Phototunable Click-based Hydrogels for 3D Cell Culture: Dynamic Biochemical and Biomechanical Tailorability of the Cell Niche

by

Cole Alexander DeForest

B.S.E., Princeton University, 2006

M.S., University of Colorado, 2008

A thesis submitted to the

Faculty of the Graduate School of the

University of Colorado in partial fulfillment

of the requirement for the degree of

Doctor of Philosophy

Department of Chemical and Biological Engineering

2011

This thesis entitled:

Phototunable Click-based Hydrogels for 3D Cell Culture:
Dynamic Biochemical and Biomechanical Tailorability of the Cell Niche

written by Cole Alexander DeForest

has been approved for the Department of Chemical and Biological Engineering

_____
Kristi S. Anseth, Ph.D.

_____
Christopher N. Bowman, Ph.D.

Date_____

The final copy of this thesis has been examined by

the signatories, and we find that both the content and the form

meet acceptable presentation standards of scholarly work

in the above mentioned discipline.

Abstract

DeForest, Cole A. (Ph.D., Chemical and Biological Engineering)

Phototunable Click-based Hydrogels for 3D Cell Culture: Dynamic Biochemical and Biomechanical Tailorability of the Cell Niche

Thesis directed by Professor Kristi S. Anseth

To better understand how cells receive and respond to signals presented by their external surroundings, polymer-based hydrogels have emerged as highly tailorable constructs for assaying cell function in well-defined microenvironments where the effects of user-dictated functionalities can be individually probed. This thesis research aimed to develop synthetic strategies to create and modify 3D cell culture platforms that permit researchers to explore in real time how cell-material interactions influence important biological function. Specifically, cytocompatible hydrogels were formed *via* a novel strain-promoted azide-alkyne cycloaddition reaction between a tetrafunctional poly(ethylene glycol) and a difunctional enzymatically-degradable peptide sequence, which enabled cell-mediated active remodeling of the local material. By varying the monomer composition during material formulation, hydrogels of different initial physical properties (*e.g.*, moduli, swelling ratio, crosslinking density) were created in the presence of encapsulated primary cells and established cell lines with high viability. Subsequently, we introduced a thiol-ene reaction as a means to alter the chemical makeup of the hydrogel post-gelation. By photoinitiating this reaction, precise spatiotemporal control over the network's biochemical functionalization was demonstrated, and synthetic peptides were patterned into the substrate to visualize enzymatic activity locally and direct 3D cell spreading within user-defined subvolumes of the gels. Additionally, a photodegradable o-nitrobenzyl ether moiety was introduced within the peptide precursors that enabled chemical

crosslinks within the network to be photocleaved and for the material physical properties to be controlled in time and space. By establishing light conditions that permitted both photoreactions to be performed independently, gels were created that enabled user-defined manipulation of material biophysical and biochemical properties that were used to direct cell motility in 3D. Finally, these chemistries were exploited to introduce reversibly biomolecules to the synthetic culture platform, and experiments demonstrate the ability to promote cell adhesion to defined regions on a hydrogel surface, along with subsequent release of the captured cells, through dynamic presentation of the RGDS epitope. Collectively, this thesis research utilized multiple orthogonal reactions for the formation of hydrogel biomaterials whose physical and chemical properties were subsequently modified in time and space to probe and direct basic cellular functions (e.g., adhesion, motility). However, the general strategies and approaches should prove quite fruitful for those seeking to answer deeper biological questions, such as the role of the culture environment in regulating stem cell self-renewal versus differentiation, and these materials should further enable newfound experiments where advances in live cell imaging of biological function can be matched with the ability to probe and direct real-time changes in the cellular niche.

To my parents, friends and family,

for their direction, love, and enthusiasm.

Acknowledgements

The work comprising this thesis would not have been possible without the generous support from a large number of incredible individuals. First and most importantly, I would like to thank my research advisor, Prof. Kristi Anseth, for providing ongoing direction and support both in and out of the laboratory. Her vision and mentorship has shaped this work into a product of which I could not be more proud. Additionally, I would like to thank my thesis committee, Profs. Christopher Bowman, Jeffrey Stansbury, Charles Musgrave, and Amy Palmer, for their insightful feedback over the years.

I have had the pleasure of interacting with many extraordinary students, post-doctoral fellows, and professors throughout this thesis including my mentees, Evan Sims, Kristen Feaver, Jennifer Bruce, Vani Vivekanandan, and Radhika Rawat; my mentors, Drs. Brian Polizzotti, April Kloxin, Benjamin Fairbanks, Chien-Chi Lin, Chris Kloxin, Robert Sebra, Melinda Cushing, Charles Cheung, Helen Simms, Danielle Benoit, Darshita Shah, and Charles Nuttelman; my collaborators, Mark Tibbitt, Drs. Leah Johnson, Brian Adzima, Julie Benton, McKinley Lawson, Jeremy Baskin, and Carolyn Bertozzi; and my colleagues, notably Patrick Hume and Abigail Bernard. I'd like to give special thanks to my officemates, collaborators, and life-long friends Alex Aimetti and Joshua McCall who have helped me grow as a researcher through regular scientific discussion and have proved invaluable sounding boards for general life decisions.

This thesis would not have been possible without the financial support of a number of agencies, including the Howard Hughes Medical Institute, the National Science Foundation (DMR 1006711), and the National Institutes of Health (HL089260). Fellowship assistance for this work was graciously provided by the U.S. Department of Education's Graduate

Assistantships in Areas of National Need (GAANN) program and the National Institutes of Health Molecular Biophysics training grant (T32 GM-065103).

Finally, I would like to thank my immediate family for their support and encouragement throughout the grand journey that has been the past five years. To my parents Marvin and Debra, parents-in-law Bill and Joan, sister Kyla, brother-in-law Sam, and nephew Dominique: thanks for understanding the times when work kept me from real life, and for providing the real life that I loved escaping work for. To Robin: your unyielding love and understanding has enabled me to pursue my dreams to their fullest and has pushed me to be the person that I am ecstatic to be today.

TABLE OF CONTENTS

LIST OF FIGURES AND SCHEMES

Figure 1.7 Mechanism of o-nitrobenzyl ether photodegradation. Upon photoexcitation, an intermediate ring is generated followed by an irreversible rearrangement that results in molecular cleavage. This results in the release of X, which is typically an amide or a carboxylic acid. Figure adapted from Li *et al*.

Figure 1.8 Phototunable click-based hydrogels for 3D cell culture thesis organization. This thesis exploits three different orthogonal reactions (SPAAC, thiol-ene photoconjugation, and photodegradation) in the development of three dynamically-tunable cell culture platforms.

Figure 3.1 Cytocompatible click hydrogel formation reaction and kinetics. (a) Click-functionalized macromolecular precursors undergo the [3+2] Huisgen cycloaddition to form a 3D ideal network hydrogel *via* a step-growth polymerization mechanism. (b) Rheology can be used to monitor dynamic network formation and indicates gelation within minutes and complete reaction occurring in less than one hour at 37 °C for a 13.5 wt% monomer solution. G' is shown as closed circles, while G'' are open circles. (c) A Live/Dead stain at 24 hours of 3T3s encapsulated within this material indicates a predominantly viable population (live cells are shown in green, while dead cells are red). Image represents a 200 μm confocal projection. Scale bar = 100 μm.

Figure 3.2 Cytocompatible, biochemical patterning within preformed click hydrogels. (a) The thiol-ene reaction mechanism provides a means to quantitatively couple sulfhydryls (-SH) with vinyl functionalities (-C=C) in the presence of light. (b) Upon swelling into the material, relevant thiol-containing biomolecules are covalently affixed to the hydrogel network at varying concentrations by altering the dosage of exposed light (intensity and exposure time). (c) A Live/Dead stain at 24 hours after photolithographic patterning of 3T3s indicates a predominantly viable population (live cells are shown in green, while dead cells are red) and that the patterning process is cytocompatible. (d) The thiol-ene reaction is confined to user-defined regions in space using photomasks to introduce three different fluorescently-labeled peptide sequences within the gel, a process that can be repeated at desired times and spatial locations to introduce additional biochemical cues. (e) By controlling the focal point of the laser light in three-dimensions using a confocal microscope, micron-scale spatial patterning resolution is achieved. Values in (b) are reported as mean ± SD (n=5). The image in (c) represents a 200 μm confocal projection. The images in (d) and (e) represent confocal micrographs of fluorescently-tagged peptides patterned within the networks. Scale bar = 100 μm for (c), 100 μm for (d), and 50 μm for (e).

Figure 3.3 Visualizing 3T3 collagenase activity *via* patterned detection peptide within 3D click hydrogels. 3T3s were encapsulated into hydrogel networks at 3 x 10^6 cells/mL. After 24 hours, a di-fluorescein collagenase-sensitive peptide sequence (DiFAM) which exhibits intramolecular self-quenching until enzymatically cleaved (a) was swollen into networks at 0.5 mgs/mL and exposed to 365 nm collimated light at 10 mW/cm^2 for 10 minutes through a variety of photomasks: (a) full mask; (b) no mask; (c) full mask with 200 μm square opening. Here, patterned regions gently fluoresce while areas of high collagenase activity (near cell surface) fluoresce with greater intensity. Images represent 200 μm confocal projections at 3 days. Scale bars = 100 μm for (b) and (c) and 50 μm for (d).

Figure 3.4 Effect of patterned RGD on 3T3 population within 3D click hydrogels. 3T3s were encapsulated into hydrogel networks at 3 x 10^6 cells/mL. After 24 hours, thiol-functionalized

RGD, a fibronectin motif known to promote cell attachment, was swollen into networks at 3 mgs/mL and exposed to 365 nm collimated light at 10 mW/cm^2 for 10 minutes through a variety of photomasks: (a) full mask; (b) no mask; (c) full mask with 250 μm square opening (illustrated by the dashed lines). 3T3s were stained at day 10 with CellTracker orange and imaged using confocal microscopy. Here, cells only adopt a spread morphology in user-defined regions of RGD. Images represent 200 μm confocal projections. Scale bars = 100 μm.

Scheme 4.1 Click-functionalized macromolecular precursors react *via* the strain-promoted [3 + 2] Huisgen cycloaddition to form an end-linked hydrogel network. By varying the molecular weight of the PEG, well-defined networks of differing crosslinking density are formed.

Figure 4.1 Final mechanical properties are dictated by gel formulation. a) The swollen hydrogel shear elastic moduli are easily tuned by changing the molecular weight of the PEG crosslinker (□ = 10,000 g/mol, ▲=15,000 g/mol, ○ = 20,000 g/mol). Alternatively, small stoichiometric imbalances between the gel-forming azide and cyclooctyne reactive groups also give rise to materials with a wide range of moduli. b) Changes in gel formulation result in hydrogels with different equilibrium swelling ratios (in PBS). c) The swelling ratio (▲) and equilibrium shear moduli (○) data scale for all conditions when normalized to crosslinking density. Data reported as mean ± std.

Figure 4.2 Network properties are largely independent of peptide crosslinker properties in buffered solutions (pH = 7.4). a) The amino acids sequence does not influence the shear elastic moduli of formed gels. b) Similarly, the overall charge of the peptide does not influence the mechanical properties of the formed networks. Data reported as mean ± std.

Scheme 4.2 Post gelation, cysteine-containing peptides are covalently affixed pendent to the hydrogel backbone *via* the radical-mediated thiol-ene reaction. Using a photoinitiator, chemical radical generation is confined to areas of light exposure, ultimately enabling spatial patterning control throughout the material.

Figure 4.3 Patterning concentration depends on the photoinitiator concentration and the total light dosage delivered to the system. a) By varying the amount of photoinitiator present, we are able to control the level of patterning concentration for a given dosage (▼ = 1.1 mM, ▲ = 2.2 mM, □ = 4.4 mM, ○ = 8.8 mM photoinitiator I2959). b) As the light intensity remains near-constant throughout the thickness of the gel, patterning concentration is largely uniform throughout the entirety of the gel. Data reported as mean ± std. Scale bar = 200 μm.

Figure 4.4 Biochemical gradients are created throughout the hydrogel network. a) By subjecting the hydrogel to a linear gradient of light exposure, well-defined gradients of fluorescent patterning agents are created across relatively large distances. b) These magnitude of these gradients is readily controlled by tuning the slope of the light gradient. c) Multiple peptide gradients are patterned within the same material. d) Using a stepped gradient of light exposure, a stepped patterning concentration is obtained. Scale bar = 200 μm.

Figure 5.1 Synthesis, photocoupling, and photodegradation for tuning chemical and physical properties of click-based hydrogels. (a) Click-functionalized macromolecular precursors (*i.e.*, PEG-tetraDIFO3 and bis(azide)-functionalized polypeptides) form a 3D ideal hydrogel structure

via a step-growth polymerization mechanism by the (b) SPAAC reaction. (c) In the presence of visible light (λ = 490 – 650 nm or 860 nm), thiol-containing biomolecules are covalently affixed to pendant vinyl functionalities throughout the hydrogel network *via* the thiol-ene reaction. (d) A nitrobenzyl ether moiety within the backbone of the polymer network undergoes photocleavage in the presence of single or multi-photon UV light (λ = 365 nm or 740 nm) that results in photodegradation of the network.

Figure 5.2 Biochemical patterning within preformed click hydrogels using visible light. Upon swelling thiol-containing biomolecules into preformed gels, pendant functionalities are affixed to the hydrogel backbone *via* the thiol-ene reaction upon exposure to visible light (λ = 490 – 650 nm). (a) The final patterned concentration of a fluorescent RGD peptide (AF_{488}-AhxRGDSC-NH_2) depends on the amount of photoinitiator present (2.5, 5, and 10 mM Eosin Y), as well as the exposure time to visible light (0 – 2 min, 10 mW cm^{-2}). (b) The network functionalization with pendant fluorescently-labeled peptides is confined to user-defined regions within preformed gels using photolithography (0.5, 1, or 2 min exposure with increased patterning concentration for increased exposure time, 10 mW cm^{-2}, 10 μM eosin Y). (c) The photocoupling reaction is controlled in 3D by rastering the focal point of multi-photon laser light (λ = 860 nm) over defined volumes within the gel, affording micron-scale resolution in all spatial dimensions. Additionally, the patterning process can be repeated many times to introduce multiple biochemical cues within the same network, as demonstrated by the red- and green- labeled patterned peptides within the same gel. Images represent confocal projections and 3D renderings. Scale bar = 400 μm for (b) and 100 μm for (c).

Figure 5.3 Biophysical patterning within preformed click hydrogels using UV light. In the presence of UV light (λ = 365 nm), photolabile functionalities within the hydrogel crosslinks undergo an irreversible cleavage, thereby decreasing the total network connectivity, resulting in local material degradation and removal of the fluorescent hydrogel material. (a) In optically-thick samples, the depth of photodegradation is directly related to the incident light intensity (5, 10 and 20 mW cm^{-2}), as well as the exposure time to visible light (0 – 45 min). (b) Using mask-based photolithographic techniques, network degradation was confined to user-defined regions within fluorescently-labeled gels (10, 15, 20, 30, and 45 min, feature height increasing with exposure time), as measured by profilometry. (c) The photodegradation reaction is controlled in 3D with micron-scale resolution in all dimensions using focused multi-photon laser light (λ = 740 nm). Images represent confocal projections and 3D renderings. Scale bar = 400 μm for (b) and 100 μm for (c).

Figure 5.4 Orthogonality of photocoupling and photodegration reactions. (a) The peak absorbance for the photoinitiator (red) and the photolabile group (blue) is well separated (~520 and ~350 nm, respectively), thus enabling photocoupling and photodegradation reactions to be performed independently from one another using different light sources (illustrated with colored bars). (b) NMR studies indicate that the photodegradable moiety cleaves readily in the presence of UV light (λ = 365 nm, 10 mW cm^{-2}), but remains intact when exposed to the visible light used to initiate the photocoupling reaction (λ = 490 – 650 nm, 10 mW cm^{-2}). (c) Multi-photon visible light was first used to couple a fluorescently-labeled peptide within the center of the hydrogel in a user-defined 3D pattern (top, buffalo), and the network was subsequently degraded locally with multi-photon UV light, thereby removing the peptide from selected regions (bottom, CU and

horn). (d) Brightfield microscopy confirms that photocleavage is confined only to user-defined locations within the gel, and that the photocoupling light conditions do not give rise to undesired degradation. Images in (c) represent 3D renderings of confocal z-stacks. Scale bars = 100 μm.

Figure 5.5 Culture and recovery of hMSCs from hydrogel microenvironments. CellTracker Orange-labeled human mesenchymal stem cells (hMSCs) were encapsulated within the click hydrogel formulation at 5 x 10^6 cells mL^{-1}. (a) 24 hours post encapsulation, perpendicular 200 μm wide lines of ~1 mM RGD and PHSRN were patterned throughout the hydrogel *via* thiol-ene photocoupling to create an array of four distinct biochemical conditions (no cue, RGD, PHSRN, RGD and PHSRN). (b) 4 hours later, channels of user-defined shape (cylindrical) were eroded down from the surface of the hydrogel to capture entrapped cells exposed to a specific cue. (c) This process was repeated 1 hour later to release entrapped cells within a different location of the material and a different shape (star-shaped cylinder). (d) The released cells were isolated by centrifugation, cultured in a 96-well plate for 48 hours, and their cytoskeleton was visualized with a fluorescent phalloidin. (a-c) RGD is shown in green, PHSRN red, and hMSCs orange. Images represent single confocal slices within the 3D gel. (d) F-actin is shown in green, nuclei blue. Image represents inverted fluorescence micrograph. Scale bars = 200 μm in (a-c), 50 μm in (d).

Figure 5.6 Directed 3D cell motility within patterned hydrogels. (a) A fibrin clot containing 3T3 fibroblasts was encapsulated within the click hydrogel formulation. Chemical channels of RGD, a cell-adhesive fibronectin motif, as well as physical channels of user-defined shape were created radially out of the roughly spherical clot. The combination of having physical space to spread as well as chemical moieties to bind to were found to be required for collective cell migration. By day 10, cells were found to migrate only down the physical channel that was functionalized with RGD. (b) By creating 3D functionalized channels, cell outgrowth was controlled in all three spatial dimensions, with the image inset illustrating a top-down projection. (c) The outgrowth of 3T3 fibroblast cells was controlled in the presence of encapsulated human mesenchymal stem cells (hMSCs) and confined to branched photodegraded channels that were functionalized with RGD. The regions of RGD-functionalization are depicted by the dashed polygons in (a) and (c). The hydrogel is shown in red, F-actin green, and cell nuclei blue. Scale bars = 100 μm.

Figure 6.1 (a) Click-based hydrogels containing pendant alkenes are functionalized with thiol-containing, photodegradable, fluorescent peptides (Ac-C-[PL]-RGDSK(AF_{488})-NH_2) *via* the thiol-ene reaction initiated with flood exposure to visible light (λ = 490 – 650 nm, 10 mW cm^{-2}) and eosin Y photoinitiator. (b) The final peptide patterning concentrations (0 – 1 mM) depended on the initiator concentration (2.5, 5, 10 μm) and visible light exposure time (0 – 120 sec). (c) Gels patterned with the photodegradable peptide by visible thiol-ene coupling (~1 mM) were subsequently exposed to UV light (λ = 365 nm) to induce an orthogonal nitrobenzyl ether photocleavage reaction and subsequent removal of the peptide, where the rate of removal was dependent on light intensity (5, 10, 20 mW cm^{-2}) and irradiation time (0 – 600 sec). Curves represent predicted concentrations based on predetermined photocleavage kinetics.

Figure 6.2 (a) Fluorescent peptides (Ac-C-[PL]-RGDSK(AF_{488})-NH_2) were patterned into the network in 2D upon exposure to masked visible light (λ = 490 – 650 nm, 10 mW cm^{-2}, 2 min, 10 μM eosin Y) and (b) in 3D *via* focused pulsed laser light (λ = 860 nm, 350 mW μm^{-2}, scan speed

= 1.27 μsec μm^{-2}, 10 μM eosin Y). (c,d) Subsets of these prepatterned cues were removed with UV light (for masked light: λ = 365 nm, 10 mW cm^{-2}, 20 min; for 3D focused laser light: λ = 740 nm, 670 mW μm^{-2}, scan speed = 1.27 μsec μm^{-2}) to yield new 2D and 3D patterns. (b) False coloring was employed for enhanced reader visualization. Scale bars = 200 μm.

Figure 6.3 Ac-C-[PL]-RGDSK(AF_{488})-NH_2 was first patterned (~1 mM) into hydrogels either uniformally throughout the bulk (a, b, d) or in 200 μm wide lines (c, e) *via* visible thiol-ene photocoupling. The samples were exposed to gradients of UV light (λ = 365 nm, 10 mW cm^{-2}) generated by a moving (1.6, 0.8, 0.4 mm min^{-1} in a; 0.4 mm min^{-1} for b-e) opaque photomask to create exponentially-decaying peptide gradient. By shuttering the light (b) or releasing pre-patterned lines (c, e), unique gradients were generated. Solid gray lines represent predicted concentrations based on predetermined photocleavage kinetics. Scale bars = 400 μm.

Figure 6.4 (a) Parallel lines (200 μm wide) of Ac-C-[PL]-RGDSK(AF_{488})-NH_2 were patterned into the hydrogel at ~1 mM *via* visible thiol-ene photocoupling. NIH 3T3s were seeded onto the gel substrates at 8 x 10^3 cells cm^{-2}, and their attachment was confined to RGD-functionalized regions of the hydrogel surface. (b) 24 hours after seeding, selective regions of RGD were removed with masked UV irradiation (λ = 365 nm, 10 mW cm^{-2}, 20 min) through the same 200 μm line mask used in the initial patterning rotated 45° clockwise, resulting in localized cell-detachment. Green = RGD, red = F-actin, blue = nuclei. Scale bar = 200 μm.

Figure 7.1 Phototunable click-based hydrogels for 3D cell culture thesis organization. This thesis exploited three different orthogonal reactions (SPAAC, thiol-ene photoconjugation, and photodegradation) in the development of three dynamically-tunable cell culture platforms.

Figure 7.2 Subset of cyclooctynes available for SPAAC copper-free click chemistry. Each molecule (*e.g.*, OCT, DIBO, BCN, BARAC, DIFBO) will react spontaneously with azides with different reaction kinetics, and could be utilized for hydrogel formation in the place of DIFO3.

Figure 7.3 Fractional release of $TGF\beta_1$ from hydrogel networks formed by different reaction mechanisms. Due to its limited interaction with encapsulated proteins, the bioorthogonal SPAAC-formed networks result in a a greated payload release when compared with radical-mediated diacrylate-based networks. *Work performed in collaboration with Joshua McCall.

Figure 7.4 Additional bioorthogonal reactions. Many different reactions have been developed that enable the chemoselective ligation of two molecules.

Figure 7.5 Single cell thiol-ene patterning. By functionalizing the hydrogel network in specific regions directly around the cell, simple questions about geometric arrangements of chemical cues and their influence on function can be assayed.

Figure 7.6 Increased moduli from thiol-ene patterning. By patterning in multifunctional thiols into the SPAAC-based hydrogel, additional crosslinks are introduced into the material, resulting in different network properties (*e.g.*, moduli, swelling ratio). *Work performed in collaboration with Kristen Feaver and Mark Tibbitt.

Figure 7.7 Directed aggregation of lung alveolar epithelial cells (AT2) within photodegraded microwells. a) Wells of a specified shape and depth are photodegraded down from the surface of the initially-flat gel. AT2 cells are seeded into the wells by centrifugation, and these wells can be arbitrarily shaped, with circles shown in (b) and three-leaf clovers in (c). d-e) After 7 days, AT2 cells have differentiated into AT1 cells and aligned with the outer wall. Blue = cell nuclei, green = AT1 marker protein T1α, red = AT2 marker surfactant protein C. Scale bars = 200 μm. *Work performed in collaboration with Dr. April Kloxin and Prof. Vivek Balasubramaniam.

Figure 7.8 2D & 3D modulation of cell shape and size. a) In 2D, cells are initially seeded on adhesive regions of a gel surface (left). At a later time point, the size or shape of the adhesive island can be changed (middle) to observe the effect on cell fate (proliferation, top right; apoptosis, bottom right). b) Similarly, cells can be seeded on posts of patterned RGD (left) that will subsequently be changed to squares *via* thiol-ene photocoupling (right). c) In 3D, voids around single cells (left) encapsulated within an RGD-containing photodegradable gel are created with UV exposure (middle). At a later time, void shape and size is altered to determine the effect on proliferation and apoptosis rates (right). d) Alternatively, only specific regions of the network can be functionalized with RGD (left, middle) to test its effect on cell function. Subsequent irradiation increases the void area or regions of adhesivity (right). *Concepts developed in collaboration with Mark Tibbitt and Dr. April Kloxin, images created by Mark Tibbitt.

CHAPTER I

INTRODUCTION AND BACKGROUND

1.1 Overview

There is a growing interest in the use of polymer-based hydrogel systems for three-dimensional (3D) cell culture applications. Their unique properties allow cells to be grown in user-defined microenvironments that recapitulate many critical aspects of native tissue. The synthetic nature of these hydrogel enables them to be engineered precisely to include desired biofunctionality *via* the tailorability of the hydrogel's chemical and mechanical properties. While hydrogels do afford this level of functional control and a great body of research has been dedicated towards their use at directing specific cell function and to engineer fully-functional tissue, it is often arduous to know which specific biological cues are important in promoting a desired cellular response and therefore which cues should be included *in vitro*. This complexity stems, in part, from a fundamental difficulty in visualizing and quantifying the dynamically-presented, spatially-complex milieu of cues found *in vivo*. A major goal of this thesis is the development and characterization of user-programmable hydrogel platforms that enable newfound experiments and specific questions concerning cell function to be probed to better understand how cells receive information from their dynamically evolving surroundings.

As the field seeks to better understand the way in which cells interact with and receive information from their extracellular niche, the ability to control dynamically material properties

enables the individual effects of these complex cues to be elucidated in a precise manner. In this thesis, a new class of biomaterials is developed that offers user-defined control of the physical and chemical nature of cell-laden hydrogels using light. These modifications to the cell environment can be performed on-demand and in real-time and are readily controlled in both time and space. The overall goal of this thesis is the development of poly(ethylene glycol) (PEG)-peptide hydrogels that undergo chemical functionalization or degradation upon exposure to light, enabling the cell's local environment to be tuned precisely. Specifically, light-programmable hydrogels are synthesized, their formation and modification are characterized, and their use as dynamic cell culture platforms is demonstrated.

This introductory chapter focuses on the use of polymer-based hydrogels for 3D cell culture. Subsequently, the main techniques that have been used to date to alter the physical and chemical properties of these hydrogels, and the degree of biological control that these systems provide, will be addressed. Finally, a variety of emerging chemical reactions will be reviewed that provide a critical foundation for this thesis work.

1.2 Hydrogels as Biomaterials for 3D Cell Culture and Tissue Engineering

Hydrogels represent an emerging and highly-attractive class of biomaterials that have been used in a number of biological applications, including drug delivery, biosensors, and contact lenses[1-4]. More recently, their unique set of properties has enabled their expanded use into that of *in vitro* cell culture platforms[5-8]. Their high water content, tissue-like elasticity, and facile transport of nutrients and waste render them ideal candidates as mimics of the cell's extracellular matrix (ECM), while their optical clarity enables microscopy-based assays of cell function to be performed and quantified readily. Furthermore, many hydrogels can be formed under mild, cytocompatible conditions that enable cell encapsulation and are modified easily to

contain user-defined chemical functionalities, mechanical properties, and degradability. Hydrogels can be synthesized from a variety of starting materials, including both naturally- and synthetically-derived polymer systems.

Naturally-derived components are commonly employed in the synthesis of hydrogels for cell culture due to their inherent bioactivity, biocompatibility, and biodegradability. Gels have been created from a wide variety of sources, including collagen[9,10], fibrin[11-13], hyaluronic acid[14-17], dextran[18,19], chitosan[20-22], and alginate[23-25], through a variety of crosslinking methods (e.g., physical, covalent, ionic interactions) with varying degrees of success. As these biomolecules inherently contain cell-signaling attributes, cells generally thrive in these materials. Nevertheless, the same endogenous epitopes and cues that enable high viability and proliferation rates within these naturally-derived materials convolute studies and make it challenging to assess the isolated effects of single cues on cell function. In addition, the non-specific interactions between the cells and the biomolecules, coupled with the batch-to-batch variability of many of these products, result in hydrogels whose physical and chemical properties are difficult to engineer. As such, synthetic-based hydrogels, where the exact composition and chemistry of the cell microenvironment are explicitly known, have become increasingly attractive as culture platforms to gain information on the effects of specific biochemical and/or biophysical signals on cell function.

Synthetic hydrogels are formed by reacting bioinert molecules, typically monomers and polymers, to form a crosslinked network in the presence of cells. As the chemical makeup of these gels is defined precisely by the selection of network components, the resulting hydrogels form with consistent and predictable properties and are readily tunable to create systems with user-desired functionality. For example, numerous synthetic hydrogels for 3D cell culture are

formed from polymer building blocks based on poly(ethylene glycol) (PEG), poly(vinyl alcohol) (PVA), and poly(*N*-isopropylacrylamide) (PNIPAm) (Figure 1.1). PEG represents the "gold standard" for synthetic scaffolds, owing to its high hydrophilicity and bioinert structure that is highly resistant to protein adsorption and enables non-fouling hydrogels to be created that resist cell and macromolecular adhesion. As PEG-based hydrogels lack the functional sites to interact directly with cells in any way other than physical support, they are generally considered a blank slate that will permit, but not promote, basic cell function. In addition, the hydroxyl endgroups of PEG are easily modified with other chemical functionalities (e.g., acrylates, methacrylates, maleimides, thiols, azides) that can be reacted together to form a 3D network[26-28]. PVA contains the same chemically-modifiable hydroxyl functionalities, which are pendant to the polymer backbone, and is also water-soluble and biocompatible. Its structure enables a high level of functionalization as each chain can be decorated with many pendant reactive groups, giving rise to hydrogels with unique and complex structures[29-33]. Hydrogels have also been formed with PNIPAm, a polymer whose backbone undergoes conformational refolding above and below 32 °C, enabling systems whose physical properties can be modulated with temperature[34-36]. A variety of other polymer-based systems are also being explored[37].

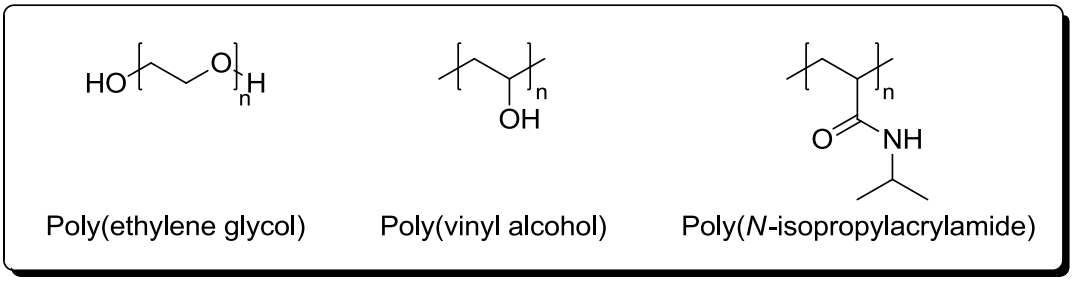

Figure 1.1 Typical synthetic hydrogel macromolecular precursors. A variety of hydrophilic polymers have been used in the formation of synthetic hydrogels for 3D cell culture, including poly(ethylene glycol), poly(vinyl alcohol), and poly(*N*-isopropylacrylamide).

Just as the selection of the hydrogel's building blocks dictates the final material properties, the method of network crosslinking also influences its structure and function, and

polymer networks are therefore often categorized by the reaction mechanism in which they are formed[38]. Chain polymerizations result when an initiator produces a monomer with a reactive center in the form of a free radical, anion, or cation, and monomer molecules are added successively across this active center, with the reactive center regenerated and the polymer lengthened upon each addition. When monofunctional monomers are polymerized *via* chain polymerization, they form linear polymers; however, when multifunctional monomers are reacted, a crosslinked, chain-growth network results. Alternatively, step growth polymerizations proceed by the one-to-one reaction of complementary functional groups. In this way, monomers proceed to dimer, trimer, tetramer, etc, until large polymer molecules are formed. When the average functionality of the reactive monomers is two or more, the result is a crosslinked step-growth network. Due to the reaction mechanism, chain-growth networks are typically characterized by an early gelation point as well as by network heterogeneity, where dense regions of kinetic chains are crosslinked by polymer[39,40]; step-growth networks require a much higher conversion to reach gelation (as predicted by the Flory-Stockmeyer equation[38]), but produce materials that are much more ideal and regular in structure[41] (Figure 1.2).

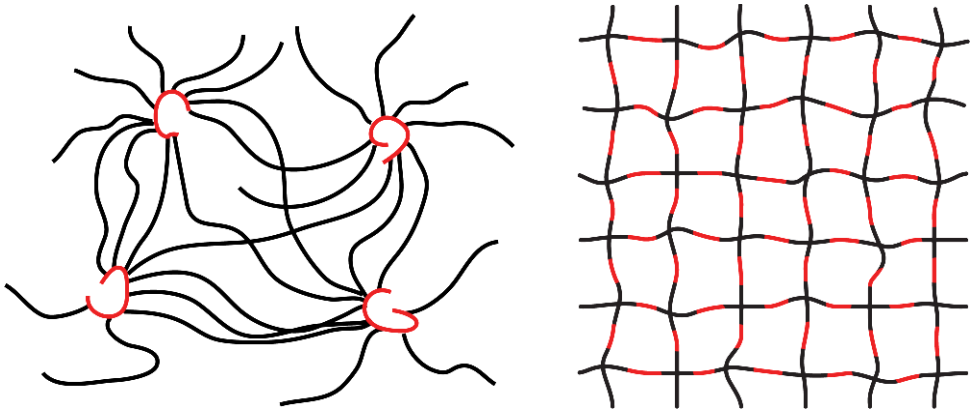

Figure 1.2 Schematics of chain- and step-growth networks. General network structures for radically-polymerized chain growth from hydrophilic, macromolecular divinyl monomers (left, kinetic chains shown in red) and step-growth networks formed from di- and tetra-functional comonomers (right).

In addition to the chemical composition and the reaction mechanism that forms the hydrogel, a variety of other parameters are important in gel properties. The crosslinking density (ρ_x) refers to the number of elastically active chains that are present in a given volume of the material and directly influences materials properties such as: (1) the water content of the hydrogel, as measured by the volumetric swelling ratio (Q, the ratio of water-swollen gel volume to dry volume); (2) the mesh size of the network (ζ), which dictates the diffusivity of molecules through the network (D); (3) the gel mechanics, including the gel shear modulus (G). Based on rubber elasticity theory, for highly-swollen networks these parameters can be related by[42]:

$$G = RT\rho_x Q^{-\frac{1}{3}}$$

where R is the universal gas constant and T is the temperature. As G can be directly measured through network formation with rheometric techniques, the network crosslinking density can be calculated as the material evolves and subsequently degrades. Nevertheless, nearly every hydrogel property is related to the crosslinking density, so it is often difficult to create materials with desired mechanical properties defined *a priori*. From Flory-Rehner theory, for highly-swollen materials, the swelling ratio scales as $Q \sim \rho_x^{-3/5}$ and implies that the shear moduli scales as $G \sim \rho_x^{6/5}$, which has been experimentally confirmed by Anseth *et al.*[43,44]

1.3 Biochemical Control of Hydrogel Properties

As cells receive a variety of complex chemical signals from their local microenvironment, there is a growing interest in developing and utilizing biochemically-functionalized polymer-based hydrogels for 3D cell culture applications that promote specific cell functions.[6,7,45] While full proteins can be entrapped within hydrogels to elicit a specific interaction, peptides have emerged as an alternative synthetic route that allows facile introduction of biofunctionality into hydrogels as covalently bound ligands. Peptides are short

chains of amino acid residues linked together by amide bonds, with each amino acid consisting of an amine and a carboxylic acid, as well as an α-carbon with an R group which can contain a variety of functionalities (e.g., amines, thiols, alcohols, acids). As peptides contain the same amino acid building blocks as proteins, they can evoke similar biological function to that of the full protein whose structure they mimic. They are easily synthesized and purified, and can be systematically engineered to include a variety of non-natural amino acids, ultimately enabling a greater level of synthetic biological control than their complex biomacromolecular counterparts[46]. Peptides have already enabled the incorporation of integrin-binding epitopes (e.g., the fibronectin-derived RGD sequence)[27,32,47,48], enzymatically-degradable sequences (e.g., the collagenase sensitive sequence GPQG↓ILGQ)[49-51], growth-factor sequestering properties (e.g., the basic fibroblast growth factor-binding KRTGQYKL sequence)[52-54], as well as additional bioactivity[55-58] into otherwise bioinert hydrogel formulations, permitting cells to interact directly with their surrounding material.

Peptides are most commonly incorporated into hydrogels during the formation of the network itself. In this approach, peptides are synthesized and functionalized to include the same reactive substituents that are employed for network formation and are simply mixed at the desired concentration into the polymer precursor solution. Upon gelation, the peptide is homogenously distributed throughout the network and is able to signal encapsulated cells. This technique was exploited by Anseth *et al.* to incorporate varying amounts of Acryl-PEG-RGD, an acrylated version of the adhesive ligand RGD created by the coupling of monoacrylated PEG-*N*-Hydroxysuccinimide (NHS) to the N-terminal α-amino group of the peptide[59-62], into a gel formed by the radical chain photopolymerization of PEG diacrylate (PEGDA)[27]. There, the authors found that osteoblasts exhibited a higher degree of spreading and cytoskeletal

organization on gels (Figure 1.3a-c) and increased mineralization within gels containing additional RGD. Alternatively, a mixed-mode photopolymerization of acrylates in the presence of thiols enables cysteine-containing peptides to be incorporated directly into materials with no post-synthetic modification[63]. In this system, the chain polymerization of acrylates is truncated with a step-addition to a thiol, giving rise to networks with unique structure compared to those described in Figure 1.2. Finally, cysteine-containing peptides are also directly incorporated into hydrogels formed *via* the base-catalyzed Michael-type addition between electron-deficient alkenes (e.g., acrylates, vinyl sulfones) and thiols[64-66], or by the radical-mediated thiol-ene reaction (which will be further examined in Section 1.5)[67]. While these approaches are fairly straightforward, the level of peptide incorporation directly influences network structure and resulting gel mechanics and the approach offers no spatiotemporal control over the gel's functionalization.

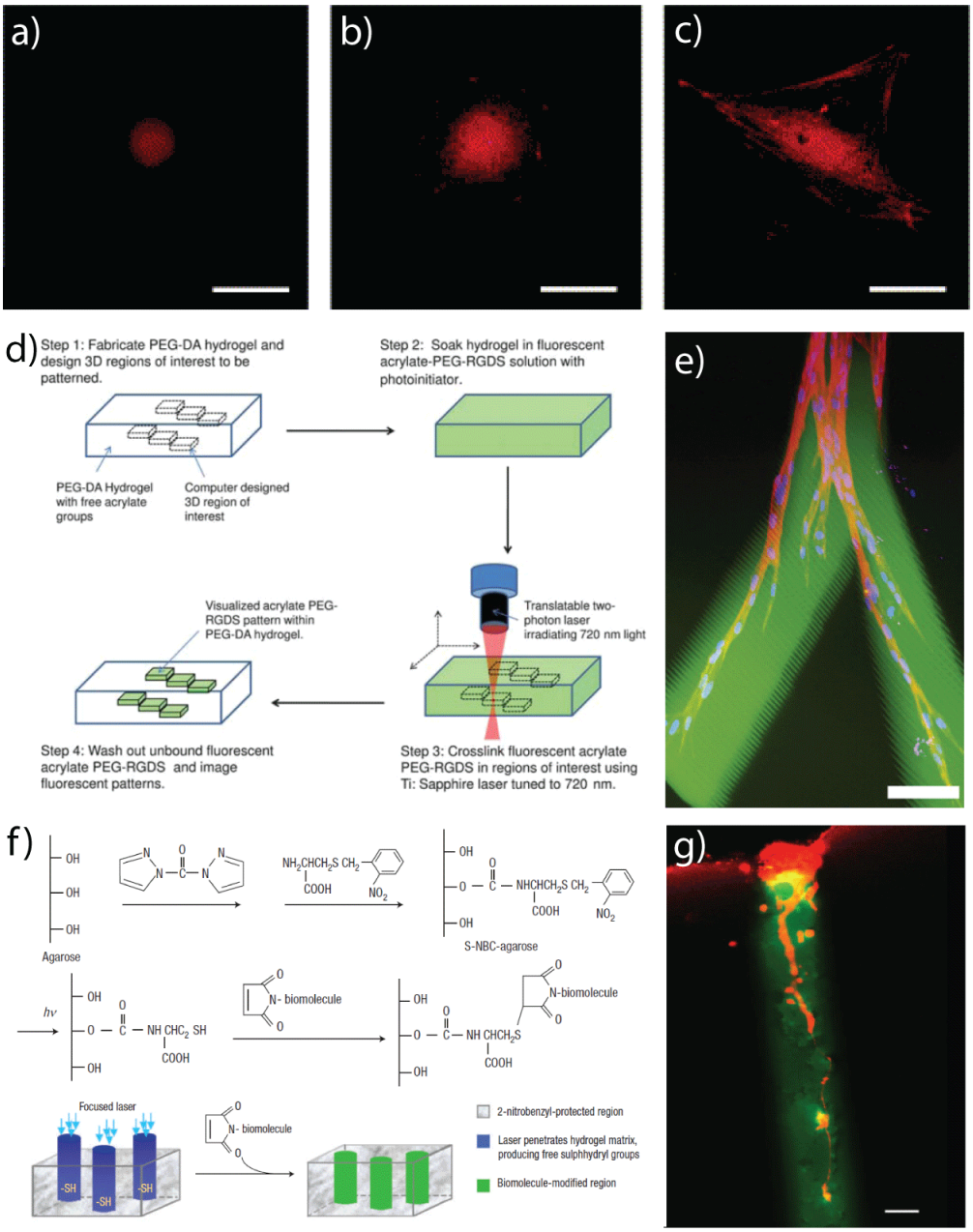

Figure 1.3 Methods for controlling biochemical aspects of hydrogel. Osteoblasts were seeded on PEGDA gels containing (a) 0 mM, (b) 0.5 mM, and (c) 5.0 mM Acry-PEG-RGD and increased cytoskeletal organization (as illustrated with F-actin staining in red) was observed with higher RGD concentrations[27]. (d) By swelling fluorescently-labeled, acrylated peptides into a preformed PEGDA gel and selectively exposing the material to light, peptides were selectively immobilized within the 3D hydrogel network[68]. (e) This technique was used to direct 3D human dermal fibroblast cell migration within an enzymatically-degradable PEG hydrogel (red = F-actin, green = RGD, blue = cell nuclei)[69]. (f) Photocaged thiols are deprotected in the presence of focused laser light, which can subsequently react with maleimide-functionalized biomolecules[70]. (g) Dorsal root ganglia cells were seeded on agarose gels containing channels of RGD, and processes extension was confined to patterned regions in the gel. Scale bars = 20 μm for (a)-(c), 100 μm for (e) and (g).

While the initial biochemical properties of synthetic hydrogels are readily controlled by approaches outlined thus far, platforms that allow dynamic tunability of the presentation of these bioepitopes are particularly beneficial as these materials enable cell function to be modulated in space and time as the experimenter sees fit. The West lab has exploited a classic photopolymerization technique which enables this level of dynamic control (Figure 1.3d)[68,69,71]. Here, hydrogels were formed *via* the photoinitated radical chain polymerization of PEGDA. Although the bulk of the acrylate functionalities were consumed during material formation, a small percentage of free reactive groups are present for subsequent conjugation to acrylate-containing monomers. Post-gelation, Acryl-PEG-RGD was swollen into the network with a small amount of photoinitiator and sub-volumes of the gel were selectively exposed to pulsed laser light, inducing chain polymerization locally and thus material functionalization. This technique enables multiple cues to be introduced post-gel formation and was used to guide human dermal fibroblast cell spreading within an enzymatically-degradable gel (Figure 1.3e). It is important to note, however, that while this technique does successfully pattern biochemical cues at desired locations in space and time, the final gel structure and composition is ill-defined and difficult to characterize.

Shoichet *et al.* have developed an alternative patterning approach that enables chemical immobilization in a more defined manner that does not modify the local gel mechanics (Figure 1.3f)[70,72]. Here, an agarose gel was synthesized that contained photocaged thiols. In the presence of focused laser light, free thiols were liberated that spontaneously reacted with maleimide-functionalized RGD that was swollen into the gel. The unreacted peptides were swollen out of the gel to yield patterned channels down from the surface of the gel. Dorsal root ganglia cells were seeded on top of these networks and were found to extend processes only into

the adhesive biochemical domains of the gel (Figure 1.3g). While this approach does enable gel patterning without altering network mechanics, the cytotoxicity of maleimides ultimately precludes the use of this patterning scheme in the presence of cells.

1.4 Biomechanical Control of Hydrogel Properties

In addition to chemical cues, mechanical signals are known to dictate local cell behavior and there is growing appreciation for the role of mechanotransduction during cell expansion and differentation. For example, in seminal studies by Discher *et al*., the differentiation of human mesenchymal stem cells (hMSCs) was found to be dependent on the 2D matrix elasticity of the substrate on which they were cultured[73,74]. hMSCs grown on soft substrates (E ~ 0.5 kPa, similar to that of brain) underwent neuronal differentiation, whereas they proceeded down an osteogenic pathway when cultured on a stiffer substrate (E ~ 35 kPa, similar to that of bone), indicating that mechanical cues alone were enough to induce lineage-specific differentiation. Similar studies have been performed in mixed differentiation media on 2D stiffness gradients[75], as well is in 3D, where the matrix stiffness was found to induce adipogenesis and osteogenesis of hMSCs within compliant (E ~ 2.5 kPa) and stiff (E ~110 kPa) agarose gels, respectively[76]. Additionally, it has been shown that the degree to which a cell is extended morphology on a 2D substrate can dictate it relative growth and apoptosis rates[77-80]. While there is significant interest in understanding these mechanobiological phenomena and in elucidating the method in which physical forces in and on a cell contribute to its function, few 3D platforms enable these fundamental studies to be performed dynamically[81,82].

As the biophysical parameters (e.g., stiffness, water content, diffusivity of molecules) of a hydrogel are directly related to the crosslinking density of the network, efforts to control gel mechanical properties have centered on ways to alter dynamically the connectivity of the

material. Some attempts have been made to synthesize 3D materials that stiffen with time. By reacting thiolated hyaluronic acid with PEGDA *via* a slow Michael-type addition, the moduli of the material stiffened from $E \sim 1$ kPa to ~8 kPa over a period of 300 hours, which was designed to match the local stiffening of heart muscle during their development from mesoderm to adult myocardium, and resulted in a higher cardiomyocyte differentiation than was found in static culture[83]. Alternative to this pre-engineered strategy, West *et al*. has exploited the use of radical photopolymerized PEGDA hydrogels that have been formed with incomplete conversion and contained free acrylates for gel modification to obtain a user-defined increase in gel mechanics (Figure 1.4a)[71]. A low molecular weight PEGDA and a small amount of photoinitiator were swollen into the network, and regions of the gel were selectively exposed to ultraviolet (UV) light, locally introducing additional crosslinks within the material, and altering the moduli from $E \sim 1$ kPa to ~3 kPa. The patterning also induced changes in the hydrogel transport properties, and fluorescently-labeled dextran was only imbibed in the unpatterned regions of the gel (Figure 1.4b). Similarly, materials containing a photosensitive amino acid *p*-azidophenylalanine were used to photocrosslink artificial ECM proteins together, where the resulting stiffness was directly related to total amount of light exposure[84]. Additionally, hydrogels have been formed *via* a Michael addition between acrylated-functionalized hyaluronic acid and a reaction-limiting amount of bis(cysteine)-containing enzymatically degradable peptides[85,86]. Patterned regions of the remaining acrylates were crosslinked with masked UV light exposure, creating a stiffer network. While cells were able to attach and spread in the base hydrogel, the increased density of non-enzymatically-degradable crosslinks in the patterned regions physically trapped the cells and prevented their migration through the material. This platform was used to pattern regions of

cell spreading of encapsulated single cells and chick aortic arches (Figure 1.4c) as well as adipogenic/osteogenic hMSC fate by regulating cell shape within the materials.

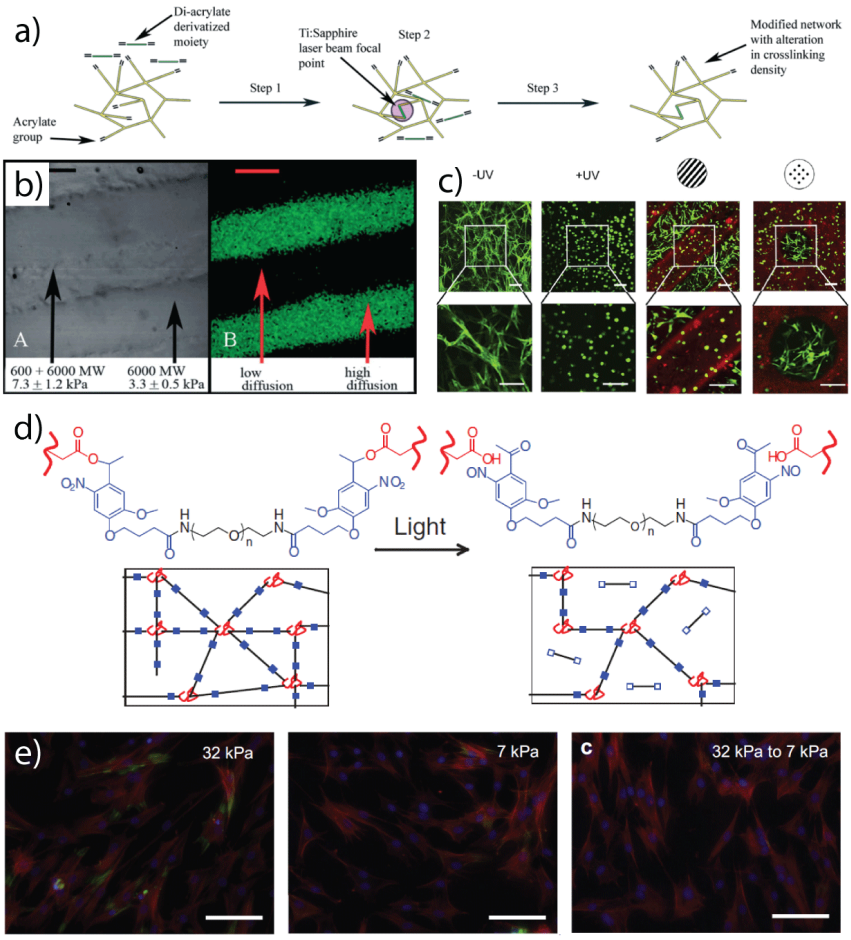

Figure 1.4 Methods for controlling biomechanical aspects of hydrogel. (a) By patterning diacrylate-derivatized monomers into a preformed PEGDA gel, the local crosslinking density was increased and the network was stiffened[71]. (b) By patterning in channels, the hydrogel transport properties were altered and fluorescently-labeled dextran (green) was found to diffuse only into unpatterned regions. (c) hMSCs within hydrogel formed by Michael addition of acrylated hyaluronic acid with a di(thiol) enzymatically-degradable peptide crosslinker. When the material was exposed to light (illuminated regions shown in red), a secondary polymerization locked up the network, entrapped the cells (green), and prevented their migration[86]. (d) By irradiating hydrogels that contained photolabile moieties in the backbone, ρ_x decreased and photodegradation occurred[87]. (e) VICs were cultured on photodegradable substrates of various moduli (E ~ 7 and 32 kPa), and activation to its myofibroblast phenotype was confined to the stiffer substrate[88]. On day 3, a portion of the 32 kPa substrates were irradiated and the moduli was decreased to 7 kPa. By day 5, activation had been reversed in the 32 kPa to 7 kPa sample (red = F-actin, green = α-smooth muscle actin, blue = cell nuclei). Scale bars = 20 μm for (b), 100 μm for (c) and (e).

Just as gels have been created that allow stiffening of the material in a pre-engineered or user-defined manner, a variety of systems have emerged that enable the gel to become more compliant with or at a specific time. This has been achieved *via* the incorporation of degradable linkers within the polymer backbone that will fracture a crosslink when cleaved and alter the gel's mechanical properties. Hydrolytically-degradable gels were first introduced by Hubbell *et al.*, where macromers having a PEG central block, extended with oligo(*dl*-lactic acid) (PLA) or oligo(glyolic acid) (PGA) and terminated with acrylates were synthesized[26]. The PLA and PGA domains contained predictably-hydrolysable ester bonds, which liberate an acid and an alcohol, and the rate of network degradation was controlled between 1 day and 4 months based on the number of PLA/PGA repeat units present. Statistical kinetic models of the degradation behavior of these materials have also been created[39,89,90], and similar methodologies have been applied to other networks[91]. PLA-PEG-PLA gels have been used for the encapsulation of a variety of cell types (e.g., chondrocytes[92], osteoblasts[93], neural precursor cells[94]), where cell function was found to be correlated directly to degradation rates, and have demonstrated some of the benefits of non-static culture platforms. Regardless, the mass profiles of these platforms are fixed by their pre-engineered rates of degradation, and are unable to be altered post gel-fabrication.

By incorporating enzymatically-degradable units into the network, the rate of material degradation is dictated locally by the amount of cell enzyme secretion and the susceptibility of the crosslinker sequence to cleavage[45,50,67,95]. A large number of peptide sequences have been incorporated into synthetic gels, each subject to different enzymatic activity and a wide range of degradation kinetics. The majority of these substrates have been susceptible to cleavage by collagenase[95], plasmin[96,97], and/or matrix metalloproteinases (MMPs)[98,99], with a variety of sequences having been engineered to cleave upon treatment with a given enzyme.

Unfortunately, most sequences have a degree of promiscuity and are not cleaved exclusively by a single enzyme making it difficult for the material degradation to be predicted *a priori*[100]. As cells are able to secrete the same enzymes responsible for network degradation, they can actively reform their surrounding microenvironment in a way that has enabled cell proliferation, migration, and differentiation over a time scale that is biologically dictated. In addition, enzyme has been exogenously delivered to these materials to degrade the network and liberate the cells[101]. While this approach does offer user-defined degradation, enzymes can have adverse affects on biological function and are often cost-prohibitive in their use for network degradation.

Light has been used to decrease the crosslinking density of the system to control network mechanical properties and had been demonstrated as advantageous as degradation is triggered externally and mechanics are tuned *in situ*. Seliktar *el al*. have used high intensity pulsed laser light to photoablate physical channels in transparent hydrogels[102]. With feature control on the micron scale, channels were created to guide neural outgrowth from a clot into a gel, opening up new avenues for the generation of guidance channels for treating nerve injuries. While this technique can be applied to most biomaterials and demonstrated patterning of cell function by altering gel physical properties, the high light requirements are cytotoxic and prohibit patterning in the presence of cells. An alternative approach has focused on the synthesis of networks based on the photoreversible dimerization of nitrocinnamate- or anthracene-functionalized polymers that are formed with 365 nm light and degraded with 254 nm light[103,104]. Unfortunately, full network degradation has not been demonstrated and the cytotoxicity of 254 nm light limits its application for cell culture. More recently, approaches have been made to create photodegradable networks that undergo reverse gelation with cytocompatable conditions[87,105-109]. Anseth *et al*. have designed linear PEG molecules that are flanked by photolabile acrylate

moieties (Figure 1.4d). This monomer was polymerized radically *via* a redox initiation scheme to create photodegradable hydrogels that were formed and whose properties were tuned in the presence of cells. These gels have been used to influence migration[87], create stiffness gradients throughout the material[110], and to study cytoskeletal reorganization of cells on 2D surfaces[111]. Perhaps the most powerful biological demonstration that has been illustrated with this material has been in the dynamic alteration of culture platform elasticity to activate and subsequently de-activate valvular interstitial cells (VICs) into their myofibroblastic phenotype, further demonstrating that the mechanical properties of a substrate are capable of directing cell fate, but illustrating for the first time that this occurs in a dynamic, reversible manner (Figure 1.4e)[88].

Covalently-adaptable networks (CANs) have recently emerged as synthetic platforms that offer dynamic control over material properties and possess reversible covalent crosslinks that respond to an externally-applied stimulus[112]. Bowman *et al.* have developed thermoreversible networks based on the Diels-Alder reaction, where a furan reversibly reacts with a maleimide to form a bicyclic compound at low temperatures and fractures into the starting compounds at high temperatures[113]. Alternatively, thiol-ene based networks containing allyl sulfide moieties undergo a radical-mediated addition-fragmentation chain transfer rearrangement, enabling rearrangement of polymer connectivity and for mechanical stress within the material to be eliminated[114-116]. Finally, disulfide crosslinked networks have been formed that degrade *via* a radical-mediated disulfide fragmentation reaction that can be spatiotemporally controlled[117]. The ability to control reversibly material properties would enable cell function to be dynamically assayed in new and exciting ways. Unfortunately, CANs have not yet been applied in the field of 3D cell culture primarily due to the reaction cytotoxicity.

1.5 Bioorthogonal Chemistry for Biomaterial Synthesis and Functionalization

As researchers have sought to develop novel approaches to create and functionalize biomaterials, specifically with control over their biophysical and biochemical properties, many have embraced the emerging "click" philosophy as a means to reach these goals. Introduced by Sharpless in 2001, the approach attempts to synthesize complex oligomers *via* a series of well-defined reactions on relatively simple subunits in a similar manner to how nature produces proteins, DNA, and carbohydrates[118-120]. These click reactions must be modular and wide in scope, orthogonal to common reactive moieties, high-yielding, have a large thermodynamic driving force, lead to no or minimally offensive byproducts, be simple to perform, and require benign or easily-removed solvent. By employing click reactions, complex and well-defined material structures are achieved readily.

Bioorthogonal reactions represent the small subset of click reactions that can be performed specifically in the plethora of functional groups that are found in biological systems[121]. This is a non-trivial requirement, as amines, alcohols, acids, sulfates, phosphates and aromatics are present on many biomolecules. Not only must these reactions be orthogonal to specific functional groups, they must be performed under stringent, physiological conditions which dictate that the reaction must proceed mildly in aqueous medium and a defined chemical environment (5% CO_2 and atmospheric O_2 levels), under regulated pH (7.4), temperature (37 °C), osmolarity (~300 mOsM), and involve reactive moieties and (by)products that are non-toxic in themselves. Though these reaction requirements represent significant constraints, these elite bioorthogonal reactions are a necessity for probing chemically and directing biological function and are fundamental in the work comprising this thesis.

The most common of the click reactions is the copper(I)-catalyzed 1,3-dipolar Huisgen cycloaddition between azides and alkynes (CuAAC, Figure 1.5)[122-124]. Mechanistically, the reaction involves the formation of a π complex between Cu(I) and the terminal alkyne, and the terminal hydrogel is subsequently deprotonated to give the activated Cu acetylide intermediate that forms a complex with the azide.[125] At this point, cyclization occurs and the weakly-coordinated copper ligand is displaced, yielding the triazole product. This quintessential click reaction has been utilized for peptide ligation[124,126] and modification[127,128], macrocyclization[129,130], dendrimer formation[131-133], and polymer grafting[134,135], among other things. Unfortunately, this reaction's catalyst, as with the majority of those reactions commanding "click" status, is cytotoxic and is unable to be performed in the presence of cells, thereby precluding its usage in the formation of peptide-functionalized materials for cell encapsulation. Recently, cyclooctyne molecules have been developed whose ring strain gives rise to an activated alkyne that reacts quickly and spontaneously with azides in the absence of a catalyst[136-139]. This strain-promoted azide-alkyne cycloaddition (SPAAC, Figure 1.5) has enabled the application of the Huisgen reaction in living organisms to label glycosylation patterns in zebrafish and mice[137,140]. Efforts have continued to develop novel cyclooctynes with enhanced reaction rates and ease of synthesis, and have included fluorinated cyclooctynes[138,141], (aza-)dibenzocyclooctynes[142,143], biarylazacyclooctynones[144], and bicyclononynes[145].

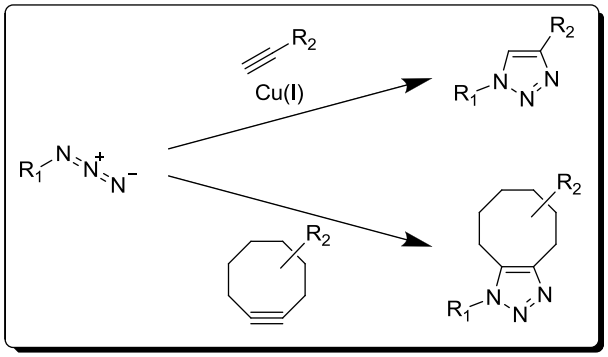

Figure 1.5 Bioorthogonal [3+2] azide-alkyne cyclooadditions to form triazoles. The reaction between terminal azides and alkynes proceeds with Cu(I)-catalyzation (CuAAC, top), while cyclooctynes will spontaneously react with azides *via* a strain-promoted reaction (SPAAC, bottom). Figure adapted from Bertozzi *et al.*[121]

Another reaction that has recently been established as a bioorthogonal process is the radical-mediated thiol-ene addition. This reaction involves an alternating propagation of a thiyl radical through a vinyl functional group and the chain transfer from the resulting thioether radical back to a thiol, resulting in a catalytic regeneration of the thiyl moiety (Figure 1.6)[146-148]. While some unsaturated carbon-carbon double bonds will undergo radical homopolymerization (e.g., acrylates, methacrylates), many alkenes do not (e.g., allyl ethers, vinyl ethers, norbornenes) and ensures the one-to-one addition of thiol-containing molecules to vinyl-functionalized moieties[149]. Initiation is most commonly achieved *via* the abstraction of a hydrogen from a thiol to form a thiyl radical, which can be accomplished by both cleavage-type and hydrogen-abstracting photoinitiators[150]. As this reaction can be initiated photochemically, it is advantageous in that it can be controlled spatially and temporally with the presentation of light. This reaction has among others been utilized for biofunctionalization[151-154], dendrimer formation[155-157], surface modification[158-161], polymerization[162-164], and idealized network generation[67,114,165].

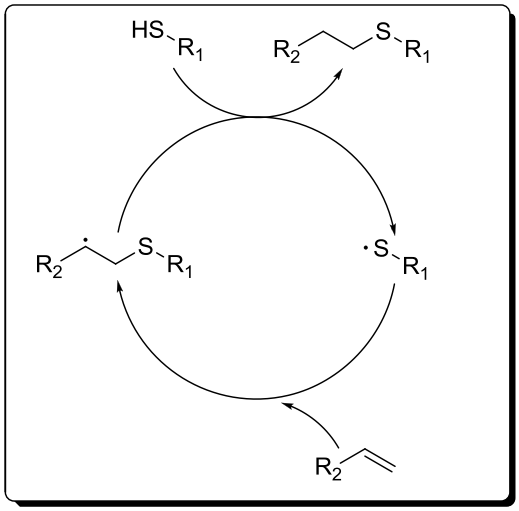

Figure 1.6 Radical thiol-ene reaction mechanism. Thiols react stoichiometrically with alkenes *via* alternating chain transfer and propagation steps. Figure adapted from Bowman *et al*.[147]

While both the thiol-ene and SPAAC reactions covalently attach functionalized monomers together, the photocleavage of an o-nitrobenzyl ether moiety permits a previously-intact chemical linkage to be cleaved photolytically and represents another powerful bioorthogonal reaction. In the presence of UV light, the moiety absorbs a photon to enter a photochemically-excited state, which subsequently undergoes an irreversible rearrangement to form a nitroso- and an acid- or amide-terminated byproduct (Figure 1.7). Unlike other photolabile functionalities, it degrades under cytocompatible irradiation conditions (e.g., 365 nm light[166]) and has been used in the uncaging of proteins[167,168], to cleave peptides from a solid support[169-171], and to control cell adhesions[172,173]. As previously mentioned, this functionality has been used to synthesize photodegradable networks[87,107,108], which enable the effects of physical material cues on cell function to be probed[88,105,109].

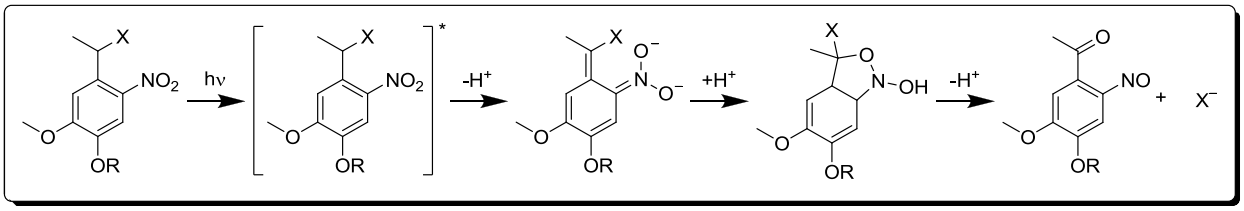

Figure 1.7 Mechanism of o-nitrobenzyl ether photodegradation. Upon photoexcitation, an intermediate ring is generated followed by an irreversible rearrangement that results in molecular cleavage. This results in the release of X, which is typically an amide or a carboxylic acid. Figure adapted from Li *et al*.[174]

1.6 Research Summary

This thesis aims to develop dynamic cell culture microenvironments, whose chemical and mechanical aspects can be independently tuned with full 3D control and in real-time (Figure 1.8). Towards this goal, Chapter II outlines the four objectives of this thesis work: developing a click-based hydrogel platform that enables biochemical cues to be introduced at specific location, expanding this platform to include biophysical control of the system in an orthogonal manner, utilizing the developed chemistries to reversibly control the presentation of biological epitopes, and to exploit these systems to pattern directed cell function. In Chapter III, the use of the SPAAC reaction for hydrogel formation is developed. Once the gel is formed, the thiol-ene reaction is utilized to decorate spatiotemporally the material with peptides that direct cell spreading and detect enzymatic activity. By tuning the monomer formulation, the initial mechanical properties of the network are readily tuned, which is demonstrated in Chapter IV. By varying the thiol-ene photocoupling conditions (e.g., light and photoinitiator concentration), we study dosage-dependent biochemical patterning which is exploited to create complex gradients of multiple epitopes within the same material. In Chapter V, we expand on this base hydrogel platform to include a photolabile moiety within the hydrogel backbone, enabling network photodegradation upon UV light exposure. Conditions are identified that enable photodegradation to be performed orthogonally to photoconjugation, providing independent

control over the gel's physical and chemical properties, and this platform is used to direct 3D cell outgrowth into complex shapes. By creating peptides that contain both the photodegradable moiety and a flanking thiol, the orthogonal photoreactions are used to decorate a gel with physiologically-relevant cues and to subsequently remove them to create biochemical gradients and to control reversibly cell attachment on a 2D surface, as demonstrated in Chapter VI. Finally, Chapter VII presents the progress in the development of light-programmable cell-culture platforms from this thesis work, as well as suggests future avenues for the utilization of these materials to probe and elicit cell function in a user-defined manner.

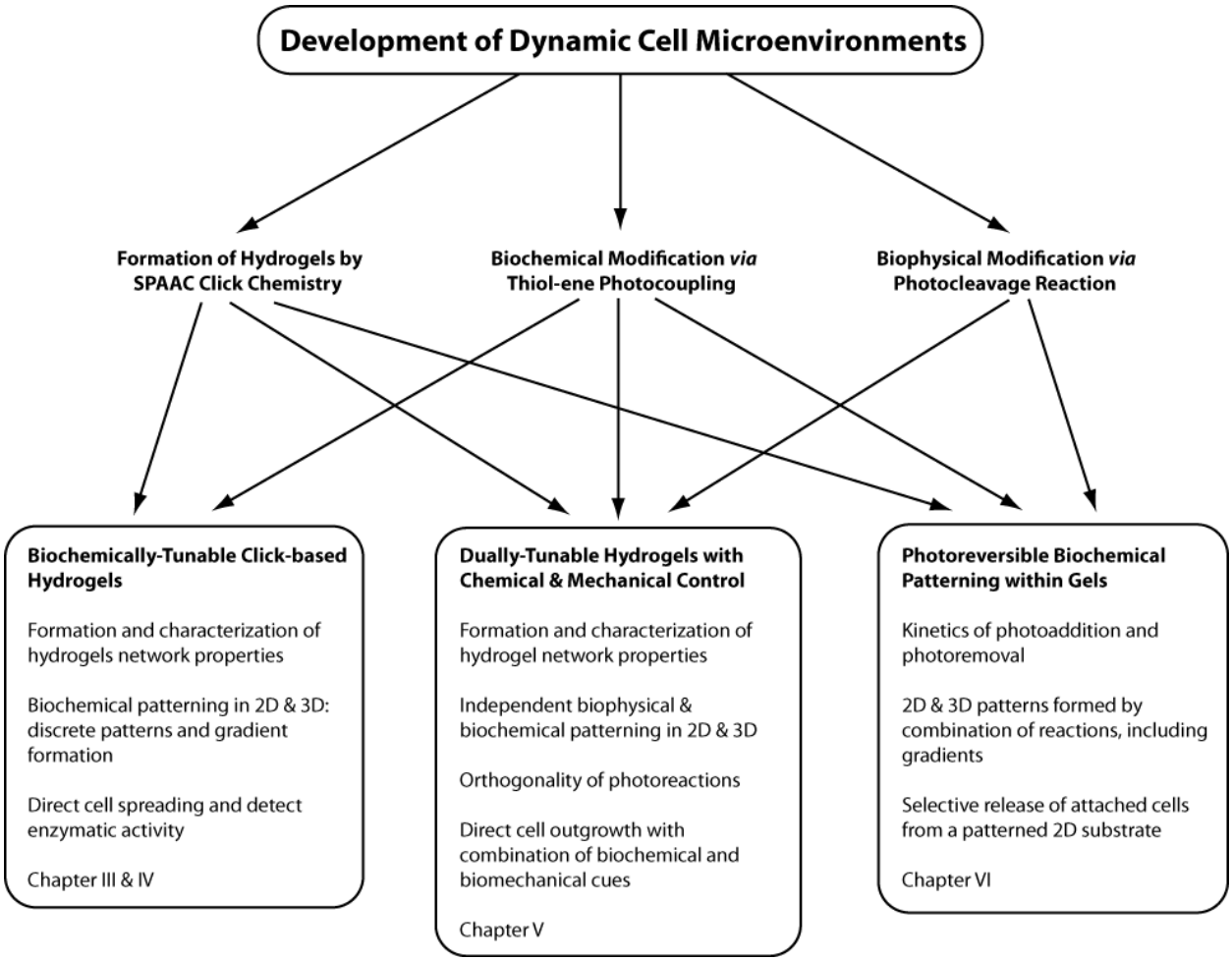

Figure 1.8 Phototunable click-based hydrogels for 3D cell culture thesis organization. This thesis exploits three different orthogonal reactions (SPAAC, thiol-ene photoconjugation, and photodegradation) in the development of three dynamically-tunable cell culture platforms.

1.7 References

1. Ratner, B.D. & Bryant, S.J. Biomaterials: Where we have been and where we are going. *Annu. Rev. Biomed. Eng.* **6**, 41-75 (2004).

2. Peppas, N.A., Hilt, J.Z., Khademhosseini, A. & Langer, R. Hydrogels in biology and medicine: From molecular principles to bionanotechnology. *Adv. Mater.* **18**, 1345-1360 (2006).

3. Langer, R. & Tirrell, D.A. Designing materials for biology and medicine. *Nature* **428**, 487-492 (2004).

4. Peppas, N.A. & Langer, R. New challenges in biomaterials. *Science* **263**, 1715-1720 (1994).

5. Langer, R. & Vacanti, J.P. Tissue engineering. *Science* **260**, 920-926 (1993).

6. Cushing, M.C. & Anseth, K.S. Materials science. Hydrogel cell cultures. *Science* **316**, 1133-1134 (2007).

7. Tibbitt, M.W. & Anseth, K.S. Hydrogels as extracellular matrix mimics for 3D cell culture. *Biotechnol. Bioeng.* **103**, 655-663 (2009).

8. Lee, K.Y. & Mooney, D.J. Hydrogels for tissue engineering. *Chem. Rev.* **101**, 1869-1879 (2001).

9. Rault, I., Frei, V., Herbage, D., AbdulMalak, N. & Huc, A. Evaluation of different chemical methods for cross-linking collagen gel, films and sponges. *J. Mater. Sci. - Mater. Med.* **7**, 215-221 (1996).

10. Butcher, J.T. & Nerem, R.M. Porcine aortic valve interstitial cells in three-dimensional culture: Comparison of phenotype with aortic smooth muscle cells. *J. Heart Valve Dis.* **13**, 478-485 (2004).

11. Eyrich, D. et al. Long-term stable fibrin gels for cartilage engineering. *Biomaterials* **28**, 55-65 (2007).

12. Ahmed, T.A., Dare, E.V. & Hincke, M. Fibrin: A versatile scaffold for tissue engineering applications. *Tissue Eng. Part B Rev.* (2008).

13. Hutmacher, D.W., Ho, S.T.B., Cool, S.M. & Hui, J.H. The influence of fibrin based hydrogels on the chondrogenic differentiation of human bone marrow stromal cells. *Biomaterials* **31**, 38-47 (2010).

14. Masters, K.S., Shah, D.N., Walker, G., Leinwand, L.A. & Anseth, K.S. Designing scaffolds for valvular interstitial cells: Cell adhesion and function on naturally derived materials. *J. Biomed. Mater. Res. A* **71**, 172-180 (2004).

15. Masters, K.S., Shah, D.N., Leinwand, L.A. & Anseth, K.S. Crosslinked hyaluronan scaffolds as a biologically active carrier for valvular interstitial cells. *Biomaterials* **26**, 2517-2525 (2005).

16. Burdick, J.A. & Prestwich, G.D. Hyaluronic acid hydrogels for biomedical applications. *Adv. Mater.* **23**, H41-56 (2011).

17. Leach, J.B., Bivens, K.A., Patrick, C.W. & Schmidt, C.E. Photocrosslinked hyaluronic acid hydrogels: Natural, biodegradable tissue engineering scaffolds. *Biotechnol. Bioeng.* **82**, 578-589 (2003).

18. Cadee, J.A. et al. In vivo biocompatibility of dextran-based hydrogels. *J. Biomed. Mater. Res.* **50**, 397-404 (2000).

19. Cascone, M.G. et al. Bioartificial polymeric materials based on polysaccharides. *J. Biomater. Sci., Polym. Ed.* **12**, 267-281 (2001).

20. Berger, J. et al. Structure and interactions in covalently and ionically crosslinked chitosan hydrogels for biomedical applications. *Eur. J. Pharm. Biopharm.* **57**, 19-34 (2004).

21. Azab, A.K. et al. Crosslinked chitosan implants as potential degradable devices for brachytherapy: In vitro and in vivo analysis. *J. Control. Release* **111**, 281-289 (2006).

22. Hoemann, C.D., Sun, J., Legare, A., McKee, M.D. & Buschmann, M.D. Tissue engineering of cartilage using an injectable and adhesive chitosan-based cell-delivery vehicle. *Osteoarthritis Cartilage* **13**, 318-329 (2005).

23. Rowley, J.A., Madlambayan, G. & Mooney, D.J. Alginate hydrogels as synthetic extracellular matrix materials. *Biomaterials* **20**, 45-53 (1999).

24. Barralet, J.E. et al. Comparison of bone marrow cell growth on 2D and 3D alginate hydrogels. *J. Mater. Sci. - Mater. Med.* **16**, 515-519 (2005).

25. Kuo, C.K. & Ma, P.X. Ionically crosslinked alginate hydrogels as scaffolds for tissue engineering: Part 1. Structure, gelation rate and mechanical properties. *Biomaterials* **22**, 511-521 (2001).

26. Sawhney, A.S., Pathak, C.P. & Hubbell, J.A. Bioerodible hydrogels based on photopolymerized poly(ethylene glycol)-co-poly(alpha-hydroxy acid) diacrylate macromers. *Macromolecules* **26**, 581-587 (1993).

27. Burdick, J.A. & Anseth, K.S. Photoencapsulation of osteoblasts in injectable RGD-modified PEG hydrogels for bone tissue engineering. *Biomaterials* **23**, 4315-4323 (2002).

28. Bryant, S.J. & Anseth, K.S. Hydrogel properties influence ECM production by chondrocytes photoencapsulated in poly(ethylene glycol) hydrogels. *J. Biomed. Mater. Res.* **59**, 63-72 (2002).

29. Hassan, C.M. & Peppas, N.A. Structure and applications of poly(vinyl alcohol) hydrogels produced by conventional crosslinking or by freezing/thawing methods. *Biopolymers/Pva Hydrogels/Anionic Polymerisation Nanocomposites* **153**, 37-65 (2000).

30. Bryant, S.J. et al. Synthesis and characterization of photopolymerized multifunctional hydrogels: Water-soluble poly(vinyl alcohol) and chondroitin sulfate macromers for chondrocyte encapsulation. *Macromolecules* **37**, 6726-6733 (2004).

31. Martens, P.J., Bryant, S.J. & Anseth, K.S. Tailoring the degradation of hydrogels formed from multivinyl poly(ethylene glycol) and poly(vinyl alcohol) macromers for cartilage tissue engineering. *Biomacromolecules* **4**, 283-292 (2003).

32. Schmedlen, K.H., Masters, K.S. & West, J.L. Photocrosslinkable polyvinyl alcohol hydrogels that can be modified with cell adhesion peptides for use in tissue engineering. *Biomaterials* **23**, 4325-4332 (2002).

33. Ossipov, D.A. & Hilborn, J. Poly(vinyl alcohol)-based hydrogels formed by "click chemistry". *Macromolecules* **39**, 1709-1718 (2006).

34. Shimizu, S. et al. In vitro studies on a new method for islet microencapsulation using a thermoreversible gelation polymer, n-isopropylacrylamide-based copolymer. *Artif. Organs* **20**, 1232-1237 (1996).

35. Lu, H.F., Targonsky, E.D., Wheeler, M.B. & Cheng, Y.L. Thermally induced gelable polymer networks for living cell encapsulation. *Biotechnol. Bioeng.* **96**, 146-155 (2007).

36. Yasuda, A. et al. In vitro culture of chondrocytes in a novel thermoreversible gelation polymer scaffold containing growth factors. *Tissue Eng.* **12**, 1237-1245 (2006).

37. Barz, M., Luxenhofer, R., Zentel, R. & Vicent, M.J. Overcoming the PEG-addiction: Well-defined alternatives to peg, from structure–property relationships to better defined therapeutics. *Polym. Chem.* (2011).

38. Odian, G.G. Principles of polymerization, Edn. 4th. (Wiley-Interscience, Hoboken, N.J.; 2004).

39. Metters, A.T., Anseth, K.S. & Bowman, C.N. A statistical kinetic model for the bulk degradation of PLA-b-PEG-b-PLA hydrogel networks: Incorporating network non-idealities. *J. Phys. Chem. B* **105**, 8069-8076 (2001).

40. Lin-Gibson, S., Jones, R.L., Washburn, N.R. & Horkay, F. Structure-property relationships of photopolymerizable poly(ethylene glycol) dimethacrylate hydrogels. *Macromolecules* **38**, 2897-2902 (2005).

41. Lin, C.C. & Anseth, K.S. PEG hydrogels for the controlled release of biomolecules in regenerative medicine. *Pharm. Res.* **26**, 631-643 (2009).

42. Anseth, K.S., Bowman, C.N. & BrannonPeppas, L. Mechanical properties of hydrogels and their experimental determination. *Biomaterials* **17**, 1647-1657 (1996).

43. Metters, A.T., Bowman, C.N. & Anseth, K.S. Verification of scaling laws for degrading PLA-b-PEG-b-PLA hydrogels. *Aiche Journal* **47**, 1432-1437 (2001).

44. Mason, M.N., Metters, A.T., Bowman, C.N. & Anseth, K.S. Predicting controlled-release behavior of degradable PLA-b-PEG-b-PLA hydrogels. *Macromolecules* **34**, 4630-4635 (2001).

45. Lutolf, M.P., Raeber, G.P., Zisch, A.H., Tirelli, N. & Hubbell, J.A. Cell-responsive synthetic hydrogels. *Adv. Mater.* **15**, 888-892 (2003).

46. Patch, J.A. & Barron, A.E. Mimicry of bioactive peptides *via* non-natural, sequence-specific peptidomimetic oligomers. *Curr. Opin. Chem. Biol.* **6**, 872-877 (2002).

47. Ruoslahti, E. & Pierschbacher, M.D. New perspectives in cell-adhesion - RGD and integrins. *Science* **238**, 491-497 (1987).

48. Hern, D.L. & Hubbell, J.A. Incorporation of adhesion peptides into nonadhesive hydrogels useful for tissue resurfacing. *Journal of Biomedical Materials Research* **39**, 266-276 (1998).

49. Lutolf, M.P. et al. Synthetic matrix metalloproteinase-sensitive hydrogels for the conduction of tissue regeneration: Engineering cell-invasion characteristics. *Proceedings of the National Academy of Sciences of the United States of America* **100**, 5413-5418 (2003).

50. Lutolf, M.P. & Hubbell, J.A. Synthetic biomaterials as instructive extracellular microenvironments for morphogenesis in tissue engineering. *Nature Biotechnology* **23**, 47-55 (2005).

51. Mann, B.K., Gobin, A.S., Tsai, A.T., Schmedlen, R.H. & West, J.L. Smooth muscle cell growth in photopolymerized hydrogels with cell adhesive and proteolytically degradable domains: Synthetic ecm analogs for tissue engineering. *Biomaterials* **22**, 3045-3051 (2001).

52. Lin, C.C. & Anseth, K.S. Controlling affinity binding with peptide-functionalized poly(ethylene glycol) hydrogels. *Advanced Functional Materials* **19**, 2325-2331 (2009).

53. Lin, C.C., Metters, A.T. & Anseth, K.S. Functional PEG-peptide hydrogels to modulate local inflammation induced by the pro-inflammatory cytokine TNF alpha. *Biomaterials* **30**, 4907-4914 (2009).

54. Tayalia, P. & Mooney, D.J. Controlled growth factor delivery for tissue engineering. *Advanced Materials* **21**, 3269-3285 (2009).

55. Mann, B.K., Schmedlen, R.H. & West, J.L. Tethered-tgf-beta increases extracellular matrix production of vascular smooth muscle cells. *Biomaterials* **22**, 439-444 (2001).

56. Zisch, A.H. et al. Cell-demanded release of VEGF from synthetic, biointeractive cell-ingrowth matrices for vascularized tissue growth. *Faseb Journal* **17**, 2260-2262 (2003).

57. Aimetti, A.A., Tibbitt, M.W. & Anseth, K.S. Human neutrophil elastase responsive delivery from poly(ethylene glycol) hydrogels. *Biomacromolecules* **10**, 1484-1489 (2009).

58. Lee, S.H., Moon, J.J., Miller, J.S. & West, J.L. Poly(ethylene glycol) hydrogels conjugated with a collagenase-sensitive fluorogenic substrate to visualize collagenase activity during three-dimensional cell migration. *Biomaterials* **28**, 3163-3170 (2007).

59. Roberts, M.J., Bentley, M.D. & Harris, J.M. Chemistry for peptide and protein pegylation. *Advanced Drug Delivery Reviews* **54**, 459-476 (2002).

60. Gobin, A.S. & West, J.L. Cell migration through defined, synthetic extracellular matrix analogues. *Faseb Journal* **16**, 751-753 (2002).

61. DeLong, S.A., Moon, J.J. & West, J.L. Covalently immobilized gradients of bFGF on hydrogel scaffolds for directed cell migration. *Biomaterials* **26**, 3227-3234 (2005).

62. Weber, L.M., Hayda, K.N., Haskins, K. & Anseth, K.S. The effects of cell-matrix interactions on encapsulated beta-cell function within hydrogels functionalized with matrix-derived adhesive peptides. *Biomaterials* **28**, 3004-3011 (2007).

63. Salinas, C.N. & Anseth, K.S. Mixed mode thiol-acrylate photopolymerizations for the synthesis of peg-peptide hydrogels. *Macromolecules* **41**, 6019-6026 (2008).

64. Lutolf, M.P., Tirelli, N., Cerritelli, S., Cavalli, L. & Hubbell, J.A. Systematic modulation of michael-type reactivity of thiols through the use of charged amino acids. *Bioconjug. Chem.* **12**, 1051-1056 (2001).

65. Park, Y., Lutolf, M.P., Hubbell, J.A., Hunziker, E.B. & Wong, M. Bovine primary chondrocyte culture in synthetic matrix metalloproteinase-sensitive poly(ethylene glycol)-based hydrogels as a scaffold for cartilage repair. *Tissue Eng.* **10**, 515-522 (2004).

66. Miller, J.S. et al. Bioactive hydrogels made from step-growth derived peg-peptide macromers. *Biomaterials* (2010).

67. Fairbanks, B.D. et al. A versatile synthetic extracellular matrix mimic *via* thiol-norbornene photopolymerization. *Adv. Mater.* **21**, 5005-5010 (2009).

68. Hoffmann, J.C. & West, J.L. Three-dimensional photolithographic patterning of multiple bioactive ligands in poly(ethylene glycol) hydrogels. *Soft Matter* **6**, 5056-5063 (2010).

69. Lee, S.H., Moon, J.J. & West, J.L. Three-dimensional micropatterning of bioactive hydrogels *via* two-photon laser scanning photolithography for guided 3d cell migration. *Biomaterials* **29**, 2962-2968 (2008).

70. Luo, Y. & Shoichet, M.S. A photolabile hydrogel for guided three-dimensional cell growth and migration. *Nat. Mater.* **3**, 249-253 (2004).

71. Hahn, M.S., Miller, J.S. & West, J.L. Three-dimensional biochemical and biomechanical patterning of hydrogels for guiding cell behavior. *Adv. Mater.* **18**, 2679-2684 (2006).

72. Wosnick, J.H. & Shoichet, M.S. Three-dimensional chemical patterning of transparent hydrogels. *Chem. Mater.* **20**, 55-60 (2008).

73. Engler, A.J., Sweeney, H.L. & Discher, D.E. Substrate elasticity alters human mesenchymal stem cell differentiation. *Biophys. J.* **88**, 500A-500A (2005).

74. Engler, A.J., Sen, S., Sweeney, H.L. & Discher, D.E. Matrix elasticity directs stem cell lineage specification. *Cell* **126**, 677-689 (2006).

75. Tse, J.R. & Engler, A.J. Stiffness gradients mimicking in vivo tissue variation regulate mesenchymal stem cell fate. *PLoS ONE* **6** (2011).

76. Huebsch, N. et al. Harnessing traction-mediated manipulation of the cell/matrix interface to control stem-cell fate. *Nat. Mater.* **9**, 518-526 (2010).

77. Singhvi, R. et al. Engineering cell-shape and function. *Science* **264**, 696-698 (1994).

78. Chen, C.S., Mrksich, M., Huang, S., Whitesides, G.M. & Ingber, D.E. Geometric control of cell life and death. *Science* **276**, 1425-1428 (1997).

79. Mammoto, A., Huang, S., Moore, K., Oh, P. & Ingber, D.E. Role of RhoA, mDia, and ROCK in cell shape-dependent control of the Skp2-p27(kip1) pathway and the G1/S transition. *J. Biol. Chem.* **279**, 26323-26330 (2004).

80. Kloxin, A.M., Kloxin, C.J., Bowman, C.N. & Anseth, K.S. Mechanical properties of cellularly responsive hydrogels and their experimental determination. *Adv. Mater.* **22**, 3484-3494 (2010).

81. Ingber, D.E. Mechanobiology and diseases of mechanotransduction. *Ann. Med.* **35**, 564-577 (2003).

82. Ingber, D.E. Cellular mechanotransduction: Putting all the pieces together again. *FASEB J.* **20**, 811-827 (2006).

83. Young, J.L. & Engler, A.J. Hydrogels with time-dependent material properties enhance cardiomyocyte differentiation in vitro. *Biomaterials* **32**, 1002-1009 (2011).

84. Nowatzki, P.J., Franck, C., Maskarinec, S.A., Ravichandran, G. & Tirrell, D.A. Mechanically tunable thin films of photosensitive artificial proteins: Preparation and characterization by nanoindentation. *Macromolecules* **41**, 1839-1845 (2008).

85. Khetan, S., Katz, J.S. & Burdick, J.A. Sequential crosslinking to control cellular spreading in 3-dimensional hydrogels. *Soft Matter* **5**, 1601-1606 (2009).

86. Khetan, S. & Burdick, J.A. Patterning network structure to spatially control cellular remodeling and stem cell fate within 3-dimensional hydrogels. *Biomaterials* **31**, 8228-8234 (2010).

87. Kloxin, A.M., Kasko, A.M., Salinas, C.N. & Anseth, K.S. Photodegradable hydrogels for dynamic tuning of physical and chemical properties. *Science* **324**, 59-63 (2009).

88. Kloxin, A.M., Benton, J.A. & Anseth, K.S. In situ elasticity modulation with dynamic substrates to direct cell phenotype. *Biomaterials* **31**, 1-8 (2010).

89. Metters, A.T., Anseth, K.S. & Bowman, C.N. Fundamental studies of a novel, biodegradable peg-b-pla hydrogel. *Polymer* **41**, 3993-4004 (2000).

90. Anseth, K.S. et al. In situ forming degradable networks and their application in tissue engineering and drug delivery. *J. Control. Release* **78**, 199-209 (2002).

91. Rydholm, A.E., Reddy, S.K., Anseth, K.S. & Bowman, C.N. Controlling network structure in degradable thiol-acrylate biomaterials to tune mass loss behavior. *Biomacromolecules* **7**, 2827-2836 (2006).

92. Bryant, S.J. & Anseth, K.S. Controlling the spatial distribution of ECM components in degradable PEG hydrogels for tissue engineering cartilage. *J. Biomed. Mater. Res. A* **64A**, 70-79 (2003).

93. Benoit, D.S.W., Durney, A.R. & Anseth, K.S. Manipulations in hydrogel degradation behavior enhance osteoblast function and mineralized tissue formation. *Tissue Eng.* **12**, 1663-1673 (2006).

94. Mahoney, M.J. & Anseth, K.S. Three-dimensional growth and function of neural tissue in degradable polyethylene glycol hydrogels. *Biomaterials* **27**, 2265-2274 (2006).

95. West, J.L. & Hubbell, J.A. Polymeric biomaterials with degradation sites for proteases involved in cell migration. *Macromolecules* **32**, 241-244 (1999).

96. Gobin, A.S. & West, J.L. Cell migration through defined, synthetic extracellular matrix analogues. *FASEB J.* **16**, 751-753 (2002).

97. Lutolf, M.P. et al. Biomimetic peg hydrogels crosslinked with minimal plasmin-sensitive tri-amino acid peptides. *J. Biomed. Mater. Res. A* **93A**, 870-877 (2010).

98. Patterson, J. & Hubbell, J.A. Enhanced proteolytic degradation of molecularly engineered PEG hydrogels in response to MMP-1 and MMP-2. *Biomaterials* **31**, 7836-7845 (2010).

99. Patterson, J. & Hubbell, J.A. Sparc-derived protease substrates to enhance the plasmin sensitivity of molecularly engineered PEG hydrogels. *Biomaterials* **32**, 1301-1310 (2011).

100. Nagase, H. & Fields, G.B. Human matrix metalloproteinase specificity studies using collagen sequence-based synthetic peptides. *Biopolymers* **40**, 399-416 (1996).

101. Rice, M.A., Sanchez-Adams, J. & Anseth, K.S. Exogenously triggered, enzymatic degradation of photopolymerized hydrogels with polycaprolactone subunits: Experimental observation and modeling of mass loss behavior. *Biomacromolecules* **7**, 1968-1975 (2006).

102. Sarig-Nadir, O., Livnat, N., Zajdman, R., Shoham, S. & Seliktar, D. Laser photoablation of guidance microchannels into hydrogels directs cell growth in three dimensions. *Biophys. J.* **96**, 4743-4752 (2009).

103. Andreopoulos, F.M. et al. Photoscissable hydrogel synthesis *via* rapid photopolymerization of novel peg-based polymers in the absence of photoinitiators. *J. Am. Chem. Soc.* **118**, 6235-6240 (1996).

104. Zheng, Y.J. et al. Peg-based hydrogel synthesis *via* the photodimerization of anthracene groups. *Macromolecules* **35**, 5228-5234 (2002).

105. Kloxin, A.M., Tibbitt, M.W. & Anseth, K.S. Synthesis of photodegradable hydrogels as dynamically tunable cell culture platforms. *Nat. Protoc.* **5**, 1867-1887 (2010).

106. Johnson, J.A., Finn, M.G., Koberstein, J.T. & Turro, N.J. Synthesis of photocleavable linear macromonomers by atrp and star macromonomers by a tandem ATRP-click reaction: Precursors to photodegradable model networks. *Macromolecules* **40**, 3589-3598 (2007).

107. Johnson, J.A., Baskin, J.M., Bertozzi, C.R., Koberstein, J.T. & Turro, N.J. Copper-free click chemistry for the in situ crosslinking of photodegradable star polymers. *Chem. Commun.*, 3064-3066 (2008).

108. Wong, D.Y., Griffin, D.R., Reed, J. & Kasko, A.M. Photodegradable hydrogels to generate positive and negative features over multiple length scales. *Macromolecules* **43**, 2824-2831 (2010).

109. Frey, M.T. & Wang, Y.L. A photo-modulatable material for probing cellular responses to substrate rigidity. *Soft Matter* **5**, 1918-1924 (2009).

110. Kloxin, A.M., Tibbitt, M.W., Kasko, A.M., Fairbairn, J.A. & Anseth, K.S. Tunable hydrogels for external manipulation of cellular microenvironments through controlled photodegradation. *Adv. Mater.* **22**, 61-66 (2010).

111. Tibbitt, M.W., Kloxin, A.M., Dyamenahalli, K.U. & Anseth, K.S. Controlled two-photon photodegradation of PEG hydrogels to study and manipulate subcellular interactions on soft materials. *Soft Matter* **6**, 5100-5108 (2010).

112. Kloxin, C.J., Scott, T.F., Adzima, B.J. & Bowman, C.N. Covalent adaptable networks (CANs): A unique paradigm in cross-linked polymers. *Macromolecules* **43**, 2643-2653 (2010).

113. Adzima, B.J., Aguirre, H.A., Kloxin, C.J., Scott, T.F. & Bowman, C.N. Rheological and chemical analysis of reverse gelation in a covalently crosslinked diels-alder polymer network. *Macromolecules* **41**, 9112-9117 (2008).

114. Scott, T.F., Schneider, A.D., Cook, W.D. & Bowman, C.N. Photoinduced plasticity in cross-linked polymers. *Science* **308**, 1615-1617 (2005).

115. Scott, T.F., Draughon, R.B. & Bowman, C.N. Actuation in crosslinked polymers *via* photoinduced stress relaxation. *Adv. Mater.* **18**, 2128-2132 (2006).

116. Kloxin, C.J., Scott, T.F. & Bowman, C.N. Stress relaxation *via* addition-fragmentation chain transfer in a thiol-ene photopolymerization. *Macromolecules* **42**, 2551-2556 (2009).

117. Fairbanks, B.D., Singh, S.P., Bowman, C.N. & Anseth, K.S. Photodegradable, photoadaptable hydrogels *via* radical-mediated disulfide fragmentation reaction. *Macromolecules* **44**, 2444-2450 (2011).

118. Kolb, H.C., Finn, M.G. & Sharpless, K.B. Click chemistry: Diverse chemical function from a few good reactions. *Angew. Chem. Int. Ed. Engl.* **40**, 2004-2021 (2001).

119. Kolb, H.C. & Sharpless, K.B. The growing impact of click chemistry on drug discovery. *Drug Discov. Today* **8**, 1128-1137 (2003).

120. Hawker, C.J. & Wooley, K.L. The convergence of synthetic organic and polymer chemistries. *Science* **309**, 1200-1205 (2005).

121. Sletten, E.M. & Bertozzi, C.R. Bioorthogonal chemistry: Fishing for selectivity in a sea of functionality. *Angew. Chem. Int. Ed. Engl.* **48**, 6974-6998 (2009).

122. Huisgen, R. 1.3-dipolare cycloadditionen - ruckschau und ausblick. *Angew. Chem. Int. Ed. Engl.* **75**, 604-637 (1963).

123. Rostovtsev, V.V., Green, L.G., Fokin, V.V. & Sharpless, K.B. A stepwise huisgen cycloaddition process: Copper(I)-catalyzed regioselective "ligation" of azides and terminal alkynes. *Angew. Chem. Int. Ed. Engl.* **41**, 2596-2599 (2002).

124. Tornoe, C.W., Christensen, C. & Meldal, M. Peptidotriazoles on solid phase: [1,2,3]-triazoles by regiospecific copper(I)-catalyzed 1,3-dipolar cycloadditions of terminal alkynes to azides. *J. Org. Chem.* **67**, 3057-3064 (2002).

125. Himo, F. et al. Copper(i)-catalyzed synthesis of azoles. Dft study predicts unprecedented reactivity and intermediates. *J. Am. Chem. Soc.* **127**, 210-216 (2005).

126. Franke, R., Doll, C. & Eichler, J. Peptide ligation through click chemistry for the generation of assembled and scaffolded peptides. *Tetrahedron Lett.* **46**, 4479-4482 (2005).

127. Moses, J.E. & Moorhouse, A.D. The growing applications of click chemistry. *Chem. Soc. Rev.* **36**, 1249-1262 (2007).

128. Binder, W.H. & Sachsenhofer, R. 'Click' chemistry in polymer and materials science. *Macromol. Rapid Commun.* **28**, 15-54 (2007).

129. Bock, V.D., Perciaccante, R., Jansen, T.P., Hiemstra, H. & van Maarseveen, J.H. Click chemistry as a route to cyclic tetrapeptide analogues: Synthesis of cyclo-[pro-val-psi(triazole)-pro-tyr]. *Org. Lett.* **8**, 919-922 (2006).

130. Jagasia, R., Holub, J.M., Bollinger, M., Kirshenbaum, K. & Finn, M.G. Peptide cyclization and cyclodimerization by cu-i-mediated azide-alkyne cycloaddition. *J. Org. Chem.* **74**, 2964-2974 (2009).

131. Franc, G. & Kakkar, A. Dendrimer design using cu-i-catalyzed alkyne-azide "click-chemistry". *Chem. Commun.*, 5267-5276 (2008).

132. Joralemon, M.J. et al. Dendrimers clicked together divergently. *Macromolecules* **38**, 5436-5443 (2005).

133. Evans, R.A. The rise of azide-alkyne 1,3-dipolar 'click' cycloaddition and its application to polymer science and surface modification. *Aust. J. Chem.* **60**, 384-395 (2007).

134. Parrish, B., Breitenkamp, R.B. & Emrick, T. PEG- and peptide-grafted aliphatic polyesters by click chemistry. *J. Am. Chem. Soc.* **127**, 7404-7410 (2005).

135. Engler, A.C., Lee, H.I. & Hammond, P.T. Highly efficient "grafting onto" a polypeptide backbone using click chemistry. *Angew. Chem. Int. Ed. Engl.* **48**, 9334-9338 (2009).

136. Agard, N.J., Prescher, J.A. & Bertozzi, C.R. A strain-promoted [3 + 2] azide-alkyne cycloaddition for covalent modification of biomolecules in living systems. *J. Am. Chem. Soc.* **126**, 15046-15047 (2004).

137. Laughlin, S.T., Baskin, J.M., Amacher, S.L. & Bertozzi, C.R. In vivo imaging of membrane-associated glycans in developing zebrafish. *Science* **320**, 664-667 (2008).

138. Baskin, J.M. et al. Copper-free click chemistry for dynamic in vivo imaging. *Proc. Natl. Acad. Sci. U. S. A.* **104**, 16793-16797 (2007).

139. Codelli, J.A., Baskin, J.M., Agard, N.J. & Berozzi, C.R. Second-generation difluorinated cyclooctynes for copper-free click chemistry. *J. Am. Chem. Soc.* **130**, 11486-11493 (2008).

140. Chang, P.V. et al. Copper-free click chemistry in living animals. *Proc. Natl. Acad. Sci. U. S. A.* **107**, 1821-1826 (2010).

141. Agard, N.J., Baskin, J.M., Prescher, J.A., Lo, A. & Bertozzi, C.R. A comparative study of bioorthogonal reactions with azides. *ACS Chem. Biol.* **1**, 644-648 (2006).

142. Ning, X.H., Guo, J., Wolfert, M.A. & Boons, G.J. Visualizing metabolically labeled glycoconjugates of living cells by copper-free and fast huisgen cycloadditions. *Angew. Chem. Int. Ed. Engl.* **47**, 2253-2255 (2008).

143. Debets, M.F. et al. Aza-dibenzocyclooctynes for fast and efficient enzyme pegylation *via* copper-free (3+2) cycloaddition. *Chem. Commun.* **46**, 97-99 (2010).

144. Jewett, J.C., Sletten, E.M. & Bertozzi, C.R. Rapid Cu-free click chemistry with readily synthesized biarylazacyclooctynones. *J. Am. Chem. Soc.* **132**, 3688-3690 (2010).

145. Dommerholt, J. et al. Readily accessible bicyclononynes for bioorthogonal labeling and three-dimensional imaging of living cells. *Angew. Chem. Int. Ed. Engl.* **49**, 9422-9425 (2010).

146. Hoyle, C.E., Lee, T.Y. & Roper, T. Thiol-enes: Chemistry of the past with promise for the future. *J. Polym. Sci., Part A: Polym. Chem.* **42**, 5301-5338 (2004).

147. Hoyle, C.E. & Bowman, C.N. Thiol-ene click chemistry. *Angew. Chem. Int. Ed. Engl.* **49**, 1540-1573 (2010).

148. Kade, M.J., Burke, D.J. & Hawker, C.J. The power of thiol-ene chemistry. *J. Polym. Sci., Part A: Polym. Chem.* **48**, 743-750 (2010).

149. Cramer, N.B., Reddy, S.K., O'Brien, A.K. & Bowman, C.N. Thiol-ene photopolymerization mechanism and rate limiting step changes for various vinyl functional group chemistries. *Macromolecules* **36**, 7964-7969 (2003).

150. Uygun, M., Tasdelen, M.A. & Yagci, Y. Influence of type of initiation on thiol-ene "click" chemistry. *Macromol. Chem. Phys.* **211**, 103-110 (2010).

151. Boyer, C. & Davis, T.P. One-pot synthesis and biofunctionalization of glycopolymers *via* raft polymerization and thiol-ene reactions. *Chem. Commun.*, 6029-6031 (2009).

152. Campos, L.M. et al. Development of thermal and photochemical strategies for thiol-ene click polymer functionalization. *Macromolecules* **41**, 7063-7070 (2008).

153. Hayashi, K. et al. One-pot biofunctionalization of magnetic nanoparticles *via* thiol-ene click reaction for magnetic hyperthermia and magnetic resonance imaging. *Chem. Mater.* **22**, 3768-3772 (2010).

154. Boyer, C., Bulmus, V. & Davis, T.P. Efficient usage of thiocarbonates for both the production and the biofunctionalization of polymers. *Macromol. Rapid Commun.* **30**, 493-497 (2009).

155. Killops, K.L., Campos, L.M. & Hawker, C.J. Robust, efficient, and orthogonal synthesis of dendrimers *via* thiol-ene "click" chemistry. *J. Am. Chem. Soc.* **130**, 5062-5064 (2008).

156. Nilsson, C., Simpson, N., Malkoch, M., Johansson, M. & Malmstrom, E. Synthesis and thiol-ene photopolymerization of allyl-ether functionalized dendrimers. *J. Polym. Sci., Part A: Polym. Chem.* **46**, 1339-1348 (2008).

157. Franc, G. & Kakkar, A.K. "Click" methodologies: Efficient, simple and greener routes to design dendrimers. *Chem. Soc. Rev.* **39**, 1536-1544 (2010).

158. Jonkheijm, P. et al. Photochemical surface patterning by the thiol-ene reaction. *Angew. Chem. Int. Ed. Engl.* **47**, 4421-4424 (2008).

159. Harant, A.W., Khire, V.S., Thibodaux, M.S. & Bowman, C.N. Thiol-ene photopolymer grafts on functionalized glass and silicon surfaces. *Macromolecules* **39**, 1461-1466 (2006).

160. Khire, V.S., Yi, Y., Clark, N.A. & Bowman, C.N. Formation and surface modification of nanopatterned thiol-ene substrates using step and flash imprint lithography. *Adv. Mater.* **20**, 3308-3313 (2008).

161. Weinrich, D. et al. Oriented immobilization of farnesylated proteins by the thiol-ene reaction. *Angew. Chem. Int. Ed. Engl.* **49**, 1252-1257 (2010).

162. Cramer, N.B. & Bowman, C.N. Kinetics of thiol-ene and thiol-acrylate photopolymerizations with real-time fourier transform infrared. *J. Polym. Sci., Part A: Polym. Chem.* **39**, 3311-3319 (2001).

163. van Dijk, M., Rijkers, D.T.S., Liskamp, R.M.J., van Nostrum, C.F. & Hennink, W.E. Synthesis and applications of biomedical and pharmaceutical polymers *via* click chemistry methodologies. *Bioconjug. Chem.* **20**, 2001-2016 (2009).

164. Chiou, B.S. & Khan, S.A. Real-time ftir and in situ rheological studies on the uv curing kinetics of thiol-ene polymers. *Macromolecules* **30**, 7322-7328 (1997).

165. Wei, H.Y., Senyurt, A.F., Jonsson, S. & Hoyle, C.E. Photopolymerization of ternary thiol-ene/acrylate systems: Film and network properties. *J. Polym. Sci., Part A: Polym. Chem.* **45**, 822-829 (2007).

166. Alvarez, M. et al. Single-photon and two-photon induced photocleavage for monolayers of an alkyltriethoxysilane with a photoprotected carboxylic ester. *Adv. Mater.* **20**, 4563-4567 (2008).

167. Wu, Y.I. et al. A genetically encoded photoactivatable Rac controls the motility of living cells. *Nature* **461**, 104-U111 (2009).

168. Deiters, A. Principles and applications of the photochemical control of cellular processes. *Chembiochem* **11**, 47-53 (2010).

169. Holmes, C.P. Model studies for new o-nitrobenzyl photolabile linkers: Substituent effects on the rates of photochemical cleavage. *J. Org. Chem.* **62**, 2370-2380 (1997).

170. Whitehouse, D.L., Savinov, S.N. & Austin, D.J. An improved synthesis and selective coupling of a hydroxy based photolabile linker for solid phase organic synthesis. *Tetrahedron Lett.* **38**, 7851-7852 (1997).

171. Holmes, C.P. & Jones, D.G. Reagents for combinatorial organic-synthesis - development of a new o-nitrobenzyl photolabile linker for solid-phase synthesis. *J. Org. Chem.* **60**, 2318-2319 (1995).

172. Ohmuro-Matsuyama, Y. & Tatsu, Y. Photocontrolled cell adhesion on a surface functionalized with a caged arginine-glycine-aspartate peptide. *Angew. Chem. Int. Ed. Engl.* **47**, 7527-7529 (2008).

173. Kaneko, S. et al. Photocontrol of cell adhesion on amino-bearing surfaces by reversible conjugation of poly(ethylene glycol) *via* a photocleavable linker. *Phys. Chem. Chem. Phys.* **13**, 4051-4059 (2011).

174. Zhao, Y. et al. New caged coumarin fluorophores with extraordinary uncaging cross sections suitable for biological imaging applications. *J. Am. Chem. Soc.* **126**, 4653-4663 (2004).

CHAPTER II

THESIS OBJECTIVES

2.1 Overview

Polymer-based hydrogels have emerged as a unique class of biomaterials that enable cells to be cultured in three-dimensions (3D) within a user-defined synthetic microenvironment[1-3]. Based on the specific hydrogel formulation, material properties of the constructs can be defined precisely to impart different moduli, chemical moieties, porosity, adhesivity, degradability, and stimuli-responsiveness over a wide range of nano-, micro-, and macroscopic scales. By tuning the initial properties of these networks, cells have been engineered to proliferate within, migrate through, and undergo differentiation inside these materials *via* the incorporation of physiologically-relevant cues. While hydrogels enable a high degree of functional tunability over the fate of encapsulated cells, it is often difficult to know the specific effects of an included signal on a cell's biological function, owing to the difficulty of monitoring and quantifying these abundant, spatially-complex, ever-evolving cues that are found *in vivo*. A major goal of this thesis work is the development of hydrogel platforms whose biochemical and biophysical characteristics are dynamically modifiable in real time to allow the capture of new information regarding basic cell function that can be ascertained through temporal/kinetic studies. Such an understanding of how cells receive information from their external environment may provide

improved insight into the engineering of scaffold systems to promote the creation of functional tissue substitutes.

Toward these concepts, the aims of this thesis focus on the synthesis of cytocompatible click-based hydrogel networks formed *via* a step-growth polymerization between multifunctional macromolecular precursors containing orthogonal chemical functionalities that undergo specific, user-defined reactions on demand. We hypothesize that the chemical and mechanical properties of these hydrogel systems can be exogenously tuned in both time and space through the incorporation of pendant photoreactive groups, as well as photolabile linkers within the polymer network, allowing for the real-time detection (*e.g.*, enzymatic activity) and direction of individual cell function (*e.g.*, migration, adhesion, outgrowth) in 3D. Subsequently, these photopatternable gels can be utilized to examine the effects of dynamic biochemical and biomechanical alterations in the material environment on cell function, including how temporal adhesive ligand presentation and pericellular mechanics affect integrin binding, focal adhesion formation, and cytoskeletal organization.

To illustrate the phototunability of hydrogel properties to direct cell behavior, the specific aims of this research are to:

1) Synthesize and characterize a peptide-functionalized poly(ethylene glycol) (PEG)-based hydrogel platform using strain-promoted azide-alkyne cycloaddition (SPAAC) click chemistry, and demonstrate cytocompatible spatial and temporal presentation of *biochemical* cues in discrete and gradient 2D and 3D patterns using an orthogonal thiol-ene photoconjugation reaction,

2) Expand the SPAAC-based, biochemically-tunable hydrogel platform to enable independent alteration of *biomechanical* properties of the network using an orthogonally-controlled photodegradable mechanism in real time and in the presence of cells,

3) Utilize the developed orthogonal initiation conditions for photocoupling and photodegradation reactions to introduce *reversibly* physiologically-relevant, biochemical cues,

4) Use the above material systems to detect encapsulated cell enzymatic activity and direct cell adhesion, motility, and outgrowth in response to biophysically- and biochemically-patterned hydrogels.

To enable biologically-relevant assessment of 3D cell function, it is vital that the culture platform adequately captures many critical aspects of the native extracellular matrix, including the spatial and temporal presentation of a variety of chemical and physical cues[4,5]. Towards this objective, the experiments in this thesis introduce a new type of chemical reaction for the formation of biomaterials based on the copper-free strain-promoted addition of an alkyne to an azide[6] (Objective 1, Chapter III and IV). As this reaction proceeds orthogonally to the other chemical moieties found in biological systems[7], including those found on proteins, cell surfaces, and in culture media, the ability to form idealized click-based biomaterial in the presence of cells is examined, and the ideality of the network formation is investigated by magic angle spinning ^{1}H-NMR and the measurement and comparison of observed moduli and network swelling for a variety of formulations to those that are predicted. Subsequently, the high selectivity of the gel formation reaction is exploited to introduce additional functional groups, including those that are photochemically active, uniformly within the material. By creating networks that contain a homogenous population of vinyl functionalities, the ability of these moieties to serve as anchor

points in the patterning of pendant biochemical cues, including cysteine-containing peptides, within the network *via* the thiol-ene photoconjugation reaction is characterized[8]. By patterning in fluorescently-labeled peptides, the degree of network bio-functionalization is studied by comparing local fluorescence intensity to that of known standard concentrations. The goal is to use light-based chemistry to enable full 4D control over the biochemical aspects of the network in time and space.

Just as biochemical cues have been implicated as crucial signals in the dictation of cell function, the mechanics of the surrounding material are also responsible for directing cell fate. By introducing a photodegradable nitrobenzyl ether moiety in the hydrogel backbone[9,10], we then study how material physical properties can be controlled by locally photocleaving chemical crosslinks (*e.g.*, a decreased network moduli or full gel degradation) and characterizing these changes with profilometry and fluorescence microscopy (Objective 2, Chapter V). The kinetics of photocleavage are examined with ^{1}H-NMR. Additionally, a broad range of light conditions are examined to identify specific conditions that enable the photodegradation and thiol-ene photoconjugation reactions to be independently controlled within the same system. This orthogonality is characterized using both ^{1}H-NMR and fluorescence and bright-field microscopy-based techniques. Through this approach, we aim to develop hydrogel systems that permit independent and spatiotemporal manipulation over both physical and chemical properties in a cytocompatible manner.

While the introduction of biologically-relevant signals in time and space is vital towards understanding of isolated effects on single cell function, these cues are generally presented in a dynamic manner *in vivo*[11]. To adequately recapitulate a cell's native, temporally-variable microenvironment, cues must be first introduced and subsequently removed with a high level of

fidelity and often in a spatially-controlled manner. As a proof of principle, we synthesize a peptide that contains both the photolabile nitrobenzyl ether and the photocouplable thiol components. Studies focus on controlling cell-material interactions and cell motility by introducing and removing the RGD epitope, a well-known integrin binding adhesive ligand. We study the introduction and patterning of RGD using visible light into and then removal with UV light from a user-defined volume within SPAAC hydrogels by photolithographic- and multiphoton-based techniques. The goal is to demonstrate how covalently-immobilized, biochemical cues can be presented to cells in a reversible manner and for complex, well-defined, biomolecular gradients over millimolar ranges and centimeter distances to be formed within the gel (Objective 3, Chapter VI).

As each of these utilized chemistries (i.e., SPAAC, thiol-ene photoconjugation, and photodegradation) is fully cytocompatible, the developed biomaterial systems can be formed and modified in the presence of cells. In addition, depending on how the hydrogel composition is altered spatially, cell function can be both detected as well as directed within user-defined regions of the material (Objective 4). Local enzymatic activity is monitored *via* the patterned incorporation of a self-quenched fluorescent, collagenase-sensitive peptide (Chapter III). Additionally, cell motility of encapsulated cells is controlled both isotropically (Chapter III), as well radially down chemically-functionalized, physical channels (Chapter V). Dynamic cell adhesion is further controlled on the surface of these click-based biomaterials by the reversible presentation of an adhesive ligand (Chapter VI). Finally, the broader implications of these studies are discussed and future directions for the work are put forth (Chapter VII).

2.2 References

1. Peppas, N.A., Hilt, J.Z., Khademhosseini, A. & Langer, R. Hydrogels in biology and medicine: From molecular principles to bionanotechnology. *Adv. Mater.* **18**, 1345-1360 (2006).

2. Peppas, N.A. & Langer, R. New challenges in biomaterials. *Science* **263**, 1715-1720 (1994).

3. Langer, R. & Vacanti, J.P. Tissue engineering. *Science* **260**, 920-926 (1993).

4. Tibbitt, M.W. & Anseth, K.S. Hydrogels as extracellular matrix mimics for 3D cell culture. *Biotechnol. Bioeng.* **103**, 655-663 (2009).

5. Cushing, M.C. & Anseth, K.S. Hydrogel cell cultures. *Science* **316**, 1133-1134 (2007).

6. Codelli, J.A., Baskin, J.M., Agard, N.J. & Berozzi, C.R. Second-generation difluorinated cyclooctynes for copper-free click chemistry. *J. Am. Chem. Soc.* **130**, 11486-11493 (2008).

7. Sletten, E.M. & Bertozzi, C.R. Bioorthogonal chemistry: Fishing for selectivity in a sea of functionality. *Angew. Chem. Int. Ed. Engl.* **48**, 6974-6998 (2009).

8. Hoyle, C.E. & Bowman, C.N. Thiol-ene click chemistry. *Angew. Chem. Int. Ed. Engl.* **49**, 1540-1573 (2010).

9. Holmes, C.P. Model studies for new o-nitrobenzyl photolabile linkers: Substituent effects on the rates of photochemical cleavage. *J. Org. Chem.* **62**, 2370-2380 (1997).

10. Kloxin, A.M., Kasko, A.M., Salinas, C.N. & Anseth, K.S. Photodegradable hydrogels for dynamic tuning of physical and chemical properties. *Science* **324**, 59-63 (2009).

11. Alberts, B. et al. Molecular biology of the cell, Edn. 5th. (Garland Science, New York; 2008).

CHAPTER III

SEQUENTIAL CLICK REACTIONS FOR SYNTHESIZING AND PATTERNING 3D CELL MICROENVIRONMENTS

As published in *Nature Materials*, 8, 659-664 (2009).

3.1 Abstract

Click chemistry provides extremely selective and orthogonal reactions that proceed with high efficiency and under a variety of mild conditions, the most common example being the copper(I)-catalyzed reaction of azides with alkynes[1,2]. While the versatility of click reactions has been broadly exploited[3-5], a major limitation is the intrinsic toxicity of the synthetic schemes and the inability to translate these approaches to biological applications. This manuscript introduces a robust synthetic strategy where macromolecular precursors react *via* a copper-free click chemistry[6], allowing for the direct encapsulation of cells within click hydrogels for the first time. Subsequently, an orthogonal thiol-ene photocoupling chemistry is introduced that enables patterning of biological functionalities within the gel in real-time and with micron-scale resolution. This material system allows one to tailor independently the biophysical and biochemical properties of the cell culture microenvironments *in situ*. This synthetic approach uniquely allows for the direct fabrication of biologically functionalized gels with ideal structures that can be photopatterned and all in the presence of cells.

3.2 Introduction

An emerging paradigm in organic synthesis is a focus on highly selective and orthogonal reactions that proceed with high efficiency and under a variety of mild conditions. A growing number of these reactions are grouped under the term "click chemistry," which have been used to produce a catalog of functional synthetic molecules and subsequent materials[1,4]. Characteristics of modular click reactions include: (a) high yields with fast kinetics, (b) regiospecificity and stereospecificity, (c) insensitivity to oxygen or water, and (d) mild, solventless reaction conditions or in water.

While the versatility of click reactions has been broadly exploited in many fields including drug discovery[7,8], material science[9-11], and bioconjugation[3,12,13], a major limitation is the intrinsic toxicity of the synthetic schemes and the inability to translate these approaches to biological applications. Though the 1,3-dipolar Huisgen cycloaddition between azides and alkynes[2] is often seen as the quintessential click reaction, the crucial copper catalyst precludes its usage with biological systems[14,15]. This drawback, however, was recently circumvented *via* the development of novel cyclooctyne moieties whose ring strain and electron-withdrawing fluorine substituents give rise to an activated alkyne. This molecule has been shown to react quickly with azides in the absence of a metal catalyst, enabling the usage of traditional click chemistry in living systems[6,16]. Specifically, azide-labeled cell-surface glycans were reacted with fluorescently-labeled cyclooctynes *in vivo* to enable the visualization of dynamic subcellular development within zebrafish embryos[17]. Though this chemistry has been exploited in the labeling of biomolecules, it has not yet been utilized for biomaterial formation.

More recently, the radical-mediated addition of a thiol to an alkene known as the thiol-ene reaction has gained attention as an emerging click reaction[18]. In addition to being bio-

orthogonal and biocompatible, the reaction is advantageous in that it is readily initiated with light, ultimately affording spatial and temporal control over where the reaction occurs.[19] This reaction has been utilized to create 2D surface gradients of biomolecules[20] as well complex materials[21].

In alignment with the evolution of click chemistry, the combined utilization of multiple orthogonal reactions presents the opportunity to fabricate multifunctional and tunable materials without sacrificing synthetic simplicity or efficiency. While materials with highly defined structures have applications in microelectronics, membrane technology, and fuel cells, one increasingly important area of research is in developing biomaterial platforms that allow researchers to culture and study cells in 3D[22]. Though initial material development has proven successful at *permitting* cell growth, a growing topic of interest is the development of bioactive materials that *promote* and *detect* specific cell function *via* spatially-presented biochemical and biomechanical cues[23]. Ultimately, a platform offering such versatility would be of particular note to those interested in well-defined niches for 3D cell culture, understanding the role of biomechanical versus biochemical signals on cell function, as well as regenerating tissue structures[24]. Appropriately developed click chemistry can provide this versatility, enabling the fabrication of increasingly complex 3D culture constructs using just a few simple reactions.

3.3 Results and Discussion

Here, a hydrogel platform is introduced that utilizes two orthogonal click chemistries; one for hydrogel formation and another for biochemical patterning within the preformed material. The modular aspect of these reactions allows for independent control of the network structure and chemistry, and facile incorporation of biological epitopes. Network formation is accomplished using a recently developed Cu-free variant to the traditional click reaction, the

Huisgen cycloaddition, between an azide (-N_3) and an alkyne (-C≡C-) to form a triazole[6]. This method employs a di-fluorinated cyclooctyne moiety (DIFO3), whose ring strain and electron-withdrawing fluorine substituents promote the [3+2] dipolar cycloaddition with azides without the use of a catalyst[25] (Figure 3.1a). This reaction has been carried out under physiological conditions in the presence of living cells with no reported toxicity[17]. Beyond this bioconjugation approach for cell labeling, multifunctional macromolecular monomers were synthesized to create ideal network structures with minimal defects and local heterogeneties. Specifically, multifunctional azides and activated alkynes were reacted in a one-to-one fashion to yield end-linked polymer gels, under reaction conditions that enable cell encapsulation and result in gels with initially uniform material properties.

A four-arm poly(ethylene glycol) (PEG) tetraazide was reacted with bis(DIFO3) di-functionalized polypeptide in an aqueous environment at 37 °C (schematic shown in Figure 3.1a). The choice of PEG allows one to tailor readily the biophysical properties of the gel, while eliminating non-specific interactions that often result when proteins adsorb to materials. Biological functionality can be readily introduced into the hydrogel backbone by the choice of the crosslinking peptide sequence. Here, a matrix metalloproteinase (MMP)-cleavable (GPQG↓ILGQ) is selected, so that cells can actively remodel their surroundings *via* secreted enzymes[26]. Cells encapsulated in hydrogels containing an enzymatically-degradable crosslinker sequence spread and migrate throughout the material with dramatically increased viability compared with non-degradable alternatives[27,28].

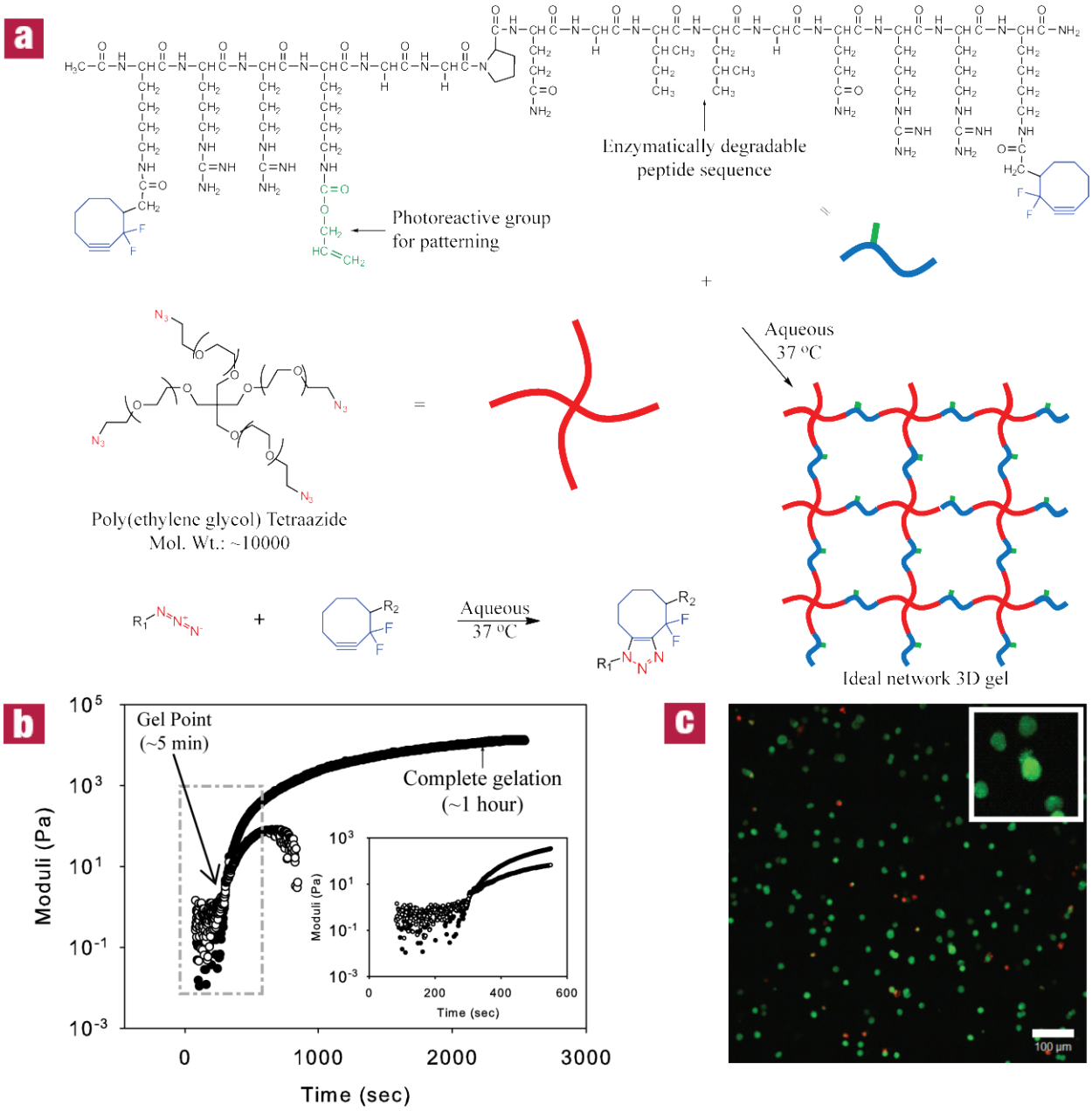

Figure 3.1 Cytocompatible click hydrogel formation reaction and kinetics. (a) Click-functionalized macromolecular precursors undergo the [3+2] Huisgen cycloaddition to form a 3D ideal network hydrogel *via* a step-growth polymerization mechanism. **(b)** Rheology can be used to monitor dynamic network formation and indicates gelation within minutes and complete reaction occurring in less than one hour at 37 °C for a 13.5 wt% monomer solution. G' is shown as closed circles, while G'' are open circles. **(c)** A Live/Dead stain at 24 hours of 3T3s encapsulated within this material indicates a predominantly viable population (live cells are shown in green, while dead cells are red). Image represents a 200 µm confocal projection. Scale bar = 100 µm.

Hydrogels were formed using a 13.5 wt% total macromer solution containing a 1:1 ratio of alkyne to azide functionalities. Ultimately, this gel composition affords a high water content, elasticity similar to many tissue matrices, and the ability to image cells in 3D. Dynamic time sweep rheological experiments were conducted to monitor network evolution during this step polymerization (Figure 3.1b). The crossover point, an estimate of gelation at which the elastic modulus (G') is equal to the storage modulus (G''), occurs in less than 5 min (290 ± 30 sec). Furthermore, the data indicates a final G' value of 12.0 ± 0.6 kPa at t ~ 1 hour, signifying a structurally robust network that maintains its 3D shape with loading. The step-growth mechanism was confirmed by the statistical gelation model for step-growth networks developed by Flory and Stockmayer (Supplementary Section 3.6.1). In addition, dynamic magic-angle spinning (MAS) ^{1}H NMR was carried out to further examine the reaction kinetics of network formation (Supplementary Section 3.6.2). Under normal solution-phase NMR conditions, the NMR spectral lines would quickly become extremely broad, yielding useless spectra as the polymer network begins to form due to dipolar relaxation in the motionally restricted (semi-solid) phase being formed. With the sample oriented at the magic-angle (ca. 54.736 degrees), rotating at a frequency that exceeds the static dipolar linewidth, this dipolar line-broadening can be eliminated, yielding high-resolution ^{1}H NMR spectra throughout the polymerization reaction. Characteristic peaks associated with the alkyne DIFO3 functionality were found to completely disappear upon reaction with azides within 1 hour with a second-order rate constant of 8.9×10^{-5} M^{-1} s^{-1}. Both the rheological and the MAS NMR data suggest that the formed hydrogel is nearly ideal, agreeing with previous work with click-based networks[10]. Ultimately, the time scale and mechanism of this reaction are such that it permits cell encapsulation with high viability

comparable to traditional hydrogel systems (>90% at 24 hours post encapsulation, Figure 3.1c & Supplementary Section 3.6.6).

Post network formation, a second click reaction allows facile modification of the cell's niche through the conjugation of biomolecules at specific locations with the gel. Specifically, by including a photoreactive allyl ester within the crosslinking peptide sequence *via* the commercially available Fmoc-Lys(alloc)-OH amino acid (Figure 3.1a), relevant biochemical cues can be covalently incorporated within the hydrogel using the bio-orthogonal thiol-ene coupling reaction. Originally designed as an orthogonal protecting group for lysine[29], allyloxycarbonyl (alloc) contains a vinyl group capable of undergoing a thiol-ene photocoupling reaction with any thiol-containing compound, including cysteine[11,30]. The alloc protecting group is stable to Fmoc deprotection and peptide trifluoroacetic acid cleavage from resin, rendering it a suitable and versatile choice as the photoreactive component of our hydrogel crosslinker. Additionally, the electron-rich alloc allyl ester is not susceptible to Michael-type addition, eliminating the possibility for non-specific chemical immobilization[31].

The thiol-ene reaction is a radical-mediated addition of a thiol to an alkene, involving the catalytic propagation of a thiyl radical through a vinyl functional group and the chain transfer from the resulting carbon radical to a thiol[32] (Figure 3.2a). Thiols can be deprotonated to thiyl radicals using photolytically-cleaved, hydrogen-abstracting initiator systems. Selectively exposing specific locations within the material to light affords spatial and temporal control of where this photocoupling reaction occurs in real time. The extent of patterning can ultimately be controlled by regulating the light intensity and exposure time (Figure 3.2b) and utilizes cytocompatible wavelengths (365 nm) and intensities (~10 mW/cm^2). Light exposure can be controlled using conventional photolithographic, single-photon, and multi-photon techniques,

each affording a higher degree of reaction specificity than the last. This thiol-ene reaction is compatible with cells, as indicated by the high viability maintained throughout patterning (>90% at 24 hours post encapsulation, Figure 3.2c & Supplementary Section 3.6.6). 2D patterns were transferred throughout the z-axis of a gel using stereolithography (Figure 3.2d & Supplementary Section 3.6.8). We demonstrate that the reaction scheme is fully additive by incorporating three different peptides at varied positions within the gel (Figure 3.2d & Supplementary Section 3.6.10). More complex 3D structures of arbitrary size and shape can be patterned within the gel by systematically scanning the focal point of a pulsed near IR laser where functionalization is desired. The latter technique affords micron-scale pattern resolution, as illustrated in Figure 3.2e & Supplementary Section 3.6.9, and is performed in time scales similar to that required for 3D confocal imaging.

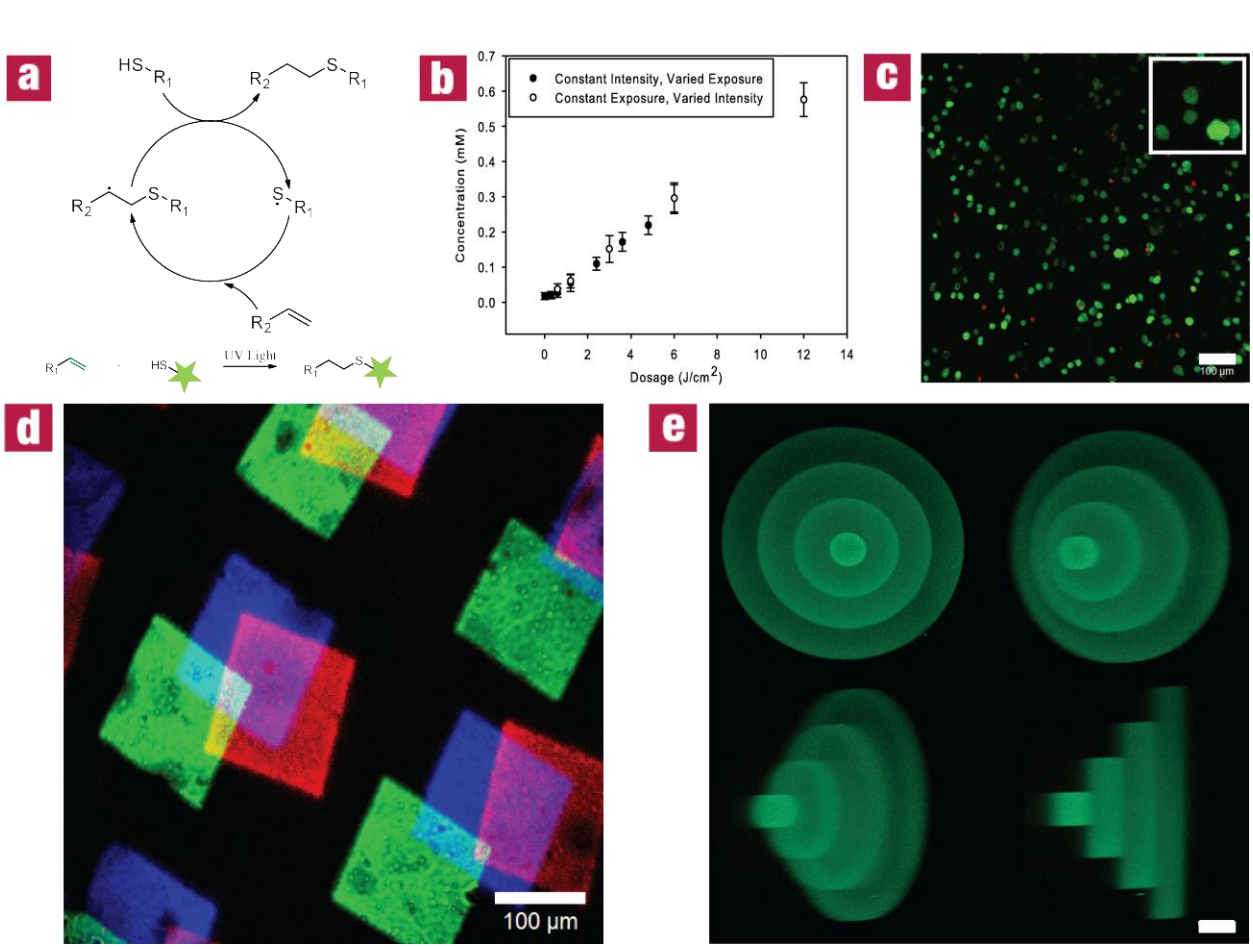

Figure 3.2 Cytocompatible, biochemical patterning within preformed click hydrogels. (a) The thiol-ene reaction mechanism provides a means to quantitatively couple sulfhydryls (-SH) with vinyl functionalities (-C=C) in the presence of light. **(b)** Upon swelling into the material, relevant thiol-containing biomolecules are covalently affixed to the hydrogel network at varying concentrations by altering the dosage of exposed light (intensity and exposure time). **(c)** A Live/Dead stain at 24 hours after photolithographic patterning of 3T3s indicates a predominantly viable population (live cells are shown in green, while dead cells are red) and that the patterning process is cytocompatible. **(d)** The thiol-ene reaction is confined to user-defined regions in space using photomasks to introduce three different fluorescently-labeled peptide sequences within the gel, a process that can be repeated at desired times and spatial locations to introduce additional biochemical cues. **(e)** By controlling the focal point of the laser light in three-dimensions using a confocal microscope, micron-scale spatial patterning resolution is achieved. Values in (b) are reported as mean ± SD (n=5). The image in (c) represents a 200 µm confocal projection. The images in (d) and (e) represent confocal micrographs of fluorescently-tagged peptides patterned within the networks. Scale bar = 100 µm for (c), 100 µm for (d), and 50 µm for (e).

The thiol-ene reaction allows any thiol-containing compound to be pendantly attached at user-defined locations within the hydrogel. While adding thiol functionality to small molecules

is fairly straightforward, cysteine-containing peptides require no additional synthetic modifications to be patterned within a gel. To illustrate the versatility that is afforded by this type of patterning scheme, a detection molecule was covalently incorporated as a pendant functionality that increases its fluorescence when exposed to cellular protease activity within the network. Specifically, a di-fluorescein collagenase-sensitive peptide sequence (DiFAM) was selectively patterned into the gels. This peptide, FAM-KGWL↓GPAK(FAM)GKC-NH_2, exhibits intramolecular self quenching until it is enzymatically cleaved (Figure 3.3a). While the gel fluoresces slightly where the quenched molecule has been patterned, the probe is found to fluoresce with much higher intensity in regions of collagenase activity immediately surrounding the cells (Figure 3.3b-d). This DiFAM probe serves as a proof of concept that these materials are able to report real-time information concerning local encapsulated cell behavior, and that these detection assays can be confined to user-defined regions within the gel.

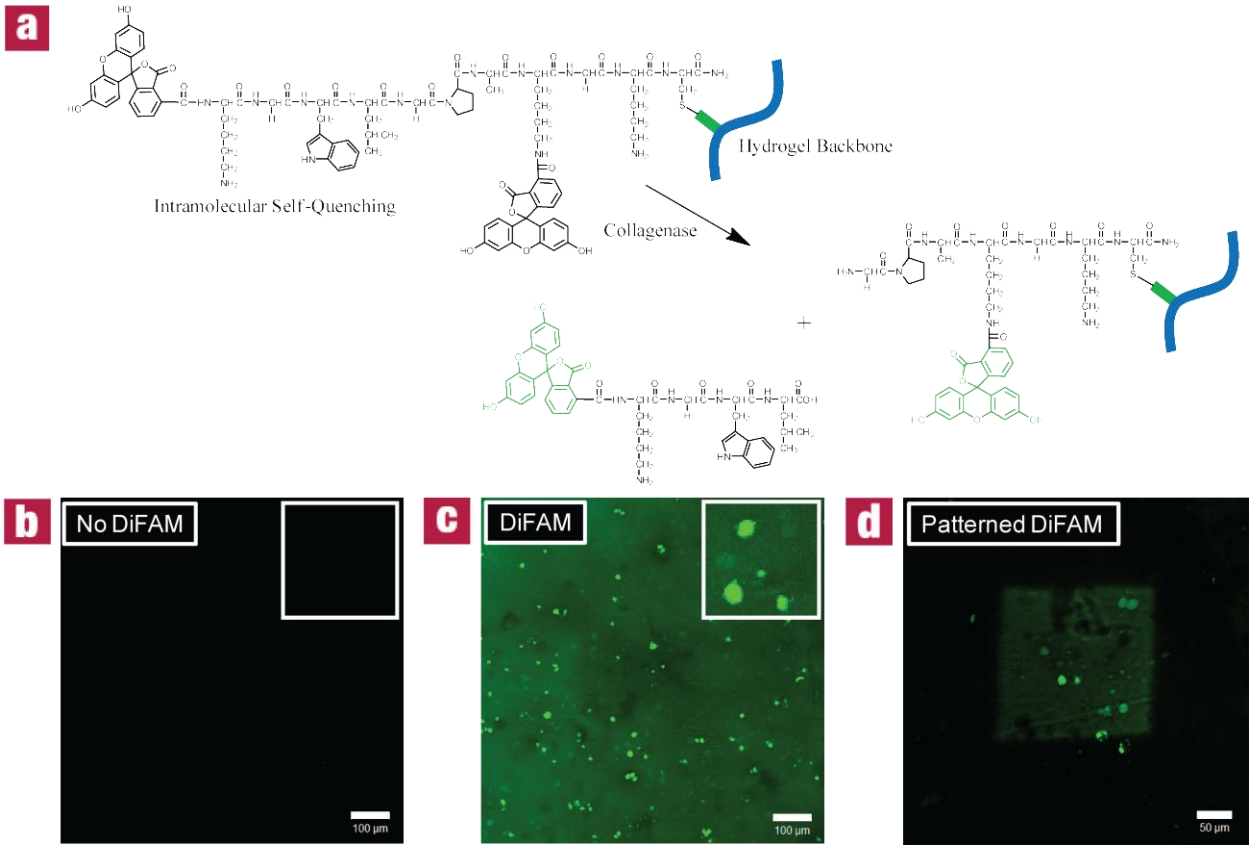

Figure 3.3 Visualizing 3T3 collagenase activity *via* patterned detection peptide within 3D click hydrogels. 3T3s were encapsulated into hydrogel networks at 3 x 10^6 cells/mL. After 24 hours, a di-fluorescein collagenase-sensitive peptide sequence (DiFAM) which exhibits intramolecular self-quenching until enzymatically cleaved **(a)** was swollen into networks at 0.5 mgs/mL and exposed to 365 nm collimated light at 10 mW/cm^2 for 10 minutes through a variety of photomasks: **(a)** full mask; **(b)** no mask; **(c)** full mask with 200 µm square opening. Here, patterned regions gently fluoresce while areas of high collagenase activity (near cell surface) fluoresce with greater intensity. Images represent 200 µm confocal projections at 3 days. Scale bars = 100 µm for (b) and (c) and 50 µm for (d).

Just as this system allows for the patterning of reporter probes, biochemical functionalities that direct cell behavior can be incorporated within these materials in a location-specific manner. Incorporation of the RGD sequence, a fibronectin motif, has been extensively used to promote cell adhesion uniformly throughout biomaterials[33,34], as well as in patterned channels[35-37]. Here, a cysteine-containing, fluorescently-labeled RGD sequence, AF_{488}-AhxRGDSC-NH_2, was selectively affixed within a cell-impregnated hydrogel. The fibronectin motif induces localized morphological and migratory changes within the patterned regions

(Figure 3.4). Where the RGD is present, cells are able to attach to and locally degrade the surrounding network, giving rise to a spread morphology. However, when this functionality is absent, cells maintain a rounded morphology. Figure 3.4c illustrates that these induced differences in cell behavior can be selectively confined to patterned regions within a single gel.

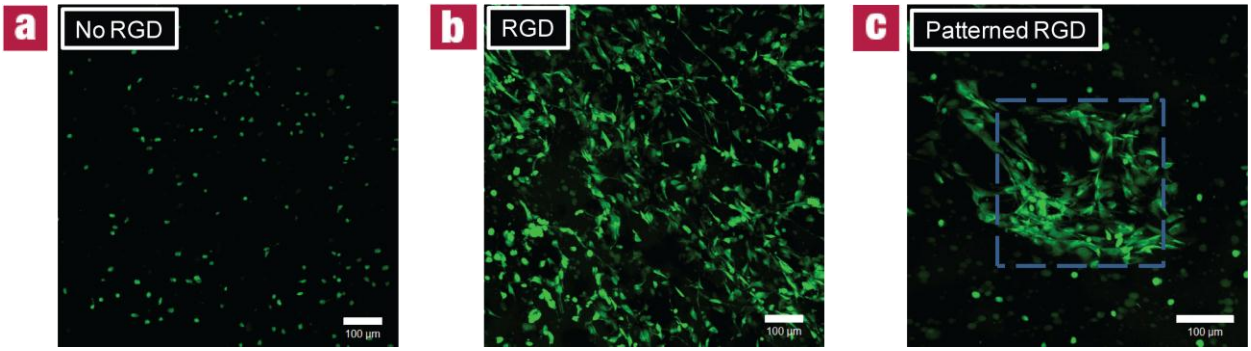

Figure 3.4 Effect of patterned RGD on 3T3 population within 3D click hydrogels. 3T3s were encapsulated into hydrogel networks at 3 x 10^6 cells/mL. After 24 hours, thiol-functionalized RGD, a fibronectin motif known to promote cell attachment, was swollen into networks at 3 mgs/mL and exposed to 365 nm collimated light at 10 mW/cm^2 for 10 minutes through a variety of photomasks: **(a)** full mask; **(b)** no mask; **(c)** full mask with 250 µm square opening (illustrated by the dashed lines). 3T3s were stained at day 10 with CellTracker orange and imaged using confocal microscopy. Here, cells only adopt a spread morphology in user-defined regions of RGD. Images represent 200 µm confocal projections. Scale bars = 100 µm.

As presented, this work utilizes two novel bio-orthogonal click chemistry schemes to combine and exploit features of previously mutually exclusive technologies. Namely, the enzymatically-degradable hydrogel platform provides an ideal network into which biomacromolecules can be photopatterned that detect, as well as promote, specific cellular functions. The material chemistry affords a simplified synthetic microenvironment that captures critical aspects of extracellular matrices, allowing for the direct observation of cellular processes in 3D, including migration, proliferation, and morphological changes. The ability to then spatially tune the material properties provides an additional tool to manipulate cell function. Since reactive monomer components can be easily exchanged, the material is readily tailorable with multiple functionalities for 3D cell studies.

3.4 Materials and Methods

3.4.1 Synthesis of PEG-tetraazide

4-arm poly(ethylene glycol) tetraazide was synthesized following a published synthetic route[11]. In short, methanesulfonyl chloride (5x) was added to 4-arm PEG (M_n ~ 10,000 Da) (Jenkem) and subsequently reacted with sodium azide (5x). Additional detail is available in Supplementary Section 3.6.11.

3.4.2 Synthesis of Bis(cyclooctyne)-functionalized peptide crosslinker

The enzymatically-degradable, allyl ester-containing peptide Ac-KRRK(alloc)GGPQGILGQRRK-NH_2 was synthesized (ABI 433A peptide synthesizer) *via* standard Fmoc solid-phase methodology and HBTU/HOBt activation. Resin was treated with trifluoroacetic acid/triisopropylsilane/water (95:2.5:2.5) for 2 hours and precipitated (3x) using ice-cold diethyl ether (Supplementary Section 3.6.3). DIFO3 was coupled to the ε-amino groups of the terminal lysines *via* standard HATU coupling chemistry. Peptides were purified using semi-preparative RP-HPLC (Waters Delta Prep 4000) using a 70 minute linear gradient (5 to 95%) of acetonitrile and 0.1% trifluoroacetic acid (Sigma). Peptide purity was confirmed by an analytical RP-HPLC and MALDI-TOF-MS (Applied Biosystems DE Voyager) using α-cyano-4-hydroxycinnamic acid matrix (Sigma): calculated ($[M+H]^+$ 2329.7); observed ($[M+H]^+$ 2329.1) (Supplementary Section 3.6.4)

3.4.3 Synthesis of self-quenched collagenase-sensitive detection peptide (DiFAM)

H-KGWLGPAK(Dde)GKC-NH_2 (0.25 mmol) was synthesized *via* standard Fmoc solid-phase methodology and HBTU/HOBt activation. Carboxyfluorescein (1 mmol, Novabiochem) was coupled to the N-terminus *via* standard HATU coupling chemistry. The Dde protecting group was removed using 2% hydrazine in DMF, and a second carboxyfluorescein (1 mmol) was

coupled to the ε-amino groups of the deprotected lysine using standard HATU coupling chemistry. Resin was treated with trifluoroacetic acid/triisopropylsilane/water (95:2.5:2.5) for 2 hours and precipitated (3x) using ice-cold diethyl ether. Peptides were purified using semi-preparative RP-HPLC (Waters Delta Prep 4000) using a 70 minute linear gradient (5 to 95%) of acetonitrile and 0.1% trifluoroacetic acid (Sigma). DiFAM peptide purity was confirmed by an analytical RP-HPLC and MALDI-TOF-MS (Applied Biosystems DE Voyager) using α-cyano-4-hydroxycinnamic acid matrix (Sigma): calculated ($[M+H]^+$ 1860.04); observed ($[M+H]^+$ 1861.94) (Supplementary Section 3.6.5).

3.4.4 Synthesis of fluorescently-labeled adhesive ligand

H-AhxRGDSC-NH_2 (0.25 mmol) was synthesized *via* standard Fmoc solid-phase methodology and HBTU/HOBt activation. Alexa Fluor® 488 carboxylic acid, 2,3,5,6-tetrafluorophenyl ester (1 mg, Invitrogen) was dissolved in NMP with a catalytic amount of DIEA and stirred with resin overnight at room temperature. Resin was treated with trifluoroacetic acid/triisopropylsilane/water/dithiothreitol (94.5:2.5:2.5:0.5) for 1 hour and precipitated (3x) using ice-cold diethyl ether. This product, denoted AF_{488}-AhxRGDSC-NH_2, was used with no further purification.

3.4.5 Rheological Experiments

Dynamic frequency, time, and strain sweep rheology experiments were performed on a TA Ares rheometer with parallel plate geometry (20 mm diameter) at 25 °C. Initial gel network formation of a 13.5 wt% solution was monitored by observing G' and G'' at a constant frequency of 100 rad/s as a function of time. Gel properties were monitored *via* frequency sweep measurements at fixed strain amplitude (10%) to measure the hydrogel storage, G', and loss, G'', moduli.

3.4.6 3T3 Fibroblast Cell Culture

General Cell Culture: NIH 3T3s were cultured in high-glucose Dulbecco's modified eagle's medium (Gibco) containing 10% fetal bovine serum (Invitrogen), 2% penicillin/streptomycin (Gibco), 0.4% fungizone (Gibco), and 0.2% gentamicin (Gibco) in 5% CO_2 at 37 °C.

Cell Encapsulation: 3T3s were suspended at 3 x 10^6 cells/mL in a 13.5 total wt% monomer solution in media and allowed to react for one hour to form a cell-laden hydrogel sheet.

3.4.7 Biochemical Patterning

Hydrogels were swollen in phenol red-free media (pH = 7.4) containing 0.05 wt% Irgacure 2959 (Ciba) and 3 mg/mL patterning agent AF_{488}-AhxRGDSC-NH_2 for one hour. Using conventional photolithographic techniques, gels were exposed to collimated UV light (365 nm wavelength at 10 mW/cm^2) through a patterned photomask for 10 minutes. Under these photopatterning conditions, 1-2% of the alloc functional groups are consumed to yield ~0.1 mM of conjugated peptide, implying that multiple signals can be incorporated at biologically relevant concentrations. Alternatively, two-photon techniques were exploited for complex patterning by placing gels on a 710 LSM NLO confocal microscope stage (Carl Zeiss) and selectively exposing to pulsing focused 720 nm laser light through a 20x/0.8 Plan-Apochromat objective (Carl Zeiss), with x-y control afforded by Region of Interest scanning and z-control by focal depth. Z-planes were scanned at 1 μm increments with a laser power of 400 mW/μm^2 and a scan speed of 2.4 μs/μm^2. For both the two-photon and photolithographic approaches, photocoupling of the patterning agent to the hydrogel network occurs only within areas exposed to light. After patterning is complete, the gel is washed for approximately two hours with fresh media to

remove any unbound material, yielding the final patterned hydrogel (Supplementary Figs. S7 & S9). The process of swelling in the patterning agent, photopatterning, and washing can be repeated for multiple cues within the same gel (Supplementary Section 3.6.10). For gels that are of reasonable thickness for 3D cell culture (~200 microns to 1 mm), characteristic diffusion times of the unreacted peptides from the gel are on the order of a few minutes to a few hours.

3.5 References

1. Kolb, H.C., Finn, M.G. & Sharpless, K.B. Click chemistry: Diverse chemical function from a few good reactions. *Angew. Chem. Int. Ed. Engl.* **40**, 2004-2021 (2001).

2. Huisgen, R. 1.3-Dipolare Cycloadditionen - Ruckschau Und Ausblick. *Angew. Chem. Int. Ed. Engl.* **75**, 604-637 (1963).

3. Moses, J.E. & Moorhouse, A.D. The growing applications of click chemistry. *Chem. Soc. Rev.* **36**, 1249-1262 (2007).

4. Kolb, H.C. & Sharpless, K.B. The growing impact of click chemistry on drug discovery. *Drug Discov. Today* **8**, 1128-1137 (2003).

5. Hawker, C.J. & Wooley, K.L. The convergence of synthetic organic and polymer chemistries. *Science* **309**, 1200-1205 (2005).

6. Baskin, J.M. et al. Copper-free click chemistry for dynamic in vivo imaging. *Proc. Natl. Acad. Sci. U. S. A.* **104**, 16793-16797 (2007).

7. Srinivasan, R., Li, J., Ng, S.L., Kalesh, K.A. & Yao, S.Q. Methods of using click chemistry in the discovery of enzyme inhibitors. *Nat. Protoc.* **2**, 2655-2664 (2007).

8. Evans, M.J., Saghatelian, A., Sorensen, E.J. & Cravatt, B.F. Target discovery in small-molecule cell-based screens by in situ proteome reactivity profiling. *Nat. Biotechnol.* **23**, 1303-1307 (2005).

9. Franc, G. & Kakkar, A. Dendrimer design using Cu-I-catalyzed alkyne-azide "click-chemistry". *Chem. Commun.*, 5267-5276 (2008).

10. Malkoch, M. et al. Synthesis of well-defined hydrogel networks using Click chemistry. *Chem. Commun.*, 2774-2776 (2006).

11. Polizzotti, B.D., Fairbanks, B.D. & Anseth, K.S. Three-dimensional biochemical patterning of click-based composite hydrogels *via* thiolene photopolymerization. *Biomacromolecules* **9**, 1084-1087 (2008).

12. Tornoe, C.W., Christensen, C. & Meldal, M. Peptidotriazoles on solid phase: [1,2,3]-triazoles by regiospecific copper(I)-catalyzed 1,3-dipolar cycloadditions of terminal alkynes to azides. *J. Org. Chem.* **67**, 3057-3064 (2002).

13. Franke, R., Doll, C. & Eichler, J. Peptide ligation through click chemistry for the generation of assembled and scaffolded peptides. *Tetrahedron Lett.* **46**, 4479-4482 (2005).

14. Prescher, J.A. & Bertozzi, C.R. Chemistry in living systems. *Nat. Chem. Biol.* **1**, 13-21 (2005).

15. Chen, J.K. Fish 'n clicks. *Nat. Chem. Biol.* **4**, 391-392 (2008).

16. Agard, N.J., Prescher, J.A. & Bertozzi, C.R. A strain-promoted [3 + 2] azide-alkyne cycloaddition for covalent modification of biomolecules in living systems. *J. Am. Chem. Soc.* **126**, 15046-15047 (2004).

17. Laughlin, S.T., Baskin, J.M., Amacher, S.L. & Bertozzi, C.R. In vivo imaging of membrane-associated glycans in developing zebrafish. *Science* **320**, 664-667 (2008).

18. Dondoni, A. The Emergence of Thiol-Ene Coupling as a Click Process for Materials and Bioorganic Chemistry. *Angew. Chem. Int. Ed. Engl.* **47**, 8995-8997 (2008).

19. Hoyle, C.E., Lee, T.Y. & Roper, T. Thiol-enes: Chemistry of the past with promise for the future. *J. Polym. Sci., Part A: Polym. Chem.* **42**, 5301-5338 (2004).

20. Khire, V.S., Benoit, D.S.W., Anseth, K.S. & Bowman, C.N. Ultrathin gradient films using thiol-ene polymerizations. *J. Polym. Sci., Part A: Polym. Chem.* **44**, 7027-7039 (2006).

21. Killops, K.L., Campos, L.M. & Hawker, C.J. Robust, efficient, and orthogonal synthesis of dendrimers *via* thiol-ene "Click" chemistry. *J. Am. Chem. Soc.* **130**, 5062-5064 (2008).

22. Langer, R. & Vacanti, J.P. Tissue Engineering. *Science* **260**, 920-926 (1993).

23. Cushing, M.C. & Anseth, K.S. Hydrogel cell cultures. *Science* **316**, 1133-1134 (2007).

24. Anseth, K.S. A biologist looks to 'click chemistry' for better three-dimensional tissue models. *Nature* **453**, 5 (2008).

25. Codelli, J.A., Baskin, J.M., Agard, N.J. & Berozzi, C.R. Second-generation difluorinated cyclooctynes for copper-free click chemistry. *J. Am. Chem. Soc.* **130**, 11486-11493 (2008).

26. Nagase, H. & Fields, G.B. Human matrix metalloproteinase specificity studies using collagen sequence-based synthetic peptides. *Biopolymers* **40**, 399-416 (1996).

27. Lutolf, M.P. et al. Synthetic matrix metalloproteinase-sensitive hydrogels for the conduction of tissue regeneration: Engineering cell-invasion characteristics. *Proc. Natl. Acad. Sci. U. S. A.* **100**, 5413-5418 (2003).

28. Lutolf, M.P. & Hubbell, J.A. Synthetic biomaterials as instructive extracellular microenvironments for morphogenesis in tissue engineering. *Nat. Biotechnol.* **23**, 47-55 (2005).

29. Kunz, H. & Unverzagt, C. The allyloxycarbonyl (aloc) moiety - Conversion of an unsuitable into a valuable amino protecting group for peptide-synthesis. *Angew. Chem. Int. Ed. Engl.* **23**, 436-437 (1984).

30. Lee, T.Y., Smith, Z., Reddy, S.K., Cramer, N.B. & Bowman, C.N. Thiol-allyl ether-methacrylate ternary systems. Polymerization mechanism. *Macromolecules* **40**, 1466-1472 (2007).

31. Mather, B.D., Viswanathan, K., Miller, K.M. & Long, T.E. Michael addition reactions in macromolecular design for emerging technologies. *Progress in Polymer Science* **31**, 487-531 (2006).

32. Cramer, N.B., Reddy, S.K., O'Brien, A.K. & Bowman, C.N. Thiol-ene photopolymerization mechanism and rate limiting step changes for various vinyl functional group chemistries. *Macromolecules* **36**, 7964-7969 (2003).

33. Ruoslahti, E. & Pierschbacher, M.D. New Perspectives in cell-adhesion - RGD and Integrins. *Science* **238**, 491-497 (1987).

34. Burdick, J.A. & Anseth, K.S. Photoencapsulation of osteoblasts in injectable RGD-modified PEG hydrogels for bone tissue engineering. *Biomaterials* **23**, 4315-4323 (2002).

35. Hahn, M.S., Miller, J.S. & West, J.L. Three-dimensional biochemical and biomechanical patterning of hydrogels for guiding cell behavior. *Adv. Mater.* **18**, 2679-2684 (2006).

36. Lee, S.H., Moon, J.J. & West, J.L. Three-dimensional micropatterning of bioactive hydrogels *via* two-photon laser scanning photolithography for guided 3D cell migration. *Biomaterials* **29**, 2962-2968 (2008).

37. Luo, Y. & Shoichet, M.S. A photolabile hydrogel for guided three-dimensional cell growth and migration. *Nat. Mater.* **3**, 249-253 (2004).

3.6 Supplementary Information

3.6.1 Statistical gelation model for step-growth networks (Flory and Stockmayer)

To verify that hydrogel network formation occurs *via* the proposed step growth mechanism, a series of stoichiometrically-imbalanced gel polymerizations were monitored *via*

real time rheology. Measurements for tan δ, ultimate elastic moduli, and the time required for gelation (estimated by the crossover point) were obtained for 13.5 wt% gels in PBS at room temperature with compositions shown in the table below. Here, tan δ is defined as the loss modulus divided by the storage modulus (tan δ = G''/G'); therefore, a value less than unity indicates a solid material, while values greater than one are indicative of a liquid.

According to the Flory-Stockmeyer equation for statistical gelation of step growth networks, the conversion required for gelation (ρ_c) can be predicted as a function of the stoichiometry ratio of reactants r where $r \leq 1$, f_{azide} and f_{yne} are the degree of functionality for the PEG azide and cyclooctyne peptide monomers, respectively. For our system, we have f_{azide}= 4 and f_{yne} = 2.

$$\rho_c = \frac{1}{\sqrt{r(f_{azide}-1)(f_{yne}-1)}} = \frac{1}{\sqrt{3r}}$$

By definition, conversion in any reactive system cannot exceed unity. As such, for a gel to form, ρ_c must be less than or equal to 1. It follows that gels will form in this system only when $r \geq 0.33$. Our data is consistent with this step-growth prediction in that gels are unable to form in systems where r = 0.3.

Azide:acetylene ratio	***r***	***ρ_c***	***Time to gel point (sec)***	***tan δ***	***Final G' (kPa)***
3.3 : 1.0	0.3	1.1	No gelation	8.1 ± 3	0 ± 0.1
2.0 : 1.0	0.5	0.82	511 ± 40	0.74 ± 0.1	2.9 ± 0.4
1.0 : 1.0	1.0	0.58	290 ± 30	0.28 ± 0.1	12 ± 0.6
1.0 : 2.0	0.5	0.82	573 ± 50	0.81 ± 0.1	2.3 ± 0.5
1.0 : 3.3	0.3	1.1	No gelation	9.8 ± 3	0 ± 0.1

3.6.2 Kinetics of network formation from dynamic MAS ^{1}H NMR

In these experiments, ^{1}H NMR spectra were acquired at 400.15 MHz using a Varian Inova-400 NMR spectrometer system equipped with a Varian gHX-Nano Probe for MAS

operation. Spectra were acquired with sample spinning speeds of 3.0-3.5KHz at the magic angle roughly every 10 minutes (left) and integral values for the characteristic peaks were exponentially fit to give a second-order rate constant for the reaction (right). The characteristic peak has completely disappeared 1 hour into the polymerization, indicating that all alkyne functionalities have fully reacted at this point.

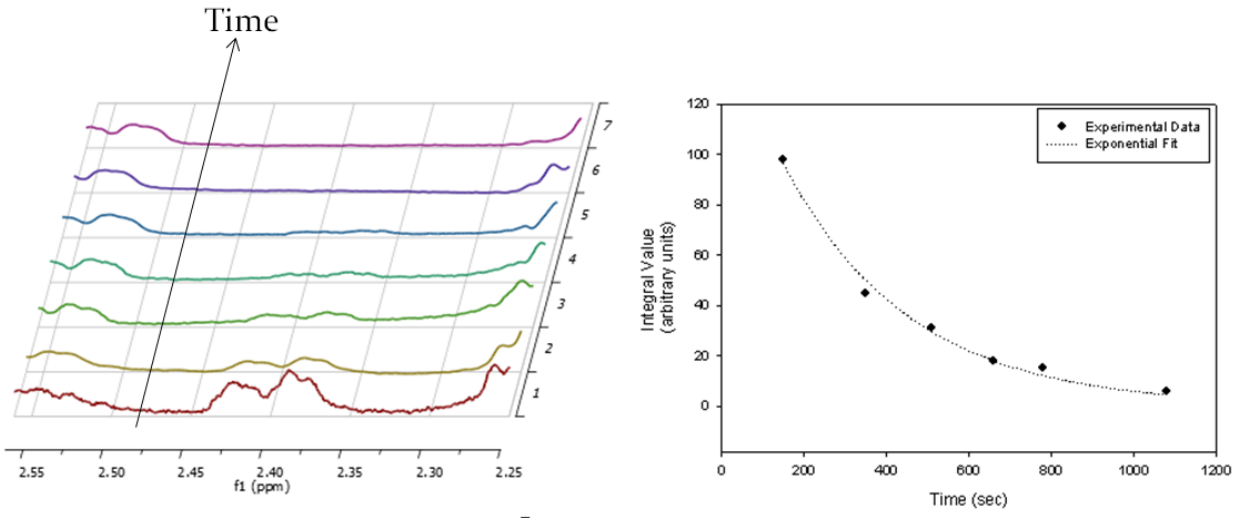

3.6.3 MALDI-TOF Spectra of Ac-KRRK(alloc)GGPQGILGQRRK-NH_2

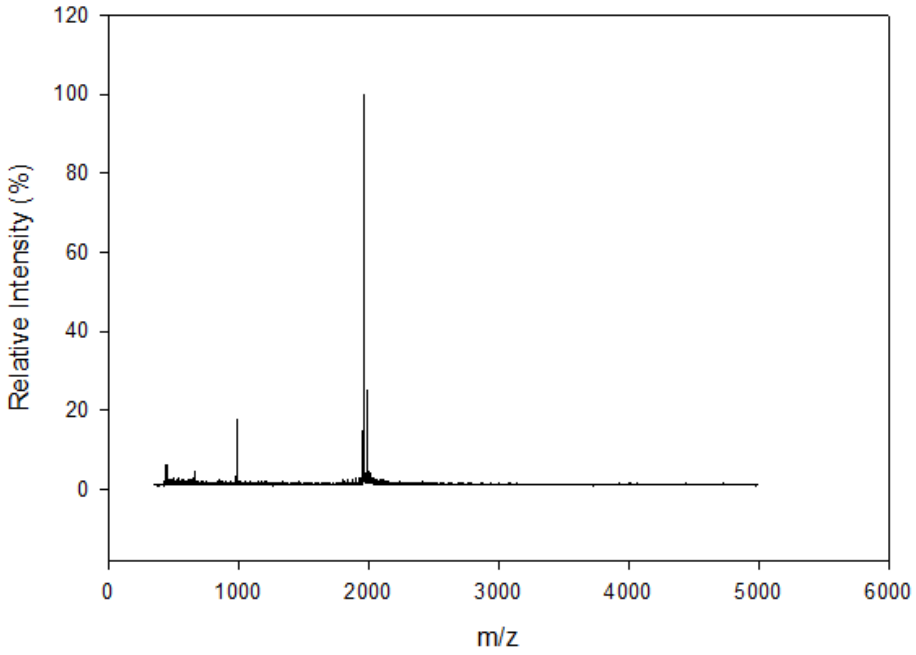

3.6.4 MALDI-TOF Spectra of Ac-K(DIFO3)RRK(alloc)GGPQGILGQRRK(DIFO3)-NH_2

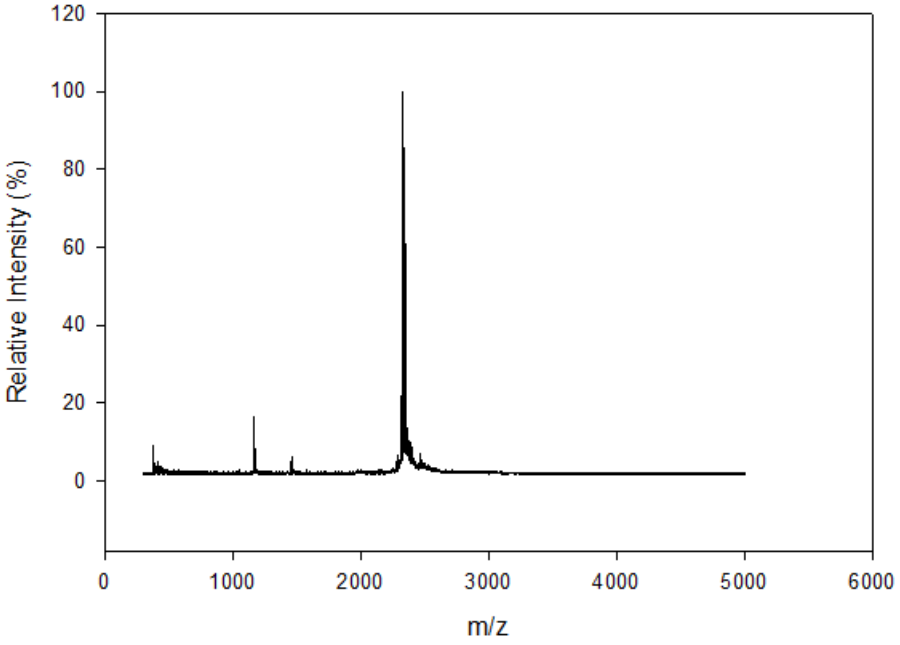

3.6.5 MALDI-TOF spectra of FAM-KGWLGPAK(FAM)GKC-NH_2

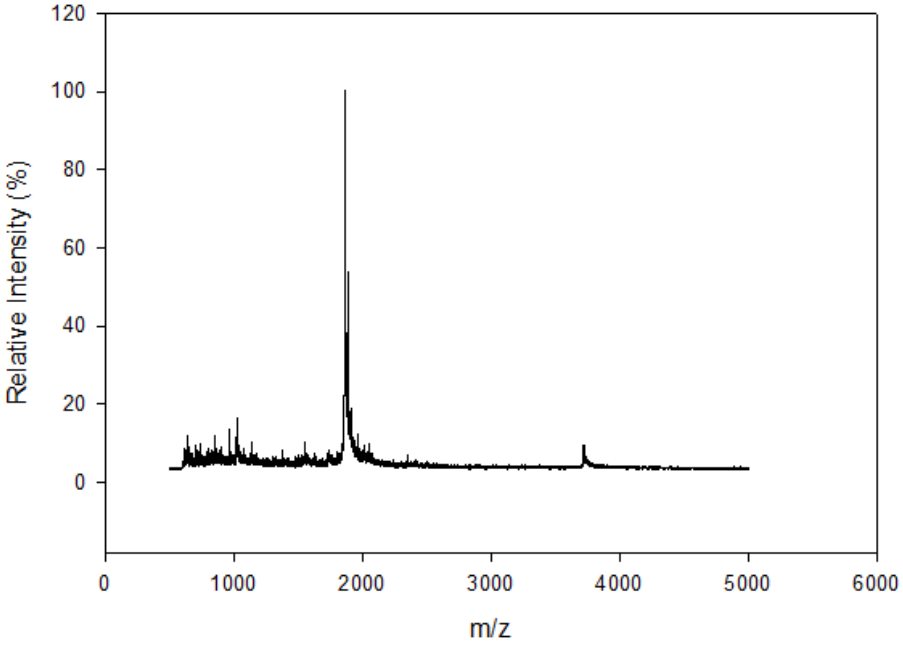

3.6.6 Viability of 3T3s and hMSCs within click-based hydrogels over 1 week of culture

To verify viability of cells following encapsulation and subsequent material patterning, 3T3s and human mesenchymal stem cells (hMSCs) were stained and imaged using confocal microscopy on days 1, 2, and 7 (live cells are shown in green, while dead cells are red). 24 hour post encapsulation, a portion of the gels were bulk modified with RGDSC *via* the thiol-ene reaction. The images indicate a predominately viable cell population for each cell type (>95% viability, no statistic significance between any two conditions). While we did not explicitly assay for proliferation, it does appear that the 3T3s are proliferating in the presence of the patterned RGDSC. Images represent 200 μm confocal projections. Scale bar = 100 μm.

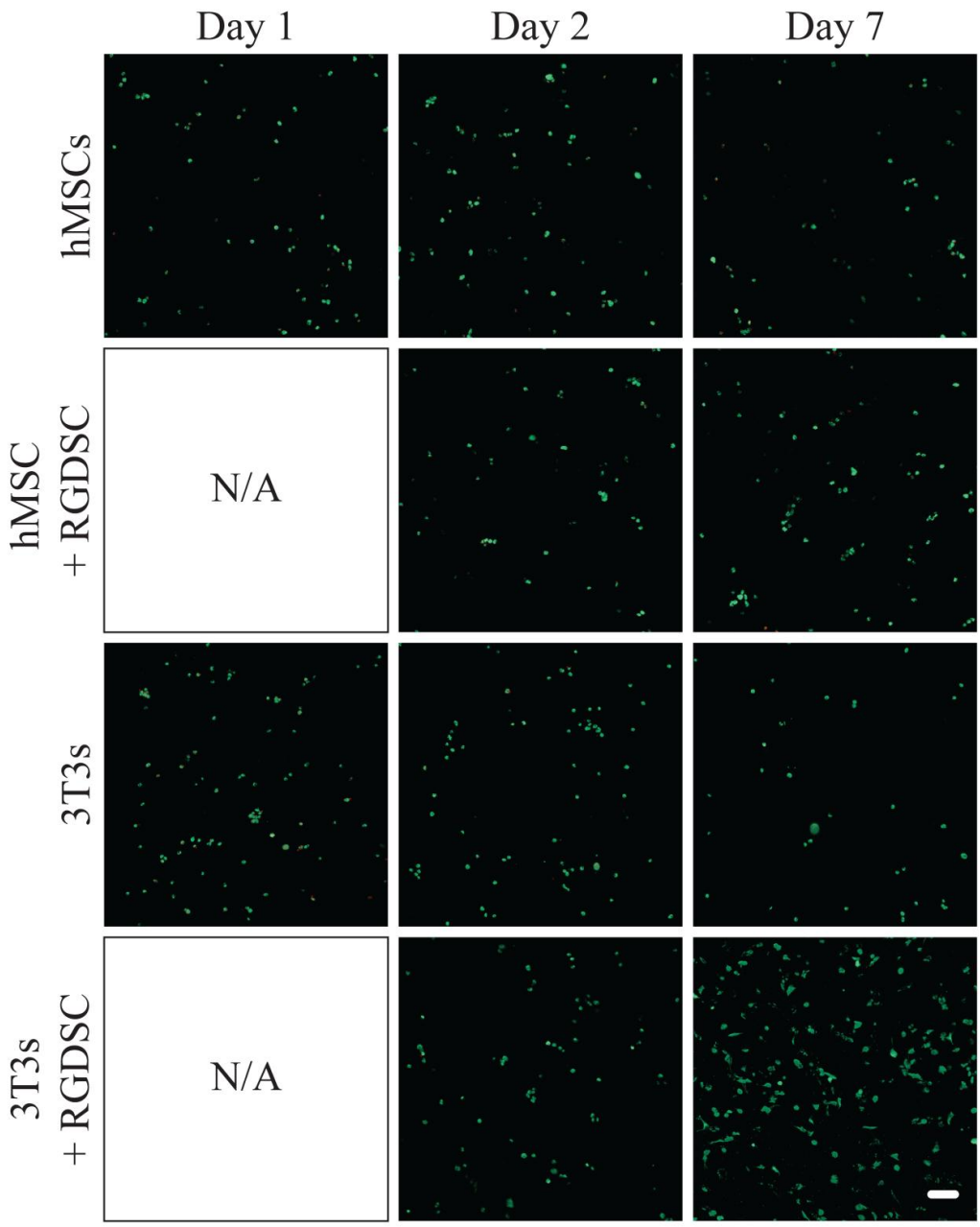

3.6.7 Post-patterning peptide diffusion from click-based hydrogels

Fluorescently-labeled peptide was swollen into the hydrogel network and allowed to equilibrate for 2 hours. Confocal microscopy was used to determine peptide concentration profiles throughout the gel with time. The gel was placed in fresh media on an orbital shaker at

room temperature in between time points to facilitate transport. The peptide was found to be completely released within two hours of treatment.

The diffusion of peptide from the click-based hydrogel was calculated using solutions to Fick's second law of diffusion for a planar sheet with a uniform initial condition ($C = C_0$, $-l < z < l$, $t = 0$), and sink boundary conditions ($C = C_l = 0$, $z = \pm l$, $t \leq 0$):

$$\frac{\partial C}{\partial t} = D\frac{\partial^2 C}{\partial z^2}$$

Using separation of variables, an exact analytical solution is achieved:

$$\frac{C - C_0}{C_l - C_0} = 1 - \frac{4}{\pi}\sum_{n=0}^{\infty}\frac{(-1)^n}{2n+1}\exp\left[-D(2n+1)^2\frac{\pi^2 t}{4l^2}\right]\cos\left[\frac{(2n+1)\pi z}{2l}\right]$$

A visual fit of experimentally obtained data for a 500 μm thick slab gel gives a diffusion coefficient on the order of 10^{-6} cm^2/s, which is comparable to that of small molecules in water (10^{-5} cm^2/s). For gels that are of reasonable thickness for 3D cell culture (~200 microns to 1 mm), this gives characteristic diffusion time scales on the order of a few minutes to a few hours.

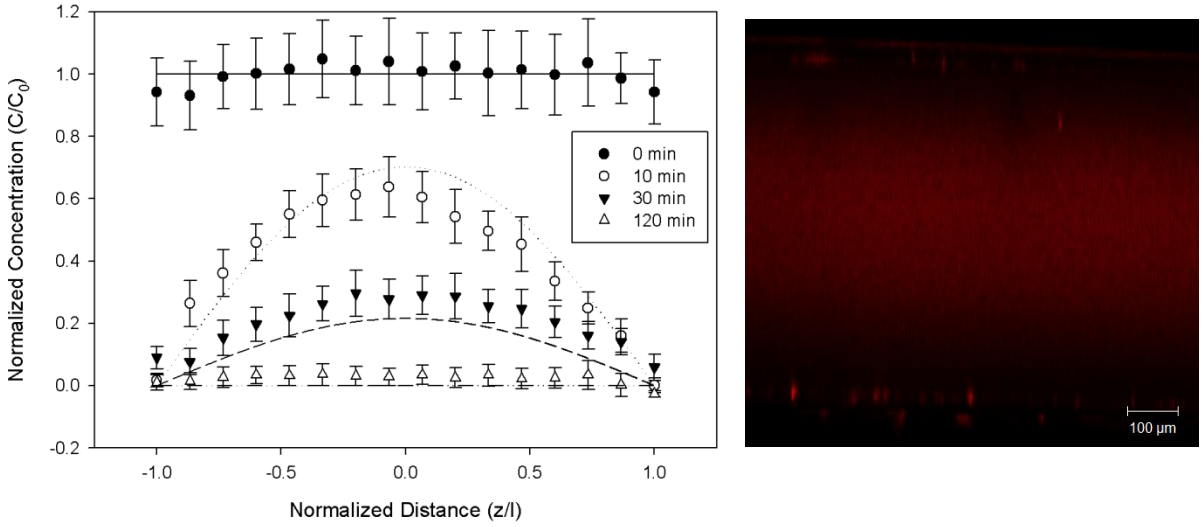

3.6.8 Stereolithographic patterning within click-based hydrogel

Scale bars = 200 μm (left) and 100 μm (mid).

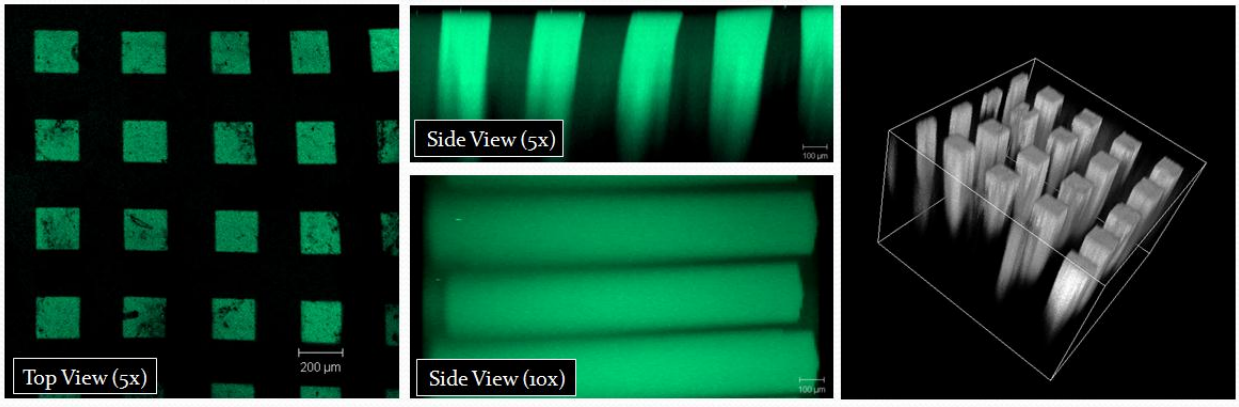

3.6.9 Additional illustration of 2-photon patterning within click-based hydrogel

False coloring was used to enhance reader visualization. Scale bar = 50 μm.

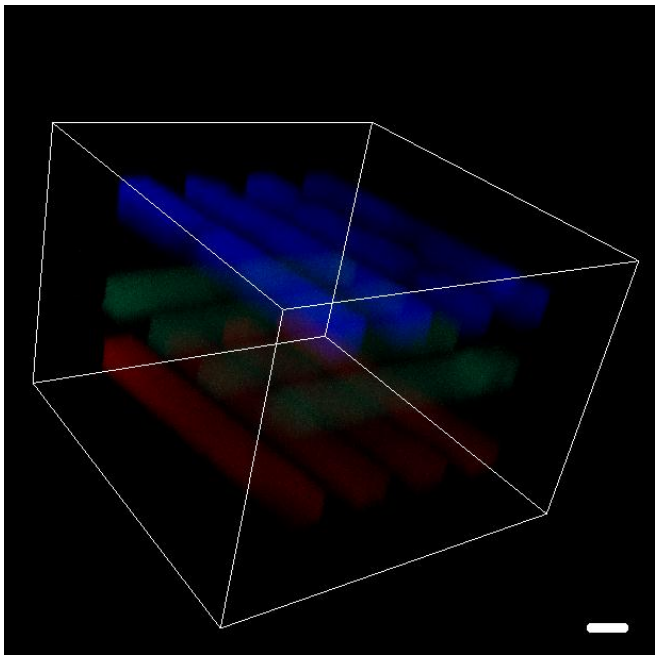

3.6.10 Patterning of multiple peptides within a single gel

AF_{488}-AhxRGDSC-NH_2 was first swollen into a gel at 3 mg/mL in 0.05 wt% I2959 in clear media for one hour. 365 nm light was exposed to the gel through a photomask at 10

mW/cm2 for 10 min. The gel was then placed in media for two hours to swell out any unreacted material. The process was repeated again for AF_{546}-AhxPHSRNC-NH_2 and then AF_{405}-AhxKRTGQYKLC-NH_2, the full process taking ~10 hours. The pattern was subsequently imaged using confocal microscopy. Images represent a single optical slice within the hydrogel. AF_{546}-AhxPHSRNC-NH_2 is shown in red on the top left, AF_{405}-AhxKRTGQYKLC-NH_2 in blue on the top right, and AF_{488}-AhxRGDSC-NH_2 in green on the bottom left. The overlay of all peptides is shown in the bottom right. Scale bar = 100 μm.

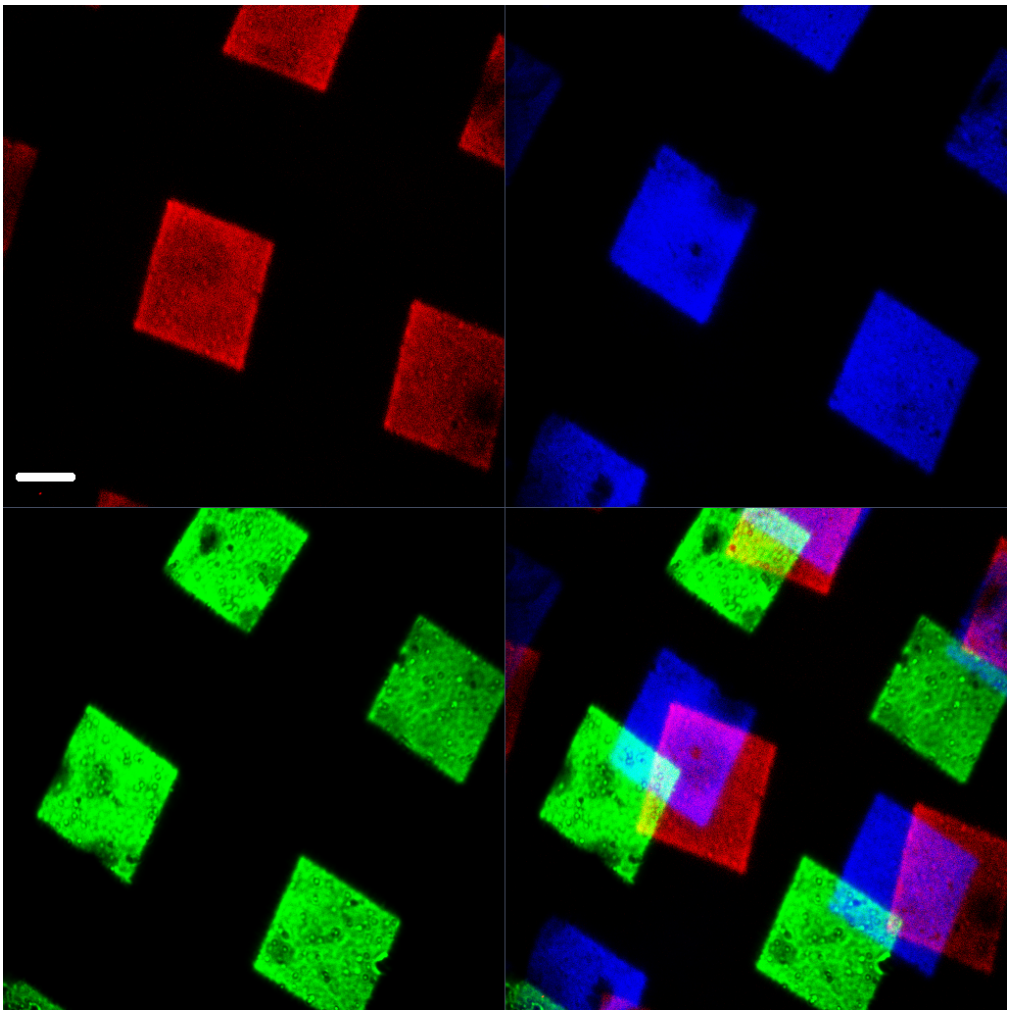

3.6.11 Synthesis and ^{1}H NMR of four-arm PEG Tetraazide (MW~10000)

5 grams of 4-arm poly(ethylene glycol) (M_n ~ 10,000 Da) (Jenkem) was dried overnight and dissolved in a 4:1 mixture of dichloromethane:pyridine under argon at 0 °C. Methanesulfonyl chloride (1.15 g, Sigma) dissolved in minimal DCM was added dropwise over 10 minutes in a five-fold molar excess to hydroxyl groups and allowed to react overnight. The solution was concentrated, washed with sodium bicarbonate (Fisher), dried over $MgSO_4$ (Fisher), and precipitated in diethyl ether (Fisher). ^{1}H NMR (DMSO-d6): 4.30 (8H, m, 4 x MsOCH_2), 3.67 (8H, m, 4 x MsOCH$_2$ CH_2), 3.47-3.57 (m, [CH_2CH_2O]$_n$), 3.18 (12H, s, 4 x CH_3SOO-). The activated mesylate was co-dissolved with 5 molar excess sodium azide (650 mg, Fluka) in 10 mL anhydrous DMF and stirred overnight under argon at 80 °C. The precipitate was removed *via* Celite filtration and subsequently concentrated. The product was dissolved in distilled water and dialyzed for two days and lyophilized to give the desired product. ^{1}H NMR ($CDCl_3$): 3.50-3.77 (m, CH_2[CH_2CH_2O]$_n$CH_2), 3.39 (8H, m, 4 x CH_2N$_3$).

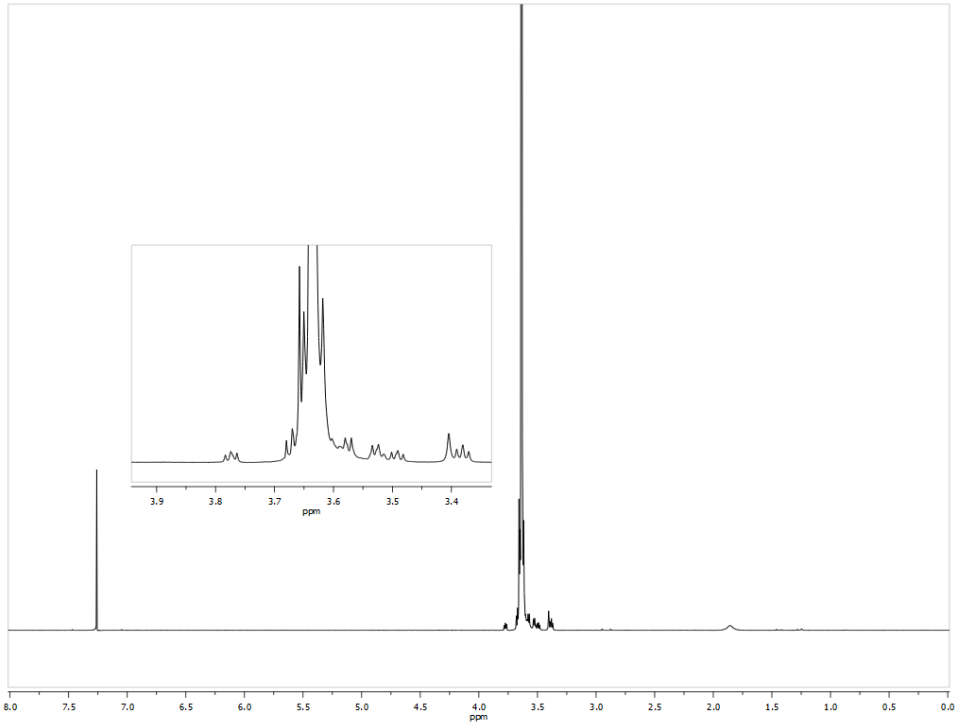

CHAPTER IV

PEPTIDE-FUNCTIONALIZED CLICK HYDROGELS WITH INDEPENDENTLY TUNABLE MECHANICS AND CHEMICAL FUNCTIONALITY FOR 3D CELL CULTURE

As published in *Chemistry of Materials*, 22, 4783-4790 (2010).

4.1 Abstract

Click chemistry offers highly selective and orthogonal reactions that proceed rapidly and under a variety of mild conditions with the opportunity to create highly defined and multifunctional materials. This work illustrates a strategy where step-growth networks are formed rapidly *via* a copper-free, azide-alkyne click chemistry between tetrafunctional poly(ethylene glycol) molecules and difunctionalized synthetic polypeptides. The molecular weight of the polymer precursors (10, 15, or 20 kDa PEG) and the stoichiometry of reactive end group functionalities (1.5:1 – 1:1.5) provide control over the material crosslinking density, enabling elastic materials with tunable moduli (G' = 1000 – 6000 Pa). A sequential photochemically-activated thiol-ene chemistry allows subsequent functionalization of the network through reaction with pendant alkene moieties on the peptide. Since the thiol-ene reaction is light-driven, the degree of modification is directly related to the dosage of light delivered to the system (0 – 6 J cm^{-2}). We exploit this feature to create complex biochemical gradients of multiple peptides with well-defined magnitude and slope throughout the three-dimensional (3D) network. Since both reactions can occur in the presence of cells, this material ultimately enables independent and *in situ* tuning of biochemical and biomechanical properties of

biomaterial networks, suggesting an avenue to direct cell function throughout specific regions within a 3D material.

4.2 Introduction

There is a growing interest to develop and utilize peptide-functionalized poly(ethylene glycol) (PEG) hydrogels for 3D cell culture applications.[1-3] Peptides are readily designed to incorporate integrin-binding epitopes (e.g., the fibronectin-derived RGD sequence),[4-7] enzymatically-degradable sequences (e.g., the collagenase-sensitive sequence GPQG↓ILGQ),[8-10] growth-factor sequestering properties (e.g., the basic fibroblast growth factor-binding KRTGQYKL sequence),[11-13] as well as additional bioactivity[14-17] into otherwise bioinert hydrogel material formulations. The inclusion of peptides within cell-laden hydrogel matrices enables tailorability of a cell's microenvironment and potential control over the biological fate of encapsulated cells. Their ease of synthesis and purification render peptides as viable options for material functionalization. Additionally, peptides can be systematically engineered and modified with a variety of non-natural amino acids,[18] ultimately enabling a greater level of synthetic biological control than their complex biomacromolecular counterparts.

Taking lead from a variety of reactions originally developed for organic synthesis, many techniques have been utilized to incorporate peptides into hydrogel materials. Most commonly, monoacrylated PEG-*N*-Hydroxysuccinimide (NHS) is coupled to the N-terminal α-amino group to yield an acrylated peptide, which can be copolymerized within PEG acrylate-based polymer networks.[19-22] The photoinitiated solution polymerization of these molecules yields hydrogel systems that are useful for cell encapsulation, but are quite heterogeneous and polydisperse in their crosslinking density.[23] Alternatively, the Michael-type addition reaction has been used to generate step-growth networks which exhibit more uniform crosslinking densities, and do not

require post-synthetic modification of the peptide sequence. In this reaction, cysteine-containing peptides (which include pendent thiols) are coupled to PEG with electron-poor olefin end groups (such as an acrylate or vinyl sulfone) under slightly basic conditions.[24-26] More recently, a photoinitiated thiol-ene hydrogel platform, which combines the advantages of step-growth and photoinitiated polymerization has been used to form enzymatically-degradable peptide-functionalized PEG gels, similar in structure to the Michael-addition reaction.[27] Further, the spatial and temporal regulation of the photopolymerization affords an additional level of control over network formation. Finally, the mixed-mode polymerization of acrylates in the presence of thiols enables non-stoichiometric amounts of cysteine-containing peptides to be directly incorporated into materials.[28] The combination of chain and step growth mechanisms give rise to networks with unique structure, where polyacrylate kinetic chains are truncated with single peptides, but the amount of peptide functionalization directly influences network structure and resulting gel mechanics. While the interest in and application of peptide-functionalized PEG gels continues to grow, we sought to use a combination of orthogonal reactions to first form peptide-functionalized hydrogels with defined structures and mechanical properties and then to modify subsequently these materials with user-defined biochemical functionalities without altering the underlying network structure.

The recent advent of click chemistry, an organic paradigm for robust, highly-efficient, highly-specific reactions,[29,30] has led to novel means to create peptide-functionalized biomaterials.[31] The orthogonal nature of these reactions ultimately allows for peptide introduction into materials both initially, as well as post-gelation without altering the initial network structure[32]. The quintessential click reaction, the copper(I)-catalyzed 1,3-dipolar Huisgen cycloaddition between azides and alkynes (CuAAC),[33] has been utilized for peptide

ligation,[34,35] modification,[36,37] macrocyclization,[38,39] and polymer grafting.[40,41] Unfortunately, this reaction's catalyst, as with the majority of those reactions commanding "click" status, is cytotoxic and is unable to be performed in the presence of cells, thereby precluding its usage in the formation of peptide-functionalized materials for cell encapsulation. Recently, a novel cyclooctyne molecule (DIFO3) was developed whose ring strain and electron-withdrawing fluorine substituents give rise to an activated alkyne that reacts quickly with azides in the absence of a catalyst.[42-44] This strain-promoted azide-alkyne cycloaddition (SPAAC) has enabled the application of the Huisgen reaction in living organisms to label glycosylation patterns in zebrafish and mice.[45] Similarly, the photoinduced thiol-ene reaction, a radical-mediated addition of a thiol across an olefin, has recently gained attention as an emerging click reaction.[46,47] In addition to being fully bioorthogonal and biocompatible, this reaction is advantageous in that it can be controlled spatially and temporally with the presentation of light.[27] The cytocompatible nature of these two click reactions render them particularly well-suited for biomaterial synthesis and functionalization.

Beyond simply creating peptide-functionalized hydrogels, we are interested in developing and exploiting these constructs to study 3D cell behavior dynamically. Recently, we introduced a two-component hydrogel system that is capable of directing and detecting 3D cell behavior at user-defined locations within the material.[48] This system, comprised of a four-arm PEG tetraazide and a bis(cyclooctyne)-peptide, utilizes two orthogonal click reactions; one for hydrogel formation (SPAAC) and another for biochemical patterning (thiol-ene). Ultimately, this formulation leads to an ideal, step growth network that enables control of the material crosslinking density and the ability to introduce pendant biochemical functionalities through the photochemical thiol-ene reaction. Exploiting these chemistries, this manuscript sought to

understand how the molecular weight and (non)stoichiometric reaction of the precursor molecules could be used to control the final material mechanical properties. Subsequently, we quantified aspects of the thiol-ene photocoupling reaction and demonstrate the advantages of the photochemical reaction in forming complex chemical gradients of multiple peptides within the same material with precise control over location and concentration. We expect that these unique gels will prove particularly beneficial in elucidating the unique role of mechanotransduction versus biochemical signaling on cell function in a well-defined 3D environment.

4.3 Results and Discussion

4.3.1 Mechanical Tunability of Click-based Hydrogels

Design of the Base Hydrogel Network

To illustrate the utility that is afforded by multiple bioorthogonal chemistries, we have developed a two-component system that enables hydrogel formation with tunable mechanics. Here, a four-arm PEG tetraazide is reacted with a bis(DIFO3) difunctional polypeptide crosslinker in an aqueous environment to form a multifunctional hydrogel (Scheme 4.1). PEG is chosen due to its biocompatibility, hydrophilicity, and resistance to non-specific protein adsorption. By ensuring minimal protein interaction with this base material, only specifically desired biofunctionality is incorporated into the system. Additionally, the biophysical properties of the gel are readily tuned by altering the length of the PEG arms as well as the stoichiometric ratio of azide:alkyne on the PEG and peptide crosslinker, respectively. Biological functionality is introduced into the matrix backbone *via* the choice of the synthetic crosslinking peptide sequence. Here, we utilize a functionalized matrix metalloproteinase cleavable sequence (GPQG↓ILGQ) that is susceptible to secreted enzymes, enabling cell-dictated local network degradation and material reformation.[49] Enzymatically-degradable hydrogels enable cells to

spread and migrate throughout the material and yield a significantly more viable population as compared to their non-degradable counterparts.[8,9] Furthermore, by utilizing a synthetic peptide crosslinker with a pendant functional group, we are able to introduce additional chemical moieties into the material at later time points or in spatially-defined regions.

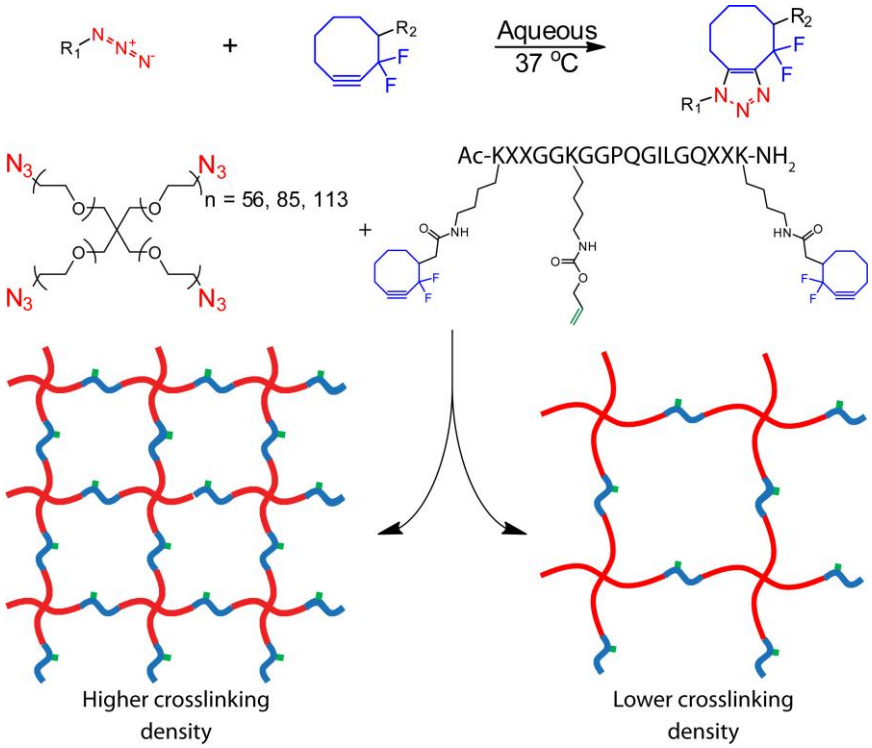

Scheme 4.1. Click-functionalized macromolecular precursors react *via* the strain-promoted [3 + 2] Huisgen cycloaddition to form an end-linked hydrogel network. By varying the molecular weight of the PEG, well-defined networks of differing crosslinking density are formed.

When the PEG tetraazide is mixed with the difunctionalized peptide, an end-linked polymerization occurs spontaneously and yields an idealized network with minimal defects and local heterogeneities. The nearly-ideal structure of this system has been previously confirmed with rheological and magic-angle spinning NMR experiments[48] and agrees with previous work with click-based networks.[50] Though the gel is formed in just a few minutes, reaction continues for ~1 hr at which point all previously-detectable azide and cyclooctyne functional groups have

been consumed. This formulation is fully cytocompatible and has been successfully used for the encapsulation of primary cells, as well as established cell lines, with high viability.[48]

Effect of PEG Size and Network Connectivity on Mechanical Properties

We first sought to determine the effects of different PEG molecular weights on the resulting hydrogel network structure and elasticity. For this, we synthesized 10, 15, and 20 kDa 4-arm PEG tetraazide, spanning a two-fold range of average repeat units per arm (~56, 85, and 113 respectively). The functionalized (>95%) PEGs were then combined with a base peptide [AcK(DIFO3)RRGGK(alloc)GGPQGILGQRRK(DIFO3)-NH_2] in a 13.5 wt% aqueous solution containing a stoichiometrically-balanced amount of azide and alkyne moieties. After formation, these gels were allowed to equilibrate overnight in phosphate buffered saline (PBS) upon which rheological frequency sweep experiments were conducted to determine the shear elastic moduli of the constructs (Figure 4.1a). In addition, equilibrium swelling ratios (q) were calculated as the mass of the swollen network divided by that of the dry system (Figure 4.1b).

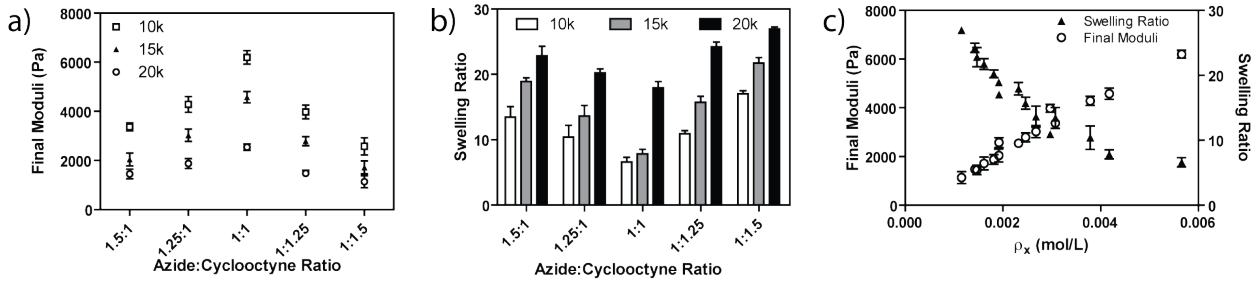

Figure 4.1 Final mechanical properties are dictated by gel formulation. a) The swollen hydrogel shear elastic moduli are easily tuned by changing the molecular weight of the PEG crosslinker (□ = 10,000 g/mol, ▲=15,000 g/mol, ○ = 20,000 g/mol). Alternatively, small stoichiometric imbalances between the gel-forming azide and cyclooctyne reactive groups also give rise to materials with a wide range of moduli. b) Changes in gel formulation result in hydrogels with different equilibrium swelling ratios (in PBS). c) The swelling ratio (▲) and equilibrium shear moduli (○) data scale for all conditions when normalized to crosslinking density. Data reported as mean ± std.

The shear moduli and overall water content varied significantly between formulations and were found to be directly related to the swollen hydrogel crosslinking density (ρ_x) (Figure

4.1c). For these networks, the ideal crosslinking density during network formation ($\rho_{x,0}$) is equal to twice the concentration of PEG tetraazide multiplied by *r*, the ratio of azide to alkyne functionalities such that $0 \leq r \leq 1$, since each arm of the PEG azide is attached to half an infinite chain.[51] The gels containing the lowest molecular weight PEG (10 kDa, ρ_x = 0.0048 mol/L) resulted in the highest moduli (6200 ± 280 Pa) and lowest swelling (6.6 ± 0.7), while those with the highest molecular weight PEG (20 kDa, ρ_x = 0.0027 mol/L) gave rise to the lowest observed moduli (2500 ± 220 Pa) and highest swelling (17.9 ± 0.9).

Since small stoichiometric imbalances can lead to significant changes in ρ_x, we quantified the changes in the elastic modulus and *q* for systems of varying ratios of azide to alkyne. Specifically, we created gels for each of the three PEG molecular weights (MWs) and the base peptide, this time varying the overall ratio of azide to alkyne functionality (1.5:1, 1.25:1, 1:1.25, and 1:1.5), and measured the resulting equilibrium swelling ratio (Figure 4.1a) and shear moduli (Figure 4.1b). Here, we find that the overall network stiffness decreases rapidly as the formulation departs from 1:1 stoichiometry with relatively modest deviations from unity resulting in large changes in mechanical properties. With one of the reactive groups in excess, a network containing fewer overall crosslinks is formed (as $r < 1$). Again, with a lower ρ_x in the system, we observe a lower elastic moduli and a higher swelling ratio (Figure 4.1c). This trend is consistent through all chosen MWs of PEG and all stoichiometries.

By comparing the obtained gel moduli and swelling ratios with that expected for a perfect system with a given $\rho_{x,0}$, the degree of network ideality can be estimated.[51] When two azide functional groups on the same PEG molecule react with both cyclooctyne moieties present on a given peptide, a primary cycle is formed. This defect fully removes the ability of the PEG molecule to form crosslinks, rendering it to behave like a difunctional linker, and lowers the final

moduli. Similarly, when the tetrafunctional PEG contains two primary cycles, it will no longer be connected to the network and becomes part of the sol fraction. For all formulations containing an equal ratio of azide to cyclooctyne functionality, we estimate the degree of network ideality (i.e., extent of crosslinking versus cyclization) to be >90% (derivations and results for all formulations are given in Supplementary Section 3.7.1).

Effect of Peptide Sequence and Charge on Network Properties

To determine the effect of the crosslinker composition on the hydrogel mechanical properties, various peptides were synthesized and gels were formed with each PEG tetraazide. We first sought to determine whether the order of amino acids in our peptide sequence had a significant effect on the gels' resulting properties. We created a scrambled peptide sequence [Ac-K(DIFO3)QGK(alloc)RIPGRRLGGRGQGK(DIFO3)-NH_2], which contained all of the internal amino acids of the original sequence in a randomly rearranged order. We find that the equilibrated shear elastic moduli of these stoichiometrically-balanced scrambled systems are statistically indistinguishable from those of the original peptide sequence (Figure 4.2a). Similarly, we were interested in determining the effect of overall peptide charge on moduli values. For this, we synthesized charge neutral [AcK(DIFO3)R<u>E</u>GGK(alloc)GGPQGILGQ<u>E</u>RK(DIFO3)-NH_2] and negatively charged [-4, AcK(DIFO3)<u>EE</u>GGK(alloc)GGPQGILGQ<u>EE</u>K(DIFO3)-NH_2] peptide variants to complement our positively charged (+4) base peptide. Here, we find that the resulting equilibrated moduli are not statistically different from one another for the 10 kDa PEG system (Figure 4.2b). This is likely due to a charge-shielding effect of the buffered PBS solution that the gel imbibes. Ultimately, this enables the sequence of the peptide crosslinker to be altered without significant changes in gel mechanics under conditions for cell culture.

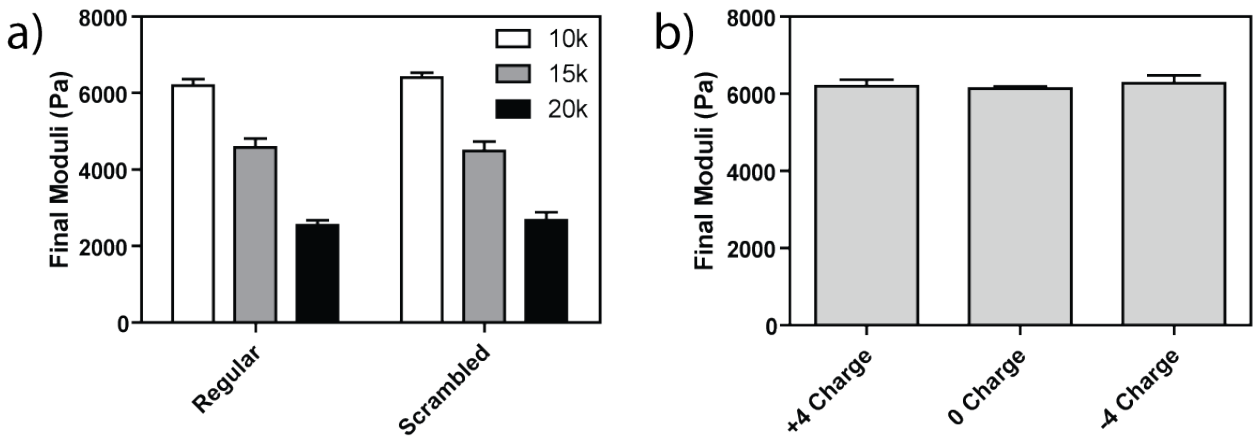

Figure 4.2 Network properties are largely independent of peptide crosslinker properties in buffered solutions (pH = 7.4). a) The amino acids sequence does not influence the shear elastic moduli of formed gels. b) Similarly, the overall charge of the peptide does not influence the mechanical properties of the formed networks. Data reported as mean ± std.

4.3.2 Biochemical Patterning within Click-based Hydrogels

Incorporating Biochemical Tunability into Base Hydrogel

An additional benefit of using a synthetic peptide crosslinker to form our hydrogel network is that we are able to dictate precisely its sequence to include a variety of biological functionalities, as well as to include non-natural amino acids that enable additional modification of the system post-gelation independent of the network mechanics. Here, we chose to include a photoreactive allyl ester within the peptide sequence *via* the commercially available Fmoc-Lys(alloc)-OH amino acid, which enables relevant biomolecules to be covalently coupled pendent to the hydrogel backbone *via* the bioorthogonal thiol-ene click reaction (Scheme 4.2). Though allyloxycarbonyl (alloc) was originally designed as a selectively-removable protecting group for peptide branch creation, it contains a vinyl group capable of undergoing the thiol-ene reaction with any thiol-containing molecule, including cysteine.[32,52] This protecting group is fully stable to Fmoc deprotection and trifluoroacetic acid peptide cleavage from resin. The electron-rich alloc allyl ester is not susceptible to the non-specific Michael-type addition,

ensuring that chemical immobilization is confined to user-defined regions of interest within the material.[53]

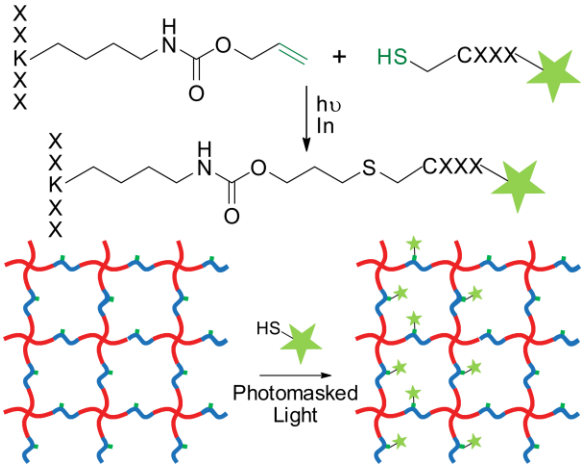

Scheme 4.2 Post gelation, cysteine-containing peptides are covalently affixed pendent to the hydrogel backbone *via* the radical-mediated thiol-ene reaction. Using a photoinitiator, chemical radical generation is confined to areas of light exposure, ultimately enabling spatial patterning control throughout the material.

The thiol-ene reaction is a radical-mediated addition of a thiol to an alkene, involving a sequential propagation of a thiyl radical with a vinyl functional group followed by a chain transfer of the radical to another thiol.[54] Thiyl radicals can be readily generated *via* the photocleavage of a hydrogen-abstracting initiator. Here, thiyl radicals are only generated in the presence of UV light, ultimately dictating when, where, and how much of the thiol-ene functionalization will occur. After functionalization is complete, unreacted thiols are allowed to diffuse out of the network, leaving the covalently-patterned substrate behind (Scheme 4.2). Additionally, spatially-controlled patterns can be formed in 3D using focused multi-photon laser light.[48]

Controlling Patterning Extent with Light Dosage and Initiator Concentration

Upon swelling cysteine-containing peptides and photoinitiator into the preformed hydrogel, UV light was used to induce thiol-ene functionalization within the network. By

varying the amount of photoinitiator present (1.1, 2.2, 4.4, and 8.8 mM Irgacure 2959, 2-Hydroxy-1-[4-(2-hydroxyethoxy)phenyl]-2-methyl-1-propanone), as well as the total dosage of light imposed on the system (0.6, 1.8, 3.0, and 6.0 J cm^{-2}), we control the extent of ene conversion, ultimately dictating the patterning concentrations of peptide within our materials. Here, fluorescently-labeled peptides (AF_{488}-AhxRGDSC-NH_2 and AF_{546}-AhxPHSRNC-NH_2) are patterned into the network and the system's resulting fluorescence is used to quantify the resulting concentration range. For a given light dosage, we find that the degree of patterning scales roughly linearly with the photoinititiator concentration (Figure 4.3a). Similarly, for a given amount of photoinitiator, we find that the patterning concentration scales roughly linearly with the light dosage. Interestingly, the patterning concentrations for a given condition remains nearly constant throughout the full ~1 mm thickness of the gel (Figure 4.3b).

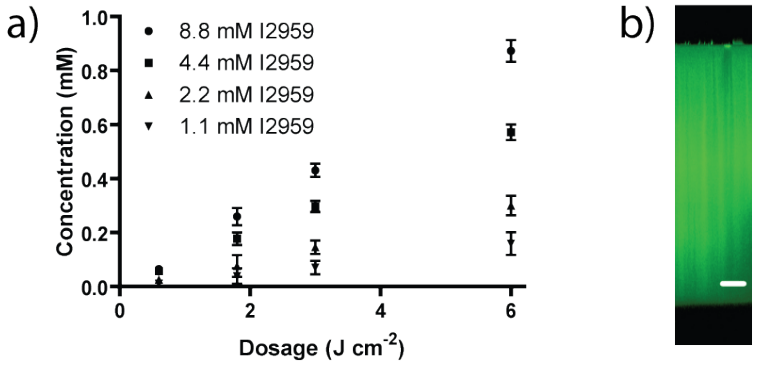

Figure 4.3 Patterning concentration depends on the photoinitiator concentration and the total light dosage delivered to the system. a) By varying the amount of photoinitiator present, we are able to control the level of patterning concentration for a given dosage (▼ = 1.1 mM, ▲ = 2.2 mM, □ = 4.4 mM, ○ = 8.8 mM photoinitiator I2959). b) As the light intensity remains near-constant throughout the thickness of the gel, patterning concentration is largely uniform throughout the entirety of the gel. Data reported as mean ± std. Scale bar = 200 μm.

For thiol–ene polymerizations, the rate of reaction (R_p) is given as:

$$R_p = -\frac{\mathrm{d}[\mathrm{C}=\mathrm{C}]}{\mathrm{d}t} = k[\mathrm{C}=\mathrm{C}][\mathrm{S}\cdot] \qquad (1)$$

where [C=C] is the ene concentration, [S·] is the thiyl radical concentration, and k is the reaction rate constant.[54] In this system, both the alkene (~20 mM) and thiol (~10 mM) functionalities are in significant excess with regards to the patterned concentrations obtained (~1 mM). Since only a small portion of the total ene functionality is consumed (<5%) in any one of our patterning experiments, the [C=C] is taken as a largely unchanging constant, leaving R_p only as a function of [S·] (i.e., pseudo-first order reaction). Additionally, the thiyl radical concentration directly depends on the rate of photoinitiation (R_i) given by:

$$R_i = \frac{2.303 f \varepsilon [\mathrm{I}] I_0 \lambda}{N_{AV} h c} \qquad (2)$$

where f = initiator efficiency, ε = molar absorptivity of initiator, [I] = initiator concentration, I_0 = light intensity, N_{AV} = Avogadro's number, h = Planck's constant, and c = speed of light.[54] Since <2% of the total initiator is consumed in any one of our patterning experiments (Supplementary Section 3.7.2), [I] can also be approximated as a constant, implying that overall degree of patterning is proportional to the light dosage and the initiator concentration. This result is consistent with our experimental findings. For example, for 4.4 mM I2959 a dosage of 6 J cm^{-2} results in 0.57 ± 0.03 mM patterning. Halving the dosage to 3 J cm^{-2} gives half the patterning (0.29 ± 0.02 mM) with the same I2959 concentration, while halving the amount of initiator to 2.2 mM I2959 with the same light conditions also results in half the patterning amount (0.30 ± 0.04 mM). Thus, the patterning concentration is observed to be roughly linear with light dosage and initiator concentration.

Generation of Peptide Gradients Throughout Hydrogel

Having established a relationship between light dosage and patterning concentration, we were interested in utilizing this information to create well-defined complex biochemical

gradients within a hydrogel. Hydrogels were exposed to a linear gradient of light exposure generated by a moving photomask (Supplementary Section 3.7.4),[55] resulting in a linear gradient of AF_{488}-AhxRGDSC-NH_2 patterning concentrations (Figure 4.4a). By varying the rate of photomask coverage (0.05, 0.1, or 0.2 cm min^{-1}), the chemical gradient slope was precisely tuned (Figure 4.4b). As only a fraction of the available alkene functionalities are consumed in any given patterning process, the thiol-ene process can be repeated to pattern multiple epitopes within a single sample. This was exploited to introduce sequential and independent gradients of arbitrarily chosen slope of multiple peptides (AF_{488}-AhxRGDSC-NH_2 and AF_{546}-AhxPHSRNC-NH_2) within the same material (Figure 4.4c). By shuttering the light as it is delivered to the system, stepped gradients are easily created (Figure 4.4d). 3D biochemical gradients are of particular note to those interested in studying fundamental biological processes *in vitro*, including induced cell migration and alignment with RGD[56] and directed neurite extension with nerve growth factor gradients.[57]

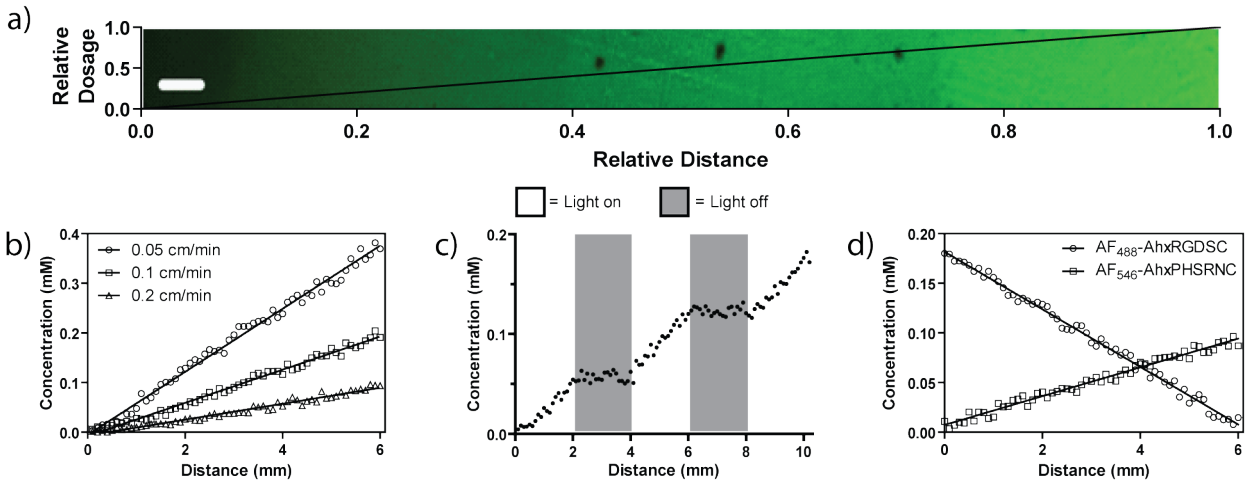

Figure 4.4 Biochemical gradients are created throughout the hydrogel network. a) By subjecting the hydrogel to a linear gradient of light exposure, well-defined gradients of fluorescent patterning agents are created across relatively large distances. b) These magnitude of these gradients is readily controlled by tuning the slope of the light gradient. c) Multiple peptide gradients are patterned within the same material. d) Using a stepped gradient of light exposure, a stepped patterning concentration is obtained. Scale bar = 200 μm.

4.4 Materials and Methods

4.4.1 Synthesis of poly(ethylene glycol) tetraazide

4-arm PEG (M_n ~ 10, 15, or 20 kDa) (0.5 mmol, Jenkem) was dried overnight in a vacuum oven and dissolved at 0 °C in a 20% mixture of pyridine in dichloromethane (DCM) under argon. A solution of methanesulfonyl chloride (1.15 g, 10 mmol, 5x/OH, Sigma) dissolved in minimal DCM was added over 10 minutes *via* syringe pump and allowed to react overnight. This solution was concentrated, washed with saturated Na_2HCO_3 (Fisher), dried over $MgSO_4$ (Fisher), and precipitated in ice-cold diethyl ether (Fisher). ^{1}H NMR (500 MHz, DMSO-d_6, δ): 4.30 (m, 8H; 4 x MsOC*H*$_2$), 3.67 (m, 8H; 4 x MsOCH$_2$C*H*$_2$), 3.57-3.47 (m, [C*H*$_2$C*H*$_2$O]$_n$), 3.18 (s, 12H; 4 x C*H*$_3$SOO-). The activated mesylate was dissolved in anhydrous dimethylformamide containing sodium azide (650 mg, 10 mmol, 5x/Ms, Fluka) and stirred over night at 80 °C under argon. The reaction was filtered through Celite and concentrated. The product was dissolved in deionized water and dialyzed for 48 hours (MWCO ~ 2 kDa, SpectraPor). The solution was lyophilized to yield the desired product. The functionality was determined as >95% for all products. ^{1}H NMR (500 MHz, $CDCl_3$, δ): 3.77-3.50 (m, [C*H*$_2$C*H*$_2$O]$_n$), 3.39 (m, 8H; 4 x C*H*$_2$N$_3$) (Supplementary Section 3.7.3).

4.4.2 Synthesis of difluorinated cyclooctyne (DIFO3*)*

DIFO3 was synthesized following a published synthetic route.[44] Briefly, 1,3-cyclooctanedione was difluorinated followed by a Wittig reaction to introduce an orthoester linker handle. The remaining ketone was converted to its vinyl triflate, and cyclooctyne was generated *via* a lithium diisopropylamide-mediated elimination. Finally, the orthoester was deprotected to yield the DIFO3 carboxylic acid product. ^{1}H NMR (500 MHz, $CDCl_3$, δ): 11.72 (br s, 1H), 2.82-2.69 (m, 2H), 2.43-2.22 (m 3H), 2.19-2.05 (m, 2H), 1.87-1.74 (m, 2H), 1.70-1.61

(m, 1H), 1.45-1.35 (m, 1H); ^{13}C NMR (101 MHz, $CDCl_3$, δ): 178.53 (s), 119.10 (dd, J = 237.7, 239.4), 110.71 (t, J = 11.1 Hz) 84.62 (dd, J = 41.6 Hz, 46.9), 52.60 (t, J = 24.3 Hz), 33.80 (d, J = 3.1 Hz), 32.84 (d, J = 4.5 Hz), 32.65 (d, J = 1.9 Hz), 27.87 (s), 20.45 (s); ^{19}F NMR (376 MHz, $CDCl_3$, δ): -95.84 (d, J = 259.9; 1F), -102.05 (ddt, J = 7.0, 21.1, 260.2; 1F); HRMS (ESI+): calculated for $C_{10}H_{12}F_2LiO_2^+$ $[M + {}^7Li]^+$, 209.0960; found 209.0965 (Δ = +2.5 ppm). NMR spectra are found in Supplementary Section 3.7.5-7.

4.4.3 Peptide synthesis and modification

Peptide sequences (Ac-KRRGGK(alloc)GGPQGILGQRRK-NH_2, regular; Ac-KQGK(alloc)RIPGRRLGGRGQGK-NH_2, scrambled; Ac-KREGGK(alloc)GGPQGILGQERK-NH_2, neutral; Ac-KEEGGK(alloc)GGPQGILGQEEK-NH_2, negative) were synthesized (Protein Technologies, Inc. Tribute Peptide Synthesizer) though standard Fmoc solid-phase methodology and 2-(1H-benzotriazole-1-yl)-1,1,3,3-tetramethyluronium hexafluorophosphate/N-hydroxybenzotriazole (HBTU/HOBt) activation. Resin was treated with trifluoroacetic acid/triisopropylsilane/water/phenol (94:2.5:2.5:1) for 3 h and precipitated and washed (3x) in ice-cold diethyl ether. DIFO3 was coupled to the ε-amino groups of the terminal lysines *via* standard 2-(7-aza-1H-benzotriazole-1-yl)-1,1,3,3-tetramethyluronium hexafluorophosphate (HATU) coupling chemistry. Peptides were purified using a semipreparative reversed-phase high-performance liquid chromatography (RP-HPLC) (Waters Delta Prep 4000) using a 70 minute linear gradient (5 to 95%) of acetonitrile and 0.1% trifluoroacetic acid (Sigma). Peptide purity was confirmed by analytical RP-HPLC and matrix-assisted laser desorption, ionization time-of-light (MALDI-TOF) mass spectrometry (Applied Biosystems DE Voyager) using α-cyano-4-hydroxycinnamic acid matrix (Sigma). Regular calculated ($[M+H]^+$ 2442.793); observed ($[M+H]^+$ 2441.815); scrambled calculated ($[M+H]^+$ 2442.793); observed ($[M+H]^+$

2443.159); neutral calculated ($[M+H]^+$ 2388.649); observed ($[M+H]^+$ 2388.568); negative calculated ($[M+Na]^+$ 2357.471); observed ($[M+H]^+$ 2357.205). MALDI spectra are found in Supplementary Section 3.7.8-11.

4.4.4 Synthesis of fluorescently-labeled patterning agents

H-AhxRGDSC-NH_2 and H-AhxPHSRNC-NH_2 (0.25 mmol) were synthesized *via* standard Fmoc solid-phase methodology and HBTU/HOBt activation. Fluorescent activated esters [Alexa Fluor® 488 carboxylic acid, 2,3,5,6-tetrafluorophenyl ester (1 mg, Invitrogen) for H-AhxRGDSC-NH_2 and Alexa Fluor® 546 carboxylic acid, succinimidyl ester (1 mg, Invitrogen) for AhxPHSRNC-NH_2] were dissolved in NMP with a catalytic amount of DIEA and stirred with respective resins overnight at room temperature. Resins were treated with trifluoroacetic acid/triisopropylsilane/water/dithiothreitol (94.5:2.5:2.5:0.5) for 1 hour and precipitated and washed (3x) using ice-cold diethyl ether. These products, denoted as AF_{488}-AhxRGDSC-NH_2 and AF_{546}-PHSRNC-NH_2, were used with no further purification.

4.4.5 Hydrogel formation

Four-arm PEG tetraazide was reacted with bis(DIFO3) di-functionalized polypeptides in an aqueous environment at room temperature. Component concentrations were based on a 13.5 wt% total macromer content for a variety of differing stoichiometric ratios of azide to alkyne functionality (1.5:1, 1.25:1, 1:1, 1:1.25, 1:1.5). Gels were allowed to swell in PBS overnight prior to patterning or mechanical testing.

4.4.6 Rheological characterization of hydrogel equilibrium properties

Dynamic rheometry was performed with parallel plate geometry on an ARES 4400 rotational rheometer (TA Instruments). Frequency sweep experiments (10% strain, $\omega = 1 – 100$

rad s^{-1}) were conducted on equilibrated hydrogels of known geometry (7 mm diameter x 1 mm tall disks). Gel moduli were determined within the linear viscoelastic regime for each sample.

4.4.7 Biochemical patterning

Hydrogels were swollen in PBS (pH = 7.4) containing Irgacure 2959 (1.1, 2.2, 4.4, or 8.8 mM, I2959, Ciba) and 10 mM patterning agent (AF_{488}-AhxRGDSC-NH_2 or AF_{546}-PHSRNC-NH_2) for one hour. Using conventional photolithographic techniques, gels were exposed to collimated UV light (365 nm wavelength at 10 mW cm^{-2}) for various times (1, 3, 5 or 10 min). After patterning is complete, the gel is washed for approximately two hours with fresh PBS to remove any unbound material, yielding the final patterned hydrogel. For gradient patterned hydrogels, a light gradient (365 nm at 10 mW cm^{-2} for 0 – 12 min of exposure time) was achieved by irradiating the hydrogel containing 2.2 mM I2959 and 10 mM patterning agent while a unidirectional moving photomask continuously covers the hydrogel at a predetermined rate (0.5, 1.0, or 2.0 cm min^{-1}).[55] For step-gradient formation, the light was shuttered on and off while the photomask continued to cover the sample at a fixed rate. Patterning concentrations were determined using confocal microscopy by comparing the fluorescence intensity at a point 200 μm below gel surface against a standard curve relating fluorescence intensity to that of gels swollen in known concentrations of the patterning agent (Supplementary Section 3.7.12). Light dosage was calculated as the product of the intensity and the exposure time.

4.5 Conclusions

In conclusion, we developed a versatile click-based PEG/peptide hydrogel system whose biomechanical properties are precisely tuned by altering the crosslinking density and network connectivity of the system. This was accomplished by (1) changing the molecular weight of the PEG crosslinker and (2) off-stoichiometric network polymerization. In classic cell culture

buffers, the sequence and charge of the peptide were found to have little effect on the mechanical properties of the gel. By incorporating a photoreactive alkene functionality pendent to the hydrogel backbone, we were able to exploit the thiol-ene click reaction for spatially-controlled, full-thickness network functionalization of cysteine-containing peptides. We demonstrate that the degree of patterning within the network is directly proportional to the dosage of light imposed on the system as well as to the initiator concentration. Exploiting this finding, we used gradients of light to synthesize well-defined linear chemical gradients of defined slope throughout a gel. This process is fully additive, and gradients of multiple peptides are easily achieved. Though not explicitly demonstrated in this work, both network formation and subsequent patterning reactions are fully cytocompatible. As such, this system can be utilized to elucidate systematically the effects of individual chemical cues in addition to gradients of multiple cues on individual cell behavior, as well as to spatially direct 3D stem cell differentiation.

4.6 References

1. Tibbitt, M.W. & Anseth, K.S. Hydrogels as extracellular matrix mimics for 3D cell culture. *Biotechnol. Bioeng.* **103**, 655-663 (2009).

2. Cushing, M.C. & Anseth, K.S. Hydrogel cell cultures. *Science* **316**, 1133-1134 (2007).

3. Lutolf, M.P., Raeber, G.P., Zisch, A.H., Tirelli, N. & Hubbell, J.A. Cell-responsive synthetic hydrogels. *Adv. Mater.* **15**, 888-892 (2003).

4. Ruoslahti, E. & Pierschbacher, M.D. New perspectives in cell-adhesion - RGD and Integrins. *Science* **238**, 491-497 (1987).

5. Burdick, J.A. & Anseth, K.S. Photoencapsulation of osteoblasts in injectable RGD-modified PEG hydrogels for bone tissue engineering. *Biomaterials* **23**, 4315-4323 (2002).

6. Hern, D.L. & Hubbell, J.A. Incorporation of adhesion peptides into nonadhesive hydrogels useful for tissue resurfacing. *J. Biomed. Mater. Res.* **39**, 266-276 (1998).

7. Schmedlen, K.H., Masters, K.S. & West, J.L. Photocrosslinkable polyvinyl alcohol hydrogels that can be modified with cell adhesion peptides for use in tissue engineering. *Biomaterials* **23**, 4325-4332 (2002).

8. Lutolf, M.P. et al. Synthetic matrix metalloproteinase-sensitive hydrogels for the conduction of tissue regeneration: Engineering cell-invasion characteristics. *Proc. Natl. Acad. Sci. U. S. A.* **100**, 5413-5418 (2003).

9. Lutolf, M.P. & Hubbell, J.A. Synthetic biomaterials as instructive extracellular microenvironments for morphogenesis in tissue engineering. *Nat. Biotechnol.* **23**, 47-55 (2005).

10. Mann, B.K., Gobin, A.S., Tsai, A.T., Schmedlen, R.H. & West, J.L. Smooth muscle cell growth in photopolymerized hydrogels with cell adhesive and proteolytically degradable domains: synthetic ECM analogs for tissue engineering. *Biomaterials* **22**, 3045-3051 (2001).

11. Lin, C.C. & Anseth, K.S. Controlling affinity binding with peptide-functionalized poly(ethylene glycol) hydrogels. *Adv. Funct. Mater.* **19**, 2325-2331 (2009).

12. Lin, C.C., Metters, A.T. & Anseth, K.S. Functional PEG-peptide hydrogels to modulate local inflammation induced by the pro-inflammatory cytokine TNF alpha. *Biomaterials* **30**, 4907-4914 (2009).

13. Tayalia, P. & Mooney, D.J. Controlled growth factor delivery for tissue engineering. *Adv. Mater.* **21**, 3269-3285 (2009).

14. Mann, B.K., Schmedlen, R.H. & West, J.L. Tethered-TGF-beta increases extracellular matrix production of vascular smooth muscle cells. *Biomaterials* **22**, 439-444 (2001).

15. Zisch, A.H. et al. Cell-demanded release of VEGF from synthetic, biointeractive cell-ingrowth matrices for vascularized tissue growth. *FASEB J.* **17**, 2260-2262 (2003).

16. Aimetti, A.A., Tibbitt, M.W. & Anseth, K.S. Human neutrophil elastase responsive delivery from poly(ethylene glycol) hydrogels. *Biomacromolecules* **10**, 1484-1489 (2009).

17. Lee, S.H., Moon, J.J., Miller, J.S. & West, J.L. Poly(ethylene glycol) hydrogels conjugated with a collagenase-sensitive fluorogenic substrate to visualize collagenase activity during three-dimensional cell migration. *Biomaterials* **28**, 3163-3170 (2007).

18. Patch, J.A. & Barron, A.E. Mimicry of bioactive peptides *via* non-natural, sequence-specific peptidomimetic oligomers. *Curr. Opin. Chem. Biol.* **6**, 872-877 (2002).

19. Roberts, M.J., Bentley, M.D. & Harris, J.M. Chemistry for peptide and protein PEGylation. *Adv. Drug Delivery Rev.* **54**, 459-476 (2002).

20. Gobin, A.S. & West, J.L. Cell migration through defined, synthetic extracellular matrix analogues. *FASEB J.* **16**, 751-753 (2002).

21. DeLong, S.A., Moon, J.J. & West, J.L. Covalently immobilized gradients of bFGF on hydrogel scaffolds for directed cell migration. *Biomaterials* **26**, 3227-3234 (2005).

22. Weber, L.M., Hayda, K.N., Haskins, K. & Anseth, K.S. The effects of cell-matrix interactions on encapsulated beta-cell function within hydrogels functionalized with matrix-derived adhesive peptides. *Biomaterials* **28**, 3004-3011 (2007).

23. Lin-Gibson, S., Jones, R.L., Washburn, N.R. & Horkay, F. Structure-property relationships of photopolymerizable poly(ethylene glycol) dimethacrylate hydrogels. *Macromolecules* **38**, 2897-2902 (2005).

24. Lutolf, M.P., Tirelli, N., Cerritelli, S., Cavalli, L. & Hubbell, J.A. Systematic modulation of Michael-type reactivity of thiols through the use of charged amino acids. *Bioconjug. Chem.* **12**, 1051-1056 (2001).

25. Park, Y., Lutolf, M.P., Hubbell, J.A., Hunziker, E.B. & Wong, M. Bovine primary chondrocyte culture in synthetic matrix metalloproteinase-sensitive poly(ethylene glycol)-based hydrogels as a scaffold for cartilage repair. *Tissue Eng.* **10**, 515-522 (2004).

26. Miller, J.S. et al. Bioactive hydrogels made from step-growth derived PEG-peptide macromers. *Biomaterials* (2010).

27. Fairbanks, B.D. et al. A versatile synthetic extracellular matrix mimic *via* thiol-norbornene photopolymerization. *Adv. Mater.* **21**, 5005-5010 (2009).

28. Salinas, C.N. & Anseth, K.S. Mixed mode thiol-acrylate photopolymerizations for the synthesis of PEG-peptide hydrogels. *Macromolecules* **41**, 6019-6026 (2008).

29. Kolb, H.C., Finn, M.G. & Sharpless, K.B. Click chemistry: Diverse chemical function from a few good reactions. *Angew. Chem. Int. Ed. Engl.* **40**, 2004-2021 (2001).

30. Kolb, H.C. & Sharpless, K.B. The growing impact of click chemistry on drug discovery. *Drug Discov. Today* **8**, 1128-1137 (2003).

31. Hawker, C.J. & Wooley, K.L. The convergence of synthetic organic and polymer chemistries. *Science* **309**, 1200-1205 (2005).

32. Polizzotti, B.D., Fairbanks, B.D. & Anseth, K.S. Three-dimensional biochemical patterning of click-based composite hydrogels *via* thiolene photopolymerization. *Biomacromolecules* **9**, 1084-1087 (2008).

33. Huisgen, R. 1.3-Dipolare Cycloadditionen - Ruckschau Und Ausblick. *Angew. Chem. Int. Ed. Engl.* **75**, 604-637 (1963).

34. Tornoe, C.W., Christensen, C. & Meldal, M. Peptidotriazoles on solid phase: [1,2,3]-triazoles by regiospecific copper(I)-catalyzed 1,3-dipolar cycloadditions of terminal alkynes to azides. *J. Org. Chem.* **67**, 3057-3064 (2002).

35. Franke, R., Doll, C. & Eichler, J. Peptide ligation through click chemistry for the generation of assembled and scaffolded peptides. *Tetrahedron Lett.* **46**, 4479-4482 (2005).

36. Moses, J.E. & Moorhouse, A.D. The growing applications of click chemistry. *Chem. Soc. Rev.* **36**, 1249-1262 (2007).

37. Binder, W.H. & Sachsenhofer, R. 'Click' chemistry in polymer and materials science. *Macromol. Rapid Commun.* **28**, 15-54 (2007).

38. Bock, V.D., Perciaccante, R., Jansen, T.P., Hiemstra, H. & van Maarseveen, J.H. Click chemistry as a route to cyclic tetrapeptide analogues: Synthesis of cyclo-[Pro-Val-Psi(triazole)-Pro-Tyr]. *Org. Lett.* **8**, 919-922 (2006).

39. Jagasia, R., Holub, J.M., Bollinger, M., Kirshenbaum, K. & Finn, M.G. Peptide Cyclization and Cyclodimerization by Cu-I-Mediated Azide-Alkyne Cycloaddition. *J. Org. Chem.* **74**, 2964-2974 (2009).

40. Parrish, B., Breitenkamp, R.B. & Emrick, T. PEG- and peptide-grafted aliphatic polyesters by click chemistry. *J. Am. Chem. Soc.* **127**, 7404-7410 (2005).

41. Engler, A.C., Lee, H.I. & Hammond, P.T. Highly Efficient "Grafting onto" a Polypeptide Backbone Using Click Chemistry. *Angew. Chem. Int. Ed. Engl.* **48**, 9334-9338 (2009).

42. Agard, N.J., Prescher, J.A. & Bertozzi, C.R. A strain-promoted [3 + 2] azide-alkyne cycloaddition for covalent modification of biomolecules in living systems. *J. Am. Chem. Soc.* **126**, 15046-15047 (2004).

43. Laughlin, S.T., Baskin, J.M., Amacher, S.L. & Bertozzi, C.R. In vivo imaging of membrane-associated glycans in developing zebrafish. *Science* **320**, 664-667 (2008).

44. Codelli, J.A., Baskin, J.M., Agard, N.J. & Berozzi, C.R. Second-generation difluorinated cyclooctynes for copper-free click chemistry. *J. Am. Chem. Soc.* **130**, 11486-11493 (2008).

45. Chang, P.V. et al. Copper-free click chemistry in living animals. *Proc. Natl. Acad. Sci. U. S. A.* **107**, 1821-1826 (2010).

46. Hoyle, C.E., Lee, T.Y. & Roper, T. Thiol-enes: Chemistry of the past with promise for the future. *J. Polym. Sci., Part A: Polym. Chem.* **42**, 5301-5338 (2004).

47. Dondoni, A. The emergence of thiol-ene coupling as a click process for materials and bioorganic chemistry. *Angew. Chem. Int. Ed. Engl.* **47**, 8995-8997 (2008).

48. DeForest, C.A., Polizzotti, B.D. & Anseth, K.S. Sequential click reactions for synthesizing and patterning three-dimensional cell microenvironments. *Nat. Mater.* **8**, 659-664 (2009).

49. Nagase, H. & Fields, G.B. Human matrix metalloproteinase specificity studies using collagen sequence-based synthetic peptides. *Biopolymers* **40**, 399-416 (1996).

50. Malkoch, M. et al. Synthesis of well-defined hydrogel networks using click chemistry. *Chem. Commun.*, 2774-2776 (2006).

51. Rydholm, A.E., Reddy, S.K., Anseth, K.S. & Bowman, C.N. Development and characterization of degradable thiol-allyl ether photopolymers. *Polymer* **48**, 4589-4600 (2007).

52. Lee, T.Y., Smith, Z., Reddy, S.K., Cramer, N.B. & Bowman, C.N. Thiol-allyl ether-methacrylate ternary systems. Polymerization mechanism. *Macromolecules* **40**, 1466-1472 (2007).

53. Mather, B.D., Viswanathan, K., Miller, K.M. & Long, T.E. Michael addition reactions in macromolecular design for emerging technologies. *Progress in Polymer Science* **31**, 487-531 (2006).

54. Cramer, N.B., Reddy, S.K., O'Brien, A.K. & Bowman, C.N. Thiol-ene photopolymerization mechanism and rate limiting step changes for various vinyl functional group chemistries. *Macromolecules* **36**, 7964-7969 (2003).

55. Johnson, P.M., Reynolds, T.B., Stansbury, J.W. & Bowman, C.N. High throughput kinetic analysis of photopolymer conversion using composition and exposure time gradients. *Polymer* **46**, 3300-3306 (2005).

56. DeLong, S.A., Gobin, A.S. & West, J.L. Covalent immobilization of RGDS on hydrogel surfaces to direct cell alignment and migration. *J. Control. Release* **109**, 139-148 (2005).

57. Yu, X.J., Dillon, G.P. & Bellamkonda, R.V. A laminin and nerve growth factor-laden three-dimensional scaffold for enhanced neurite extension. *Tissue Eng.* **5**, 291-304 (1999).

4.7 Supplementary Information

4.7.1 Amount of cyclic non-idealities in step-growth hydrogel

For a step-growth network, we define the fraction of pairs of the azide functional groups that are part of primary cycles as *c*. From this, the probability of having azide monomers with 1, 2, or 0 primary cycles is given as c', c'', and c''', respectively:

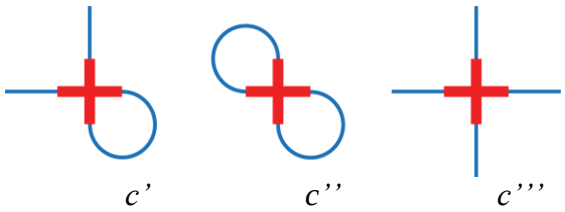

$$c' = 2c(1-c) \tag{2}$$

$$c'' = c^2 \tag{3}$$

$$c''' = (1-c)^2 \tag{4}$$

In a perfectly ideal network containing no primary cycles, $c = c' = c'' = 0$ and $c''' = 1$. For these networks, the ideal crosslinking density during network formation ($\rho_{x,0}$) is equal to twice the concentration of PEG tetraazide multiplied by r, the ratio of azide to alkyne functionalities such that $0 \leq r \leq 1$, since each arm of the PEG azide is attached to half an infinite chain. The formation of primary cycles decreases the network crosslinking density and the experimentally measured compressive moduli from values predicted using $c''' = 1$. By comparing the ratio of the initial bulk moduli (K_0) and the predicted bulk moduli (K_{theo}), we can estimate the degree of cyclization present in the network. K_0 can be calculated from the swelling ratio during network formation (q_{NF}), the initial swelling ratio (q_0), and the measured swollen bulk moduli ($K_{measured}$).

$$\rho_x = \frac{2(\text{moles of PEG tetraazide})r}{\text{total polymerization volume}} \tag{5}$$

$$\frac{K_0}{K_{theo}} = (1-c)^2 = c''' \tag{6}$$

$$K_0 = K_{measured}(q_0)^{1/3}(q_{NF})^{2/3} \tag{7}$$

The theoretical bulk modulus (K_{theo}) is readily calculated from the $\rho_{x,0}$ and the Poisson ratio (v_p, assumed = 0.42), [3,4] where R is the universal gas constant and T is the absolute temperature.

$$E_{theo} = 3RT\rho_{x,0} \tag{9}$$

$$K_{theo} = \frac{E_{theo}}{3(1-2v_p)} \tag{10}$$

In addition, we must calculate the obtained bulk moduli ($K_{measured}$) from the measured shear elastic moduli ($G_{measured}$).

$$K_{measured} = \frac{2G_{measured}(1+v_p)}{3(1-2v_p)} \tag{11}$$

With these equations, as well as known values for $\rho_{x,0}$, $G_{measured}$, and swelling ratios (q_0 and q_{NF}), we can calculate *c, c', c'', and c'''* for our different formulations. For mean values of $G_{measured}$ and the swelling ratios, the values for *c* and *c'''* are calculated as:

Azide: Alkyne	**10k**		**15k**		**20k**	
	c	*c'''*	*c*	*c'''*	*c*	*c'''*
1.5:1	0.075	0.86	0.106	0.80	0.122	0.77
1.25:1	0.066	0.87	0.024	0.95	0.093	0.82
1:1	0.035	0.93	0.015	0.97	0.057	0.89
1:1.25	0.023	0.95	0.005	0.99	0.134	0.75
1:1.5	0.038	0.92	0.071	0.86	0.133	0.75

We find that the networks are highly ideal (>95%) for the 1:1 stoichiometry case. As expected, ideality decreases as the system is formed further off-stoichiometry.

4.7.2 Equilibrium shear moduli and swelling ratios post patterning

Experiments were performed with 2.2 mM I2959 and a 6 J cm^{-2} dosage of 365 nm light.

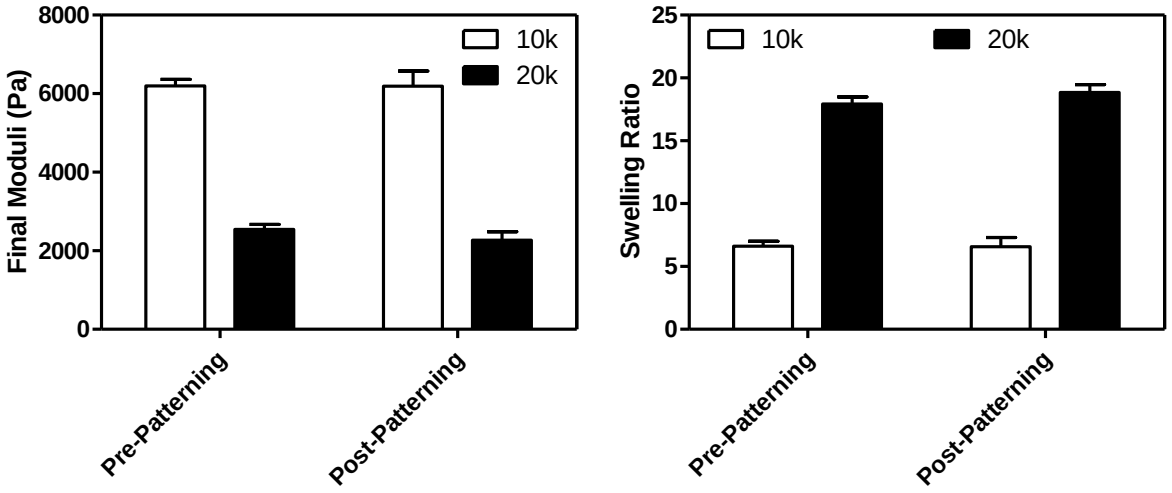

4.7.3 Total amount of photoinitiator consumed over photofunctionalization process

The volume-averaged initiator concentration versus irradiation time is given as:

$$\frac{[\mathrm{I}]}{[\mathrm{I}]_0} = \frac{1}{\varepsilon[\mathrm{I}]_0 L} \ln\left[1 - \left(1 - e^{\varepsilon[\mathrm{I}]_0 L}\right) e^{-\varepsilon \Phi I_0 t}\right] \qquad (1)$$

where:

[I] = photoinitiator concentration as a function of time

$[I]_0$ = initial photoinitiator concentration (chosen here as 2.2 mM)

I_0 = irradiance at the base of the sample = 3.05 x 10^{-8} moles photons s^{-1} cm^{-2} for 365 nm light at 10 mW cm^{-2}

ε = the wavelength dependent absorption coefficient = 2.302 x extinction coefficient (6.7 L mol^{-1} cm^{-1} for I2959)

L = sample thickness = 1 mm

Φ = quantum yield of the photoinitiator consumption = 0.05 for I2959 at 365 nm[2]

Plotting Eq. 1 as a function of time gives the representative curve:

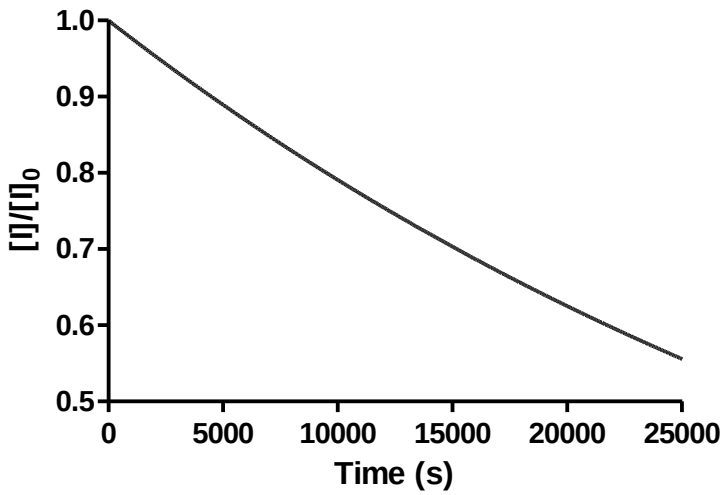

Even for our longest reaction time (600 s), <2% of the total photoinitiator is consumed.

4.7.4 Biochemical gradient generation within hydrogel

Hydrogels are exposed to collimated UV light (365 nm at 10 mW cm^{-2}) while a moving photomask covers the sample. This rate of coverage is easily controlled and enables different gradients of light to be imposed on the hydrogel. This ultimately results in well-defined gradients of patterning concentrations across relatively large distances.

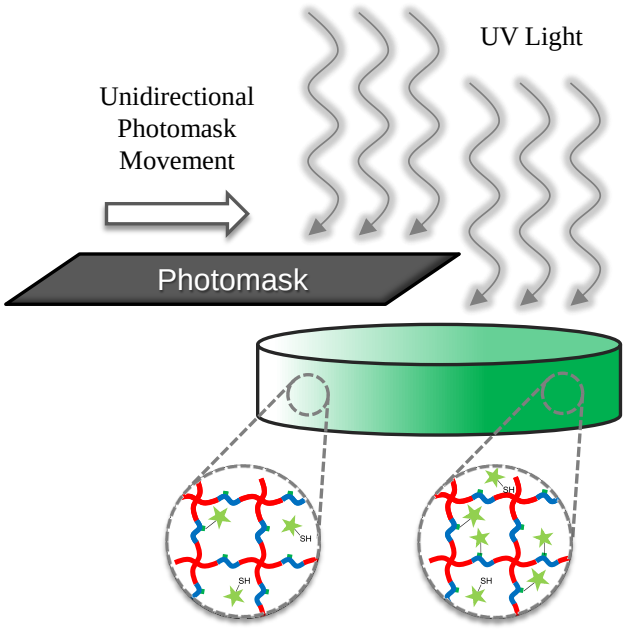

4.7.5 ^{1}H-NMR spectrum of PEG tetraazide (here, M_n ~ 10,000 g/mol).

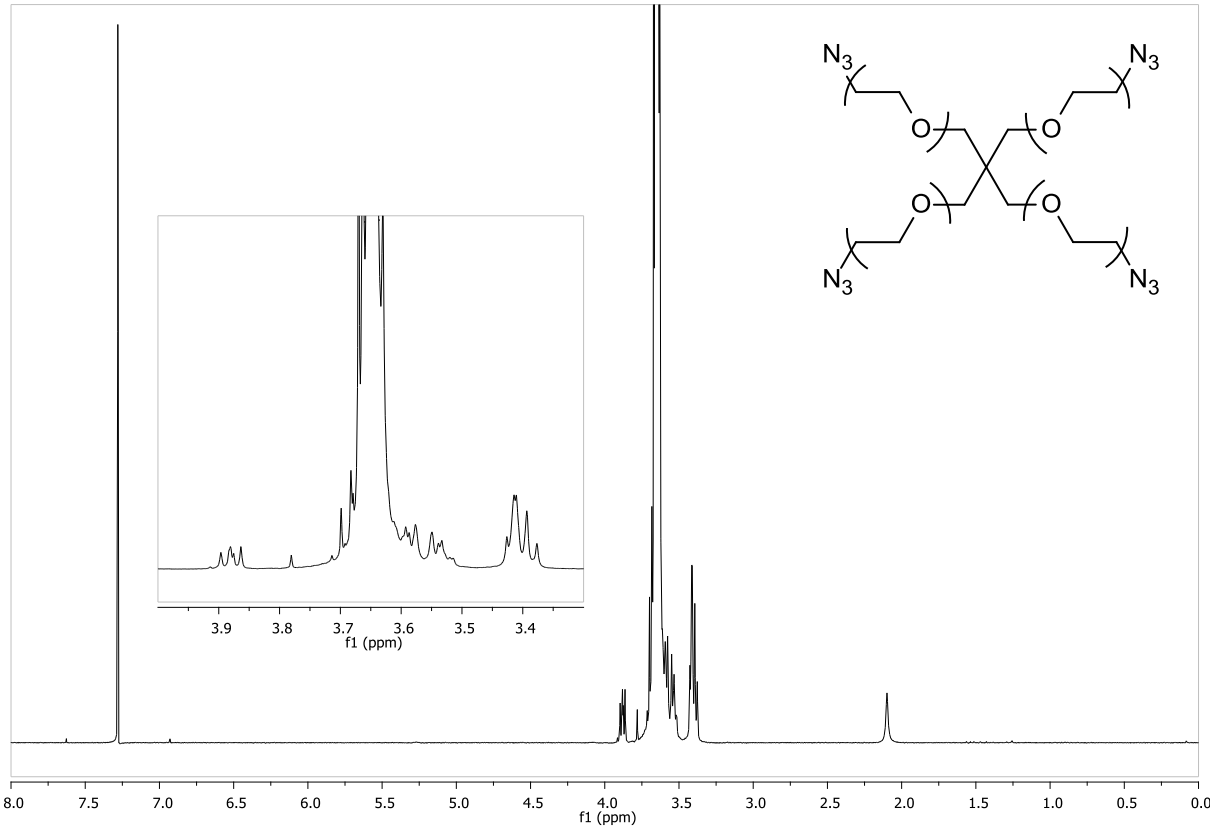

4.7.6 ^{1}H-NMR spectrum of DIFO3.

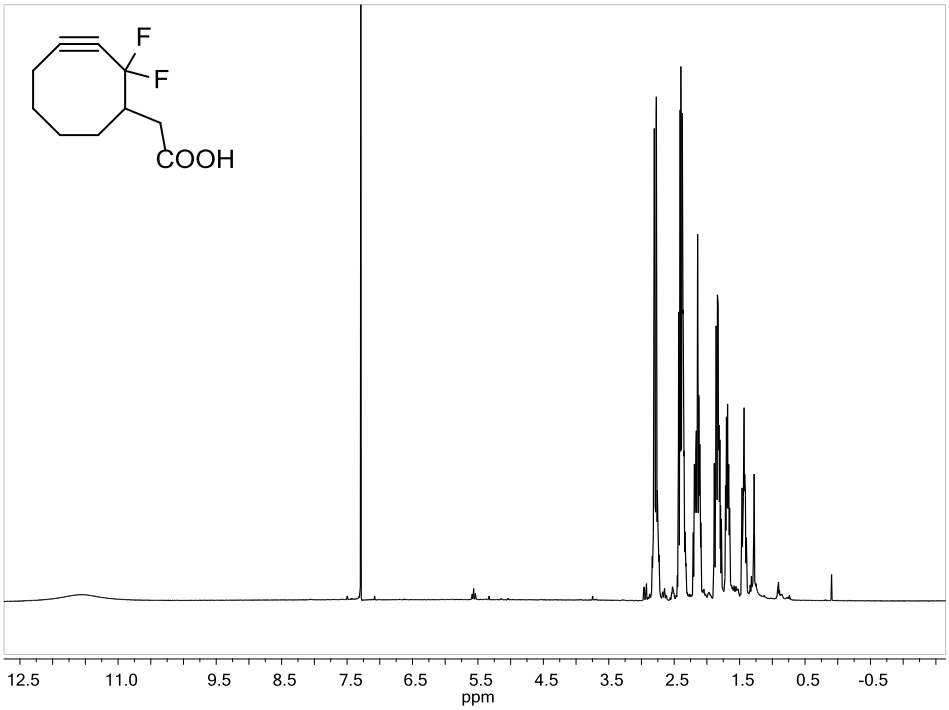

4.7.7 ^{13}C-NMR spectrum of DIFO3.

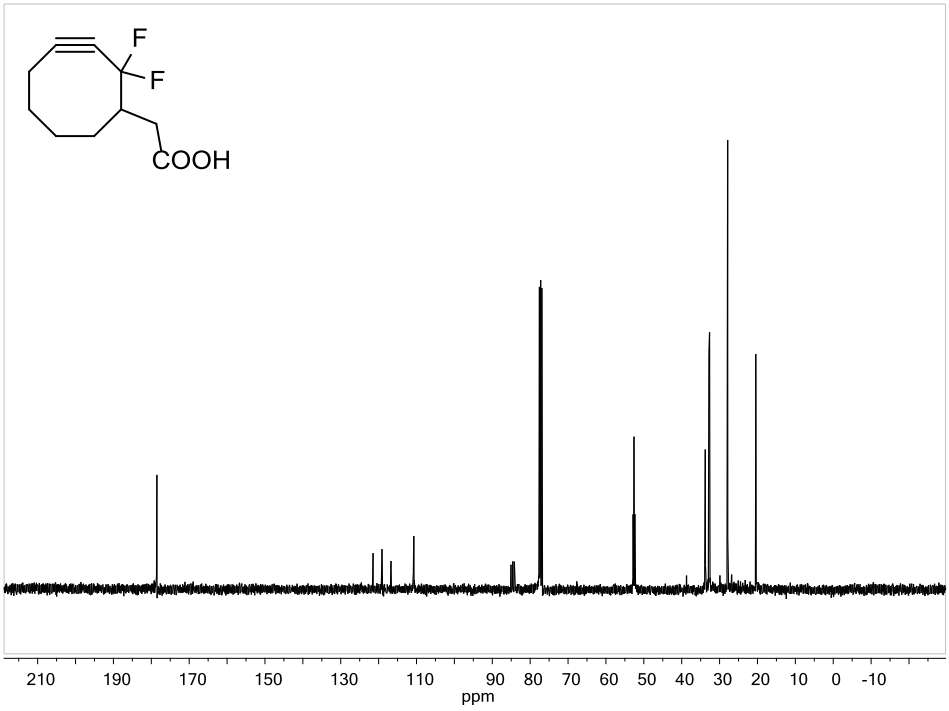

4.7.8 ^{19}F-NMR spectrum of DIFO3.

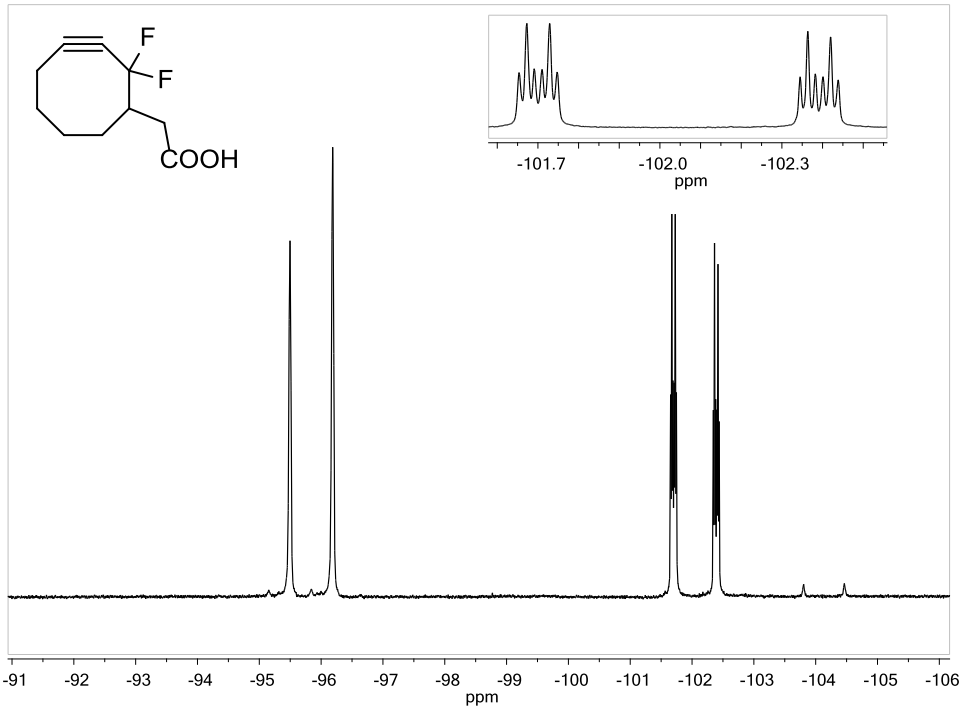

4.7.9 MALDI-TOF spectrum of regular peptide (+4 charge)

Ac-K(DIFO3)RRGGK(alloc)GGPQGILGQRRK(DIFO3)-NH_2

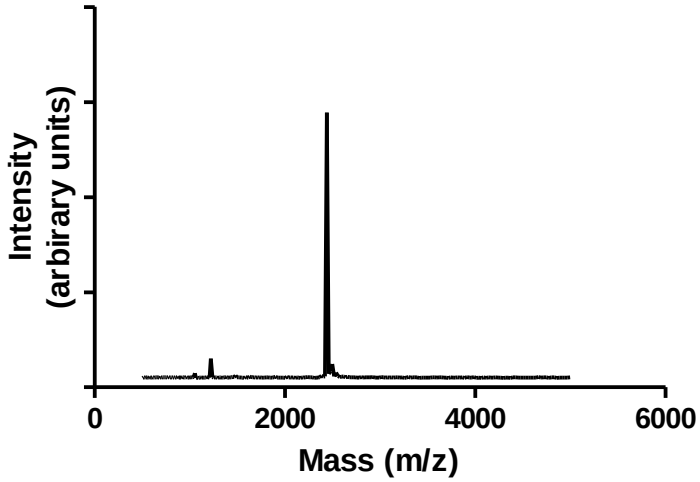

4.7.10 MALDI-TOF spectrum of scrambled peptide (+4 charge)

Ac-K(DIFO3)QGK(alloc)RIPGRRLGGRGQGK(DIFO3)-NH_2

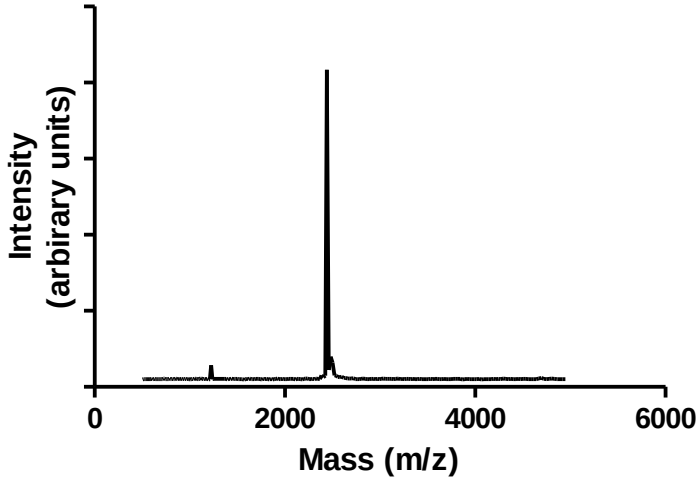

4.7.11 MALDI-TOF spectrum of neutral peptide (no net charge)

Ac-K(DIFO3)REGGK(alloc)GGPQGILGQERK(DIFO3)-NH_2

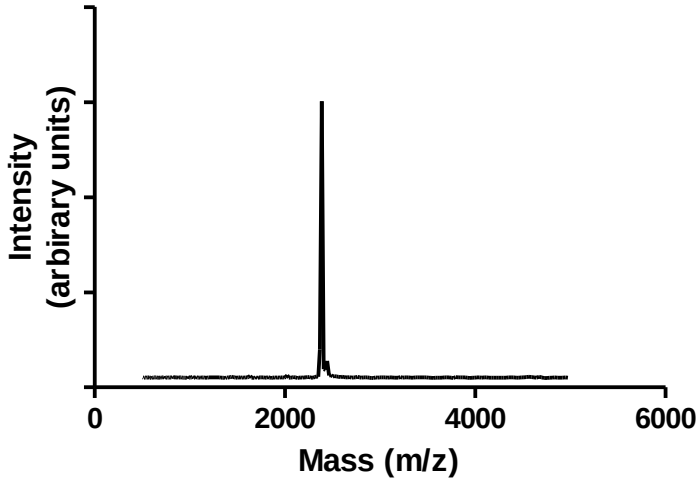

4.7.12 MALDI-TOF spectrum of negatively charged peptide (-4 charge)

Ac-K(DIFO3)EEGGK(alloc)GGPQGILGQEEK(DIFO3)-NH_2

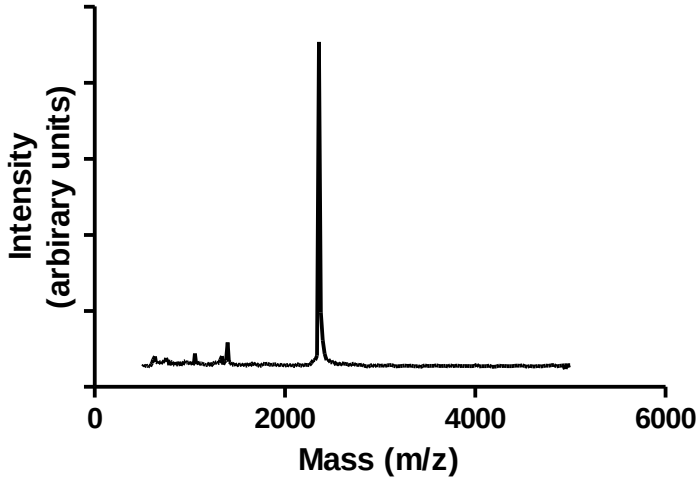

4.7.13. Calibration curve of fluorescence versus concentration of patterning agent swollen into network

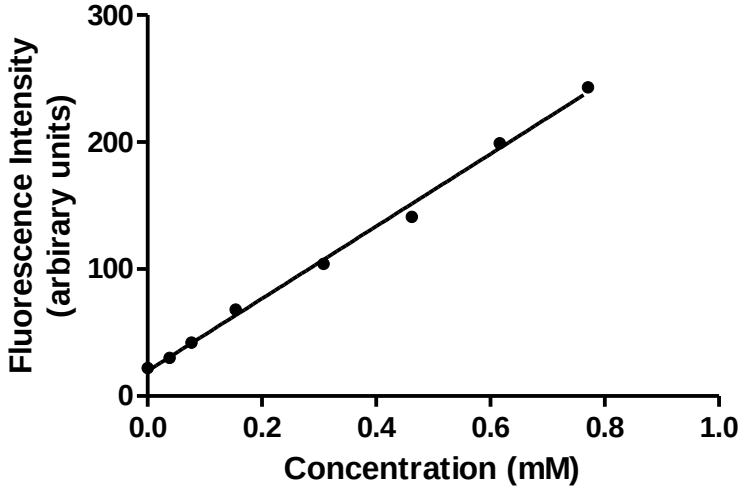

CHAPTER V

CYTOCOMPATIBLE CLICK-BASED HYDROGELS WITH DYNAMICALLY-TUNABLE PROPERTIES THROUGH ORTHOGONAL PHOTOCONJUGATION AND PHOTOCLEAVAGE REACTIONS

Under review at *Nature Chemistry*, Summer 2011.

5.1 Abstract

To provide insight as to how cells receive information from their external surroundings, synthetic hydrogels have emerged as systems for assaying cell function in well-defined microenvironments where single cues can be introduced and subsequent effects individually elucidated. However, as the field seeks to answer more complex biological questions, advanced material systems are needed that allow dynamic alteration of the 3D cellular environment with orthogonal reactions that enable multiple levels of control of biochemical and biomechanical signals. Here, we sought to synthesize one such 3D culture system using cytocompatible and wavelength-specific photochemical reactions to create hydrogels that allow orthogonal and dynamic control of the material properties through independent spatiotemporally-regulated photocleavage of crosslinks and photoconjugation of pendant functionalities. Results demonstrate the versatile nature of the chemistry to create programmable niches to study and direct cell function by modifying the local hydrogel environment.

5.2 Introduction

Since its conception by Sharpless in 2001[1], the concept of click chemistry has been rapidly adopted in many disciplines, perhaps most notably in material science, with annual publication numbers continuing to increase exponentially[2-5]. The click philosophy idealizes reactions that enable researchers to link covalently two reactants in a straightforward, modular, high-yielding manner. The copper(I)-catalyzed azide-alkyne cycloaddition (CuAAC) is frequently billed as the quintessential example in meeting these criteria. Though each of the click reactions has a variety of desirable properties, their true benefit lies in the orthogonality of these reactions with respect to many common reactive groups (*e.g.*, amines, alcohols, acids)[6]. Reaction orthogonality enables independent control over multiple functional groups in a single system and opens the door for the synthesis of materials with ever-increasing complexity for an ever-expanding list of applications.

There is also a growing interest in chemical reactions that can be performed in the presence of live cells[6]. These reactions must proceed mildly in aqueous medium and a defined chemical environment (5% CO_2 and atmospheric O_2 levels), under regulated pH (7.4), temperature (37°C), osmolarity (~300 mOsM), and involve non-toxic reactive moieties and (by)products. The requirement of reactions that proceed under physiological conditions is a stringent constraint and presents severe limitations on reaction selection. In particular, there are even fewer chemistries that proceed in a specific manner, while limiting side reactions with the plethora of functional groups that are found in biological systems. These elite reactions are considered bio-orthogonal and are a necessity for probing chemically and directing biological function.

In many instances, the ideal cytocompatible reaction would not only be selected by its bio-orthogonality, but also by its capacity to be controlled in both time and space. In this regard, photochemical reactions are widely regarded for their spatiotemporal control, where the reaction of interest is defined by when and where the light is delivered to the system[7]. Photolithographic techniques, where masked light is projected directly onto a sample, enable photoreactions to be confined to specific regions within a sample as defined by a 2D mask pattern, while focused laser light (either single- or multi-photon) provides full 3D control over where a specific reaction occurs within the volume of a material. While the effects of attenuation and scattering must be carefully taken into consideration, light-based chemistries have become a powerful tool for material synthesis and spatial modification, owing to their ease of implementation and readily available inexpensive light sources, and have become indispensible in formation and subsequent modification of biomaterials.

To date, biocompatible light-based chemistries have enabled control in space and time of *either* the gel degradation or gel chemistry of synthetic cell culture systems. By introducing chemical functionalities in user-defined patterns within the material, cell spreading and migration have been explicitly controlled in 3D[8-13]. Alternatively, cell outgrowth and stem cell fate have been directed by altering the gel's structural properties[14-18]. Nevertheless, independent control over *both* the material's physical and chemical makeup in 3D, along with in time, allow dynamic tailoring of a cell's microenvironment, and has not been demonstrated. Such 4D control of material properties would be tremendously advantageous in a number of biomaterial applications, including 3D cell culture, stem cell expansion, cancer metastasis, and tissue regeneration. Of further importance and novelty, the ability for the experimenter to control gel properties at any point in space and time enables opportunities for unique experiments, such as

the ability to introduce dynamically a cell ligand or allow cell-cell interactions at specified locations. These programmable cell culture niches facilitate the ability to perform newfound experiments and answer questions about the dynamic exchange of information between a cell and its niche. In this work, we present one such system where multiple wavelengths of light are utilized to control independently the functionality and architecture of a hydrogel network formed *via* a copper-free alkyne-azide reaction (Fig. 5.1). Each of the reactions is cytocompatible, and both photoconjugation and photocleavage reactions were used to spatiotemporally regulate materials properties, including the presentation of integrin-binding motifs and network erosion through cleavage of crosslinking moieties. This platform allows gel parameters to be tuned in real-time, and results demonstrate how spatiotemporal regulation of material properties can be used to direct the function of embedded cells.

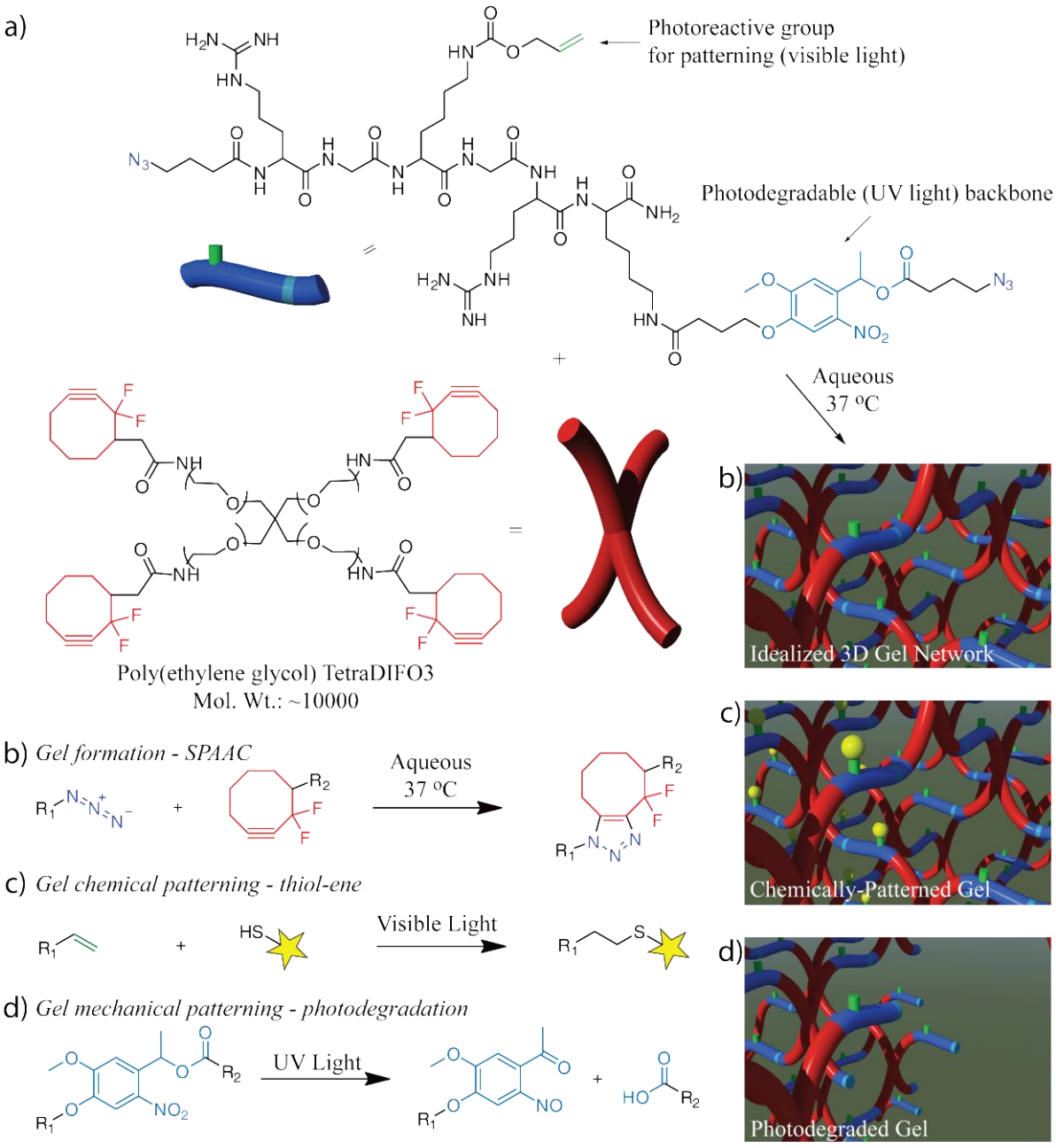

Figure 5.1 Synthesis, photocoupling, and photodegradation for tuning chemical and physical properties of click-based hydrogels. **(a)** Click-functionalized macromolecular precursors (*i.e.*, PEG-tetraDIFO3 and bis(azide)-functionalized polypeptides) form a 3D ideal hydrogel structure *via* a step-growth polymerization mechanism by the **(b)** SPAAC reaction. **(c)** In the presence of visible light (λ = 490 – 650 nm or 860 nm), thiol-containing biomolecules are covalently affixed to pendant vinyl functionalities throughout the hydrogel network *via* the thiol-ene reaction. **(d)** A nitrobenzyl ether moiety within the backbone of the polymer network undergoes photocleavage in the presence of single or multi-photon UV light (λ = 365 nm or 740 nm) that results in photodegradation of the network.

5.3 Results and Discussion

A four-arm poly(ethylene glycol) (PEG) tetracyclooctyne (M_n ~ 10,000 Da) was reacted with a bis(azide) di-functionalized polypeptide (Azide-RGK(alloc)GRK(PLazide)-NH_2) *via* a copper-free, strain promoted azide-alkyne cycloaddition (SPAAC) reaction between terminal difluorinated cyclooctyne (DIFO3) and azide ($–N_3$) moieties with 1:1 stoichiometry at 10 wt% total macromer concentration to form an idealized 3D network with minimal local defects. The ring strain and electronegative fluorine substituents of DIFO3 enable the SPAAC reaction to proceed rapidly, without a catalyst, and in the presence of cells[19]. Network gelation occurs ~2 min after mixing as estimated by the crossover point of G' and G'' (Supplementary Section 5.6.1). By including a synthetic polypeptide in the gel formulation, the precise chemical makeup of the material is tailored readily by choice of the amino acid sequence, allowing one to tailor the biofunctionality (e.g., enzymatic degradability, integrin binding ligands, protein affinity binding sites) and introduce bioorthogonal reactive moieties (e.g., vinyl groups, azides). Ultimately, the timescale and mechanism of the SPAAC reaction permits high viability (>95%) during encapsulation of both established cell lines, as well as primary cell types (Supplementary Section 5.6.11)[8].

5.3.1 Biochemical Control *via* Thiol-ene Photoconjugation

Incorporated into the synthetic peptide is the commercially-available lysine(allyloxycarbonyl) (alloc) amino acid, whose alloc protecting group is stable to standard solid phase peptide synthesis methods and contains a vinyl functionality that is readily photocoupled to thiol-containing compounds, such as cysteine, *via* the thiol-ene reaction. Although a number of reactions can be controlled with light, including the CuAAC by a photogenerated copper(I) catalyst[20], the radical-mediated thiol-ene addition has emerged as a

versatile click reaction that can be photochemically initiated[21,22]. This reaction, which involves the catalytic propagation of a thiyl radical across an olefin (–C=C) and subsequent chain transfer from the resulting carbon radical to a thiol (–SH), has gained recent interest as an approach to functionalize systems with biomolecules[8,23,24], control dendrimer formation[25], as well as synthesize other complex materials[26,27]. The propagating thiyl radical is readily generated in the presence of both cleavage-type, as well as hydrogen-abstracting photoinitiators[28], enabling thiol-containing molecules to be physically linked to vinyl-functionalized moieties over a variety of light conditions including in the visible range. This reaction can be employed with peptides, thiolated full proteins, and small molecules that are individually capable of diffusing throughout the hydrogel (Supplementary Sections 5.6.2 & 5.6.3), though peptides that contain free thiols in their bioactive domain may exhibit reduced biological effect upon thiol-ene coupling. The reaction is regarded as cytocompatible (Supplementary Section 5.6.11), as well as bioorthogonal, facilitating its use in biological systems[21] and enables materials to be functionalized dynamically with specific molecules of interest at any given location and time.

After gel formation, fluorescently-labeled thiol-containing biomolecules were swollen into the network along with a small amount of eosin Y photoinitiator (2.5 – 10 μM), which was followed by visible light irradiation (λ = 490 – 650 nm) at low intensities (10 mW cm^{-2}) and short durations (0.5 – 2 min). The extent of photocoupling was visualized and quantified using confocal microscopy and was controlled by the photoinitiator concentration and exposure time (Fig. 5.2a). Specifically, patterning concentrations between 0 and 1 mM were obtained with short light exposures of only a few minutes. By irradiating through a photomask, patterning was confined to specific locations throughout the gel, as demonstrated by the transfer of a 400 μm wide line pattern through the depth of the sample (Fig. 5.2b, Supplementary Section 5.6.4).

Additionally, multi-photon initiation techniques (λ = 860 nm) were used to create elaborate, user-defined, 3D biochemical patterns within the hydrogel (Fig. 5.2c). Here, a 300 x 400 x 400 μm interconnected 3D structure composed of multiple shapes and two distinct peptides was created. The resolution that we achieve with multiphoton-based patterning is ~1 μm in the x-y plane and ~3-5 μm in the z plane, which are values typical of multiphoton imaging methods and represent a limitation of the optics and not the chemistry. The photocoupling process can be repeated many times over, with each cycle requiring on the time scale of a few hours for introduction and removal of the signal *via* diffusion (depending on the gel dimensions). Thus, multiple signals can be incorporated with micron-scale patterning resolution on time and size scales that are relevant for many cell culture experiments.

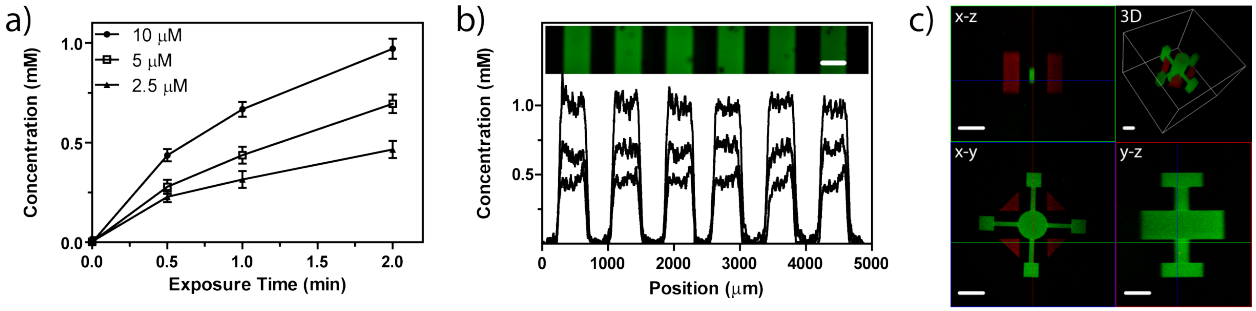

Figure 5.2 Biochemical patterning within preformed click hydrogels using visible light. Upon swelling thiol-containing biomolecules into preformed gels, pendant functionalities are affixed to the hydrogel backbone *via* the thiol-ene reaction upon exposure to visible light (λ = 490 – 650 nm). **(a)** The final patterned concentration of a fluorescent RGD peptide (AF_{488}-AhxRGDSC-NH_2) depends on the amount of photoinitiator present (2.5, 5, and 10 mM Eosin Y), as well as the exposure time to visible light (0 – 2 min, 10 mW cm^{-2}). **(b)** The network functionalization with pendant fluorescently-labeled peptides is confined to user-defined regions within preformed gels using photolithography (0.5, 1, or 2 min exposure with increased patterning concentration for increased exposure time, 10 mW cm^{-2}, 10 μM eosin Y). **(c)** The photocoupling reaction is controlled in 3D by rastering the focal point of multi-photon laser light (λ = 860 nm) over defined volumes within the gel, affording micron-scale resolution in all spatial dimensions. Additionally, the patterning process can be repeated many times to introduce multiple biochemical cues within the same network, as demonstrated by the red- and green-labeled patterned peptides within the same gel. Images represent confocal projections and 3D renderings. Scale bar = 400 μm for (b) and 100 μm for (c).

5.3.2 Biophysical Control *via* Photodegradation

The utility of a peptide linker enables desired sequences, as well as desired functionalities, to be precisely incorporated in a modular fashion. In addition to the pendant alloc vinyl functionality, the peptide includes a photodegradable nitrobenzyl ether moiety (PLazide) within its backbone, enabling photocleavage of the crosslinks upon exposure to UV light (either λ = 365 nm for single photon of λ = 740 nm for multiphoton[14,29]). Specifically, the irreversible photocleavage of an *o*-nitrobenzyl ether moiety into nitroso- and acid-terminated byproducts permits a previously-intact chemical linkage to be cleaved photolytically. The photolabile group degrades under cytocompatible irradiation conditions, including 365 nm light[29], and has been used for the uncaging of proteins[30], to cleave peptides from a solid support[31], as well as to control cell adhesion[9,32]. The functionality has also been incorporated into materials to produce networks that are capable of degrading in the presence of light[14,33,34], allowing the effects of physical material cues on cell function to be probed[35-37].

Based on kinetic nuclear magnetic resonance (NMR) as well as photorheometry studies, the photoscission of the PLazide moiety (Supplementary Section 5.6.5) was found to follow a first order degradation with a rate constant (k) that can be expressed as:

$$k = \frac{\varphi \varepsilon I}{N_A h \nu}$$

where ϕ is the quantum yield (determined to be 0.020), ε is the molar absorptivity of the sample (4780 M^{-1} cm^{-1} for PLazide at λ = 365 nm), I is the intensity of light, N_A is Avogadro's number, h is the Planck constant, and ν is the frequency of the associated electromagnetic wave (Supplementary Section 5.6.6, 5.6.7, & 5.6.8). For typical exposure conditions (λ = 365 nm, 10 mW cm^{-2}), k was determined to be 2.9 x 10^{-3} sec^{-1}, and correlates well with other photodegradable moieties[14,31]. Physical channels were eroded downward from the surface of

optically-thick samples, with the depth of photodegradation directly related to the total light intensity (5, 10 and 20 mW cm^{-2}), as well as the exposure time of UV light (0 – 45 min) (Fig. 5.3a, Supplementary Section 5.6.9), and the total light dosage delivered to the material (Supplementary Section 5.6.10). As with the photocoupling reaction, the photocleavage reaction was confined to regions of interest within the sample using photolithographic processes to create channels of varying depth (~150 – 600 μm) (Fig. 5.3b), as well as multi-photon patterning approaches to erode precisely defined 3D regions of interest with user-defined shapes and connectivity (Fig. 5.3c, λ = 740 nm). Each process affords a high level of patterning fidelity, similar to that by the photocoupling reaction.

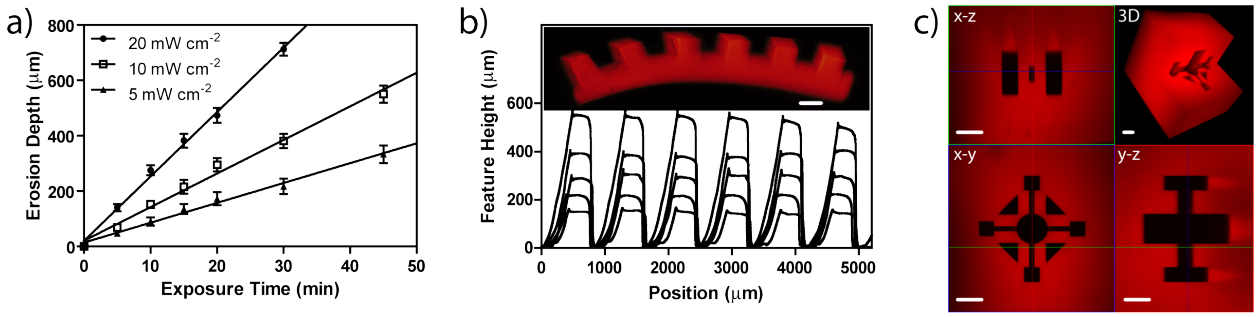

Figure 5.3 Biophysical patterning within preformed click hydrogels using UV light. In the presence of UV light (λ = 365 nm), photolabile functionalities within the hydrogel crosslinks undergo an irreversible cleavage, thereby decreasing the total network connectivity, resulting in local material degradation and removal of the fluorescent hydrogel material. **(a)** In optically-thick samples, the depth of photodegradation is directly related to the incident light intensity (5, 10 and 20 mW cm^{-2}), as well as the exposure time to visible light (0 – 45 min). **(b)** Using mask-based photolithographic techniques, network degradation was confined to user-defined regions within fluorescently-labeled gels (10, 15, 20, 30, and 45 min, feature height increasing with exposure time), as measured by profilometry. **(c)** The photodegradation reaction is controlled in 3D with micron-scale resolution in all dimensions using focused multi-photon laser light (λ = 740 nm). Images represent confocal projections and 3D renderings. Scale bar = 400 μm for (b) and 100 μm for (c).

5.3.3 Orthogonal Photoreactions for Advanced 3D Cell Culture

The utility of the photocoupling and photocleavage reactions ultimately stems from their ability to be performed orthogonally, such that both network mechanical and chemical makeup

are controlled independently. The peak absorbance for the photolabile group and the visible photoinitiator was found to be ~350 and ~520 nm, respectively, with relatively little overlap of the absorbance spectra (Fig. 5.4a). As eosin Y also has a low absorbance at λ = 365 nm, photocoupling during photodegradation was readily prevented by performing degradation only in the absence of photoinitiator. Alternatively, photocoupling was initiated first with visible light (λ = 490 – 650 nm) and photodegradation was commenced with subsequent UV irradiation. The orthogonality of these reactions was confirmed by solution NMR studies where photocleavage was quantified under both visible and UV light initiation conditions using model compounds (Fig. 5.4b). To illustrate orthogonality of the reactions within the same material system, a buffalo logo was first photocoupled within the 3D network using visible light, and user-defined letters (CU) were eroded within the fluorescent logo at a later time (Fig. 5.4c). Photodegradation was confirmed to be confined only to the areas of interest by brightfield microscopy (Fig. 5.4d), as well as with the disappearance of the fluorescently-labeled reporter peptide, indicating that cues can be spatially coupled and subsequently removed with orthogonal reactions.

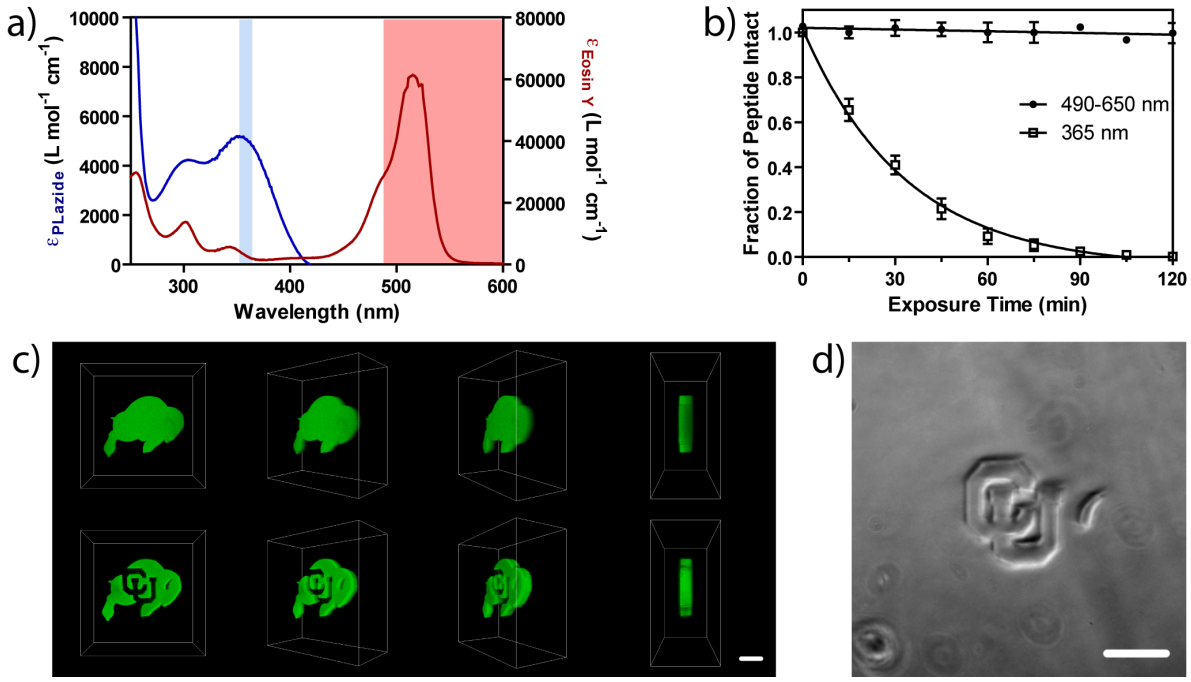

Figure 5.4 Orthogonality of photocoupling and photodegration reactions. **(a)** The peak absorbance for the photoinitiator (red) and the photolabile group (blue) is well separated (~520 and ~350 nm, respectively), thus enabling photocoupling and photodegradation reactions to be performed independently from one another using different light sources (illustrated with colored bars). **(b)** NMR studies indicate that the photodegradable moiety cleaves readily in the presence of UV light (λ = 365 nm, 10 mW cm^{-2}), but remains intact when exposed to the visible light used to initiate the photocoupling reaction (λ = 490 – 650 nm, 10 mW cm^{-2}). **(c)** Multi-photon visible light was first used to couple a fluorescently-labeled peptide within the center of the hydrogel in a user-defined 3D pattern (top, buffalo), and the network was subsequently degraded locally with multi-photon UV light, thereby removing the peptide from selected regions (bottom, CU and horn). **(d)** Brightfield microscopy confirms that photocleavage is confined only to user-defined locations within the gel, and that the photocoupling light conditions do not give rise to undesired degradation. Images in (c) represent 3D renderings of confocal z-stacks. Scale bars = 100 μm.

To provide a demonstration of the potential utility of these two photoreactions for advanced 3D cell culture, Figure 5.5 presents an approach where one might assay the specific effects of a variety of biomolecular cues on cell function within an otherwise uniform gel culture platform. Here, human mesenchymal stem cells (hMSCs) were encapsulated in gels synthesized *via* SPAAC chemistry, and their cellular microenvironment was patterned *via* the thiol-ene photocoupling reaction with perpendicular lines of width = 200 μm of integrin-binding peptide ligands, RGD and PHSRN, at ~1 mM each. These peptide sequences are both derived from

sequences found in fibronectin and are known to elicit some degree of synergy on cell adhesion[38]. The patterning created a repeating array of four distinct biochemical culture conditions (no cue, RGD alone, PHSRN alone, or both RGD and PHSRN) within the same gel (Fig. 5.5a). At a later time point, the photodegradation reaction was exploited to capture cells in spatially-defined regions of interest by exposing the gel to a given condition of light to induce erosion and liberate cells from their 3D culture environment (Fig. 5.5b). This process can be repeated many times over at different time points and locations to collect cells that have been exposed to either the same or different biochemical conditions, demonstrating full spatiotemporal control over cell subpopulation sampling (Fig. 5.5c). The released cells are readily collected, subsequently plated, expanded, and available for additional biological assays, including those that may be more difficult to perform on encapsulated cells. hMSCs remained viable (>95%) throughout the entire process (Supplementary Section 5.6.11). Here, we plated the released hMSCs and visualized their cytoskeletal organization using a fluorescent phalloidin, which stains for F-actin (Fig. 5.5d).

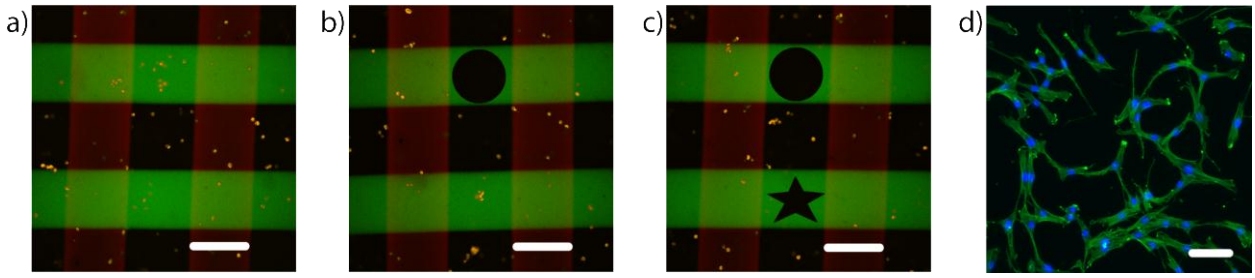

Figure 5.5 Culture and recovery of hMSCs from hydrogel microenvironments. CellTracker Orange-labeled human mesenchymal stem cells (hMSCs) were encapsulated within the click hydrogel formulation at 5 x 10^6 cells mL^{-1}. (a) 24 hours post encapsulation, perpendicular 200 μm wide lines of ~1 mM RGD and PHSRN were patterned throughout the hydrogel *via* thiol-ene photocoupling to create an array of four distinct biochemical conditions (no cue, RGD, PHSRN, RGD and PHSRN). (b) 4 hours later, channels of user-defined shape (cylindrical) were eroded down from the surface of the hydrogel to capture entrapped cells exposed to a specific cue. (c) This process was repeated 1 hour later to release entrapped cells within a different location of the material and a different shape (star-shaped cylinder). (d) The released cells were isolated by centrifugation, cultured in a 96-well plate for 48 hours, and their cytoskeleton was visualized with a fluorescent phalloidin. (a-c) RGD is shown in green, PHSRN red, and hMSCs orange. Images represent single confocal slices within the 3D gel. (d) F-actin is shown in green, nuclei blue. Image represents inverted fluorescence micrograph. Scale bars = 200 μm in (a-c), 50 μm in (d).

To further demonstrate how these reactions can be used to manipulate cellular functions in a spatiotemporally-regulated manner, a cell-laden (3T3 fibroblasts) fibrin clot was encapsulated within the click hydrogel formulation. After 2 hours, physical channels were eroded radially from the spherical clot *via* multi-photon photodegradation of the network to direct collective cell migration. Additionally, only specific regions of the gel were functionalized with RGD *via* the thiol-ene photocoupling reaction. Cells were found to leave the clot and migrate into the patterned hydrogel channels, but *only* when eroded migration channels were present *and* their surfaces decorated with the RGD adhesive ligand (Fig. 5.6a). Using two-photon patterning techniques, cell outgrowth was explicitly directed in all three spatial dimensions (Fig. 5.6b). This directed outgrowth can be performed in the presence of other encapsulated cells or with combinations of cell types. For example, hMSCs were encapsulated in the gel surrounding the 3T3-fibroblast-laden clot, and the fibroblasts were directed into the

surrounding hMSC microenvironment in a manner controlled by changes in the local gel environment. The patterned 3T3 fibroblasts were found to create complex structures in the presence of encapsulated hMSCs (Fig. 5.6c). These photoreactions are included to demonstrate how one might engineer complex, multicellular structures, ultimately expanding the potential for engineering tissue constructs with spatially varying cellularity in advanced bioreactors or culture systems.

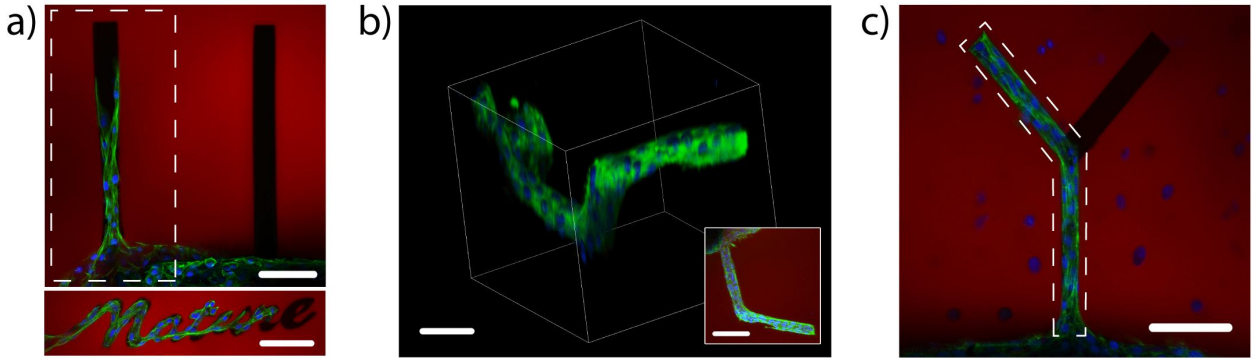

Figure 5.6 Directed 3D cell motility within patterned hydrogels. (a) A fibrin clot containing 3T3 fibroblasts was encapsulated within the click hydrogel formulation. Chemical channels of RGD, a cell-adhesive fibronectin motif, as well as physical channels of user-defined shape were created radially out of the roughly spherical clot. The combination of having physical space to spread as well as chemical moieties to bind to were found to be required for collective cell migration. By day 10, cells were found to migrate only down the physical channel that was functionalized with RGD. **(b)** By creating 3D functionalized channels, cell outgrowth was controlled in all three spatial dimensions, with the image inset illustrating a top-down projection. **(c)** The outgrowth of 3T3 fibroblast cells was controlled in the presence of encapsulated human mesenchymal stem cells (hMSCs) and confined to branched photodegraded channels that were functionalized with RGD. The regions of RGD-functionalization are depicted by the dashed polygons in (a) and (c). The hydrogel is shown in red, F-actin green, and cell nuclei blue. Scale bars = 100 μm.

As presented, this work utilizes two novel photoreaction schemes to combine and exploit features of previously mutually exclusive technologies. Namely, the physical and chemical properties of the network can be controlled independently with orthogonal light-based chemistries, allowing for real-time manipulation of cell function within a simplified synthetic microenvironment. These reactions are performed dynamically with full spatiotemporal control,

enabling full user-direction over these programmable cell niches. The cytocompatibility of the reaction processes should enable newfound opportunities for experiments to test basic hypotheses about critical events regulating cell-materials interactions at multiple time and size scales and, with this knowledge, improve strategies for stem cell culture, biomaterial design, 3D cell culture assays and tissue regeneration.

5.4 Materials and Methods

5.4.1 Synthesis of Click-Functionalized Macromolecular Precursors

Synthesis of PEG-tetraDIFO3: DIFO3[19,39] (121 mg, 0.6 mmol, Supplementary Section 5.6.12) and 2-(1H-7-Azabenzotriazol-1-yl)--1,1,3,3-tetramethyl uronium hexafluorophosphate Methanaminium (HATU, 225 mg, 0.6 mmol, Anaspec) were dissolved in minimal dimethylformamide (DMF, 5 mL) with N,N-diisopropylethylamine (DIEA, 210 μL, 1.2 mmol) and reacted for 5 min at RT. This solution was then added to 4-arm PEG tetraamine (M_n ~ 10,000 Da, 1 g, 0.4 mmol NH_2, JenKem) and stirred overnight, concentrated, dissolved in dH_2O, dialyzed (MWCO ~ 2 kDa, SpectraPor), filtered, and lyophilized to yield a white powder (1.03 g, 96%). Functionalization was confirmed to be >95% by ^{1}H-NMR.

Synthesis of Bis(azide)-functionalized photodegradable peptide crosslinker: The allyl-ester containing peptide H-RGK(alloc)GRK(dde)-NH_2 was synthesized (Protein Technologies Tribute peptide synthesizer) through Fmoc solid-phase methodology and HATU activation. 4-azidobutanoic acid (Supplementary Section 5.6.13) was coupled to the N-terminal amine with HATU, the 1-(4,4-dimethyl-2,6-dioxacyclohexylidene)ethyl (Dde) group was removed with 2% hydrazine monohydrate (Sigma) in DMF (3 x 10 min), and 4-(4-(1-(4-azidobutanoyloxy)ethyl)-2-methoxy-5-nitrophenoxy)butanoic acid (PLazide, Supplementary Section 5.6.13) was coupled to the ε-amino group of the C-terminal lysine. Resin was treated with trifluoroacetic

acid/triisopropylsilane/water (95:2.5:2.5) for 2 h and precipitated in and washed with (2x) ice-cold diethyl ether. The crude peptide was purified using semipreparative reversed-phase high-performance liquid chromatography (RP-HPLC) (Waters Delta Prep 4000) using a 70 min linear gradient (5 – 95% of acetonitrile and 0.1% trifluoroacetic acid) and lyophilized to give the product (Azide-RGK(alloc)GRK(PLazide)-NH_2) as a fluffy, yellow solid. Peptide purity was confirmed with analytical RP-HPLC and matrix-assisted laser desorption-ionization time-of-flight mass spectrometry (Applied Biosystems DE Voyage) using a-cyano-4-hydroxycinnamic acid matrix (Sigma): Calculated ($[M+H]^+$ 1288.4); observed ($[M+H]^+$ 1288.1) (Supplementary Section 5.6.14).

Synthesis of fluorescently-labeled adhesive ligand: H-AhxRGDSC-NH_2 (0.5 mmol) was synthesized and modified with Alexa Fluor® 488 carboxylic acid, 2,3,5,6-tetrafluorophenyl ester (2 mg, Invitrogen) in DMF overnight at room temp. The peptide was cleaved from resin, precipitated, and lyophilized to give a yellow solid (denoted AF_{488}-AhxRGDSC-NH_2). AF_{633}-AhxPHSRNC-NH_2 was synthesized in a similar manner.

5.4.2 Gel Formation

Hydrogels were created by mixing 10 wt% total macromer photodegradable, photocouplable click gel formulation in media in between an azide-functionalized (Supplementary Section 5.6.15) and Rain-X®-treated glass slides spaced at a known distance (typically 500 μm), and reacted for 30 min at 37 °C. The slides were separated, and the gel remained covalently attached to the azide-functionalized slide.

5.4.3 Biochemical Patterning

Hydrogels were swollen in phenol red-free media containing 3 mg mL^{-1} patterning agent AF_{488}-AhxRGDSC-NH_2 and eosin Y (10 μM) for one hour. For photolithographic-based

experiments, gels were exposed to collimated visible light (λ = 490 – 650 nm), achieved with an Acticure (EXFO) high pressure mercury lamp equipped with an internal bandpass filter (350 – 650 nm) and an external 490 nm longpass filter (Edmund Optics), through a patterned chrome photomask. Alternatively, 3D patterning was obtained *via* two-photon techniques where subvolumes within the hydrogel were selectively exposed to pulsed laser light (λ = 860 nm, power = 350 mW/μm^2, scan speed = 1.27 $\mu sec/\mu m^2$) at 1 μm z-plane increments on a 710 LSM NLO confocal microscope stage (Carl Zeiss) equipped with a 20x/0.8 Plan-Apochromat objective (NA = 1.0). Unreacted patterning agent and initiator were swollen into fresh media (2 hours), yielding the final patterned hydrogel. In both the photolithographic and multi-photon patterning techniques, photocoupling of the peptide was confined to volumes exposed to light within the material and was visualized by fluorescent confocal microscopy.

5.4.4 Biophysical Patterning

Gels containing 0.125 mM Alexa Fluor® 594 azide (Invitrogen) were patterned using photolithographic techniques, where hydrogels were exposed to collimated UV light (λ = 365 nm) from an Omnicure S1000 (EXFO) high pressure mercury lamp equipped with an internal bandpass filter (365 nm). 3D patterning was obtained *via* two-photon techniques where regions of interest (x-y control) within the hydrogel were selectively exposed to pulsed laser light (λ = 740 nm, power = 670 mW/μm^2, scan speed = 1.27 $\mu sec/\mu m^2$). Photodegraded monomer was swollen into fresh media, yielding the final patterned hydrogel.

5.4.5 Cell Culture

NIH 3T3s (mouse) were cultured in high-glucose Dulbecco's modified Eagle's medium (DMEM, Gibco) containing 10% fetal bovine serum (Invitrogen), 1% penicillin/streptomycin (Gibco), 0.2% fungizone, and 0.4% gentamicin. hMSCs were cultured in low-glucose DMEM

with 10% fetal bovine serum, 1% penicillin/streptomycin, 0.2% fungizone, and 0.4% gentamicin. All cells were maintained in 5% CO_2 at 37 °C. Cells were used between passages P4 and P6.

5.4.6 Fibrin Clot Encapsulation

Cells were suspended at 10 x 10^6 cells mL^{-1} in a fibrinogen solution (10 mg mL^{-1} in PBS, Sigma) containing thrombin (5 U mL^{-1}, Sigma) and reacted for 30 min at 37 °C. The formed cell-laden clots were suspended in a 10 wt% total macromer photodegradable, photocouplable click gel formulation sandwiched between azide-functionalized (Supplementary Section 5.6.10) and Rain-X®-treated glass slides spaced at 1 mm, and reacted for an additional 30 min at 37 °C. The slides were separated, and the gel remained covalently attached to the azide-functionalized slide. After 2 hours in media, physical channels were patterned into the network with two-photon patterning (λ = 740 nm). The media was then supplemented with Ac-RGDSC-NH_2 (3 mg mL^{-1}) and eosin Y (10 μM), equilibrated for 1 hr, and selected regions within the gel were biochemically decorated with RGD (λ = 860 nm). On day 10, the hydrogels were fixed in formalin for 1.5 h, followed by cell permeabilization with 0.5% Triton® X-100 (Fisher) in PBS for 2 h. The samples were blocked with 3% bovine serum albumin (BSA, Sigma) in PBS for 1 h and rinsed with PBS. F-actin was visualized using Alexa Fluor® 488 Phalloidin Conjugate (5 U/mL, Invitrogen), while nuclei were stained with DAPI (500 nM, Invitrogen), each for 2 h. The samples were washed with PBS prior to confocal visualization.

5.5 References

1. Kolb, H.C., Finn, M.G. & Sharpless, K.B. Click chemistry: Diverse chemical function from a few good reactions. *Angew. Chem. Int. Ed.* **40**, 2004-2021 (2001).

2. Kolb, H.C. & Sharpless, K.B. The growing impact of click chemistry on drug discovery. *Drug Discov. Today* **8**, 1128-1137 (2003).

3. Moses, J.E. & Moorhouse, A.D. The growing applications of click chemistry. *Chem. Soc. Rev.* **36**, 1249-1262 (2007).

4. Hawker, C.J. & Wooley, K.L. The convergence of synthetic organic and polymer chemistries. *Science* **309**, 1200-1205 (2005).

5. Barner-Kowollik, C. et al. "Clicking" polymers or just efficient linking: What is the difference? *Angew. Chem. Int. Ed. Engl.* **50**, 60-62 (2011).

6. Sletten, E.M. & Bertozzi, C.R. Bioorthogonal chemistry: Fishing for selectivity in a sea of functionality. *Angew. Chem. Int. Ed. Engl.* **48**, 6974-6998 (2009).

7. Bowman, C.N. & Kloxin, C.J. Toward an enhanced understanding and implementation of photopolymerization reactions. *Aiche J* **54**, 2775-2795 (2008).

8. DeForest, C.A., Polizzotti, B.D. & Anseth, K.S. Sequential click reactions for synthesizing and patterning three-dimensional cell microenvironments. *Nat. Mater.* **8**, 659-664 (2009).

9. Luo, Y. & Shoichet, M.S. A photolabile hydrogel for guided three-dimensional cell growth and migration. *Nat. Mater.* **3**, 249-253 (2004).

10. Aizawa, Y., Wylie, R. & Shoichet, M. Endothelial cell guidance in 3d patterned scaffolds. *Adv. Mater.* **22**, 4831-+ (2010).

11. Lee, S.H., Moon, J.J. & West, J.L. Three-dimensional micropatterning of bioactive hydrogels *via* two-photon laser scanning photolithography for guided 3d cell migration. *Biomaterials* **29**, 2962-2968 (2008).

12. Hoffmann, J.C. & West, J.L. Three-dimensional photolithographic patterning of multiple bioactive ligands in poly(ethylene glycol) hydrogels. *Soft Matter* **6**, 5056-5063 (2010).

13. Seidlits, S.K., Schmidt, C.E. & Shear, J.B. High-resolution patterning of hydrogels in three dimensions using direct-write photofabrication for cell guidance. *Adv Funct Mater* **19**, 3543-3551 (2009).

14. Kloxin, A.M., Kasko, A.M., Salinas, C.N. & Anseth, K.S. Photodegradable hydrogels for dynamic tuning of physical and chemical properties. *Science* **324**, 59-63 (2009).

15. Khetan, S., Katz, J.S. & Burdick, J.A. Sequential crosslinking to control cellular spreading in 3-dimensional hydrogels. *Soft Matter* **5**, 1601-1606 (2009).

16. Khetan, S. & Burdick, J.A. Patterning network structure to spatially control cellular remodeling and stem cell fate within 3-dimensional hydrogels. *Biomaterials* **31**, 8228-8234 (2010).

17. Sarig-Nadir, O., Livnat, N., Zajdman, R., Shoham, S. & Seliktar, D. Laser photoablation of guidance microchannels into hydrogels directs cell growth in three dimensions. *Biophys. J.* **96**, 4743-4752 (2009).

18. Ilina, O., Bakker, G.J., Vasaturo, A., Hofmann, R.M. & Friedl, P. Two-photon laser-generated microtracks in 3d collagen lattices: Principles of mmp-dependent and -independent collective cancer cell invasion. *Phys. Biol.* **8** (2011).

19. Codelli, J.A., Baskin, J.M., Agard, N.J. & Berozzi, C.R. Second-generation difluorinated cyclooctynes for copper-free click chemistry. *J. Am. Chem. Soc.* **130**, 11486-11493 (2008).

20. Adzima, B.J. et al. Spatial and temporal control of the alkyne-azide cycloaddition by photoinitiated cu(ii) reduction. *Nat. Chem.* **3**, 258-261 (2011).

21. Hoyle, C.E. & Bowman, C.N. Thiol-ene click chemistry. *Angew. Chem. Int. Ed.* **49**, 1540-1573 (2010).

22. Dondoni, A. The emergence of thiol-ene coupling as a click process for materials and bioorganic chemistry. *Angew. Chem. Int. Ed.* **47**, 8995-8997 (2008).

23. Polizzotti, B.D., Fairbanks, B.D. & Anseth, K.S. Three-dimensional biochemical patterning of click-based composite hydrogels *via* thiolene photopolymerization. *Biomacromolecules* **9**, 1084-1087 (2008).

24. DeForest, C.A., Sims, E.A. & Anseth, K.S. Peptide-functionalized click hydrogels with independently tunable mechanics and chemical functionality for 3d cell culture. *Chem. Mater.* **22**, 4783-4790 (2010).

25. Killops, K.L., Campos, L.M. & Hawker, C.J. Robust, efficient, and orthogonal synthesis of dendrimers *via* thiol-ene "click" chemistry. *J. Am. Chem. Soc.* **130**, 5062-5064 (2008).

26. Fairbanks, B.D. et al. A versatile synthetic extracellular matrix mimic *via* thiol-norbornene photopolymerization. *Adv. Mater.* **21**, 5005-5010 (2009).

27. Gupta, N. et al. A versatile approach to high-throughput microarrays using thiol-ene chemistry. *Nat. Chem.* **2**, 138-145 (2010).

28. Uygun, M., Tasdelen, M.A. & Yagci, Y. Influence of type of initiation on thiol-ene "click" chemistry. *Macromol Chem Phys* **211**, 103-110 (2010).

29. Alvarez, M. et al. Single-photon and two-photon induced photocleavage for monolayers of an alkyltriethoxysilane with a photoprotected carboxylic ester. *Adv. Mater.* **20**, 4563-4567 (2008).

30. Deiters, A. Principles and applications of the photochemical control of cellular processes. *Chembiochem* **11**, 47-53 (2010).

31. Holmes, C.P. Model studies for new o-nitrobenzyl photolabile linkers: Substituent effects on the rates of photochemical cleavage. *J. Org. Chem.* **62**, 2370-2380 (1997).

32. Ohmuro-Matsuyama, Y. & Tatsu, Y. Photocontrolled cell adhesion on a surface functionalized with a caged arginine-glycine-aspartate peptide. *Angew. Chem. Int. Ed.* **47**, 7527-7529 (2008).

33. Johnson, J.A., Baskin, J.M., Bertozzi, C.R., Koberstein, J.T. & Turro, N.J. Copper-free click chemistry for the in situ crosslinking of photodegradable star polymers. *Chem. Commun.*, 3064-3066 (2008).

34. Wong, D.Y., Griffin, D.R., Reed, J. & Kasko, A.M. Photodegradable hydrogels to generate positive and negative features over multiple length scales. *Macromolecules* **43**, 2824-2831 (2010).

35. Kloxin, A.M., Tibbitt, M.W. & Anseth, K.S. Synthesis of photodegradable hydrogels as dynamically tunable cell culture platforms. *Nat. Protoc.* **5**, 1867-1887 (2010).

36. Kloxin, A.M., Benton, J.A. & Anseth, K.S. In situ elasticity modulation with dynamic substrates to direct cell phenotype. *Biomaterials* **31**, 1-8 (2010).

37. Frey, M.T. & Wang, Y.L. A photo-modulatable material for probing cellular responses to substrate rigidity. *Soft Matter* **5**, 1918-1924 (2009).

38. Redick, S.D., Settles, D.L., Briscoe, G. & Erickson, H.P. Defining fibronectin's cell adhesion synergy site by site-directed mutagenesis. *J. Cell Biol.* **149**, 521-527 (2000).

39. Sims, E.A., DeForest, C.A. & Anseth, K.S. A mild, large-scale synthesis of 1,3-cyclooctanedione: Expanding access to difluorinated cyclooctyne for copper-free click chemistry. *Tetrahedron Lett.* **52**, 1871-1873 (2011).

5.6 Supplementary Information

5.6.1 *In situ* rheometry of gel formation

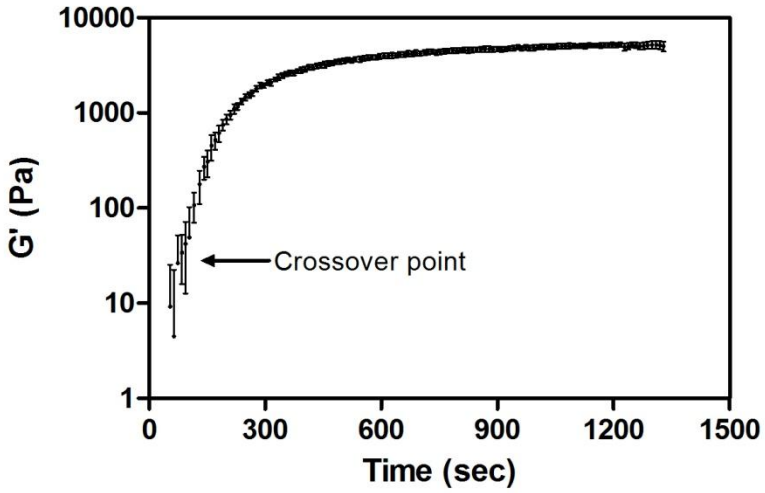

Dynamic frequency, time, and strain sweep rheological experiments were performed on a TA Ares rheometer with parallel plate geometry (8 mm diameter) at 25 °C. Initial gel network formation of a 10 wt% solution was monitored by observing G' and G'' at a constant frequency of 100 rad/s as a function of time. Gel properties were monitored *via* frequency sweep measurements at fixed strain amplitude (10%) to measure the hydrogel storage, G', and loss, G'', moduli. The crossover point was found to be at 100 ± 20 sec. Final modulus was determined to be 5100 ± 500 Pa.

5.6.2 Protein patterning within click gels

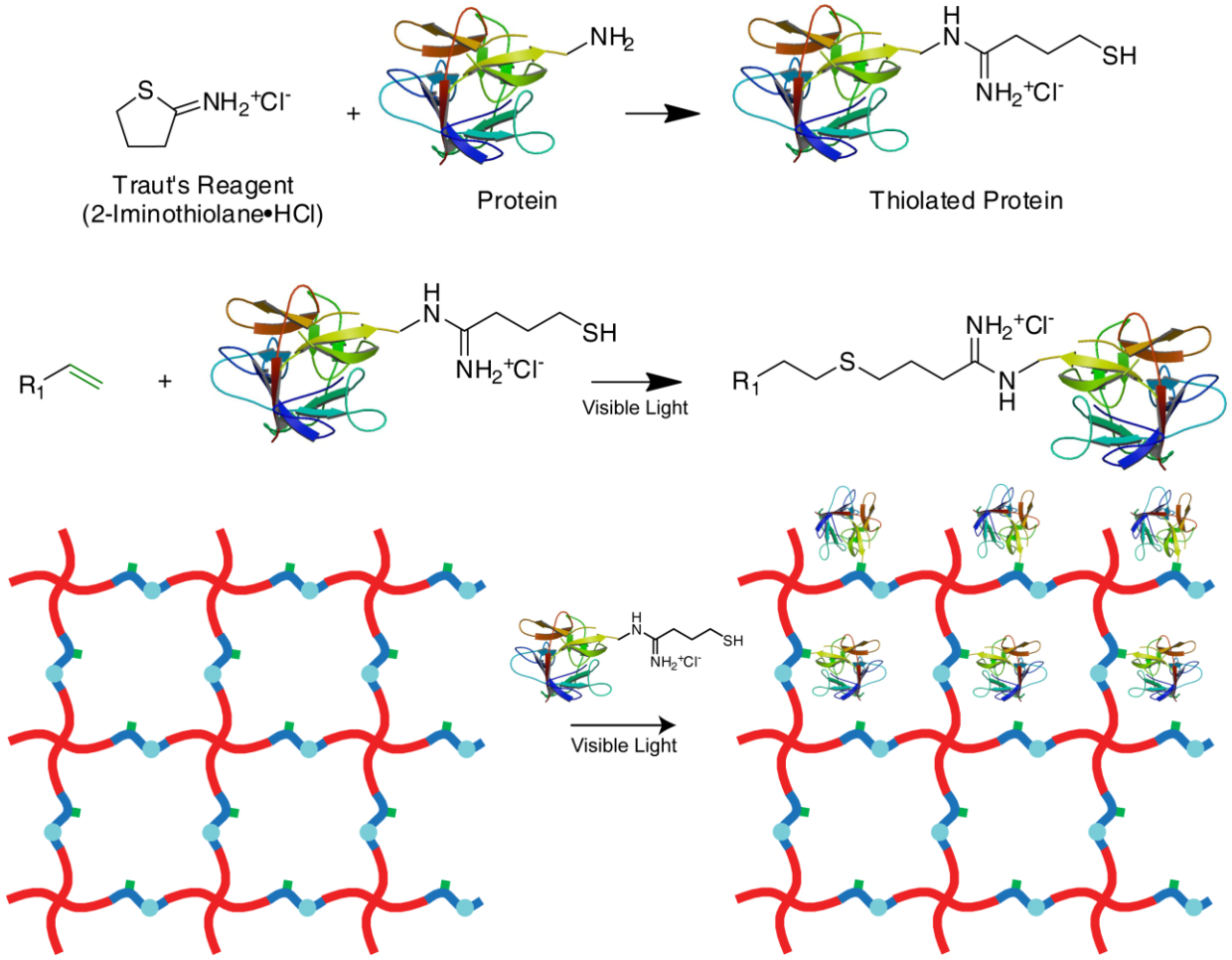

Traut's reagent (2-Iminothiolane•HCl, Thermo Scientific, 2x) was added to soybean trypsin inhibitor, Alexa Fluor® 488 conjugate (STI_{488}, 21 kDa, Invitrogen) dissolved in PBS at 0.67 mg mL^{-1} and reacted at room temperature for 1 hr to yield the thiolated protein (STI_{488}-SH). Traut's reagent reacts with primary amines on the ST_{488} and converts them to thiols to be used in the thiol-ene reaction.

Hydrogels were swollen in phenol red-free media containing STI_{488}-SH (0.1 mg mL^{-1}) and eosin Y (10 μM) for one hour. Gels were exposed to collimated visible light (λ = 490 – 650 nm), achieved with an Acticure (EXFO) high pressure mercury lamp equipped with an internal bandpass filter (350 – 650 nm) and an external 490 nm longpass filter (Edmund Optics), through

a patterned chrome photomask with 200 x 200 μm square openings. Unreacted STI_{488}-SH and initiator were removed by swelling into fresh media, and the sample was visualized by fluorescent confocal microscopy (image below).

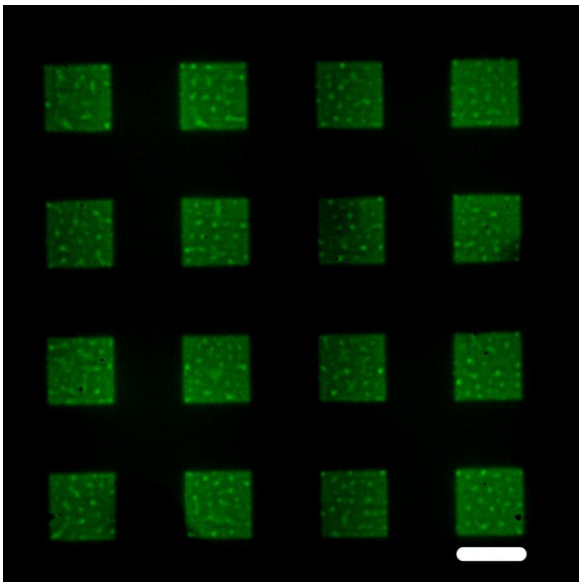

Scale bar = 200 μm.

5.6.3 Small molecule patterning within click gels

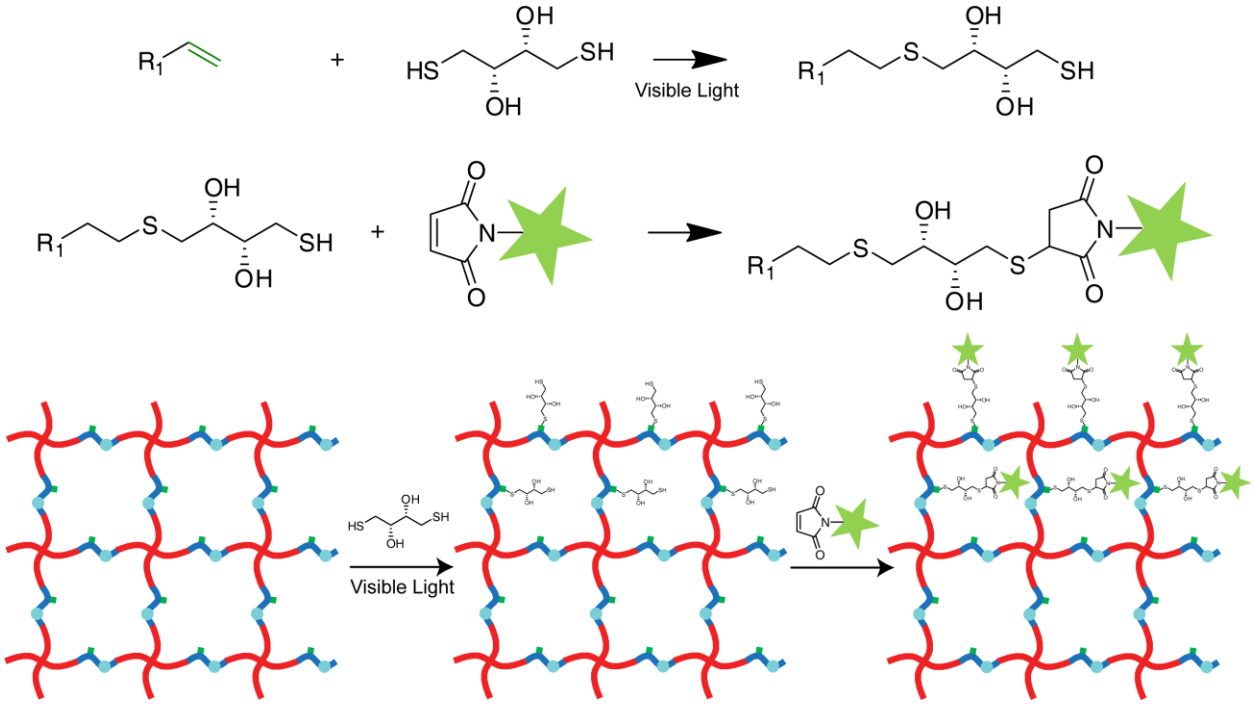

Hydrogels were swollen in phenol red-free media containing dithiothreitol (DTT, 0.3 mg mL^{-1}) and eosin Y (10 μM) for one hour. Gels were exposed to collimated visible light (λ = 490 – 650 nm), achieved with an Acticure (EXFO) high pressure mercury lamp equipped with an internal bandpass filter (350 – 650 nm) and an external 490 nm longpass filter (Edmund Optics), through a patterned chrome photomask with 50, 100, 150, 200, 250, and 300 μm diameter circle openings. Unreacted DTT and initiator were removed by swelling into fresh media, yielding the chemically-patterned hydrogel.

To visualize the patterned thiol molecules, phenol red-free media containing Alexa Fluor® 488 C5 maleimide (0.2 mg mL^{-1}) was swollen into the network. Here, the maleimides covalently react with the patterned pendant thiols, which are present only where light was previously shone. The unreacted dye was swollen into fresh media, and the sample was visualized by fluorescent confocal microscopy (image below).

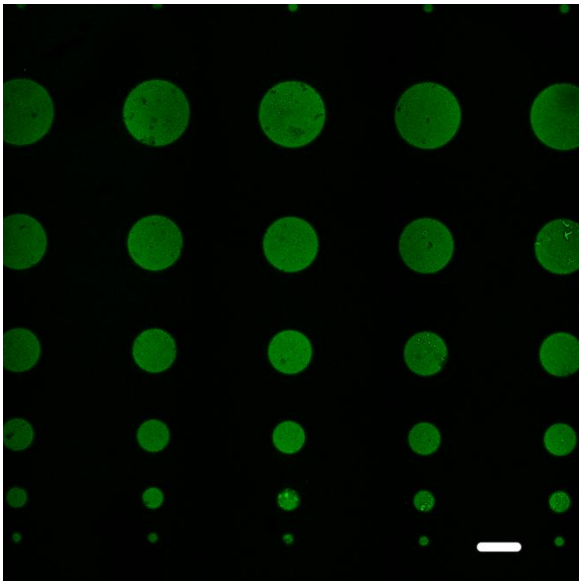

Scale bar = 200 μm.

5.6.4 3D visualization of photolithographically-based thiol-ene patterning

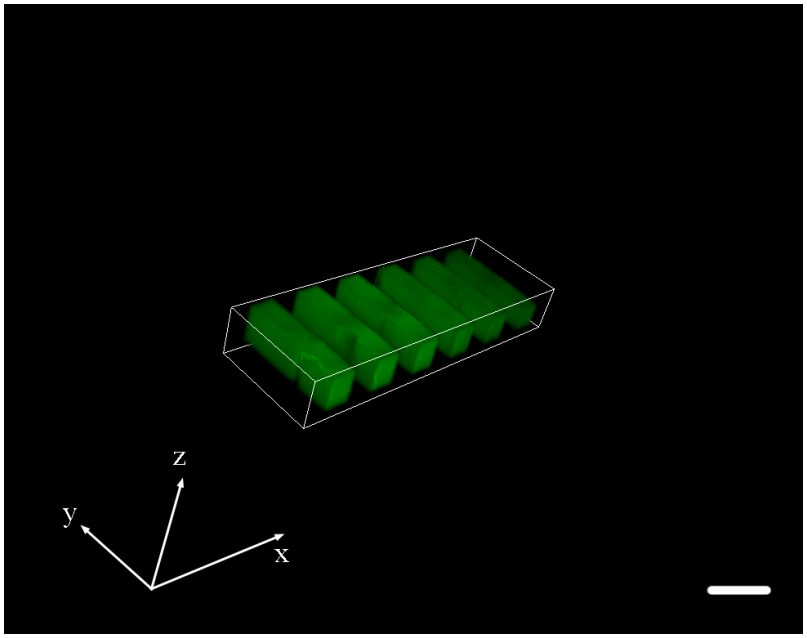

Channels are 400 μm wide (in x) and extend through the full thickness of the gel (~500 μm, in z) with roughly constant intensity. Scale bar = 800 μm.

5.6.5 NMR studies of small molecule PLazide photodegradation

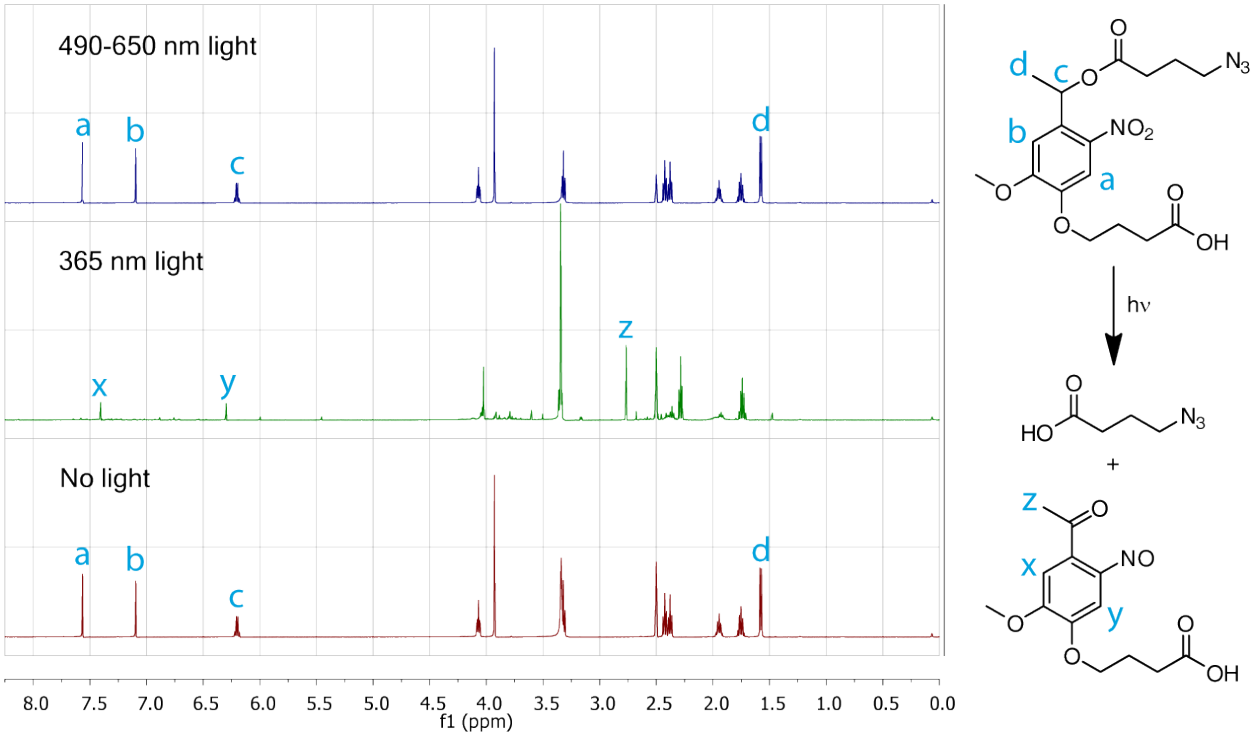

Upon exposure to UV light (λ = 365 nm), characteristic peaks in ^{1}H NMR shift drastically indicating photodegradation. In similar exposure to visible light (λ = 490 – 650 nm), these peak shifts are not observed indicating negligible photodegradation.

5.6.6 Kinetic NMR studies of PLazide photodegradation

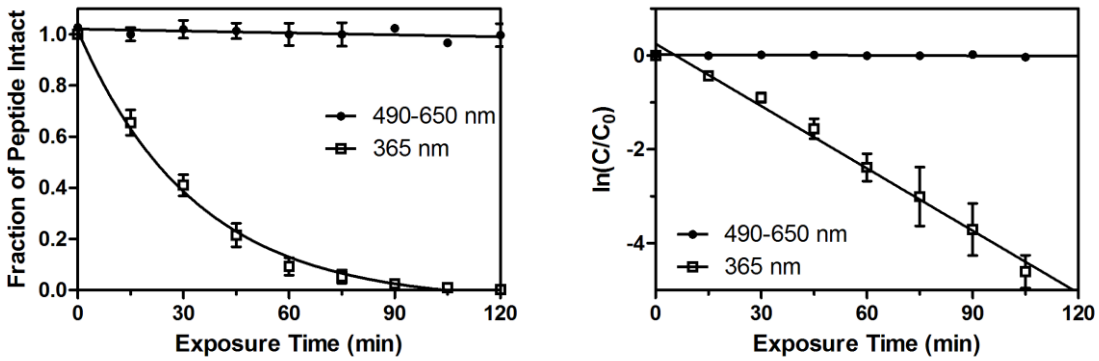

The photodegradable peptide (Azide-RGK(alloc)GRK(PLazide)-NH_2) was dissolved in dH_2O at 15.5 mM, roughly the concentration present in a 10 wt% gel formation, and injected into

a glass sample chamber measuring 3" x 2" x 500 μm. The solution was exposed to collimated light (λ = 365 nm or 490 – 650 nm, 10 mW cm^{-2}) for various amounts of time. The solution was collected, lyophilized, redissolved in D_2O, and ^1H NMR experiments were performed for each time point. The fraction of intact peptide was calculated by comparing integral values for the alloc vinyl protons (δ = 5.84, 1H), which do not shift significantly upon degradation and thus give the amount of peptide present in the sample, with the aromatic protons of the intact PLazide (δ = 7.50, 1H; δ = 7.11, 1H).

The photodegradation process follows first-order reaction kinetics:

$$\frac{C}{C_0} = e^{-k_{avg} \cdot t}$$

Where *C* is the concentration of intact PLazide at any time *t*, C_0 is the initial concentration of the PLazide (15.5 mM), and k_{avg} is the kinetic constant of degradation averaged throughout the thickness of the sample. It is important to note that k_{avg} does not account for light attenuation in our specific system and is specific to each experimental setup. From this, it follows that:

$$\ln \frac{C}{C_0} = -k_{avg} \cdot t$$

Plotting our data (left) in this form (shown on the right) gives us a linear plot with a slope:

$$k_{avg} = 7.36 \times 10^{-4} \frac{1}{\text{sec}}$$

Similarly, the kinetic constant can be written in more fundamental terms:

$$k_{avg} = \frac{\varphi \varepsilon I_{avg}}{N_A \hbar \nu}$$

$$\varphi = \frac{N_A \hbar \nu k_{avg}}{\varepsilon I_{avg}}$$

Where ϕ is the quantum yield; N_A is Avogadro's number; h is the Planck constant; c is the speed of light; I is the intensity of light; I_0 is the incident light intensity; ε is the molar absorptivity of the sample (4780 M^{-1} cm^{-1} for PLazide at λ = 365 nm); and ν is the frequency of the associated electromagnetic wave.

Also, the light intensity at any given depth (z) is a function of C and ε.

$$I = I_0 e^{-\varepsilon C z}$$

As both the degradable precursor and the degraded product have similar molar absorptivities (ε) at λ = 365 nm (see 5.6.4), the light attenuation is roughly constant throughout the degradation process and can be described as:

$$I = I_0 e^{-\varepsilon C_0 z}$$

We can calculate the average intensity as:

$$I_{avg} = \frac{\int_{0\ \mu\text{m}}^{500\ \mu\text{m}} I_0 e^{-\varepsilon C_0 z} dz}{\int_{0\ \mu\text{m}}^{500\ \mu\text{m}} dz} = 2.53 \frac{\text{mW}}{\text{cm}^2}$$

Thus, all variables in our equation for ϕ are known:

$$\varphi = 0.01995$$

Using this quantum yield, we can calculate the kinetic constant for degradation at any intensity, I.

$$k = \frac{\varphi \varepsilon I}{N_A \hbar \nu}$$

For 10 mW cm^{-2}:

$$k = 0.00291 \frac{1}{\text{sec}}$$

This value, unlike k_{avg}, is intrinsic to the photodegradation reaction and is not specific to a given experimental setup.

5.6.7 Temporally controlled photodegradation and material properties of optically thin gels

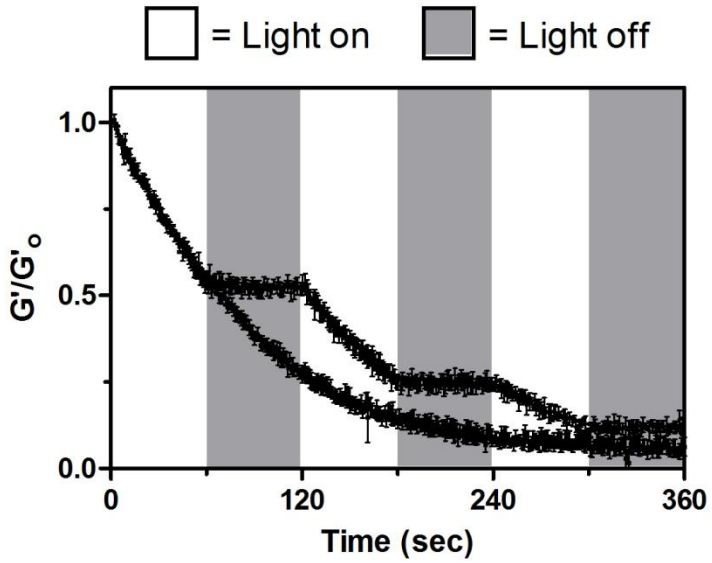

Optically thin gels (50 μm) were polymerized *in situ* between a Peltier plate (25 °C) and a clear quartz plate (8 mm) on a photorheometer (TA Ares). Dynamic time sweep experiments were performed to monitor gel formation (Supplementary Section 5.6.1). After full gelation had occurred (~20 min), the sample was exposed to UV light (λ = 365 nm, 10 mW cm^{-2}) and degradation was quantified by monitoring G' with constant exposure (bottom curve). By shuttering the light exposure, temporal control over network properties was obtained (top curve).

The crosslinking density (ρ_x) scales with the measured storage modulus (G'), we can calculate the degradation kinetic constant (k) from the continuous exposure data as:

$$\frac{\ln(G')}{\ln(G'_0)} = \frac{\ln(\rho_x)}{\ln(\rho_{x,0})} = -4kt$$

Here, G'_0 is the initial storage modulus (5100 ± 500 Pa), $\rho_{x,0}$ is the initial crosslinking density, and t is the irradiation time. The factor of 4 is included as photolytic cleavage on any side of the 4-arm PEG will lead to a decrease in crosslinking density.

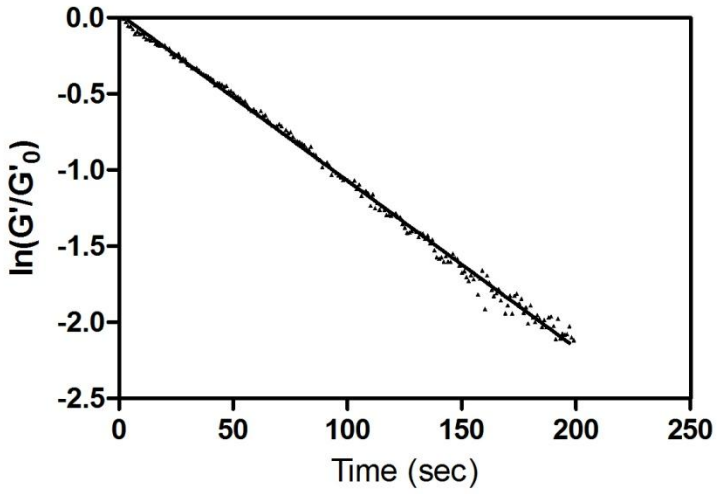

From the slope of the $\frac{\ln(G')}{\ln(G'_0)}$ vs *t* plot, we obtain:

$$k = 0.00275 \frac{1}{\text{sec}}$$

which is in good agreement with that obtained by NMR studies of PLazide degradation in Supplementary Section 5.6.6.

5.6.8 Visible color change upon Azide-RGK(alloc)GRK(PLazide)-NH_2 photodegradation

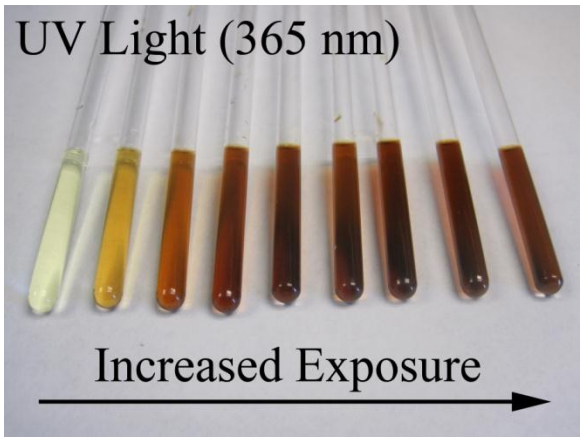

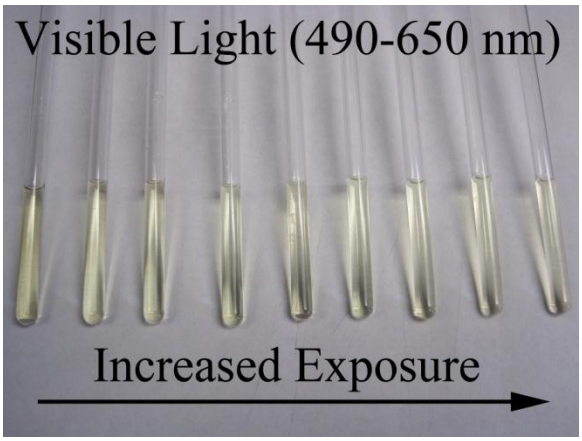

Digital photographs of Azide-RGK(alloc)GRK(PLazide)-NH_2 after light treatment (as described in Supplementary Section 5.6.6). Images each represent 0, 15, 30, 45, 60, 75, 90, 105,

and 120 min light exposure from left to right for 10 mW cm^{-2} for λ = 365 nm and λ = 490 – 650 nm.

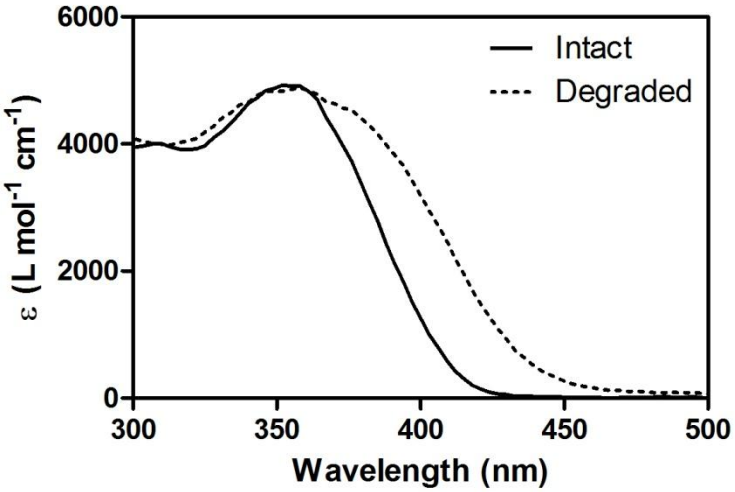

The darkening of the samples upon degradation is seen by a shift in the absorption spectrum for PLazide.

5.6.9 Digital photo of photodegraded channels in optically-thick sample

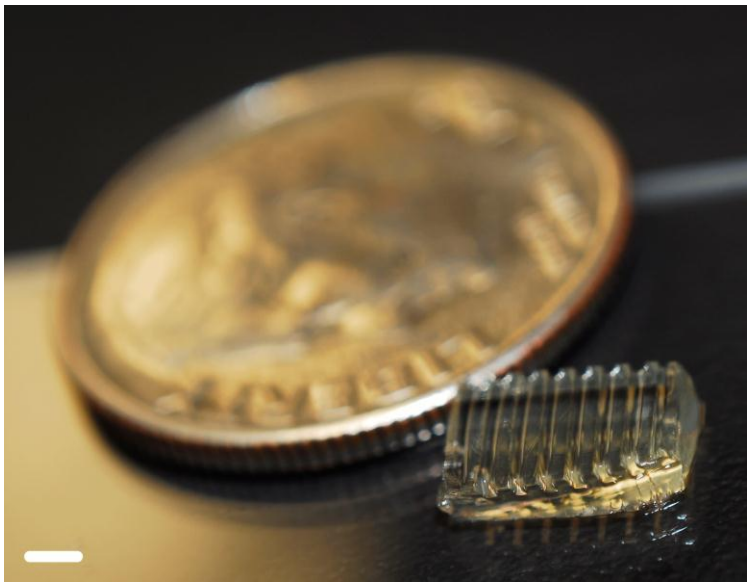

Channels are 400 μm wide and 400 μm deep. Scale bar = 1.6 mm.

5.6.10 Photodegradation erosion depth versus total light dosage

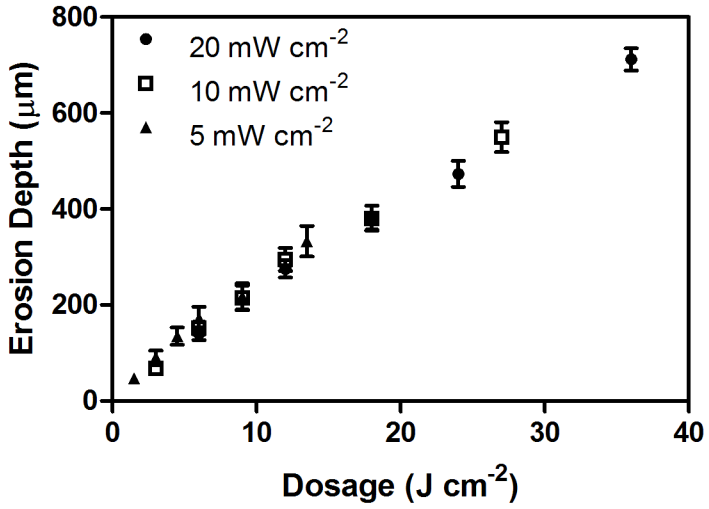

Here, dosage represents the total amount of energy delivered to the system and is calculated as the product of exposure time and light intensity. The erosion depth is measured by profilometry.

5.6.11 Viability of hMSCs after SPAAC encapsulation, thiol-ene coupling, and network photodegradation

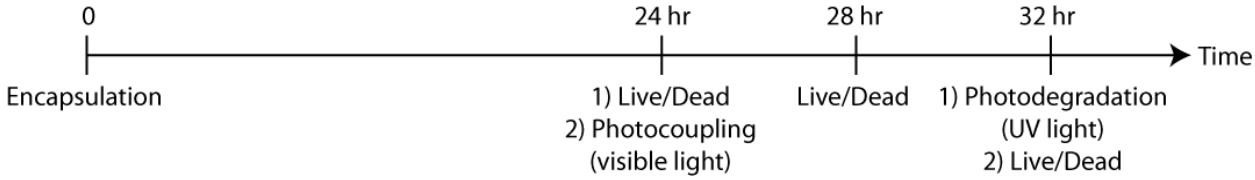

Time 0 – Human mesenchymal stem cells (hMSCs, between P3 and P6) were encapsulated in 10 wt% photodegradable, photocouplable click formulation in PBS at a density of 2.5 x 10^6 cells mL^{-1}. The solution was sandwiched between azide-functionalized (Supplementary Section 5.6.15) and Rain-X®-treated glass slides spaced at 0.5 mm, and reacted for 30 min. The gels were transferred to growth media (consisting of low-glucose Dulbecco's modified Eagle's medium (Gibco) containing 10% fetal bovine serum (Invitrogen), 1%

penicillin/streptomycin (Gibco), 0.2% fungizone, and 0.4% gentamicin) and incubated in 5% CO_2 at 37 °C.

24 hrs – A subset of the cell-laden gels were stained with a Live/Dead assay (Invitrogen) and visualized with fluorescent confocal microscopy. A high viability post-encapsulation (>95%) was observed. The unstained hydrogels were then swollen in phenol red-free media containing H-RGDSC-NH_2 (3 mg mL^{-1}) and eosin Y (10 μM) for one hour. Gels were bulk irradiated (2 min) with collimated visible light (λ = 490 – 650 nm, 10 mW cm^{-2}), achieved with an Acticure (EXFO) high pressure mercury lamp equipped with an internal bandpass filter (350 – 650 nm) and an external 490 nm longpass filter (Edmund Optics). Unreacted peptide and initiator were removed by swelling into fresh media, yielding the chemically-modified hydrogel.

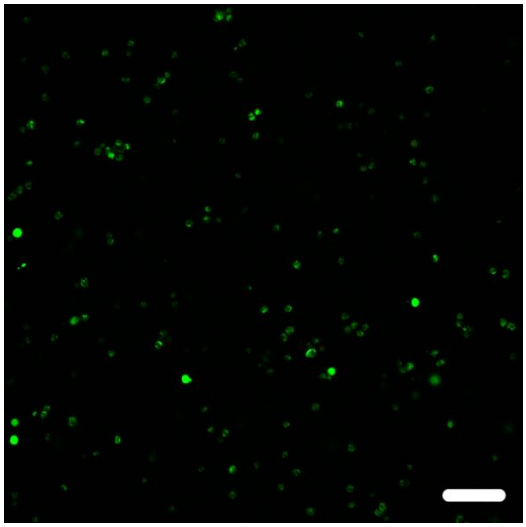

Scale bar = 100 μm, 100 μm projection

28 hr – A subset of the cell-laden, H-RGDSC-NH_2 thiol-ene labeled gels were stained with Live/Dead (Invitrogen) and visualized with fluorescent confocal microscopy, and a high viability post-encapsulation and photocoupling (>95%) was observed.

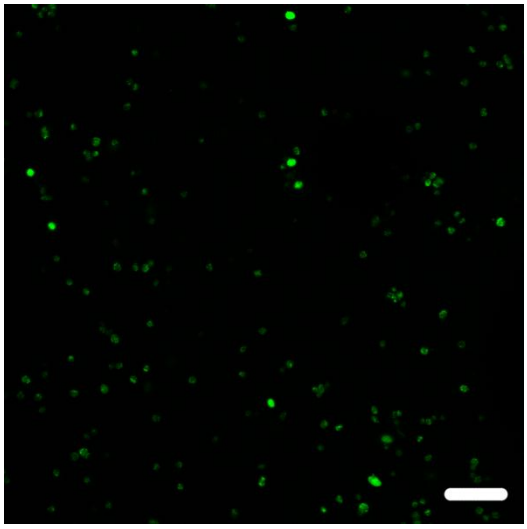

Scale bar = 100 μm, 100 μm projection

32 hr – Cell-laden gels, previously patterned with H-RGDSC-NH_2 by thiol-ene photocoupling, were bulk irradiated (15 min) with collimated UV light (λ = 365 nm, 10 mW cm^{-2}), resulting in full degradation of the top ~200 μm of the initially 500 μm thick gel. This degradation resulted in the complete release of the encapsulated cells in the eroded regions. The gel was then washed with fresh media, and the cells were concentrated by centrifugation (1000 rpm x 6 min). The cells were resuspended in media containing the Live/Dead stain (Invitrogen) for 30 min, centrifuged again (1000 rpm x 6 min), resuspended in fresh media (10^6 cells mL^{-1}), and imaged with fluorescent confocal microscopy. Again, a high viability post-encapsulation, photocoupling, and photodegradation (>95%) was observed.

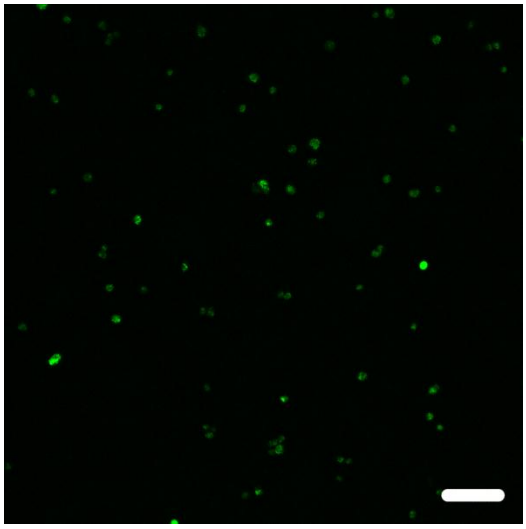

Scale bar = 100 μm, 100 μm projection

The photoreleased cells were then plated in a 96-well tissue culture polystyrene plate and imaged 48 hours later with brightfield microscopy. Cells attached and exhibited typical morphology of plated hMSCs, further demonstrating their viability throughout the encapsulation and subsequent patterning processes.

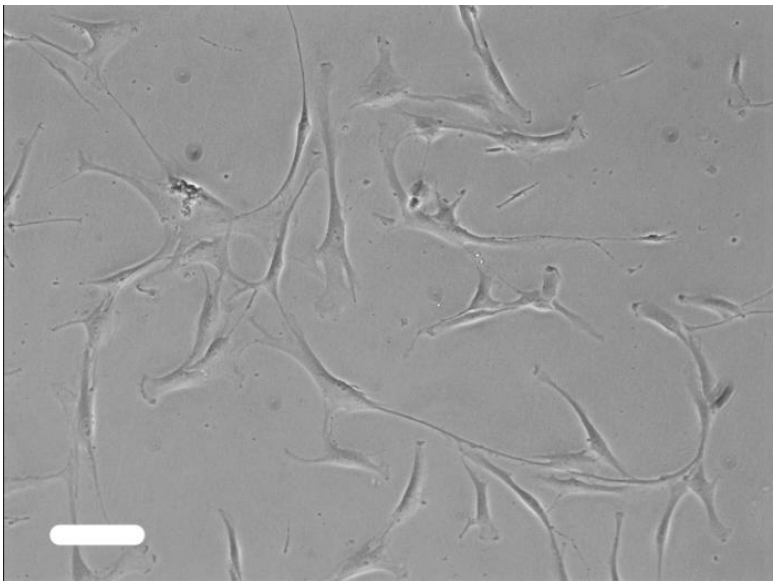

Scale bar = 25 μm

5.6.12 Synthesis of difluorinated cyclooctyne (DIFO3):

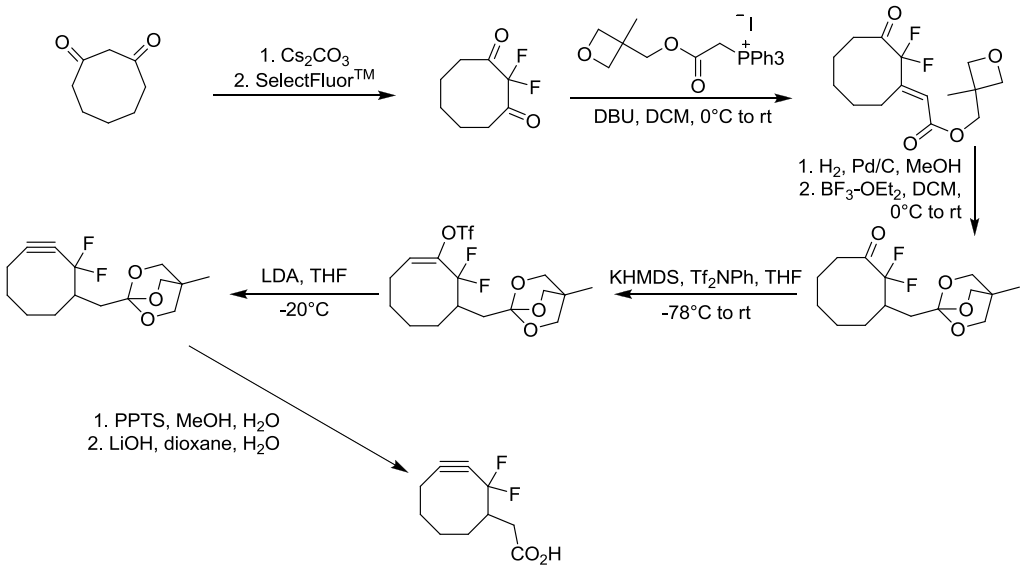

DIFO3 was synthesized following a published synthetic route, starting with 12.4 g of 1,3-cyclooctanedione. All reactions were performed with linearly-scaled reaction conditions with respect to reported amounts. Yields were comparable for all reported steps. ^{1}H NMR (500 MHz, $CDCl_3$, δ): 11.72 (br s, 1H), 2.82-2.69 (m, 2H), 2.43-2.22 (m 3H), 2.19-2.05 (m, 2H), 1.87-1.74 (m, 2H), 1.70-1.61 (m, 1H), 1.45-1.35 (m, 1H); ^{13}C NMR (101 MHz, $CDCl_3$, δ): 178.53 (s), 119.10 (dd, J = 237.7, 239.4), 110.71 (t, J = 11.1 Hz) 84.62 (dd, J = 41.6 Hz, 46.9), 52.60 (t, J = 24.3 Hz), 33.80 (d, J = 3.1 Hz), 32.84 (d, J = 4.5 Hz), 32.65 (d, J = 1.9 Hz), 27.87 (s), 20.45 (s); ^{19}F NMR (376 MHz, $CDCl_3$, δ): -95.84 (d, J = 259.9; 1F), -102.05 (ddt, J = 7.0, 21.1, 260.2; 1F); HRMS (ESI+): calculated for $C_{10}H_{12}F_2LiO_2^+$ [M + ^{7}Li]$^+$, 209.0940; found 209.0965 (Δ = +2.5 ppm).

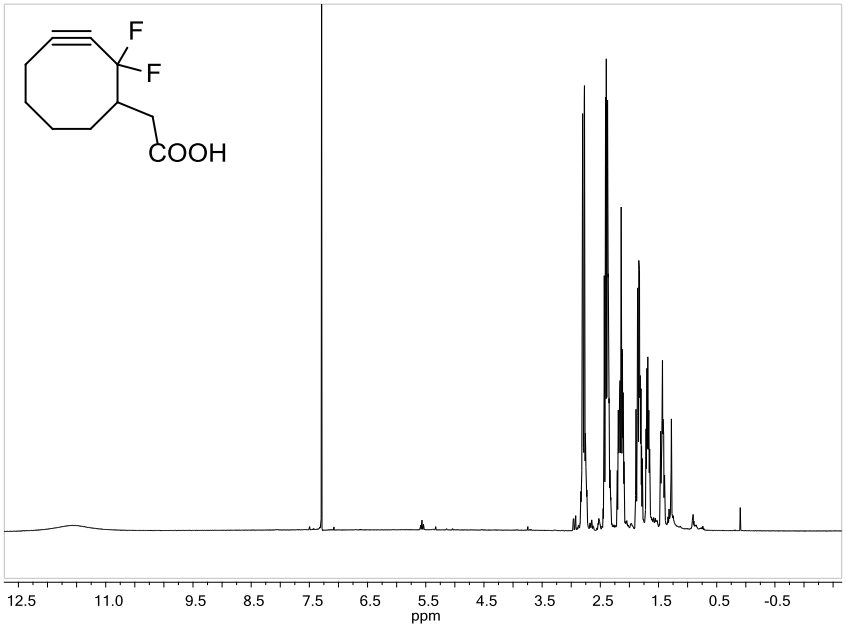

5.6.13 Synthesis of Azide-functionalized Photodegradable Precursor (PLazide)

Synthesis of 4-azidobutanoic acid:

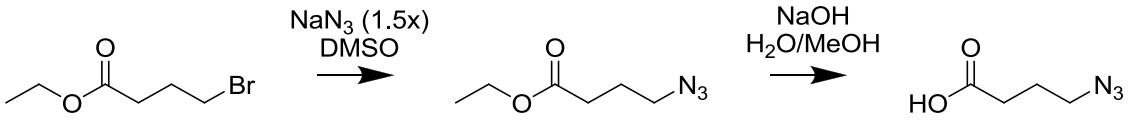

Ethyl-4-bromobutrate (100 g, 513 mmol) was dissolved in DMSO (750 mL) and stirred under argon overnight at 55 °C with sodium azide (50 g, 1.5x, 769 mmol). The crude reaction mixture was diluted with dH_2O (500 mL) and extracted into diethyl ether (3 x 500 mL). The combined organic phases were washed with water (500 mL), brine (500 mL), dried over $MgSO_4$, filtered, and concentrated to yield 80.5 g (512 mmol, quantitative yield) of ethyl 4-azidobutanoate. This intermediate was dissolved in a mixture of 1 N NaOH (500 mL) and methanol (300 mL) and stirred at room temperature for 3 h. The methanol was then removed by rotary evaporation, and the aqueous phase's pH was brought to 0 with dropwise addition of HCl, and the product was extracted into diethyl ether (3 x 500 mL). The combined organic phases

were dried over $MgSO_4$, filtered, and concentrated to yield 64.9 g (502 mmol, quantitative yield) of the 4-azidobutanoic acid product. ^1H NMR (500 MHz, $CDCl_3$, δ): 9.64 (br s, 1H), 3.34 (t, 2H), 2.44 (t, 2H), 1.88 (p, 2H); ^{13}C NMR (101 MHz, $CDCl_3$, δ): 50.46, 30.92, 23.94; HRMS (ESI+): calculated for $C_4H_6N_3O_2^-$ [M – $^1H]^-$, 128.0485; found 128.0462 (Δ = -2.3 ppm).

Synthesis of 4-azidobutanoic anhydride:

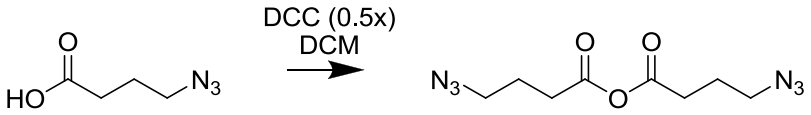

4-azidobutanoic acid (25.7 g,199 mmol) and N,N'-Dicyclohexylcarbodiimide (DCC, 13.2 g, 64 mmol) were purged with argon, dissolved in anhydrous DCM (160 mL), and stirred at room temperature for 45 min. The dicyclohexylurea byproduct was removed *via* celite filtration. The crude mixture was redissolved in DCM (30 mL), concentrated, and filtered, and was repeated until no urea was observed.

Synthesis of PLazide:

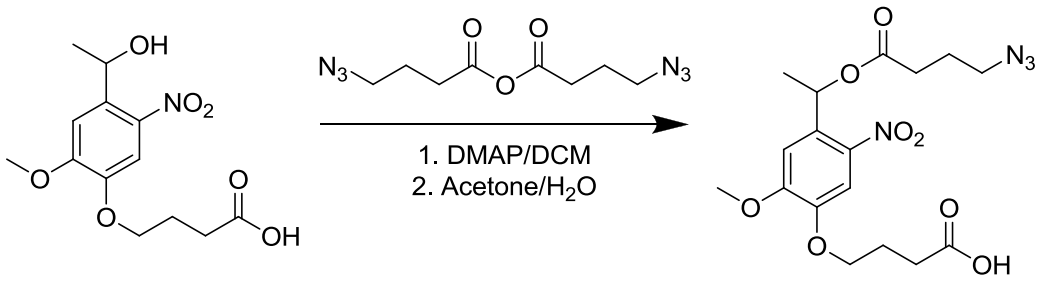

4-[4-(1-Hydroxyethyl)-2-methoxy-5-nitrophenoxy]butanoic acid (Hydroxyethyl photolinker, EMD Novabiochem, 4 g, 13.4 mmol) and 4-Dimethylaminopyridine (DMAP, 80 mg, 0.65 mmol) was added to the anhydride mixture, dissolved in minimal DCM (100 mL) with pyridine (1.08 mL, 13.4 mmol), and stirred under argon overnight. The crude mixture was washed with aq. $NaHCO_3$ (100 mL), 1 N HCl (100 mL), and brine (100 mL). The combined organics were dried over $MgSO_4$ and concentrated. This mixture was then dissolved in a 50:50

mixture of acetone/dH_2O (1400 mL) and stirred overnight, upon which acetone was removed *via* rotary evaporation, and the product was extracted into DCM (700 mL). The organic layer was washed with 1 N HCl (500 mL), brine (500 mL), dried over $MgSO_4$, filtered, concentrated under reduced pressure, and purified by flash chromatography (5:1 to 1:1 hexanes/EtOAc with 1% acetic acid) to yield a yellow solid (5.05 g, 12.3 mmol) in excellent yield (92%). ^{1}H NMR (500 MHz, DMSO, δ): 12.18 (s, 1H), 7.57 (s, 1H), 7.10 (s, 1H), 6.21 (q, 1H), 4.07 (t, 2H), 3.93 (s, 3H), 3.32 (t, 2H), 2.4 (p, 4H), 1.95 (p, 2H), 1.76 (p, 2H), 1.58 (d, 3H); ^{13}C NMR (101 MHz, DMSO, δ): 173.98, 171.56, 153.53, 146.89, 139.66, 131.87, 108.66, 108.42, 67.94, 67.48, 56.25, 49.87, 30.70, 29.92, 23.98, 23.72, 21.30; HRMS (ESI+): calculated for $C_{17}H_{21}N_4O_8^-$ [M – ^{1}H]$^-$, 409.1368; found 409.1363 (Δ = -0.5 ppm).

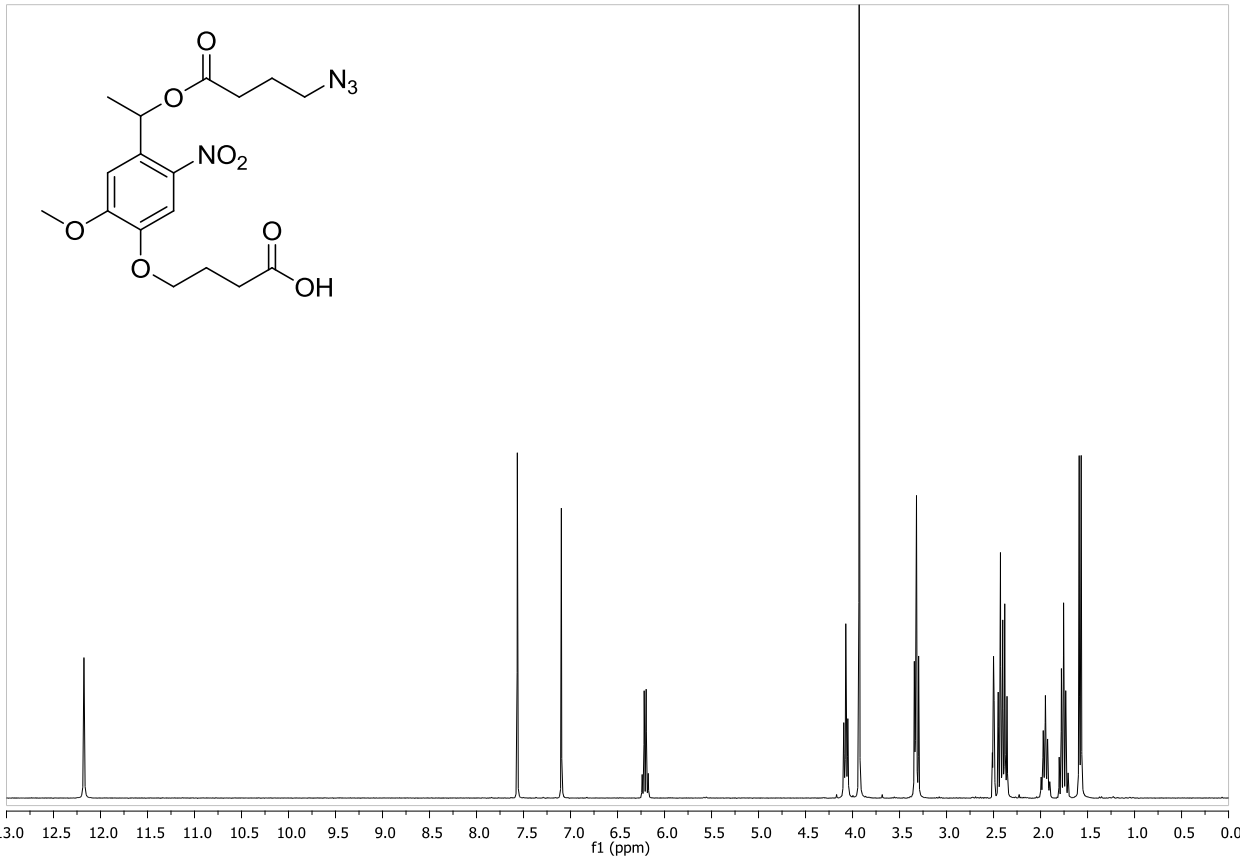

5.6.14 MALDI-TOF of Azide-RGK(alloc)GRK(PLazide)-NH_2

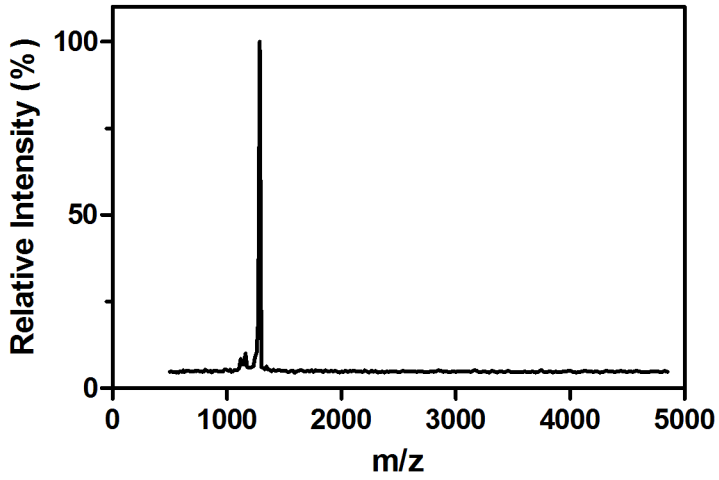

5.6.15 Synthesis of azide-functionalized glass slides:

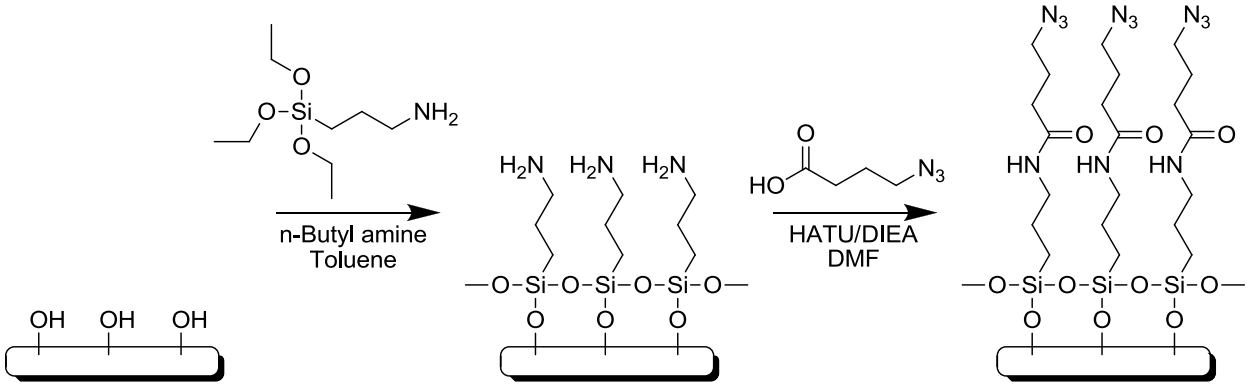

Glass slides (Fisher) were cleaned with piranha solution (50% sulfuric acid, 35% dH_2O, 15% H_2O_2) for 30 min at room temperature. The slides were dried after rinsing with water and acetone (3x) and then placed in a solution of (3-aminopropyl)-triethoxysilane (70 mM) and n-butyl amine (70 mM) in toluene for 90 min. The slides were cleaned with toluene, wiped dry, and baked at 80 °C overnight. The amine-functionalized slides were submerged in a solution containing 4-azidobutanoic acid (Supplementary Section 5.6.13, 100 mM), HATU (100 mM), and DIEA (100 mM) in DMF. After 3 hours, the slides were rinsed with acetone and dried prior to use.

CHAPTER VI

PHOTOREVERSIBLE PATTERNING OF BIOMOLECULES WITHIN CLICK-BASED HYDROGELS

Prepared for submission to *Angewandte Chemie International Edition*, Summer 2011.

6.1 Introduction

Polymer-based hydrogels have emerged as a unique class of biomaterials that enable cells to be cultured in three-dimensions (3D) within user-defined synthetic microenvironments.[1-3] Based on the specific hydrogel formulation, material properties of the cell-laden constructs can be precisely defined to impart different moduli, chemical moieties, porosity, adhesivity, degradability, and stimuli-responsiveness over a wide range of nano-, micro-, and macroscopic scales. By tuning the initial properties of these networks, cells have been engineered to proliferate within, migrate through, and undergo differentiation inside these materials *via* the incorporation of physiologically-relevant cues defined *a priori*[4].

More recently, hydrogel platforms have been developed that permit researchers to introduce biochemical epitopes post-encapsulation at any point in time and space within these materials to affect dynamically cell function[5]. These programmable microenvironments are enabling newfound control of cellular events. For example, the West lab has synthesized poly(ethylene glycol) diacrylate-based networks containing a small percentage of free reactive groups to pattern spatially acrylated peptides into pre-formed hydrogels[6]. Using this approach, the adhesive peptide sequence RGD was selectively incorporated into subvolumes of the material

to guide human dermal fibroblast cell spreading within an enzymatically-degradable gel. Additionally, Shoichet *et al.* prefabricated networks containing photocaged thiols that were selectively deprotected with light and subsequently reacted with maleimide-functionalized biomolecules[7]. By seeding dorsal root ganglia cells on gels containing channels of RGD, neuronal cell process extension was guided into a patterned material substrate.

Alternative to the introduction of chemical cues within the material at specific locations at a given time, techniques have been developed to remove existing signals with spatiotemporal control. The Burdick group encapsulated cells in methacrylated hyaluronic acid-based hydrogels formed *via* a Michael addition with a dithiol peptide crosslinker[8,9]. By forming these networks to contain an excess of methacrylates, these materials could be further crosslinked *via* a photoinitiated chain polymerization upon exposure to UV light, thereby physically entrapping cells locally and limiting their ability to sense the natural cell-signaling hyaluronic acid epitopes. Furthermore, Anseth *et al*. included pendant peptide functionalities in chain-polymerized PEG hydrogels where the peptide linker contained a photodegradable moiety[10]. While the biological cues must be present initially within the material, the signal could be selectively removed with light and results demonstrated the impact of temporal release of RGDS on chondrogenic differentiation of human mesenchymal stem cells.

While existing biochemical patterning techniques have been successfully utilized to control 3D cell adhesion and motility[6,11], promote endothelial tubulogenesis[12,13], and direct cell outgrowth[14,15], no platform enables the introduction and subsequent removal of these signals. Such a system would allow one to more closely recapitulate the dynamic presentation of signaling biomolecules found in a stem cell's native, temporally-variable niche. In this work, we demonstrate that the combination of two bio-orthogonal light-based chemistries enables the

reversible spatial presentation of a biological cue, as well as the formation of complex, well-defined, biomolecular gradients within a hydrogel. Results further highlight how the regulation of the biochemical environment can be used in the development of more sophisticated cell culture substrates.

6.2 Materials and Methods

6.2.1 Synthesis of PLazide

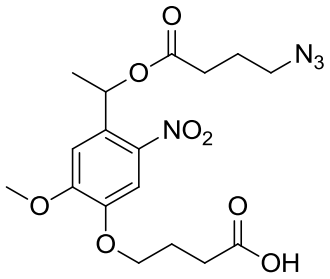

The photolabile nitrobenzyl ether moiety containing flanking carboxylic acid and azide functionality (PLazide) was synthesized as previously described[15]. Briefly, 4-azidobutanoic acid was synthesized by the azidification and deprotection of ethyl-4-bromobutyrate, and its anhydride was reacted (5X/OH) overnight with 4-[4-(1-Hydroxyethyl)-2-methoxy-5-nitrophenoxy]butanoic acid (Hydroxyethyl photolinker, EMD Novabiochem) in minimal dichloromethane (DCM). After washing, the pure product (PLazide) was recovered by flash chromatography in excellent yield (92%) as a yellow solid. ^{1}H NMR (500 MHz, DMSO-d_6, δ): 12.18 (s, 1H), 7.57 (s, 1H), 7.10 (s, 1H), 6.21 (q, 1H), 4.07 (t, 2H), 3.93 (s, 3H), 3.32 (t, 2H), 2.4 (p, 4H), 1.95 (p, 2H), 1.76 (p, 2H), 1.58 (d, 3H); ^{13}C NMR (101 MHz, DMSO-d_6, δ): 173.98, 171.56, 153.53, 146.89, 139.66, 131.87, 108.66, 108.42, 67.94, 67.48, 56.25, 49.87, 30.70, 29.92, 23.98, 23.72, 21.30; HRMS (ESI, m/z): $[M - {}^{1}H]^{-}$ calc for $C_{17}H_{21}N_4O_8^{-}$, 409.1368; found, 409.1363.

6.2.2 Synthesis of PEG tetraDIFO3

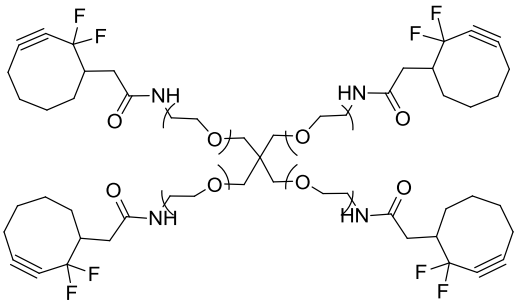

Difluorinated cyclooctyne (DIFO3) was synthesized from 1,3-cyclooctanedione[16] following a published synthetic route[17] and was reacted

(1.5X/NH_2) overnight with 2-(1H-7-Azabenzotriazol-1-yl)--1,1,3,3-tetramethyl uronium hexafluorophosphate Methanaminium (HATU, 1.5X/NH_2) and 4-arm PEG tetraamine (M_n ~ 10,000 Da, JenKem) in minimal dimethylformamide (DMF). The crude product was concentrated by rotary evaporation, dissolved in dH_2O, dialyzed (MWCO ~ 2 kDa, SpectraPor) for 72 hrs, filtered, and lyophilized to give a white powder in excellent yield (96%). By comparing characteristic DIFO3 ^{1}H-NMR peaks with those from the PEG backbone, the percentage modification was confirmed to be >95%.

6.2.3 Synthesis of Peptide Crosslinker

The allyl ester-containing polypeptide H-RGK(alloc)GRK(Dde)-NH_2 was synthesized (Protein Technologies Tribute peptide synthesizer) *via* Fmoc solid-phase methodology and HATU activation. The 1-(4,4-dimethyl-2,6-dioxacyclohexylidene)ethyl (Dde) group was removed with 2% hydrazine monohydrate (Sigma) in DMF (3 x 10 min), and 4-azidobutanoic acid was coupled *via* standard HATU coupling chemistry to the N-terminus and the ε-amino group of the C-terminal lysine. Resin was treated with trifluoroacetic acid (TFA)/triisopropylsilane (TIPS)/water (95:2.5:2.5) for 2 hours, and precipitated in and washed with ice-cold diethyl ether (3x). Crude peptide was purified to give N_3-RGK(alloc)GRK(N_3)-NH_2 using semi-preparative RP-HPLC (Waters Delta Prep 4000) using a 70 minute linear gradient (5 to 95%) of acetonitrile and 0.1% TFA (Sigma), and purity was confirmed by analytical RP-HPLC and MALDI-TOF-MS: $[M + {}^1H]^+$ calc for $C_{40}H_{72}N_{21}O_{10}^+$, 1007.1; found, 1007.7.

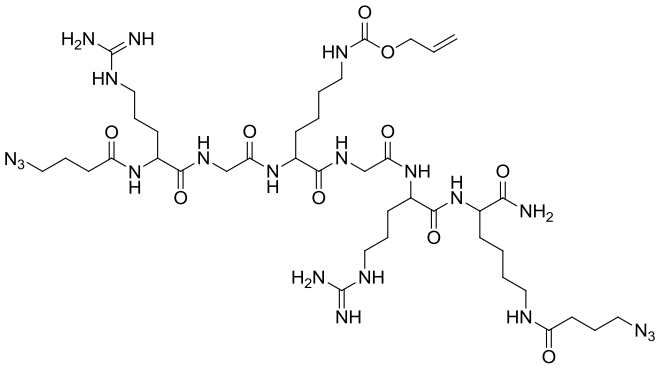

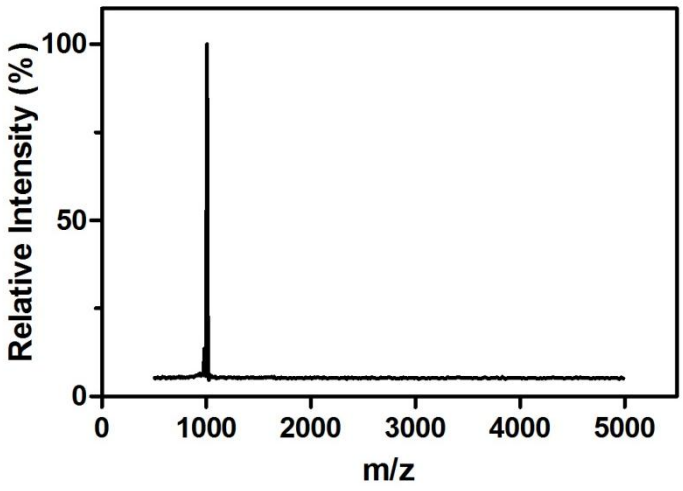

6.2.4 Synthesis of Photoreleasable Patterning Peptide (Ac-C-[PL]-RGDSK(AF_{488})-NH_2):

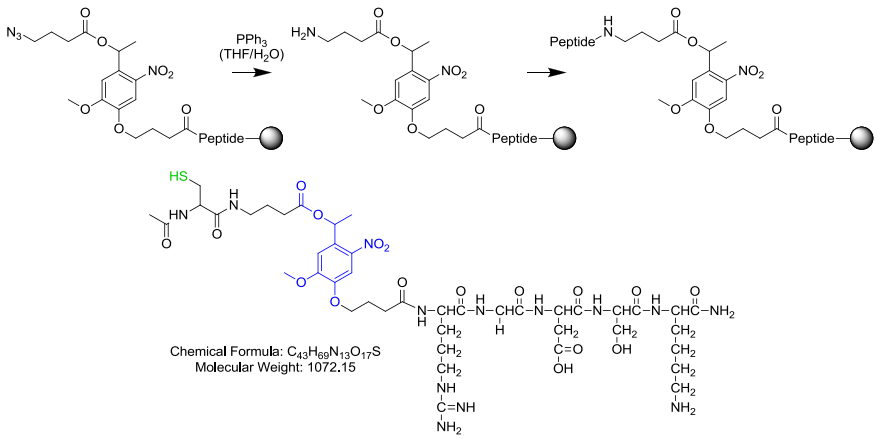

The peptide H-RGDSK-NH_2 was synthesized *via* Fmoc solid-phase methodology and HATU activation, and PLazide was coupled to the N-terminal amine by standard HATU coupling chemistry. Resin was treated with 5 wt% triphenylphosphine in tetrahydrofuran (THF)/water (90:10) for 12 hours to reduce the terminal azido functionality to a primary amine to which Fmoc-Cys(Trt)-OH (Anaspec) was coupled. The terminal Fmoc functionality was cleaved (20% piperidine in DMF) and the peptide was capped with acetic anhydride. Resin was treated with TFA/TIPS/water (95:2.5:2.5) for 2 hours, and precipitated in and washed with ice-cold diethyl ether (3x). Crude peptide was purified to give Ac-C-[PL]-RGDSK-NH_2 using semi-preparative RP-HPLC using a 70 minute linear gradient (5 to 95%) of acetonitrile and 0.1% TFA. The product was lyophilized to give a yellow solid, and purity was confirmed by analytical RP-HPLC and MALDI-TOF-MS: $[M + {}^1H]^+$ calc

for $C_{43}H_{70}N_{13}O_{17}S^+$, 1073.2; found, 1072.4. Ac-C-[PL]-RGDSK-NH_2 (20 mg) was dissolved in DMF (4 mL) containing Alexa Fluor® 488 carboxylic acid, 2,3,5,6-tetrafluorophenyl ester (1 mg) with N,N-Diisopropylethylamine (DIEA, 50 μL) and reacted overnight protected from light. The sample was concentrated, dissolved in dH_2O, dialyzed for 72 hrs (MWCO ~ 500 Da, SpectraPor), and lyophilized to give a yellow solid, denoted Ac-C-[PL]-RGDSK(AF_{488})-NH_2.

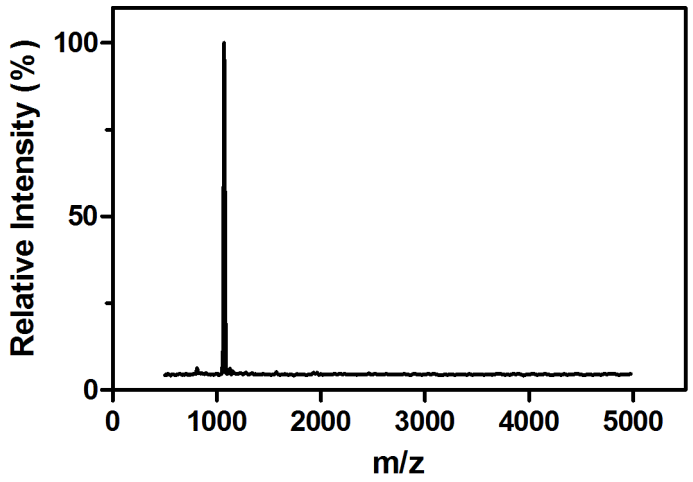

6.2.5 Formation of SPAAC-based Hydrogel

A 10 wt% solution of PEG tetraDIFO3 and N_3-RGK(alloc)GRK(N_3)-NH_2 was prepared in phosphate buffered saline (PBS) with equal concentrations of azide and alkyne functionalities. The macromer solution was reacted between azide-functionalized[15] and Rain-X®-treated glass slides separated with 1 mm thick gaskets for 1 hr. The slides were separated and gels were swollen overnight in PBS prior to usage.

6.2.6 Biological Patterning within Click-based Hydrogel

Click-based hydrogels were swollen for 1 hr in Ac-C-[PL]-RGDSK(AF_{488})-NH_2 (3 mg mL^{-1}) and eosin Y (2.5 – 10 μM). Gels were then exposed through a patterned chrome photomask (Photo Sciences, Inc.) to collimated visible light (λ = 490 – 650 nm, 10 mW cm^{-2}, 0 –

2 min), achieved with an Acticure (EXFO) high pressure mercury lamp equipped with an internal bandpass filter (350 – 650 nm) and an external 490 nm longpass filter (Edmund Optics). Alternatively, multiphoton-based techniques were used to achieve 3D photocoupling, where selected regions of interest (x-y) at 1 μm z-plane increments within the hydrogel were scanned with pulsed laser light (λ = 860 nm, power = 350 mW μm^{-2}, scan speed = 1.27 μsec μm^{-2}) on a 710 LSM NLO confocal microscope stage (Carl Zeiss) equipped with a 20x/0.8 Plan-Apochromat objective (NA = 1.0, Carl Zeiss). Upon completion of the photocoupling process, unreacted patterning agent and photoinitiator were swollen into PBS to yield the biochemically-patterned hydrogel by photoaddition. Photolithographic photoremoval of the peptide was accomplished using UV light (λ = 365 nm, 5 – 20 mW cm^{-2}, 0 – 10 min) shown through a patterned chrome mask. The photoremoval process was controlled in 3D with multiphoton-based techniques (λ = 740 nm, power = 670 mW μm^{-2}, scan speed = 1.27 μsec μm^{-2}). For both the photocoupling and photoremoval processes, the reaction was visualized with confocal microscopy and found to be confined to only those volumes within the material that were exposed to light.

6.2.7 Quantification of Patterning Concentration

The level of peptide incorporation (Ac-C-[PL]-RGDSK(AF_{488})-NH_2) was quantified by comparing the patterned fluorescence from the AF_{488} against that from gels swollen with known uncoupled free concentrations of the same patterning agent. As expected, the fluorescence of the swollen gels increased linearly with peptide concentration and provided a standard curve for relating fluorescence intensity with concentration. Though this method required a standard curve to be generated for each peptide of interest, it only required a small subset of the peptide population to be fluorescently labeled (<1%).

6.2.8 Cell Culture and Seeding

NIH 3T3s were cultured in high-glucose Dulbecco's modified Eagle's medium (Gibco) containing 10% fetal bovine serum (Invitrogen), 1% penicillin/streptomycin (Gibco), 0.2% fungizone, and 0.4% gentamicin. Cells were seeded on click hydrogels at a density of 20 x 10^3 cells cm^{-2}.

6.2.9 Cell Staining

24 hours after seeding, or 4 hours after releasing RGD, cells were fixed in formalin for 1 h, followed by cell permeabilization with 0.5% Triton® X-100 (Fisher) in PBS for 45 min. The gels were blocked with 3% bovine serum albumin (BSA, Sigma) in PBS for 30 min and rinsed with PBS. F-actin was visualized using Alexa Fluor® 488 Phalloidin Conjugate (5 U/mL, Invitrogen), while nuclei were stained with DAPI (500 nM, Invitrogen), each of which was applied for 1 h. The samples were washed with PBS prior to visualization with confocal microscopy.

6.3 Results and Discussion

A reversible patterning strategy is presented based on the combination of two orthogonal, biocompatible photoreactions[15]. The thiol-ene reaction, which involves the radical-mediated addition of a thiol to an alkene, is readily initiated with visible light (λ = 490 – 650 nm) and an appropriate photoinitiator (*e.g.*, eosin Y)[18,19]. The second reaction involves the photoscission of an o-nitrobenzyl ether to yield a nitroso and an acid byproduct upon UV light exposure (λ = 365 nm)[10,20]. By synthesizing the biological molecule of interest to include both the photocouplable thiol and the photolabile moiety, we can use the thiol-ene reaction to modify hydrogel networks with covalently-bound bioepitopes and subsequently remove these signals *via* photocleavage (Figure 6.1a). As these reactions are photochemically-based, both the introduction and

subsequent removal of relevant biomolecules can be explicitly controlled in space and time with presentation of light.

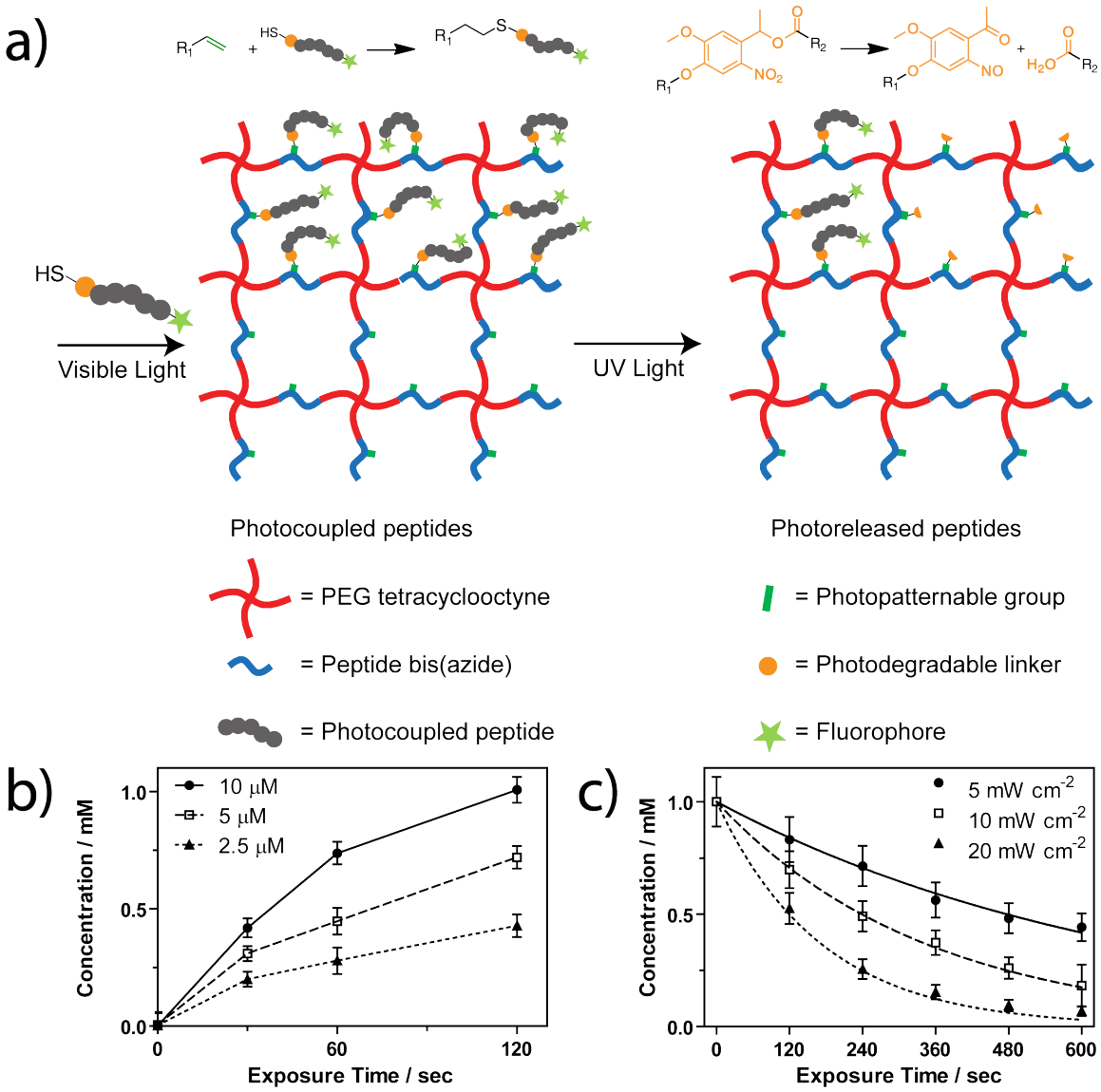

Figure 6.1 (a) Click-based hydrogels containing pendant alkenes are functionalized with thiol-containing, photodegradable, fluorescent peptides (Ac-C-[PL]-RGDSK(AF_{488})-NH_2) *via* the thiol-ene reaction initiated with flood exposure to visible light (λ = 490 – 650 nm, 10 mW cm^{-2}) and eosin Y photoinitiator. (b) The final peptide patterning concentrations (0 – 1 mM) depended on the initiator concentration (2.5, 5, 10 μm) and visible light exposure time (0 – 120 sec). (c) Gels patterned with the photodegradable peptide by visible thiol-ene coupling (~1 mM) were subsequently exposed to UV light (λ = 365 nm) to induce an orthogonal nitrobenzyl ether photocleavage reaction and subsequent removal of the peptide, where the rate of removal was dependent on light intensity (5, 10, 20 mW cm^{-2}) and irradiation time (0 – 600 sec). Curves represent predicted concentrations based on predetermined photocleavage kinetics.

The multifunctional patterning peptide was synthesized by a combination of standard Fmoc solid-phase methodologies, where a photodegradable azide acid (4-(4-(1-(4-azidobutanoyloxy)ethyl)-2-methoxy-5-nitrophenoxy)butanoic acid)[15] was coupled to the N-terminus of a peptide sequence of interest. The terminal azide moiety served as a protecting group during peptide synthesis, ensuring that only one photodegradable moiety was present per peptide, and was readily reduced by the Staudinger reaction[21] on resin *via* treatment with triphenylphosphine to liberate an N-terminal primary amine for continued peptide synthesis. In this manner, the chosen photoreversible patterning agent (Ac-C-[PL]-RGDSK-NH_2), based on the ubiquitous cell adhesive ligand RGD, was prepared and contained both a photoreactive thiol (*i.e.*, cysteine) and the adjacent photodegradable moiety.

The patternable hydrogel was formed by the copper-free strain-promoted azide-alkyne cyclooaddition (SPAAC) click reaction between a poly(ethylene glycol) tetra-cyclooctyne[16,17] and a bis(azide) allyloxycarbonyl (alloc)-protected polypeptide (N_3-RGK(alloc)GRK-N_3) in aqueous medium[11,15,22]. The resulting idealized, SPAAC-based network is homogenously populated with alloc functionalities, which contain photoreactive alkenes that serve as anchor points for the introduction of pendantly-tethered biochemical cues within the network *via* the thiol-ene photoconjugation reaction. As a side note, this reaction is fully cytocompatible[11,23], which means that cells can be readily encapsulated and cultured in these patternable gels.

Upon swelling a fluorescently-labeled, cysteine-containing peptide into the hydrogel network (Ac-C-[PL]-RGDSK(AF_{488})-NH_2), the degree of thiol-ene photoconjugation was controlled by varying the visible light irradiation (λ = 490 – 650 nm, 10 mW cm^{-2}) exposure time (0 – 120 sec) and/or initiator concentration (2.5, 5, 10 μM eosin Y) present (Figure 6.1b). Here, the visible absorbance of eosin Y extends from λ = 450 – 550 nm with a maximum absorbance at

λ ~ 515 nm and the patterned peptide concentrations ranged from between 0 to 1.0 mM. Subsequently, gels containing ~1.0 mM of patterned Ac-C-[PL]-RGDSK(AF_{488})-NH_2 were exposed to UV light (λ = 365 nm) at different intensities (5, 10, 20 mW cm^{-2}) for various times (0 – 600 sec) to cleave the *o*-nitrobenzyl ether group, which absorbs strongly between λ = 325 – 415 nm, and photorelease the previously patterned peptide (Figure 6.1c). As the photodegradable *o*-nitrobenzyl ether moiety absorbs light and cleaves with light where λ < 415 nm, both the addition and cleavage photoreactions can be performed independently by delivering different wavelengths of light to the system. Additionally, each of these reactions can be initiated with multiphoton light (λ = 860 nm for addition, 740 nm for cleavage), opening up avenues for independent 3D control of these reactions. Photocleavage was found to follow a first order degradation with a rate constant (*k*) given by:

$$k = \frac{\varphi \varepsilon I}{N_A h \nu}$$

where ϕ is the quantum yield (0.020)[15], ε is the molar absorptivity (4780 M^{-1} cm^{-1} at λ = 365 nm)[15], I is the intensity of light, N_A is Avogadro's number, h is the Planck constant, and ν is the light frequency. This indicates that the patterned peptide is nearly fully removed (>97%) upon 10 min irradiation of 20 mW cm^{-2} light (λ = 365 nm) or in real time with multiphoton light (λ = 740 nm), which represents a relevant time scale for cell applications. From this analysis, the precise amount of photoreleased peptide was readily predicted for a given light exposure (lines in Figure 6.1c). Then, by employing traditional photolithographic or multiphoton-based techniques, spatial control of the photoaddition and photoremoval reactions is demonstrated through micron-scale patterning of arbitrary shapes in both 2D (Figure 6.2a and 6.2c) and 3D (Figure 6.2b and 6.2d), respectively.

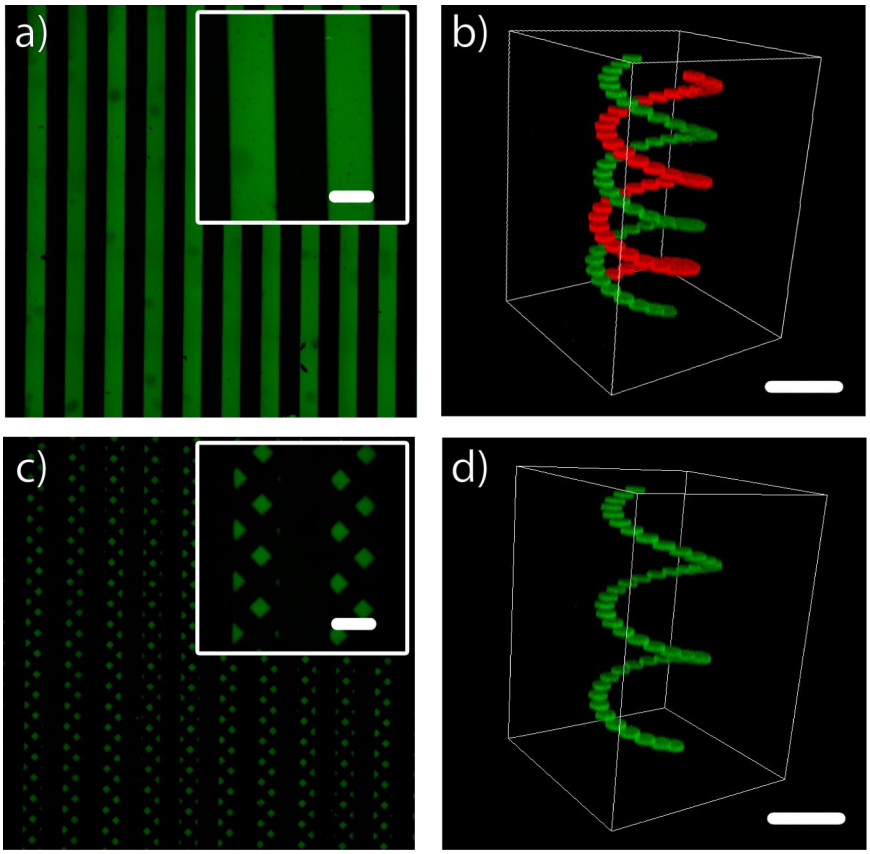

Figure 6.2 (a) Fluorescent peptides (Ac-C-[PL]-RGDSK(AF_{488})-NH_2) were patterned into the network in 2D upon exposure to masked visible light (λ = 490 – 650 nm, 10 mW cm^{-2}, 2 min, 10 μM eosin Y) and (b) in 3D *via* focused pulsed laser light (λ = 860 nm, 350 mW μm^{-2}, scan speed = 1.27 μsec μm^{-2}, 10 μM eosin Y). (c,d) Subsets of these prepatterned cues were removed with UV light (for masked light: λ = 365 nm, 10 mW cm^{-2}, 20 min; for 3D focused laser light: λ = 740 nm, 670 mW μm^{-2}, scan speed = 1.27 μsec μm^{-2}) to yield new 2D and 3D patterns. (b) False coloring was employed for enhanced reader visualization. Scale bars = 200 μm.

By first patterning in a fixed amount (~1 mM) of our biomolecule of interest (Ac-C-[PL]-RGDSK(AF_{488})-NH_2) with visible light, non-linear gradients were formed within the material by exposing the patterned substrate to a user-defined gradient of UV light exposure (λ = 365 nm, 10 mW cm^{-2}), generated with a moving opaque photomask[24] that covered the sample at a rate of 0.4, 0.8, 1.6 mm min^{-1}. For continuous gradients, this approach resulted in exponential gradients with decay constants of 0.175 min^{-1} / [rate of sample coverage] to be generated, corresponding to 0.44, 0.22, 0.11 mm^{-1} for the increasing sample coverage rates. We further demonstrate that by photoreleasing peptides that are initially present uniformly throughout the bulk (Figure 6.3a, d)

or within line patterns (Figure 6.3c, e), intricate exponential gradients within the material environment that are either continuous or line patterned can be formed over millimeter-scale distances. Alternatively, by shuttering the delivered light, more complex stepped gradients were formed where regions of constant peptide concentration were interspaced with regions of decreasing concentration (Figure 6.3b). Each of these gradients was readily predicted for a given light exposure, which correlated well with experimental findings.

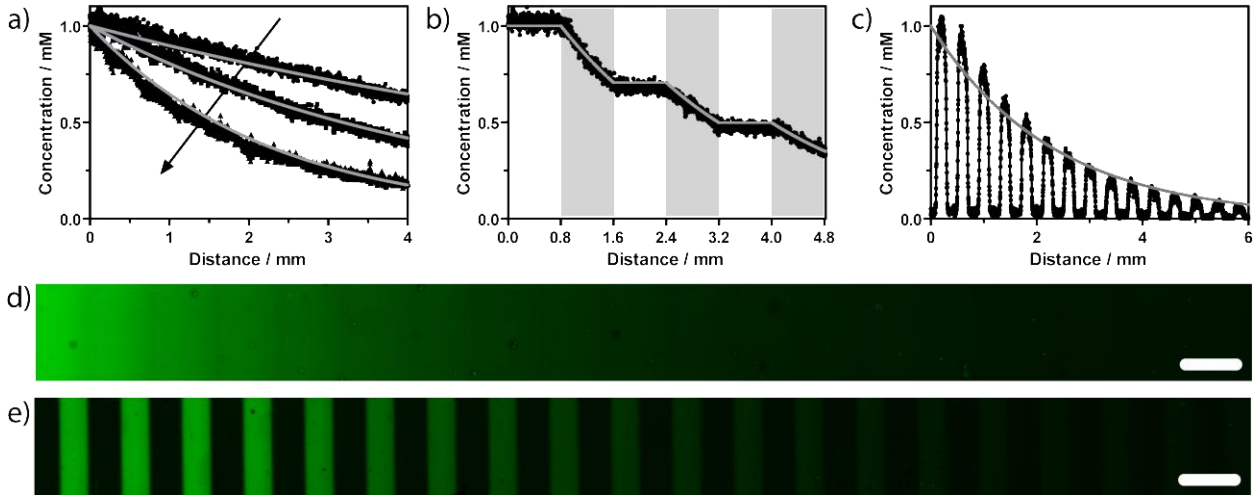

Figure 6.3 Ac-C-[PL]-RGDSK(AF_{488})-NH_2 was first patterned (~1 mM) into hydrogels either uniformally throughout the bulk (a, b, d) or in 200 μm wide lines (c, e) *via* visible thiol-ene photocoupling. The samples were exposed to gradients of UV light (λ = 365 nm, 10 mW cm^{-2}) generated by a moving (1.6, 0.8, 0.4 mm min^{-1} in a; 0.4 mm min^{-1} for b-e) opaque photomask to create exponentially-decaying peptide gradient. By shuttering the light (b) or releasing pre-patterned lines (c, e), unique gradients were generated. Solid gray lines represent predicted concentrations based on predetermined photocleavage kinetics. Scale bars = 400 μm.

Ultimately, these chemistries are useful in that they can be performed in the presence of cells. To demonstrate that this patterning approach offers dynamic control over cell function, NIH 3T3 fibroblast cells were seeded (8 x 10^3 cells cm^{-2}) onto constructs containing patterned islands of RGD. Initial cell attachment was confined to RGD-functionalized adhesive regions of the material (Figure 6.4a). On these regions, 200 μm lines of RGD spaced 200 μm apart, cells attached to the RGD-functionalized material and exhibited a spread morphology. 24 hours after

seeding, this adhesive ligand was removed within selective areas of the initial pattern, generated with the same 200 μm line pattern rotated 45° clockwise, causing only cells within these user-defined regions to detach and be removed from the surface within minutes after exposure (Figure 6.4b). These cells can be isolated and expanded, providing an efficient way of sampling a subset of a total cell population for assaying proliferation, gene expression, metabolic activity, and differentiation of stem cells within user-defined regions of the culture substrate.

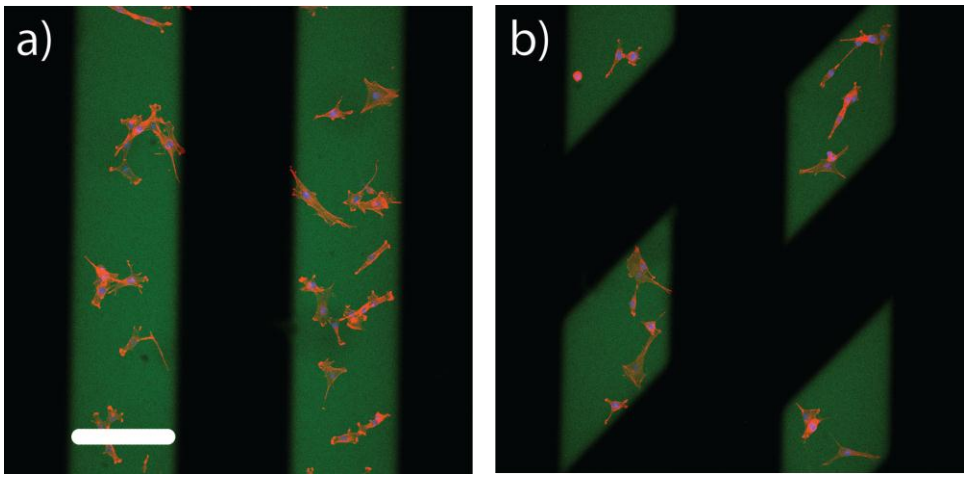

Figure 6.4 (a) Parallel lines (200 μm wide) of Ac-C-[PL]-RGDSK(AF_{488})-NH_2 were patterned into the hydrogel at ~1 mM *via* visible thiol-ene photocoupling. NIH 3T3s were seeded onto the gel substrates at 8 x 10^3 cells cm^{-2}, and their attachment was confined to RGD-functionalized regions of the hydrogel surface. (b) 24 hours after seeding, selective regions of RGD were removed with masked UV irradiation (λ = 365 nm, 10 mW cm^{-2}, 20 min) through the same 200 μm line mask used in the initial patterning rotated 45° clockwise, resulting in localized cell-detachment. Green = RGD, red = F-actin, blue = nuclei. Scale bar = 200 μm.

6.4 Conclusions

By utilizing multiple bio-orthogonal light-based chemistries, we were able to afford spatiotemporal control over the reversible presentation of biologically-relevant chemical cues. The afforded level of control over the biochemical aspects of the hydrogel platform enables dynamic cell function to be assayed in a new manner and for experimenters to program the cellular microenvironment on demand. We expect such approaches to control dynamically material properties to be crucial in establishing a more complete understanding of how cells

respond to their extracellular environment and assist in the rational design of cell delivery systems for regenerative medicine applications.

6.4 References

1. Peppas, N.A., Hilt, J.Z., Khademhosseini, A. & Langer, R. Hydrogels in biology and medicine: From molecular principles to bionanotechnology. *Adv. Mater.* **18**, 1345-1360 (2006).

2. Tibbitt, M.W. & Anseth, K.S. Hydrogels as extracellular matrix mimics for 3D cell culture. *Biotechnol. Bioeng.* **103**, 655-663 (2009).

3. Cushing, M.C. & Anseth, K.S. Hydrogel cell cultures. *Science* **316**, 1133-1134 (2007).

4. Lutolf, M.P., Gilbert, P.M. & Blau, H.M. Designing materials to direct stem-cell fate. *Nature* **462**, 433-441 (2009).

5. Khetan, S. & Burdick, J.A. Patterning hydrogels in three dimensions towards controlling cellular interactions. *Soft Matter* **7**, 830-838 (2011).

6. Hahn, M.S., Miller, J.S. & West, J.L. Three-dimensional biochemical and biomechanical patterning of hydrogels for guiding cell behavior. *Adv. Mater.* **18**, 2679-2684 (2006).

7. Luo, Y. & Shoichet, M.S. A photolabile hydrogel for guided three-dimensional cell growth and migration. *Nat. Mater.* **3**, 249-253 (2004).

8. Khetan, S., Katz, J.S. & Burdick, J.A. Sequential crosslinking to control cellular spreading in 3-dimensional hydrogels. *Soft Matter* **5**, 1601-1606 (2009).

9. Khetan, S. & Burdick, J.A. Patterning network structure to spatially control cellular remodeling and stem cell fate within 3-dimensional hydrogels. *Biomaterials* **31**, 8228-8234 (2010).

10. Kloxin, A.M., Kasko, A.M., Salinas, C.N. & Anseth, K.S. Photodegradable hydrogels for dynamic tuning of physical and chemical properties. *Science* **324**, 59-63 (2009).

11. DeForest, C.A., Polizzotti, B.D. & Anseth, K.S. Sequential click reactions for synthesizing and patterning three-dimensional cell microenvironments. *Nat. Mater.* **8**, 659-664 (2009).

12. Aizawa, Y., Wylie, R. & Shoichet, M. Endothelial cell guidance in 3D patterned scaffolds. *Adv. Mater.* **22**, 4831-4835 (2010).

13. Leslie-Barbick, J.E., Shen, C., Chen, C. & West, J.L. Micron-scale spatially patterned, covalently immobilized vascular endothelial growth factor on hydrogels accelerates

endothelial tubulogenesis and increases cellular angiogenic responses. *Tissue Eng. Part A* **17**, 221-229 (2011).

14. Lee, S.H., Moon, J.J. & West, J.L. Three-dimensional micropatterning of bioactive hydrogels *via* two-photon laser scanning photolithography for guided 3D cell migration. *Biomaterials* **29**, 2962-2968 (2008).

15. DeForest, C.A. & Anseth, K.S. Cytocompatible click-based hydrogels with dynamically-tunable properties through orthogonal photocoupling and photodegradation reactions. *In Review* (2011).

16. Sims, E.A., DeForest, C.A. & Anseth, K.S. A mild, large-scale synthesis of 1,3-cyclooctanedione: Expanding access to difluorinated cyclooctyne for copper-free click chemistry. *Tetrahedron Lett.* **52**, 1871-1873 (2011).

17. Codelli, J.A., Baskin, J.M., Agard, N.J. & Berozzi, C.R. Second-generation difluorinated cyclooctynes for copper-free click chemistry. *J. Am. Chem. Soc.* **130**, 11486-11493 (2008).

18. Hoyle, C.E. & Bowman, C.N. Thiol-ene click chemistry. *Angew. Chem. Int. Ed. Engl.* **49**, 1540-1573 (2010).

19. Uygun, M., Tasdelen, M.A. & Yagci, Y. Influence of type of initiation on thiol-ene "click" chemistry. *Macromol. Chem. Phys.* **211**, 103-110 (2010).

20. Holmes, C.P. & Jones, D.G. Reagents for combinatorial organic-synthesis - development of a new o-nitrobenzyl photolabile linker for solid-phase synthesis. *J. Org. Chem.* **60**, 2318-2319 (1995).

21. Vaultier, M., Knouzi, N. & Carrié, R. Reduction d'azides en amines primaires par une methode generale utilisant la reaction de staudinger. *Tetrahedron Lett.* **24**, 763-764 (1983).

22. DeForest, C.A., Sims, E.A. & Anseth, K.S. Peptide-functionalized click hydrogels with independently tunable mechanics and chemical functionality for 3d cell culture. *Chem. Mater.* **22**, 4783-4790 (2010).

23. Fairbanks, B.D. et al. A versatile synthetic extracellular matrix mimic *via* thiol-norbornene photopolymerization. *Adv. Mater.* **21**, 5005-5010 (2009).

24. Johnson, P.M., Reynolds, T.B., Stansbury, J.W. & Bowman, C.N. High throughput kinetic analysis of photopolymer conversion using composition and exposure time gradients. *Polymer* **46**, 3300-3306 (2005).

CHAPTER VII

CONCLUSIONS AND FUTURE DIRECTIONS

Cell functions, including migration, proliferation, and differentiation, are dictated by a wide variety of physical and chemical cues that are dynamically presented within the surrounding extracellular matrix. This complex, locally-derived information supplements the cell's genetic preprogramming, and enables elaborate decisions concerning biological fate to be made. The specific effects of these individual cues, while important in both understanding fundamental biological functions as well in the rational design of advanced biomaterials for regenerative medicine applications, are difficult to assay within the cell's native environment due to the myriad of ever-present, ever-changing signals found *in vivo*. Towards this, we have utilized three orthogonal reactions in the development of light-programmable, synthetic hydrogel platforms that enable specific questions concerning cell function to be probed *via* the spatiotemporal introduction of relevant microenvironmental cues.

First, we developed a 3D cell culture platform based of the copper-free addition of an azide to a strained alkyne *via* the SPAAC reaction between a tetrafunctional PEG and a difunctionalized peptide (Chapter III, IV). PEG was chosen due to its hydrophilicity and non-fouling characteristics that give rise to materials with tissue-like elasticity and minimal protein fouling, while the peptide component enabled biological function (*e.g.*, enzymatic degradability) to be engineered within the material and provided a means to create complex multifunctional

monomers in well-defined and repeatable manners. When macromolecular precursors are functionalized with these moieties and reacted together, gelation occurred rapidly and cytocompatibly in a time scale that was appropriate for cell encapsulation. As this SPAAC click reaction proceeds orthogonal to many reactive functionalities (*e.g.*, alcohols, carboxylic acids, amines, vinyls), additional reactive groups were included in the gel formulation without hindering gel formation. By including a photoreactive allyl ester pendent to the peptide, anchor points for localized biofunctionalization *via* the thiol-ene reaction were introduced within the material that enabled biochemical cues to be introduced at any point in time and space within the hydrogel network. Additionally, a photocleavable o-nitrobenzyl ether moiety was introduced that rendered the material photodegradable (Chapter V). Conditions were developed where photoreactions could be performed independently, ensuring that the synthesized material offered dynamic control over both the physical and chemical nature of the gel. Subsequently, the orthogonal light conditions were exploited to create a system where biochemical cues could be dynamically introduced in a reversible manner (Chapter VI). Finally, each of these systems was used to direct and study cell motility (Chapters III, V, VI). The general design for this thesis research is outlined in Figure 7.1. Utilizing these developed materials, we demonstrated that the biochemical and biophysical properties of the network can be regulated in real-time with light to detect and direct cell function. While many material- and biological-based questions have been explored throughout the course of this thesis, many others remain unanswered. In this chapter, we will explore additional capacities of these materials and discuss future directions for utilizing these materials to answer increasingly complex biological questions.

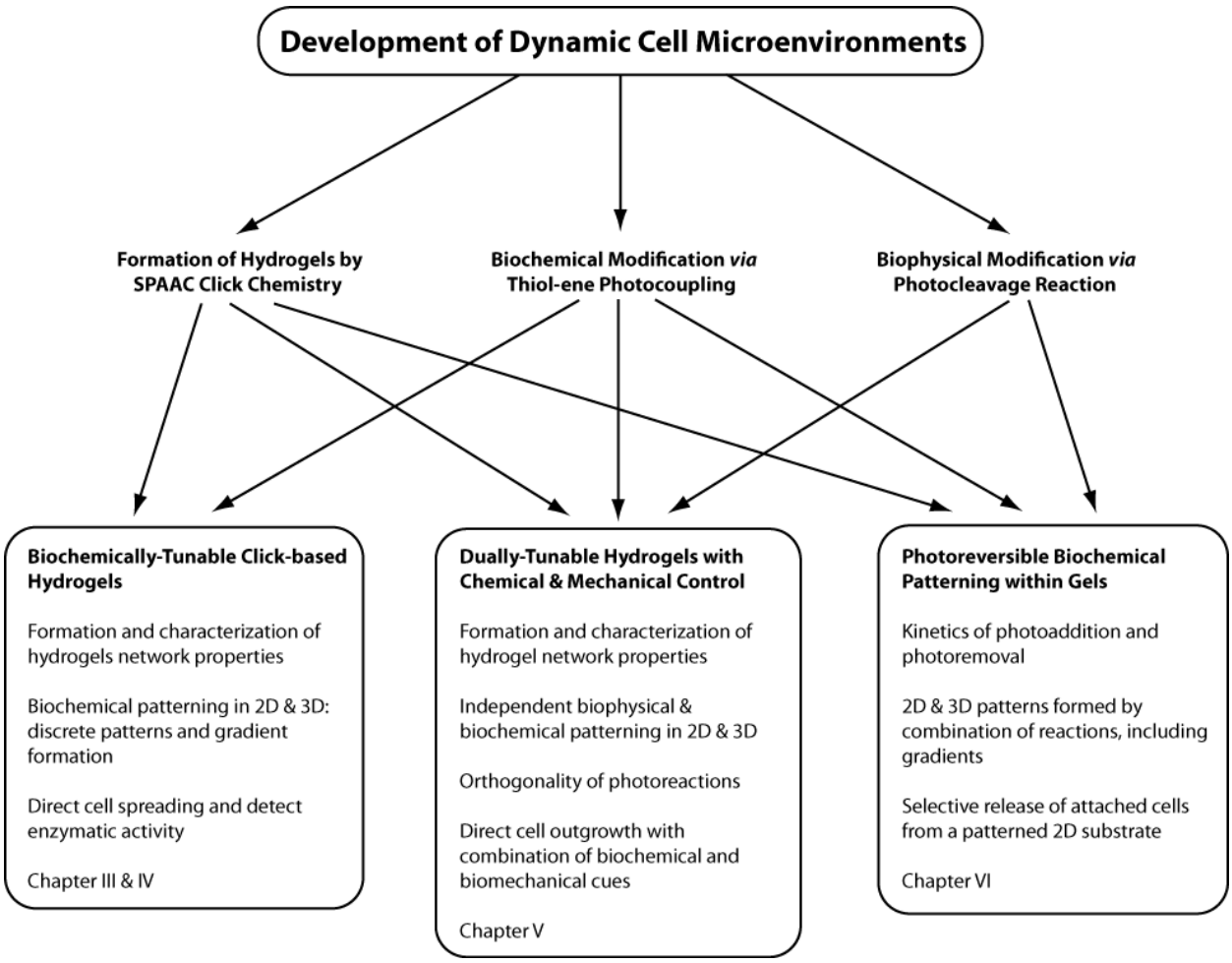

Figure 7.1 Phototunable click-based hydrogels for 3D cell culture thesis organization. This thesis exploited three different orthogonal reactions (SPAAC, thiol-ene photoconjugation, and photodegradation) in the development of three dynamically-tunable cell culture platforms.

In Chapter III, we introduced the SPAAC reaction as a quantitative means to couple azido-functionalized macromolecular precursors to those that contained cyclooctyne moieties. In this work, we synthesized and utilized a difluorinated cyclooctyne (DIFO3), whose ring strain and electron-withdrawing fluorine groups gave rise to an "activated" alkyne that spontaneously reacted with azides under physiological conditions and circumvented the use of a cytotoxic copper(I) catalyst traditionally employed in the 1,3-dipolar Huisgen cycloaddition click reaction. Following a published procedure, we were able to produce successfully DIFO3 in quantities sufficient for the purposes of this thesis[1], but the synthesis involves 14 steps, poor overall yield,

and was not readily amenable to reaction scale up (Appendix B). Thus, we devised a novel synthetic route to the key intermediate of this synthesis, 1,3-cyclooctadione (Appendix A) that enabled DIFO3 to be synthesized on the gram-scale; however, many new cyclooctynes have been identified that contain different kinetic reactivity and exhibit diverse degrees of synthetic accessibility (Figure 7.2). While DIFO3 gained its increased reactivity over that of regular cyclooctyne (OCT[2]) with its electrophilic fluorine substituents, the majority of the newer approaches have utilized polycyclic compounds to introduce additional ring strain that affords increased reactivity; dibenzocyclooctynols (DIBO[3]), biarylazacyclooctynones (BARAC[4]), and difluorobenzocyclooctynes (DIFBO[5]) employ aromatic rings, while bicyclononynes (BCN[6]) use a cyclopropane. As novel cyclooctynes continue to be developed, these functionalities can be readily interchanged with DIFO3 in our developed monomeric materials to create hydrogels that will form with different rates of reaction or can be produced on a significantly larger scale and can be chosen depending on the specific application.

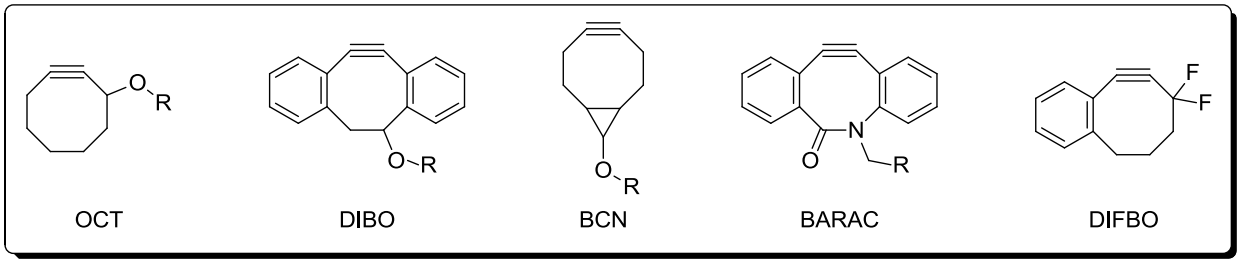

Figure 7.2 Subset of cyclooctynes available for SPAAC copper-free click chemistry. Each molecule (*e.g.*, OCT[2], DIBO[3], BCN[6], BARAC[4], DIFBO[5]) will react spontaneously with azides with different reaction kinetics, and could be utilized for hydrogel formation in the place of DIFO3.

Additionally, as the SPAAC reaction proceeds orthogonally to common reactive groups found in cellular proteins and media components, it can be used in other biological applications that require highly selective reactivity. Though hydrogels formed *via* radical solution chain polymerization are frequently employed in drug delivery applications, chemical radicals have

been shown to interact with encapsulated proteins and conjugate them to the forming material, ultimately preventing their desired localized and sustained release[7]. For a given concentration of encapsulated transforming growth factor beta ($TGF\beta_1$, 25 nM), a significantly higher fractional release, detected by an enzyme-linked immunosorbent assay (ELISA), was delivered by SPAAC-formed gels, as compared with those produced by the thiol-ene reaction between a PEG tetra(norbornene) (M_n ~ 10,000 Da) and a PEG dithiol (M_n ~ 2,000), as well as a,PEGDA-based (M_n ~ 4,600 DA) network (Figure 7.3).

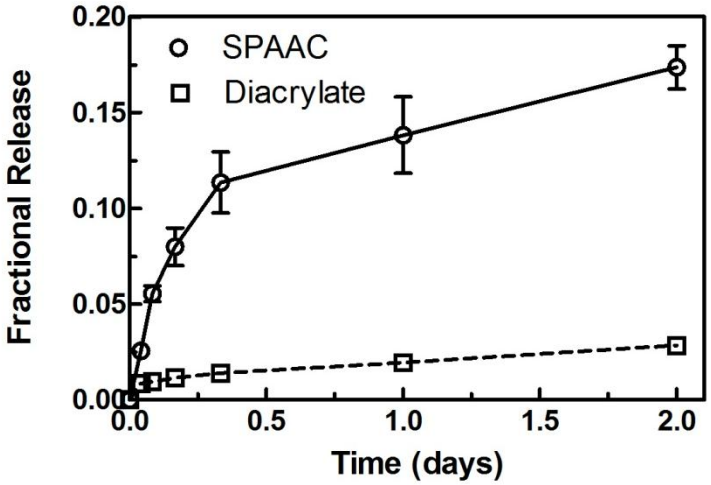

Figure 7.3 Fractional release of $TGF\beta_1$ from hydrogel networks formed by different reaction mechanisms. Due to its limited interaction with encapsulated proteins, the bioorthogonal SPAAC-formed networks result in a a greated payload release when compared with radical-mediated diacrylate-based networks. *Work performed in collaboration with Joshua McCall.

Additionally, the SPAAC chemistry was utilized for hydrogel network formation due to its high reactivity, bioorthogonality, and cytocompatibility. The reaction's spontaneous nature did not require an external initiation process and enabled the reaction to be performed in the presence of photoactive compounds that could be utilized for further light-based chemistries. As the field of click chemistry continues to progress, new reactions (*e.g.*, the inverse-demand Diels-Alder reaction of dipyridyl tetrazines and trans-cyclooctenes[8] or monoaryl tetrazines and norbornenes[9], reaction of oxanorbornadienes and azides[10], photoinduced 1,3-dipolar

cycloaddition of tetrazoles and alkenes[11], the Staudinger ligation[12], the strain-promoted acetylene-nitrone cycloaddition[13]) are being (re)discovered that meet these same criteria, but are more synthetically tractable[14] (Figure 7.4). These reactive pairs could be readily substituted for the azide/DIFO3 combination in our formulation to enable networks of similar structure to form *via* a different reaction mechanism. Alternatively, these reactions could be utilized to introduce orthogonally additional functionality within the network post-formulation.

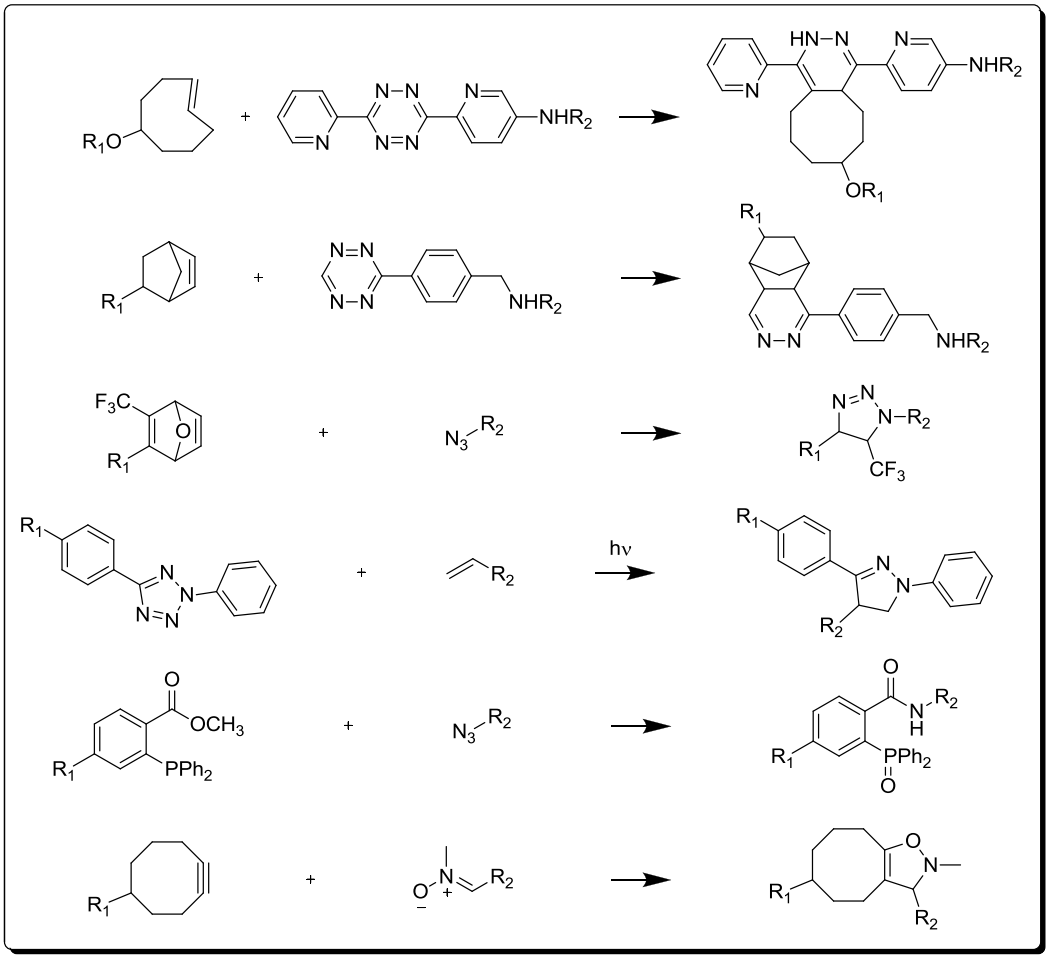

Figure 7.4 Additional bioorthogonal reactions. Many different reactions have been developed that enable the chemoselective ligation of two molecules.

In Chapter III, we introduced the concept of utilizing the thiol-ene photoconjugation reaction to introduce covalently biochemical functionality into the SPAAC-based, ene-containing, hydrogel network. We were able to pattern in a variety of peptides with full 4D

control *via* traditional photolithographic as well as multiphoton-based techniques, and used this approach to create complex, well-defined gradients within the materials (Chapter IV). By patterning the cell-adhesive peptide RGD in a matrix metalloproteinase-degradable gel, we were able to control local isotropic spreading of encapsulated cells. Additionally, we developed a Förster resonance energy transfer (FRET)-based peptide probe which increased its fluorescence in the presence of collagenase. By patterning this moiety into our hydrogel, we demonstrated spatial control over the detection of cell enzymatic function within the 3D material.

A variety of different cell functions can be detected and directed depending on which molecules are patterned into the network. As any thiol-containing molecule with a size scale less than that of the mesh of the network can be introduced with the photoconjugation reaction, this opens up the door for the patterning of many different types of compounds into the gel. Different synthetic peptide sequences can be used to stimulate specific cell function, sequester growth factors from the surrounding solutions, and to induce proliferation or differentiation within an initially-uniform population of stem cells. Thiolated full proteins, which can be readily generated with treatment of Traut's Reagent[15] (2-Iminothiolane·HCl), can also be used to elicit cell functions when peptide mimics are inadequate or unavailable. In addition to patterning discrete regions of the functional molecule into the gel at different concentrations, gradients can be generated with different slopes and magnitudes, enabling assays concerning cell behavior in response to covalently-immobilized biomolecules to be performed in 3D. Finally, chemical cues can be patterned directly around single encapsulated cells to assay the effects of geometric presentation of signals on cell function (Figure 7.5). By patterning in adhesive signals at discrete locations in the pericellular region of the hydrogel, cells can be forced into specific 3D geometric shapes and their differentiation assayed.

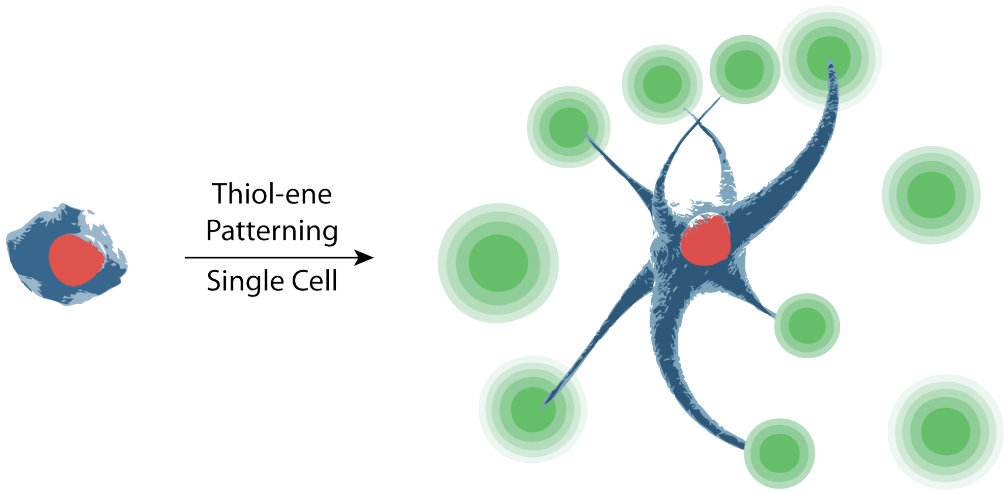

Figure 7.5 Single cell thiol-ene patterning. By functionalizing the hydrogel network in specific regions directly around the cell, simple questions about geometric arrangements of chemical cues and their influence on function can be assayed.

In this thesis, we have demonstrated that the simple patterning of monofunctional, thiol-containing biological molecules can be used to direct cell function. As this approach does not introduce additional chemical crosslinks into the network, the material properties of the system remain unchanged post-functionalization. Alternatively, by patterning in multifunctional thiol-containing molecules, thiol-ene coupling can result in a localized increase in crosslinking density and an increase in the stiffness of a material (Figure 7.6). This was preliminarily demonstrated by swelling a PEG-bis(thiol) (M_n ~ 2,000 Da) along with a small amount of photoinitator (Irgacure 2959, 0.05 wt%) into the preformed, ene-containing, SPAAC-based network and exposing the sample to light (λ = 365 nm, 10 mW cm^{-2}) for various amounts of time. Here, the swollen shear moduli increased fourfold from ~1 kPa to ~4 kPa with a 20 minute exposure. Interestingly, preliminary results suggest an almost linear increase in moduli with light dosage. This provides a means to increase spatially the moduli of a substrate, discretely or in gradient fashion, and opens up the door for elucidating the effects of increased material rigidity on cell function.

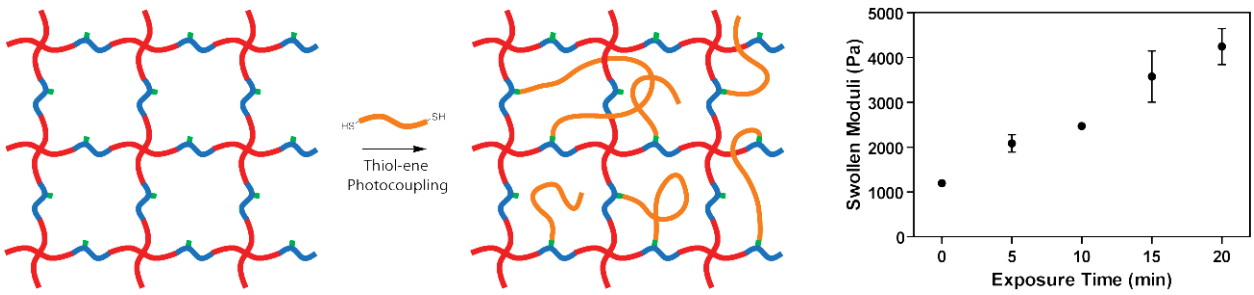

Figure 7.6 Increased moduli from thiol-ene patterning. By patterning in multifunctional thiols into the SPAAC-based hydrogel, additional crosslinks are introduced into the material, resulting in different network properties (*e.g.*, moduli, swelling ratio). *Work performed in collaboration with Kristen Feaver and Mark Tibbitt.

In Chapter V, we introduced a photolabile o-nitrobenyl ether moiety into the backbone of SPAAC-based hydrogel that enabled the user-mediated photoscission of chemical crosslinks and eventual photodegradation of the material. We utilized this reaction to create degraded channels down from the surface of the gel, where the feature height was directly related to the total amount of light dosage that was imposed on the system. Alternatively, we created elaborate 3D structural voids with the gel using focused multiphoton laser light techniques. These gels degraded substantially faster than those based on a radical chain polymerization mechanism[16], owing to the fact that fewer crosslinks are required to be broken to achieve reverse gelation in a step-growth system as compared to chain-growth materials[17]. We can utilize these materials to create quickly microwells of arbitrary size, shape, and depth that can be used to control reproducibly cell aggregation in a variety of geometries *in vitro* (Figure 7.7). As geometric cues have been implicated in directing cell function (*e.g.*, apoptosis[18], differentiation[19]), this platform provides a means to test how morphogenesis within a cluster is dictated by aggregate shape. Preliminary work has been performed with lung epithelial cells, where alveolar type II (AV2) progenitor cells differentiate into the alveolar type I (AV1) cells that facilitate gas exchange and act as a fluid barrier at the alveolar surface. After seeding a uniform population of AV2 cells into these microwell arrays, whose size was based off of that of human alveoli, we observe

progenitor differentiation of AV2 to AV1 and cell alignment along the surface of the wells, similar to what is observed *in vivo*. Less differentiation was observed in the shapes with more pinch-points along their walls.

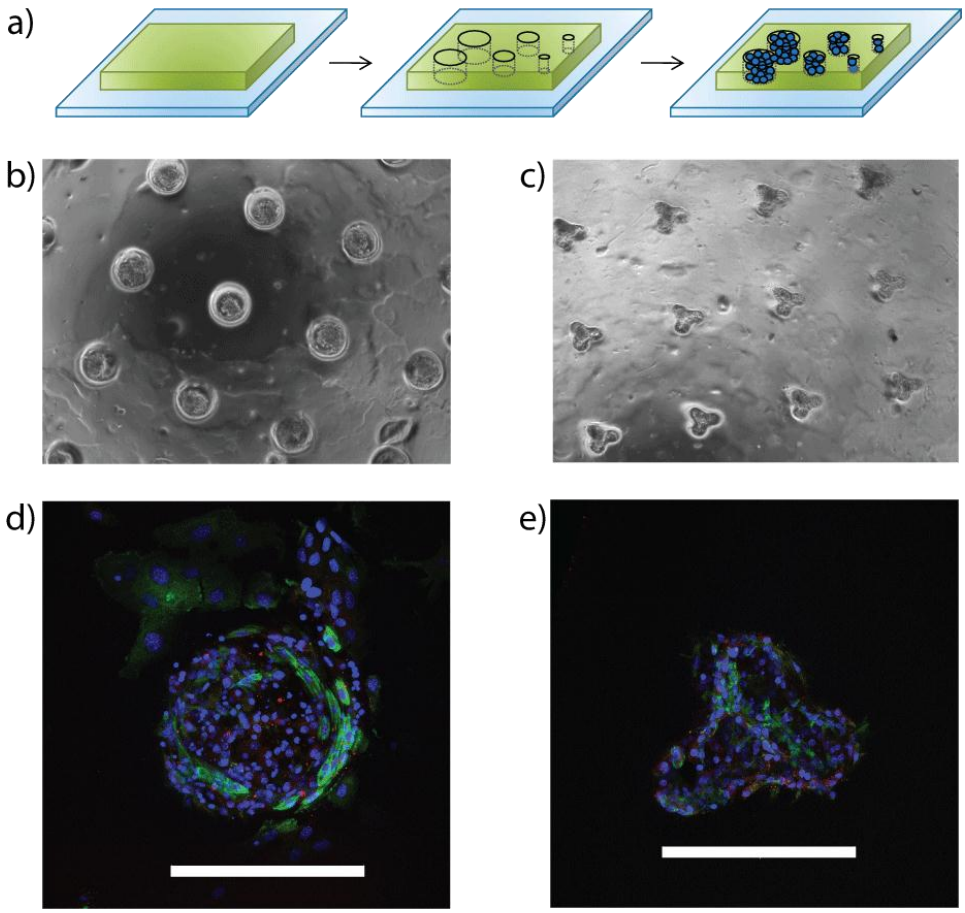

Figure 7.7 Directed aggregation of lung alveolar epithelial cells (AT2) within photodegraded microwells. a) Wells of a specified shape and depth are photodegraded down from the surface of the initially-flat gel. AT2 cells are seeded into the wells by centrifugation, and these wells can be arbitrarily shaped, with circles shown in (b) and three-leaf clovers in (c). d-e) After 7 days, AT2 cells have differentiated into AT1 cells and aligned with the outer wall. Blue = cell nuclei, green = AT1 marker protein T1α, red = AT2 marker surfactant protein C. Scale bars = 200 μm. *Work performed in collaboration with Dr. April Kloxin and Prof. Vivek Balasubramaniam.

In Chapter V, we developed light conditions that enabled the thiol-ene photoconjugation and the nitrobenzyl ether photocleavage to be performed independently within the same system. The thiol-ene reaction was initiated with visible light (λ = 490 – 650 nm) in combination with

the type II photoinitator eosin Y, while photoscission was controlled with UV (λ = 365 nm). By including both the photoreactive ene pendant to and the nitrobenzyl ether within our peptide backbone, a hydrogel material was created that was both photodegradable and photocouplable. We exploited this system to guide NIH 3T3 fibroblast cell outgrowth into a synthetic environment with full 3D control in the presence of encapsulated human mesenchymal stem cells. In Chapter VI, we combined these chemistries in a slightly different manner that enabled the reversible patterning of biomolecules within a 3D SPAAC-based gel. In this work, a thiol-containing peptide was synthesized that contained the photodegradable moiety adjacent to the amino acid sequence of interest. This peptide was patterned into the network using visible light and subsequently removed with UV light. This approach yielded predictable photorelease of peptides, which was exploited to create complex biochemical gradients within the hydrogels. Additionally, we utilized this chemistry to control reversibly cell adhesion on a gel surface, based on the dynamic presentation of the RGD adhesive ligand.

Recent work has demonstrated that cell morphology and cytoskeletal organization are directly related to the properties of its surrounding microenvironment.[20,21] The presentation of adhesive ligands, as well as the shape and moduli of the material substrate, has effects on cell viability, motility, and stem cell differentation.[18,22] Though much information about the cell's interaction with its local environment has already been determined, previous studies have been limited to static cell shapes or substrate properties due to a lack of a dynamically-tunable materials. We propose studying the effects of dynamic changes in cell shape and adhesive ligand presentation on cytoskeletal organization and cell fate (Figure 7.8). These studies will provide insight into how and how quickly cells translate changes in the biochemical and biophysical makeup of their surrounding environment into biological responses.

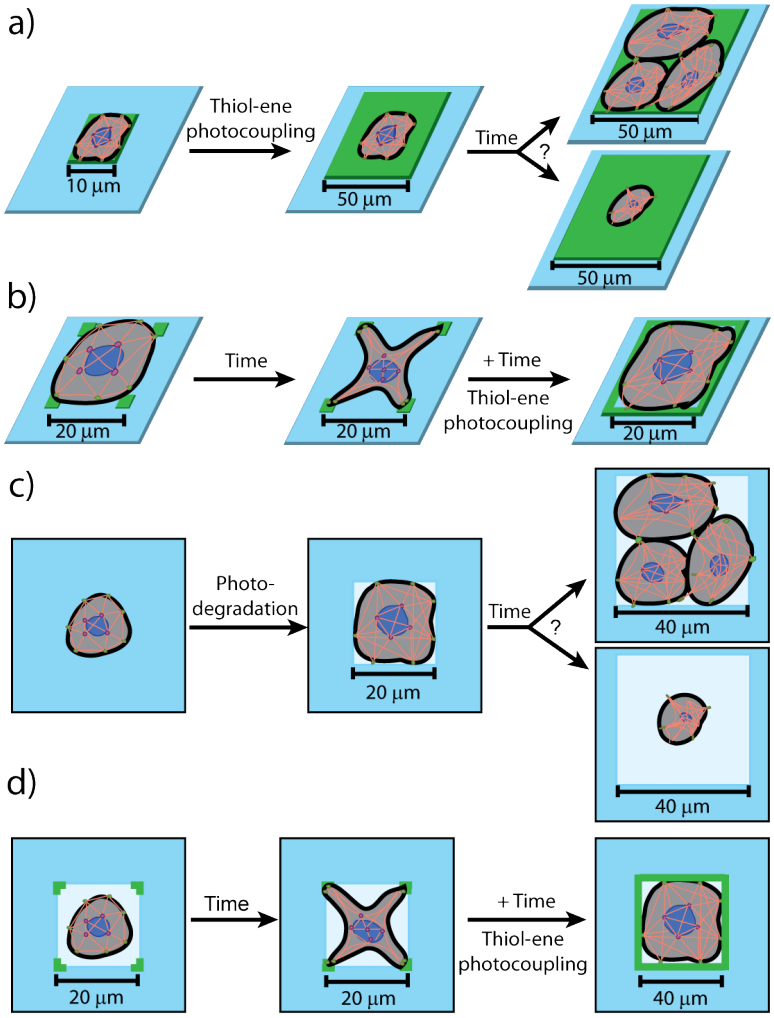

Figure 7.8 2D & 3D modulation of cell shape and size. a) In 2D, cells are initially seeded on adhesive regions of a gel surface (left). At a later time point, the size or shape of the adhesive island can be changed (middle) to observe the effect on cell fate (proliferation, top right; apoptosis, bottom right). b) Similarly, cells can be seeded on posts of patterned RGD (left) that will subsequently be changed to squares *via* thiol-ene photocoupling (right). c) In 3D, voids around single cells (left) encapsulated within an RGD-containing photodegradable gel are created with UV exposure (middle). At a later time, void shape and size is altered to determine the effect on proliferation and apoptosis rates (right). d) Alternatively, only specific regions of the network can be functionalized with RGD (left, middle) to test its effect on cell function. Subsequent irradiation increases the void area or regions of adhesivity (right). *Concepts developed in collaboration with Mark Tibbitt and Dr. April Kloxin, images created by Mark Tibbitt.

In summary, through the combined utilization of three independent bioorthogonal chemistries, we have developed hydrogel platforms whose biochemical and biophysical characteristics were modifiable dynamically and in real time to detect and direct encapsulated

cell function. These systems enable new information regarding diverse biological questions concerning cell function in response to temporal changes of the pericellular environment to be ascertained. Such an increased understanding of fundamental cell response to its external environment may provide improved insight into the rational design of synthetic biomaterial scaffolds in applications ranging from the expansion and differentiation of stem cells to carriers for cell delivery and regenerative medicine.

7.1 References

1. Codelli, J.A., Baskin, J.M., Agard, N.J. & Berozzi, C.R. Second-generation difluorinated cyclooctynes for copper-free click chemistry. *J. Am. Chem. Soc.* **130**, 11486-11493 (2008).

2. Ornelas, C., Broichhagen, J. & Weck, M. Strain-promoted alkyne azide cycloaddition for the functionalization of poly(amide)-based dendrons and dendrimers. *J. Am. Chem. Soc.* **132**, 3923-3931 (2010).

3. Ning, X.H., Guo, J., Wolfert, M.A. & Boons, G.J. Visualizing metabolically labeled glycoconjugates of living cells by copper-free and fast huisgen cycloadditions. *Angew. Chem. Int. Ed. Engl.* **47**, 2253-2255 (2008).

4. Jewett, J.C., Sletten, E.M. & Bertozzi, C.R. Rapid cu-free click chemistry with readily synthesized biarylazacyclooctynones. *J. Am. Chem. Soc.* **132**, 3688-3690 (2010).

5. Sletten, E.M., Nakamura, H., Jewett, J.C. & Bertozzi, C.R. Difluorobenzocyclooctyne: Synthesis, reactivity, and stabilization by beta-cyclodextrin. *J. Am. Chem. Soc.* **132**, 11799-11805 (2010).

6. Dommerholt, J. et al. Readily accessible bicyclononynes for bioorthogonal labeling and three-dimensional imaging of living cells. *Angew. Chem. Int. Ed. Engl.* **49**, 9422-9425 (2010).

7. McCall, J.D., Lin, C.C. & Anseth, K.S. Affinity peptides protect transforming growth factor beta during encapsulation in poly(ethylene glycol) hydrogels. *Biomacromolecules* **12**, 1051-1057 (2011).

8. Blackman, M.L., Royzen, M. & Fox, J.M. Tetrazine ligation: Fast bioconjugation based on inverse-electron-demand diels-alder reactivity. *J. Am. Chem. Soc.* **130**, 13518-13519 (2008).

9. Devaraj, N.K., Weissleder, R. & Hilderbrand, S.A. Tetrazine-based cycloadditions: Application to pretargeted live cell imaging. *Bioconjug. Chem.* **19**, 2297-2299 (2008).

10. van Berkel, S.S. et al. Metal-free triazole formation as a tool for bioconjugation. *Chembiochem* **8**, 1504-1508 (2007).

11. Song, W., Wang, Y., Qu, J., Madden, M.M. & Lin, Q. A photoinducible 1,3-dipolar cycloaddition reaction for rapid, selective modification of tetrazole-containing proteins. *Angew. Chem. Int. Ed. Engl.* **47**, 2832-2835 (2008).

12. Saxon, E. & Bertozzi, C.R. Cell surface engineering by a modified staudinger reaction. *Science* **287**, 2007-2010 (2000).

13. Ning, X.H. et al. Protein modification by strain-promoted alkyne-nitrone cycloaddition. *Angew. Chem. Int. Ed. Engl.* **49**, 3065-3068 (2010).

14. Sletten, E.M. & Bertozzi, C.R. Bioorthogonal chemistry: Fishing for selectivity in a sea of functionality. *Angew. Chem. Int. Ed. Engl.* **48**, 6974-6998 (2009).

15. Traut, R.R. et al. Methyl 4-mercaptobutyrimidate as a cleavable cross-linking reagent and its application to the escherichia coli 30s ribosome. *Biochemistry (Mosc.)* **12**, 3266-3273 (1973).

16. Kloxin, A.M., Kasko, A.M., Salinas, C.N. & Anseth, K.S. Photodegradable hydrogels for dynamic tuning of physical and chemical properties. *Science* **324**, 59-63 (2009).

17. Odian, G.G. Principles of polymerization, Edn. 4th. (Wiley-Interscience, Hoboken, N.J.; 2004).

18. Chen, C.S., Mrksich, M., Huang, S., Whitesides, G.M. & Ingber, D.E. Geometric control of cell life and death. *Science* **276**, 1425-1428 (1997).

19. Kilian, K.A., Bugarija, B., Lahn, B.T. & Mrksich, M. Geometric cues for directing the differentiation of mesenchymal stem cells. *Proc. Natl. Acad. Sci. U. S. A.* **107**, 4872-4877 (2010).

20. Wong, J.Y., Velasco, A., Rajagopalan, P. & Pham, Q. Directed movement of vascular smooth muscle cells on gradient-compliant hydrogels. *Langmuir* **19**, 1908-1913 (2003).

21. Nelson, C.M. et al. Emergent patterns of growth controlled by multicellular form and mechanics. *Proc. Natl. Acad. Sci. U. S. A.* **102**, 11594-11599 (2005).

22. Engler, A.J., Sen, S., Sweeney, H.L. & Discher, D.E. Matrix elasticity directs stem cell lineage specification. *Cell* **126**, 677-689 (2006).

CHAPTER VIII

BIBLIOGRAPHY

Adzima, B.J. et al. Spatial and temporal control of the alkyne-azide cycloaddition by photoinitiated Cu(II) reduction. *Nat. Chem.* **3**, 258-261 (2011).

Adzima, B.J., Aguirre, H.A., Kloxin, C.J., Scott, T.F. & Bowman, C.N. Rheological and chemical analysis of reverse gelation in a covalently crosslinked diels-alder polymer network. *Macromolecules* **41**, 9112-9117 (2008).

Agard, N.J., Baskin, J.M., Prescher, J.A., Lo, A. & Bertozzi, C.R. A comparative study of bioorthogonal reactions with azides. *ACS Chem. Biol.* **1**, 644-648 (2006).

Agard, N.J., Prescher, J.A. & Bertozzi, C.R. A strain-promoted [3 + 2] azide-alkyne cycloaddition for covalent modification of biomolecules in living systems. *J. Am. Chem. Soc.* **126**, 15046-15047 (2004).

Ahmed, T.A., Dare, E.V. & Hincke, M. Fibrin: A versatile scaffold for tissue engineering applications. *Tissue Eng. Part B Rev.* (2008).

Aimetti, A.A., Tibbitt, M.W. & Anseth, K.S. Human neutrophil elastase responsive delivery from poly(ethylene glycol) hydrogels. *Biomacromolecules* **10**, 1484-1489 (2009).

Aizawa, Y., Wylie, R. & Shoichet, M. Endothelial cell guidance in 3D patterned scaffolds. *Adv. Mater.* **22**, 4831-4835 (2010).

Alberts, B. et al. Molecular biology of the cell, Edn. 5th. (Garland Science, New York; 2008).

Aljarilla, A. et al. Stereochemistry of the tetrabutylammonium cyanide-catalyzed cyanosylilation of cyclic alpha,beta-epoxyketones - Dependence of the diastereoselectivity on the ring size. *Eur. J. Org. Chem.*, 3969-3976 (2006).

Alvarez, M. et al. Single-photon and two-photon induced photocleavage for monolayers of an alkyltriethoxysilane with a photoprotected carboxylic ester. *Adv. Mater.* **20**, 4563-4567 (2008).

Andreopoulos, F.M. et al. Photoscissable hydrogel synthesis *via* rapid photopolymerization of novel PEG-based polymers in the absence of photoinitiators. *J. Am. Chem. Soc.* **118**, 6235-6240 (1996).

Anseth, K.S. A biologist looks to 'click chemistry' for better three-dimensional tissue models. *Nature* **453**, 5 (2008).

Anseth, K.S. et al. In situ forming degradable networks and their application in tissue engineering and drug delivery. *J. Control. Release* **78**, 199-209 (2002).

Anseth, K.S., Bowman, C.N. & BrannonPeppas, L. Mechanical properties of hydrogels and their experimental determination. *Biomaterials* **17**, 1647-1657 (1996).

Azab, A.K. et al. Crosslinked chitosan implants as potential degradable devices for brachytherapy: In vitro and in vivo analysis. *J. Control. Release* **111**, 281-289 (2006).

Barner-Kowollik, C. et al. "Clicking" polymers or just efficient linking: What is the difference? *Angew. Chem. Int. Ed. Engl.* **50**, 60-62 (2011).

Barralet, J.E. et al. Comparison of bone marrow cell growth on 2d and 3D alginate hydrogels. *J. Mater. Sci. - Mater. Med.* **16**, 515-519 (2005).

Barz, M., Luxenhofer, R., Zentel, R. & Vicent, M.J. Overcoming the PEG-addiction: Well-defined alternatives to PEG, from structure–property relationships to better defined therapeutics. *Polym. Chem.* (2011).

Baskin, J.M. & Bertozzi, C.R. Bioorthogonal click chemistry: Covalent labeling in living systems. *Qsar & Combinatorial Science* **26**, 1211-1219 (2007).

Baskin, J.M. et al. Copper-free click chemistry for dynamic in vivo imaging. *Proc. Natl. Acad. Sci. U. S. A.* **104**, 16793-16797 (2007).

Benoit, D.S.W., Durney, A.R. & Anseth, K.S. Manipulations in hydrogel degradation behavior enhance osteoblast function and mineralized tissue formation. *Tissue Eng.* **12**, 1663-1673 (2006).

Berger, J. et al. Structure and interactions in covalently and ionically crosslinked chitosan hydrogels for biomedical applications. *Eur. J. Pharm. Biopharm.* **57**, 19-34 (2004).

Binder, W.H. & Sachsenhofer, R. 'Click' chemistry in polymer and materials science. *Macromol. Rapid Commun.* **28**, 15-54 (2007).

Blackman, M.L., Royzen, M. & Fox, J.M. Tetrazine ligation: Fast bioconjugation based on inverse-electron-demand diels-alder reactivity. *J. Am. Chem. Soc.* **130**, 13518-13519 (2008).

Bloomfield, J.J. & Nelke, J.M. Acyloin condensation in which chlorotrimethylsilane is used as a trapping Agent - 1,2-Bis(Trimethylsilyloxy)-Cyclobutene and 2-Hydroxycyclobutanone. *Org. Synth.* **50-9**, 167-172 (1988).

Bock, V.D., Perciaccante, R., Jansen, T.P., Hiemstra, H. & van Maarseveen, J.H. Click chemistry as a route to cyclic tetrapeptide analogues: Synthesis of cyclo-[pro-val-psi(triazole)-pro-tyr]. *Org. Lett.* **8**, 919-922 (2006).

Bowman, C.N. & Kloxin, C.J. Toward an enhanced understanding and implementation of photopolymerization reactions. *AIChE J* **54**, 2775-2795 (2008).

Boyer, C. & Davis, T.P. One-pot synthesis and biofunctionalization of glycopolymers *via* raft polymerization and thiol-ene reactions. *Chem. Commun.*, 6029-6031 (2009).

Boyer, C., Bulmus, V. & Davis, T.P. Efficient usage of thiocarbonates for both the production and the biofunctionalization of polymers. *Macromol. Rapid Commun.* **30**, 493-497 (2009).

Bryant, S.J. & Anseth, K.S. Controlling the spatial distribution of ECM components in degradable PEG hydrogels for tissue engineering cartilage. *J. Biomed. Mater. Res. A* **64A**, 70-79 (2003).

Bryant, S.J. & Anseth, K.S. Hydrogel properties influence ECM production by chondrocytes photoencapsulated in poly(ethylene glycol) hydrogels. *J. Biomed. Mater. Res.* **59**, 63-72 (2002).

Bryant, S.J. et al. Synthesis and characterization of photopolymerized multifunctional hydrogels: Water-soluble poly(vinyl alcohol) and chondroitin sulfate macromers for chondrocyte encapsulation. *Macromolecules* **37**, 6726-6733 (2004).

Burdick, J.A. & Anseth, K.S. Photoencapsulation of osteoblasts in injectable RGD-modified PEG hydrogels for bone tissue engineering. *Biomaterials* **23**, 4315-4323 (2002).

Burdick, J.A. & Prestwich, G.D. Hyaluronic acid hydrogels for biomedical applications. *Adv. Mater.* **23**, H41-56 (2011).

Butcher, J.T. & Nerem, R.M. Porcine aortic valve interstitial cells in three-dimensional culture: Comparison of phenotype with aortic smooth muscle cells. *J. Heart Valve Dis.* **13**, 478-485 (2004).

Cadee, J.A. et al. In vivo biocompatibility of dextran-based hydrogels. *J. Biomed. Mater. Res.* **50**, 397-404 (2000).

Campos, L.M. et al. Development of thermal and photochemical strategies for thiol-ene click polymer functionalization. *Macromolecules* **41**, 7063-7070 (2008).

Cascone, M.G. et al. Bioartificial polymeric materials based on polysaccharides. *J. Biomater. Sci., Polym. Ed.* **12**, 267-281 (2001).

Chang, P.V. et al. Copper-free click chemistry in living animals. *Proc. Natl. Acad. Sci. U. S. A.* **107**, 1821-1826 (2010).

Chen, C.S., Mrksich, M., Huang, S., Whitesides, G.M. & Ingber, D.E. Geometric control of cell life and death. *Science* **276**, 1425-1428 (1997).

Chen, J.K. Fish 'n clicks. *Nat. Chem. Biol.* **4**, 391-392 (2008).

Chiou, B.S. & Khan, S.A. Real-time FTIR and in situ rheological studies on the UV curing kinetics of thiol-ene polymers. *Macromolecules* **30**, 7322-7328 (1997).

Codelli, J.A., Baskin, J.M., Agard, N.J. & Berozzi, C.R. Second-generation difluorinated cyclooctynes for copper-free click chemistry. *J. Am. Chem. Soc.* **130**, 11486-11493 (2008).

Cramer, N.B. & Bowman, C.N. Kinetics of thiol-ene and thiol-acrylate photopolymerizations with real-time fourier transform infrared. *J. Polym. Sci., Part A: Polym. Chem.* **39**, 3311-3319 (2001).

Cramer, N.B., Reddy, S.K., O'Brien, A.K. & Bowman, C.N. Thiol-ene photopolymerization mechanism and rate limiting step changes for various vinyl functional group chemistries. *Macromolecules* **36**, 7964-7969 (2003).

Cushing, M.C. & Anseth, K.S. Hydrogel cell cultures. *Science* **316**, 1133-1134 (2007).

Debets, M.F. et al. Aza-dibenzocyclooctynes for fast and efficient enzyme PEGylation *via* copper-free (3+2) cycloaddition. *Chem. Commun.* **46**, 97-99 (2010).

DeForest, C.A. & Anseth, K.S. Cytocompatible click-based hydrogels with dynamically-tunable properties through orthogonal photocoupling and photodegradation reactions. *In Review* (2011).

DeForest, C.A., Polizzotti, B.D. & Anseth, K.S. Sequential click reactions for synthesizing and patterning three-dimensional cell microenvironments. *Nat. Mater.* **8**, 659-664 (2009).

DeForest, C.A., Sims, E.A. & Anseth, K.S. Peptide-functionalized click hydrogels with independently tunable mechanics and chemical functionality for 3D cell culture. *Chem. Mater.* **22**, 4783-4790 (2010).

Deiters, A. Principles and applications of the photochemical control of cellular processes. *Chembiochem* **11**, 47-53 (2010).

DeLong, S.A., Gobin, A.S. & West, J.L. Covalent immobilization of RGDS on hydrogel surfaces to direct cell alignment and migration. *J. Control. Release* **109**, 139-148 (2005).

DeLong, S.A., Moon, J.J. & West, J.L. Covalently immobilized gradients of bFGF on hydrogel scaffolds for directed cell migration. *Biomaterials* **26**, 3227-3234 (2005).

Devaraj, N.K., Weissleder, R. & Hilderbrand, S.A. Tetrazine-based cycloadditions: Application to pretargeted live cell imaging. *Bioconjug. Chem.* **19**, 2297-2299 (2008).

Do, N., McDermott, R.E. & Ragan, J.A. Preparation of cycloheptane-1,3-dione *via* reductive ring expansion of 1-trimethylsilyloxy-7,7-dichlorobicyclo[3.2.0]heptan-6-one. *Org. Synth.* **85**, 138-146 (2008).

Dommerholt, J. et al. Readily accessible bicyclononynes for bioorthogonal labeling and three-dimensional imaging of living cells. *Angew. Chem. Int. Ed. Engl.* **49**, 9422-9425 (2010).

Dondoni, A. The emergence of thiol-ene coupling as a click process for materials and bioorganic chemistry. *Angew. Chem. Int. Ed. Engl.* **47**, 8995-8997 (2008).

Engler, A.C., Lee, H.I. & Hammond, P.T. Highly efficient "grafting onto" a polypeptide backbone using click chemistry. *Angew. Chem. Int. Ed. Engl.* **48**, 9334-9338 (2009).

Engler, A.J., Sen, S., Sweeney, H.L. & Discher, D.E. Matrix elasticity directs stem cell lineage specification. *Cell* **126**, 677-689 (2006).

Engler, A.J., Sweeney, H.L. & Discher, D.E. Substrate elasticity alters human mesenchymal stem cell differentiation. *Biophys. J.* **88**, 500A-500A (2005).

Evans, M.J., Saghatelian, A., Sorensen, E.J. & Cravatt, B.F. Target discovery in small-molecule cell-based screens by in situ proteome reactivity profiling. *Nat. Biotechnol.* **23**, 1303-1307 (2005).

Evans, R.A. The rise of azide-alkyne 1,3-dipolar 'click' cycloaddition and its application to polymer science and surface modification. *Aust. J. Chem.* **60**, 384-395 (2007).

Eyrich, D. et al. Long-term stable fibrin gels for cartilage engineering. *Biomaterials* **28**, 55-65 (2007).

Fairbanks, B.D. et al. A versatile synthetic extracellular matrix mimic *via* thiol-norbornene photopolymerization. *Adv. Mater.* **21**, 5005-5010 (2009).

Fairbanks, B.D., Singh, S.P., Bowman, C.N. & Anseth, K.S. Photodegradable, photoadaptable hydrogels *via* radical-mediated disulfide fragmentation reaction. *Macromolecules* **44**, 2444-2450 (2011).

Floyd, M.B. & Weiss, M.J. Prostaglandins and congeners. 21. Synthesis of some cyclohexyl analogs (11a-Homoprostaglandins). *J. Org. Chem.* **44**, 71-75 (1978).

Franc, G. & Kakkar, A. Dendrimer design using Cu-I-catalyzed alkyne-azide "click-chemistry". *Chem. Commun.*, 5267-5276 (2008).

Franc, G. & Kakkar, A.K. "Click" methodologies: Efficient, simple and greener routes to design dendrimers. *Chem. Soc. Rev.* **39**, 1536-1544 (2010).

Franke, R., Doll, C. & Eichler, J. Peptide ligation through click chemistry for the generation of assembled and scaffolded peptides. *Tetrahedron Lett.* **46**, 4479-4482 (2005).

Frey, M.T. & Wang, Y.L. A photo-modulatable material for probing cellular responses to substrate rigidity. *Soft Matter* **5**, 1918-1924 (2009).

Gobin, A.S. & West, J.L. Cell migration through defined, synthetic extracellular matrix analogues. *FASEB J.* **16**, 751-753 (2002).

Gupta, N. et al. A versatile approach to high-throughput microarrays using thiol-ene chemistry. *Nat. Chem.* **2**, 138-145 (2010).

Hahn, M.S., Miller, J.S. & West, J.L. Three-dimensional biochemical and biomechanical patterning of hydrogels for guiding cell behavior. *Adv. Mater.* **18**, 2679-2684 (2006).

Harant, A.W., Khire, V.S., Thibodaux, M.S. & Bowman, C.N. Thiol-ene photopolymer grafts on functionalized glass and silicon surfaces. *Macromolecules* **39**, 1461-1466 (2006).

Hassan, C.M. & Peppas, N.A. Structure and applications of poly(vinyl alcohol) hydrogels produced by conventional crosslinking or by freezing/thawing methods. *Biopolymers/Pva Hydrogels/Anionic Polymerisation Nanocomposites* **153**, 37-65 (2000).

Hawker, C.J. & Wooley, K.L. The convergence of synthetic organic and polymer chemistries. *Science* **309**, 1200-1205 (2005).

Hayashi, K. et al. One-pot biofunctionalization of magnetic nanoparticles *via* thiol-ene click reaction for magnetic hyperthermia and magnetic resonance imaging. *Chem. Mater.* **22**, 3768-3772 (2010).

Hern, D.L. & Hubbell, J.A. Incorporation of adhesion peptides into nonadhesive hydrogels useful for tissue resurfacing. *J. Biomed. Mater. Res.* **39**, 266-276 (1998).

Himo, F. et al. Copper(i)-catalyzed synthesis of azoles. DFT study predicts unprecedented reactivity and intermediates. *J. Am. Chem. Soc.* **127**, 210-216 (2005).

Hoemann, C.D., Sun, J., Legare, A., McKee, M.D. & Buschmann, M.D. Tissue engineering of cartilage using an injectable and adhesive chitosan-based cell-delivery vehicle. *Osteoarthritis Cartilage* **13**, 318-329 (2005).

Hoffmann, J.C. & West, J.L. Three-dimensional photolithographic patterning of multiple bioactive ligands in poly(ethylene glycol) hydrogels. *Soft Matter* **6**, 5056-5063 (2010).

Holmes, C.P. & Jones, D.G. Reagents for combinatorial organic-synthesis - development of a new o-nitrobenzyl photolabile linker for solid-phase synthesis. *J. Org. Chem.* **60**, 2318-2319 (1995).

Holmes, C.P. Model studies for new o-nitrobenzyl photolabile linkers: Substituent effects on the rates of photochemical cleavage. *J. Org. Chem.* **62**, 2370-2380 (1997).

House, H.O., Sieloff, R.F., Lee, T.V. & Detar, M.B. Enones with strained double-bonds. 4. The bicyclo[5.3.1]undecane system. *J. Org. Chem.* **45**, 1800-1806 (1980).

Hoyle, C.E. & Bowman, C.N. Thiol-ene click chemistry. *Angew. Chem. Int. Ed. Engl.* **49**, 1540-1573 (2010).

Hoyle, C.E., Lee, T.Y. & Roper, T. Thiol-enes: Chemistry of the past with promise for the future. *J. Polym. Sci., Part A: Polym. Chem.* **42**, 5301-5338 (2004).

Huebsch, N. et al. Harnessing traction-mediated manipulation of the cell/matrix interface to control stem-cell fate. *Nat. Mater.* **9**, 518-526 (2010).

Huisgen, R. 1.3-dipolare cycloadditionen - ruckschau und ausblick. *Angew. Chem. Int. Ed. Engl.* **75**, 604-637 (1963).

Hutmacher, D.W., Ho, S.T.B., Cool, S.M. & Hui, J.H. The influence of fibrin based hydrogels on the chondrogenic differentiation of human bone marrow stromal cells. *Biomaterials* **31**, 38-47 (2010).

Ilina, O., Bakker, G.J., Vasaturo, A., Hofmann, R.M. & Friedl, P. Two-photon laser-generated microtracks in 3D collagen lattices: Principles of MMP-dependent and -independent collective cancer cell invasion. *Phys. Biol.* **8** (2011).

Ingber, D.E. Cellular mechanotransduction: Putting all the pieces together again. *FASEB J.* **20**, 811-827 (2006).

Ingber, D.E. Mechanobiology and diseases of mechanotransduction. *Ann. Med.* **35**, 564-577 (2003).

Jagasia, R., Holub, J.M., Bollinger, M., Kirshenbaum, K. & Finn, M.G. Peptide cyclization and cyclodimerization by Cu-I-mediated azide-alkyne cycloaddition. *J. Org. Chem.* **74**, 2964-2974 (2009).

Jewett, J.C., Sletten, E.M. & Bertozzi, C.R. Rapid Cu-free click chemistry with readily synthesized biarylazacyclooctynones. *J. Am. Chem. Soc.* **132**, 3688-3690 (2010).

Johnson, J.A., Baskin, J.M., Bertozzi, C.R., Koberstein, J.T. & Turro, N.J. Copper-free click chemistry for the in situ crosslinking of photodegradable star polymers. *Chem. Commun.*, 3064-3066 (2008).

Johnson, J.A., Finn, M.G., Koberstein, J.T. & Turro, N.J. Synthesis of photocleavable linear macromonomers by ATRP and star macromonomers by a tandem ATRP-click reaction: Precursors to photodegradable model networks. *Macromolecules* **40**, 3589-3598 (2007).

Johnson, P.M., Reynolds, T.B., Stansbury, J.W. & Bowman, C.N. High throughput kinetic analysis of photopolymer conversion using composition and exposure time gradients. *Polymer* **46**, 3300-3306 (2005).

Jonkheijm, P. et al. Photochemical surface patterning by the thiol-ene reaction. *Angew. Chem. Int. Ed. Engl.* **47**, 4421-4424 (2008).

Joralemon, M.J. et al. Dendrimers clicked together divergently. *Macromolecules* **38**, 5436-5443 (2005).

Kade, M.J., Burke, D.J. & Hawker, C.J. The power of thiol-ene chemistry. *J. Polym. Sci., Part A: Polym. Chem.* **48**, 743-750 (2010).

Kaneko, S. et al. Photocontrol of cell adhesion on amino-bearing surfaces by reversible conjugation of poly(ethylene glycol) *via* a photocleavable linker. *Phys. Chem. Chem. Phys.* **13**, 4051-4059 (2011).

Kemsley, J. Learning from UCLA. *Chemical & Engineering News* **87**, 29-31 (2009).

Khetan, S. & Burdick, J.A. Patterning hydrogels in three dimensions towards controlling cellular interactions. *Soft Matter* **7**, 830-838 (2011).

Khetan, S. & Burdick, J.A. Patterning network structure to spatially control cellular remodeling and stem cell fate within 3-dimensional hydrogels. *Biomaterials* **31**, 8228-8234 (2010).

Khetan, S., Katz, J.S. & Burdick, J.A. Sequential crosslinking to control cellular spreading in 3-dimensional hydrogels. *Soft Matter* **5**, 1601-1606 (2009).

Khire, V.S., Benoit, D.S.W., Anseth, K.S. & Bowman, C.N. Ultrathin gradient films using thiol-ene polymerizations. *J. Polym. Sci., Part A: Polym. Chem.* **44**, 7027-7039 (2006).

Khire, V.S., Yi, Y., Clark, N.A. & Bowman, C.N. Formation and surface modification of nanopatterned thiol-ene substrates using step and flash imprint lithography. *Adv. Mater.* **20**, 3308-3313 (2008).

Kilian, K.A., Bugarija, B., Lahn, B.T. & Mrksich, M. Geometric cues for directing the differentiation of mesenchymal stem cells. *Proc. Natl. Acad. Sci. U. S. A.* **107**, 4872-4877 (2010).

Killops, K.L., Campos, L.M. & Hawker, C.J. Robust, efficient, and orthogonal synthesis of dendrimers *via* thiol-ene "click" chemistry. *J. Am. Chem. Soc.* **130**, 5062-5064 (2008).

Kloxin, A.M., Benton, J.A. & Anseth, K.S. In situ elasticity modulation with dynamic substrates to direct cell phenotype. *Biomaterials* **31**, 1-8 (2010).

Kloxin, A.M., Kasko, A.M., Salinas, C.N. & Anseth, K.S. Photodegradable hydrogels for dynamic tuning of physical and chemical properties. *Science* **324**, 59-63 (2009).

Kloxin, A.M., Kloxin, C.J., Bowman, C.N. & Anseth, K.S. Mechanical properties of cellularly responsive hydrogels and their experimental determination. *Adv. Mater.* **22**, 3484-3494 (2010).

Kloxin, A.M., Tibbitt, M.W. & Anseth, K.S. Synthesis of photodegradable hydrogels as dynamically tunable cell culture PLAtforms. *Nat. Protoc.* **5**, 1867-1887 (2010).

Kloxin, A.M., Tibbitt, M.W., Kasko, A.M., Fairbairn, J.A. & Anseth, K.S. Tunable hydrogels for external manipulation of cellular microenvironments through controlled photodegradation. *Adv. Mater.* **22**, 61-66 (2010).

Kloxin, C.J., Scott, T.F. & Bowman, C.N. Stress relaxation *via* addition-fragmentation chain transfer in a thiol-ene photopolymerization. *Macromolecules* **42**, 2551-2556 (2009).

Kloxin, C.J., Scott, T.F., Adzima, B.J. & Bowman, C.N. Covalent adaptable networks (CANs): A unique paradigm in cross-linked polymers. *Macromolecules* **43**, 2643-2653 (2010).

Kolb, H.C. & Sharpless, K.B. The growing impact of click chemistry on drug discovery. *Drug Discov. Today* **8**, 1128-1137 (2003).

Kolb, H.C., Finn, M.G. & Sharpless, K.B. Click chemistry: Diverse chemical function from a few good reactions. *Angew. Chem. Int. Ed. Engl.* **40**, 2004-2021 (2001).

Kunz, H. & Unverzagt, C. The allyloxycarbonyl (aloc) moiety - Conversion of an unsuitable into a valuable amino protecting group for peptide-synthesis. *Angew. Chem. Int. Ed. Engl.* **23**, 436-437 (1984).

Kuo, C.K. & Ma, P.X. Ionically crosslinked alginate hydrogels as scaffolds for tissue engineering: Part 1. Structure, gelation rate and mechanical properties. *Biomaterials* **22**, 511-521 (2001).

Langer, R. & Tirrell, D.A. Designing materials for biology and medicine. *Nature* **428**, 487-492 (2004).

Langer, R. & Vacanti, J.P. Tissue Engineering. *Science* **260**, 920-926 (1993).

Larock, R.C. Comprehensive organic transformations: a guide to functional group preparations, Edn. 2nd. (Wiley-VCH, New York ; Chichester [England]; 1999).

Laughlin, S.T., Baskin, J.M., Amacher, S.L. & Bertozzi, C.R. In vivo imaging of membrane-associated glycans in developing zebrafish. *Science* **320**, 664-667 (2008).

Leach, J.B., Bivens, K.A., Patrick, C.W. & Schmidt, C.E. Photocrosslinked hyaluronic acid hydrogels: Natural, biodegradable tissue engineering scaffolds. *Biotechnol. Bioeng.* **82**, 578-589 (2003).

Lee, K.Y. & Mooney, D.J. Hydrogels for tissue engineering. *Chem. Rev.* **101**, 1869-1879 (2001).

Lee, S.H., Moon, J.J. & West, J.L. Three-dimensional micropatterning of bioactive hydrogels *via* two-photon laser scanning photolithography for guided 3D cell migration. *Biomaterials* **29**, 2962-2968 (2008).

Lee, S.H., Moon, J.J., Miller, J.S. & West, J.L. Poly(ethylene glycol) hydrogels conjugated with a collagenase-sensitive fluorogenic substrate to visualize collagenase activity during three-dimensional cell migration. *Biomaterials* **28**, 3163-3170 (2007).

Lee, T.Y., Smith, Z., Reddy, S.K., Cramer, N.B. & Bowman, C.N. Thiol-allyl ether-methacrylate ternary systems. Polymerization mechanism. *Macromolecules* **40**, 1466-1472 (2007).

Lehmann, T.E., Kuhn, O. & Kruger, J. Process development and pilot plant scale synthesis of spiro[3.5]nonane-6,8-dione. *Org. Process Res. Dev.* **7**, 913-916 (2003).

Leslie-Barbick, J.E., Shen, C., Chen, C. & West, J.L. Micron-scale spatially patterned, covalently immobilized vascular endothelial growth factor on hydrogels accelerates endothelial tubulogenesis and increases cellular angiogenic responses. *Tissue Eng. Part A* **17**, 221-229 (2011).

Lin, C.C. & Anseth, K.S. Controlling affinity binding with peptide-functionalized poly(ethylene glycol) hydrogels. *Advanced Functional Materials* **19**, 2325-2331 (2009).

Lin, C.C. & Anseth, K.S. PEG hydrogels for the controlled release of biomolecules in regenerative medicine. *Pharm. Res.* **26**, 631-643 (2009).

Lin, C.C., Metters, A.T. & Anseth, K.S. Functional PEG-peptide hydrogels to modulate local inflammation induced by the pro-inflammatory cytokine TNF alpha. *Biomaterials* **30**, 4907-4914 (2009).

Lin-Gibson, S., Jones, R.L., Washburn, N.R. & Horkay, F. Structure-property relationships of photopolymerizable poly(ethylene glycol) dimethacrylate hydrogels. *Macromolecules* **38**, 2897-2902 (2005).

Lu, H.F., Targonsky, E.D., Wheeler, M.B. & Cheng, Y.L. Thermally induced gelable polymer networks for living cell encapsulation. *Biotechnol. Bioeng.* **96**, 146-155 (2007).

Luo, Y. & Shoichet, M.S. A photolabile hydrogel for guided three-dimensional cell growth and migration. *Nat. Mater.* **3**, 249-253 (2004).

Lutolf, M.P. & Hubbell, J.A. Synthetic biomaterials as instructive extracellular microenvironments for morphogenesis in tissue engineering. *Nat. Biotechnol.* **23**, 47-55 (2005).

Lutolf, M.P. et al. Biomimetic PEG hydrogels crosslinked with minimal plasmin-sensitive tri-amino acid peptides. *J. Biomed. Mater. Res. A* **93A**, 870-877 (2010).

Lutolf, M.P. et al. Synthetic matrix metalloproteinase-sensitive hydrogels for the conduction of tissue regeneration: Engineering cell-invasion characteristics. *Proc. Natl. Acad. Sci. U. S. A.* **100**, 5413-5418 (2003).

Lutolf, M.P., Gilbert, P.M. & Blau, H.M. Designing materials to direct stem-cell fate. *Nature* **462**, 433-441 (2009).

Lutolf, M.P., Raeber, G.P., Zisch, A.H., Tirelli, N. & Hubbell, J.A. Cell-responsive synthetic hydrogels. *Adv. Mater.* **15**, 888-892 (2003).

Lutolf, M.P., Tirelli, N., Cerritelli, S., Cavalli, L. & Hubbell, J.A. Systematic modulation of michael-type reactivity of thiols through the use of charged amino acids. *Bioconjug. Chem.* **12**, 1051-1056 (2001).

Mahoney, M.J. & Anseth, K.S. Three-dimensional growth and function of neural tissue in degradable polyethylene glycol hydrogels. *Biomaterials* **27**, 2265-2274 (2006).

Malkoch, M. et al. Synthesis of well-defined hydrogel networks using click chemistry. *Chem. Commun.*, 2774-2776 (2006).

Mammoto, A., Huang, S., Moore, K., Oh, P. & Ingber, D.E. Role of RhoA, mDia, and ROCK in cell shape-dependent control of the Skp2-p27(kip1) pathway and the G1/S transition. *J. Biol. Chem.* **279**, 26323-26330 (2004).

Mann, B.K., Gobin, A.S., Tsai, A.T., Schmedlen, R.H. & West, J.L. Smooth muscle cell growth in photopolymerized hydrogels with cell adhesive and proteolytically degradable domains: synthetic ECM analogs for tissue engineering. *Biomaterials* **22**, 3045-3051 (2001).

Mann, B.K., Schmedlen, R.H. & West, J.L. Tethered-TGF-beta increases extracellular matrix production of vascular smooth muscle cells. *Biomaterials* **22**, 439-444 (2001).

Martens, P.J., Bryant, S.J. & Anseth, K.S. Tailoring the degradation of hydrogels formed from multivinyl poly(ethylene glycol) and poly(vinyl alcohol) macromers for cartilage tissue engineering. *Biomacromolecules* **4**, 283-292 (2003).

Mason, M.N., Metters, A.T., Bowman, C.N. & Anseth, K.S. Predicting controlled-release behavior of degradable PLA-b-PEG-b-PLA hydrogels. *Macromolecules* **34**, 4630-4635 (2001).

Masters, K.S., Shah, D.N., Leinwand, L.A. & Anseth, K.S. Crosslinked hyaluronan scaffolds as a biologically active carrier for valvular interstitial cells. *Biomaterials* **26**, 2517-2525 (2005).

Masters, K.S., Shah, D.N., Walker, G., Leinwand, L.A. & Anseth, K.S. Designing scaffolds for valvular interstitial cells: Cell adhesion and function on naturally derived materials. *J. Biomed. Mater. Res. A* **71**, 172-180 (2004).

Mather, B.D., Viswanathan, K., Miller, K.M. & Long, T.E. Michael addition reactions in macromolecular design for emerging technologies. *Progress in Polymer Science* **31**, 487-531 (2006).

McCall, J.D., Lin, C.C. & Anseth, K.S. Affinity peptides protect transforming growth factor beta during encapsulation in poly(ethylene glycol) hydrogels. *Biomacromolecules* **12**, 1051-1057 (2011).

Meier, H., Antony-Mayer, C., Schulz-Popitz, C. & Zerban, G. Einführung einer Dreifachbindung in das Bicyclo[6.1.0]nonan-Gerüst. *Liebigs Ann. Chem.* **12**, 1087-1094 (1987).

Metters, A.T., Anseth, K.S. & Bowman, C.N. A statistical kinetic model for the bulk degradation of PLA-b-PEG-b-PLA hydrogel networks: Incorporating network non-idealities. *J. Phys. Chem. B* **105**, 8069-8076 (2001).

Metters, A.T., Anseth, K.S. & Bowman, C.N. Fundamental studies of a novel, biodegradable PEG-b-PLA hydrogel. *Polymer* **41**, 3993-4004 (2000).

Metters, A.T., Bowman, C.N. & Anseth, K.S. Verification of scaling laws for degrading PLA-b-PEG-b-PLA hydrogels. *AIChE Journal* **47**, 1432-1437 (2001).

Miller, J.S. et al. Bioactive hydrogels made from step-growth derived PEG-peptide macromers. *Biomaterials* (2010).

Moses, J.E. & Moorhouse, A.D. The growing applications of click chemistry. *Chem. Soc. Rev.* **36**, 1249-1262 (2007).

Nagase, H. & Fields, G.B. Human matrix metalloproteinase specificity studies using collagen sequence-based synthetic peptides. *Biopolymers* **40**, 399-416 (1996).

Nelson, C.M. et al. Emergent patterns of growth controlled by multicellular form and mechanics. *Proc. Natl. Acad. Sci. U. S. A.* **102**, 11594-11599 (2005).

Nilsson, C., Simpson, N., Malkoch, M., Johansson, M. & Malmstrom, E. Synthesis and thiol-ene photopolymerization of allyl-ether functionalized dendrimers. *J. Polym. Sci., Part A: Polym. Chem.* **46**, 1339-1348 (2008).

Ning, X.H. et al. Protein modification by strain-promoted alkyne-nitrone cycloaddition. *Angew. Chem. Int. Ed. Engl.* **49**, 3065-3068 (2010).

Ning, X.H., Guo, J., Wolfert, M.A. & Boons, G.J. Visualizing metabolically labeled glycoconjugates of living cells by copper-free and fast huisgen cycloadditions. *Angew. Chem. Int. Ed. Engl.* **47**, 2253-2255 (2008).

Nowatzki, P.J., Franck, C., Maskarinec, S.A., Ravichandran, G. & Tirrell, D.A. Mechanically tunable thin films of photosensitive artificial proteins: Preparation and characterization by nanoindentation. *Macromolecules* **41**, 1839-1845 (2008).

Odian, G.G. Principles of polymerization, Edn. 4th. (Wiley-Interscience, Hoboken, N.J.; 2004).

Ohmuro-Matsuyama, Y. & Tatsu, Y. Photocontrolled cell adhesion on a surface functionalized with a caged arginine-glycine-aspartate peptide. *Angew. Chem. Int. Ed. Engl.* **47**, 7527-7529 (2008).

Ornelas, C., Broichhagen, J. & Weck, M. Strain-promoted alkyne azide cycloaddition for the functionalization of poly(amide)-based dendrons and dendrimers. *J. Am. Chem. Soc.* **132**, 3923-3931 (2010).

Ossipov, D.A. & Hilborn, J. Poly(vinyl alcohol)-based hydrogels formed by "click chemistry". *Macromolecules* **39**, 1709-1718 (2006).

Paquette, L.A., Ross, R.J. & Springer, J.P. Stereocontrolled construction of an ingenol prototype having a complete array of oxygenated and unsaturated centers. *J. Am. Chem. Soc.* **110**, 6192-6204 (1988).

Park, Y., Lutolf, M.P., Hubbell, J.A., Hunziker, E.B. & Wong, M. Bovine primary chondrocyte culture in synthetic matrix metalloproteinase-sensitive poly(ethylene glycol)-based hydrogels as a scaffold for cartilage repair. *Tissue Eng.* **10**, 515-522 (2004).

Parrish, B., Breitenkamp, R.B. & Emrick, T. PEG- and peptide-grafted aliphatic polyesters by click chemistry. *J. Am. Chem. Soc.* **127**, 7404-7410 (2005).

Patch, J.A. & Barron, A.E. Mimicry of bioactive peptides *via* non-natural, sequence-specific peptidomimetic oligomers. *Curr. Opin. Chem. Biol.* **6**, 872-877 (2002).

Patterson, J. & Hubbell, J.A. Enhanced proteolytic degradation of molecularly engineered PEG hydrogels in response to MMP-1 and MMP-2. *Biomaterials* **31**, 7836-7845 (2010).

Patterson, J. & Hubbell, J.A. SPARC-derived protease substrates to enhance the plasmin sensitivity of molecularly engineered PEG hydrogels. *Biomaterials* **32**, 1301-1310 (2011).

Peppas, N.A. & Langer, R. New challenges in biomaterials. *Science* **263**, 1715-1720 (1994).

Peppas, N.A., Hilt, J.Z., Khademhosseini, A. & Langer, R. Hydrogels in biology and medicine: From molecular principles to bionanotechnology. *Adv. Mater.* **18**, 1345-1360 (2006).

Pirrung, M.C. & Webster, N.J.G. Mechanism of intramolecular photocycloadditions of cyclooctenones. *J. Org. Chem.* **52**, 3603-3613 (1987).

Polizzotti, B.D., Fairbanks, B.D. & Anseth, K.S. Three-dimensional biochemical patterning of click-based composite hydrogels *via* thiolene photopolymerization. *Biomacromolecules* **9**, 1084-1087 (2008).

Prescher, J.A. & Bertozzi, C.R. Chemistry in living systems. *Nat. Chem. Biol.* **1**, 13-21 (2005).

Ragan, J.A. et al. A practical synthesis of cycloheptane-1,3-dione. *Org. Process Res. Dev.* **2**, 379-381 (1998).

Ratner, B.D. & Bryant, S.J. Biomaterials: Where we have been and where we are going. *Annu. Rev. Biomed. Eng.* **6**, 41-75 (2004).

Rault, I., Frei, V., Herbage, D., AbdulMalak, N. & Huc, A. Evaluation of different chemical methods for cross-linking collagen gel, films and sponges. *J. Mater. Sci. - Mater. Med.* **7**, 215-221 (1996).

Rice, M.A., Sanchez-Adams, J. & Anseth, K.S. Exogenously triggered, enzymatic degradation of photopolymerized hydrogels with polycaprolactone subunits: Experimental observation and modeling of mass loss behavior. *Biomacromolecules* **7**, 1968-1975 (2006).

Roberts, M.J., Bentley, M.D. & Harris, J.M. Chemistry for peptide and protein PEGylation. *Adv. Drug Delivery Rev.* **54**, 459-476 (2002).

Rostovtsev, V.V., Green, L.G., Fokin, V.V. & Sharpless, K.B. A stepwise huisgen cycloaddition process: Copper(I)-catalyzed regioselective "ligation" of azides and terminal alkynes. *Angew. Chem. Int. Ed. Engl.* **41**, 2596-2599 (2002).

Rowley, J.A., Madlambayan, G. & Mooney, D.J. Alginate hydrogels as synthetic extracellular matrix materials. *Biomaterials* **20**, 45-53 (1999).

Ruedi, G. & Hansen, H.J. Diradical-promoted two-carbon ring-expansion reactions by thermal isomerization: Synthesis of functionalized macrocyclic ketones. *Helv. Chim. Acta* **87**, 1628-1665 (2004).

Ruoslahti, E. & Pierschbacher, M.D. New perspectives in cell-adhesion - RGD and integrins. *Science* **238**, 491-497 (1987).

Rydholm, A.E., Reddy, S.K., Anseth, K.S. & Bowman, C.N. Controlling network structure in degradable thiol-acrylate biomaterials to tune mass loss behavior. *Biomacromolecules* **7**, 2827-2836 (2006).

Rydholm, A.E., Reddy, S.K., Anseth, K.S. & Bowman, C.N. Development and characterization of degradable thiol-allyl ether photopolymers. *Polymer* **48**, 4589-4600 (2007).

Salinas, C.N. & Anseth, K.S. Mixed mode thiol-acrylate photopolymerizations for the synthesis of PEG-peptide hydrogels. *Macromolecules* **41**, 6019-6026 (2008).

Sander, S.v.B. et al. Metal-Free Triazole Formation as a Tool for Bioconjugation. *Chembiochem* **8**, 1504-1508 (2007).

Sarig-Nadir, O., Livnat, N., Zajdman, R., Shoham, S. & Seliktar, D. Laser photoablation of guidance microchannels into hydrogels directs cell growth in three dimensions. *Biophys. J.* **96**, 4743-4752 (2009).

Sawhney, A.S., Pathak, C.P. & Hubbell, J.A. Bioerodible hydrogels based on photopolymerized poly(ethylene glycol)-co-poly(alpha-hydroxy acid) diacrylate macromers. *Macromolecules* **26**, 581-587 (1993).

Saxon, E. & Bertozzi, C.R. Cell surface engineering by a modified staudinger reaction. *Science* **287**, 2007-2010 (2000).

Schmedlen, K.H., Masters, K.S. & West, J.L. Photocrosslinkable polyvinyl alcohol hydrogels that can be modified with cell adhesion peptides for use in tissue engineering. *Biomaterials* **23**, 4325-4332 (2002).

Scott, T.F., Draughon, R.B. & Bowman, C.N. Actuation in crosslinked polymers *via* photoinduced stress relaxation. *Adv. Mater.* **18**, 2128-2132 (2006).

Scott, T.F., Schneider, A.D., Cook, W.D. & Bowman, C.N. Photoinduced plasticity in cross-linked polymers. *Science* **308**, 1615-1617 (2005).

Seidlits, S.K., Schmidt, C.E. & Shear, J.B. High-resolution patterning of hydrogels in three dimensions using direct-write photofabrication for cell guidance. *Adv Funct Mater* **19**, 3543-3551 (2009).

Shimizu, S. et al. In vitro studies on a new method for islet microencapsulation using a thermoreversible gelation polymer, n-isopropylacrylamide-based copolymer. *Artif. Organs* **20**, 1232-1237 (1996).

Sims, E.A., DeForest, C.A. & Anseth, K.S. A mild, large-scale synthesis of 1,3-cyclooctanedione: Expanding access to difluorinated cyclooctyne for copper-free click chemistry. *Tetrahedron Lett.* **52**, 1871-1873 (2011).

Singhvi, R. et al. Engineering cell-shape and function. *Science* **264**, 696-698 (1994).

Sletten, E.M. & Bertozzi, C.R. Bioorthogonal chemistry: Fishing for selectivity in a sea of functionality. *Angew. Chem. Int. Ed. Engl.* **48**, 6974-6998 (2009).

Sletten, E.M., Nakamura, H., Jewett, J.C. & Bertozzi, C.R. Difluorobenzocyclooctyne: Synthesis, reactivity, and stabilization by beta-cyclodextrin. *J. Am. Chem. Soc.* **132**, 11799-11805 (2010).

Song, W., Wang, Y., Qu, J., Madden, M.M. & Lin, Q. A photoinducible 1,3-dipolar cycloaddition reaction for rapid, selective modification of tetrazole-containing proteins. *Angew. Chem. Int. Ed. Engl.* **47**, 2832-2835 (2008).

Speers, A.E., Adam, G.C. & Cravatt, B.F. Activity-based protein profiling in vivo using a copper(I)-catalyzed azide-alkyne [3+2] cycloaddition. *J. Am. Chem. Soc.* **125**, 4686-4687 (2003).

Srinivasan, R., Li, J., Ng, S.L., Kalesh, K.A. & Yao, S.Q. Methods of using click chemistry in the discovery of enzyme inhibitors. *Nat. Protoc.* **2**, 2655-2664 (2007).

Suzuki, M., Watanabe, A. & Noyori, R. Palladium(0)-catalyzed reaction of alpha,beta-epoxy ketones leading to beta-diketones. *J. Am. Chem. Soc.* **102**, 2095-2096 (1980).

Tayalia, P. & Mooney, D.J. Controlled growth factor delivery for tissue engineering. *Adv. Mater.* **21**, 3269-3285 (2009).

Tibbitt, M.W. & Anseth, K.S. Hydrogels as extracellular matrix mimics for 3D cell culture. *Biotechnol. Bioeng.* **103**, 655-663 (2009).

Tibbitt, M.W., Kloxin, A.M., Dyamenahalli, K.U. & Anseth, K.S. Controlled two-photon photodegradation of PEG hydrogels to study and manipulate subcellular interactions on soft materials. *Soft Matter* **6**, 5100-5108 (2010).

Tornoe, C.W., Christensen, C. & Meldal, M. Peptidotriazoles on solid phase: [1,2,3]-triazoles by regiospecific copper(i)-catalyzed 1,3-dipolar cycloadditions of terminal alkynes to azides. *J. Org. Chem.* **67**, 3057-3064 (2002).

Traut, R.R. et al. Methyl 4-mercaptobutyrimidate as a cleavable cross-linking reagent and its application to the escherichia coli 30s ribosome. *Biochemistry (Mosc.)* **12**, 3266-3273 (1973).

Tse, J.R. & Engler, A.J. Stiffness gradients mimicking in vivo tissue variation regulate mesenchymal stem cell fate. *PLoS ONE* **6** (2011).

Tsuji, J., Nagashima, H. & Hori, K. A new preparative method for 1,3-dicarbonyl compounds by the regioselective oxidation of alpha,beta-unsaturated carbonyl-compounds, catalyzed by $PdCl_2$ using hydroperoxides as the reoxidant of Pd^0. *Chem. Lett.*, 257-260 (1980).

Uygun, M., Tasdelen, M.A. & Yagci, Y. Influence of type of initiation on thiol-ene "click" chemistry. *Macromol. Chem. Phys.* **211**, 103-110 (2010).

van Berkel, S.S. et al. Metal-free triazole formation as a tool for bioconjugation. *Chembiochem* **8**, 1504-1508 (2007).

van Dijk, M., Rijkers, D.T.S., Liskamp, R.M.J., van Nostrum, C.F. & Hennink, W.E. Synthesis and applications of biomedical and pharmaceutical polymers *via* click chemistry methodologies. *Bioconjug. Chem.* **20**, 2001-2016 (2009).

Vaultier, M., Knouzi, N. & Carrié, R. Reduction d'azides en amines primaires par une methode generale utilisant la reaction de staudinger. *Tetrahedron Lett.* **24**, 763-764 (1983).

von Maltzahn, G. et al. In vivo tumor cell targeting with "click" nanoparticles. *Bioconjug. Chem.* **19**, 1570-1578 (2008).

Weber, L.M., Hayda, K.N., Haskins, K. & Anseth, K.S. The effects of cell-matrix interactions on encapsulated beta-cell function within hydrogels functionalized with matrix-derived adhesive peptides. *Biomaterials* **28**, 3004-3011 (2007).

Wei, H.Y., Senyurt, A.F., Jonsson, S. & Hoyle, C.E. Photopolymerization of ternary thiol-ene/acrylate systems: Film and network properties. *J. Polym. Sci., Part A: Polym. Chem.* **45**, 822-829 (2007).

Weinrich, D. et al. Oriented immobilization of farnesylated proteins by the thiol-ene reaction. *Angew. Chem. Int. Ed. Engl.* **49**, 1252-1257 (2010).

Weitz, E. & Scheffer, A. The impact of alkali hydrogen superoxyde on unsaturated compounds. *Ber. Dtsch. Chem. Ges.* **54**, 2327-2344 (1921).

West, J.L. & Hubbell, J.A. Polymeric biomaterials with degradation sites for proteases involved in cell migration. *Macromolecules* **32**, 241-244 (1999).

Whitehouse, D.L., Savinov, S.N. & Austin, D.J. An improved synthesis and selective coupling of a hydroxy based photolabile linker for solid phase organic synthesis. *Tetrahedron Lett.* **38**, 7851-7852 (1997).

Wolbers, F. et al. Viability study of HL60 cells in contact with commonly used microchip materials. *Electrophoresis* **27**, 5073-5080 (2006).

Wong, D.Y., Griffin, D.R., Reed, J. & Kasko, A.M. Photodegradable hydrogels to generate positive and negative features over multiple length scales. *Macromolecules* **43**, 2824-2831 (2010).

Wong, J.Y., Velasco, A., Rajagopalan, P. & Pham, Q. Directed movement of vascular smooth muscle cells on gradient-compliant hydrogels. *Langmuir* **19**, 1908-1913 (2003).

Wosnick, J.H. & Shoichet, M.S. Three-dimensional chemical patterning of transparent hydrogels. *Chem. Mater.* **20**, 55-60 (2008).

Wu, Y.I. et al. A genetically encoded photoactivatable Rac controls the motility of living cells. *Nature* **461**, 104-U111 (2009).

Yasuda, A. et al. In vitro culture of chondrocytes in a novel thermoreversible gelation polymer scaffold containing growth factors. *Tissue Eng.* **12**, 1237-1245 (2006).

Young, J.L. & Engler, A.J. Hydrogels with time-dependent material properties enhance cardiomyocyte differentiation in vitro. *Biomaterials* **32**, 1002-1009 (2011).

Yu, X.J., Dillon, G.P. & Bellamkonda, R.V. A laminin and nerve growth factor-laden three-dimensional scaffold for enhanced neurite extension. *Tissue Eng.* **5**, 291-304 (1999).

Zhao, Y. et al. New caged coumarin fluorophores with extraordinary uncaging cross sections suitable for biological imaging applications. *J. Am. Chem. Soc.* **126**, 4653-4663 (2004).

Zheng, Y.J. et al. PEG-based hydrogel synthesis *via* the photodimerization of anthracene groups. *Macromolecules* **35**, 5228-5234 (2002).

Zisch, A.H. et al. Cell-demanded release of VEGF from synthetic, biointeractive cell-ingrowth matrices for vascularized tissue growth. *FASEB J.* **17**, 2260-2262 (2003).

APPENDIX A

A MILD, LARGE-SCALE SYNTHESIS OF 1,3-CYCLOOCTANEDIONE: EXPANDING ACCESS TO DIFLUORINATED CYCLOOCTYNE FOR COPPER-FREE CLICK CHEMISTRY

As published in *Tetrahedron Letters*, 52, 1871-1873 (2011).

9.1 Abstract

We report the large-scale synthesis of 1,3-cyclooctanedione in five steps with 29% yield. This molecule is a synthetic precurser to difluorinated cyclooctyne, which participates in a bioorthogonal copper-free click reaction with azides. The final step demonstrates the first successful application of the Wacker-Tsuji oxidation to form a cyclic 1,3-dione.

9.2 Introduction

In the past decade, bioorthogonal conjugation methods have emerged as powerful and increasingly indispensable tools for performing chemistry in biological contexts[1-3]. Notably, the strain-promoted azide-alkyne cycloaddition (SPAAC) has proven especially promising as a cytocompatible ligation method. The reaction boasts nearly all the advantages of the canonical copper(I)-catalyzed Huisgen [2+3] cycloaddition between an azide and a terminal alkyne, but requires no copper catalyst, which is cytotoxic at >0.1 mM concentrations[4,5]. Thus, the chemistry can be performed readily ($k \sim 10^{-1}$ M^{-1} s^{-1}) in the presence of individual cells as well as full living organisms[6]. Bertozzi and coworkers have pioneered the synthesis of several cyclooctyne reagents and have successfully applied their use as chemical probes to

perform *in vivo* imaging to study glycosylation in zebrafish and mice[7,8]. In addition, other molecules for strain-promoted ractions with azides have recently been developed including (aza-)dibenzocyclooctynes[9,10], biarylazacyclooctynone[11], and oxanorbornadienes[12] which exhibit similar utility.

More recently, the use of Cu-free click chemistry has expanded from simple labeling procedures to include the formation of complex materials[13-15]. By end-functionalizing synthetic polypeptides with a difluorinated cyclooctyne reagent (DIFO3)[16] and reacting with a four-arm poly(ethylene glycol) tetraazide in an aqueous medium, hydrogels are formed that allow for the direct encapsulation of cells.[13,15] Despite this preliminary success, the difficulty of the cyclooctyne synthetic preparation has ultimately hampered the widespread implementation of SPAAC in material formation to date. Additionally, utilizing these reagents in material fabrication requires gram-quantities of the reagents as opposed to the μg- to mg-scale required for labeling experiments. Thus, we sought to develop an improved synthetic route that enables DIFO3 to be formed on the multi-gram scale.

We found the main difficulty in preparing DIFO3 in significant quantity lies in producing large amounts of the key synthetic intermediate 1,3-cyclooctanedione. The published route of Pirrung and Webster[17] (Scheme 1) for preparation of this compound has several undesirable characteristics, including the use of large molar equivalents of water-reactive sodium metal and diethylzinc[18]. Pyrophoric organometallic reagents are not ideal for larger scale reactions and have in some cases been implicated in laboratory accidents[19]. Moreover, the acyloin condensation (Scheme 1, first step) exhibited highly-variable yields in our hands. This is in part due to the nature of cyclizing larger rings: significant oligomerization/polymerization likely occured, as evidenced by the formation of a non-

volatile, colored byproduct and reduced product recovery, even with high dilution and slow addition of diester. Thus, we sought to develop a mild, high-yielding synthesis of 1,3-cyclooctanedione starting from an inexpensive, readily-available substrate.

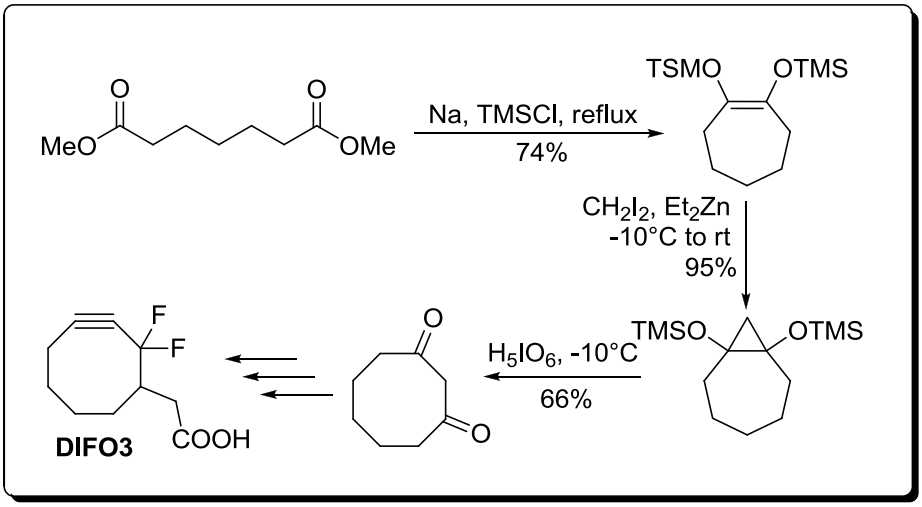

S**cheme 9.1** Traditional synthesis of DIFO3 from 1,3-cyclooctanedione intermediate.

9.3 Results and Discussion

Initially, we were inspired by a kg-scale preparation of 1,3-cycloheptanedione[20,21], whose key step relies on the cycloaddition between dichloroacetyl chloride and 1-trimethylsilyloxycyclopentene. We hypothesized that this synthetic approach could be easily adapted to prepare 1,3-cyclooctanedione. However, we abandoned this route after experiencing difficulty obtaining significant coupling between 1-trimethylsilyloxycyclohexene and dichloroacetyl chloride. Ultimately, cyclooctanone was chosen as a starting point as it is inexpensive ($77 per 100 g *via* Aldrich), readily available, and several potential methods for installing the ketone functionality at the β-position were identified, including epoxidation and subsequent Pd-catalyzed rearrangement[22,23] as well as the direct Wacker-Tsuji oxidation[24] (Scheme 2).

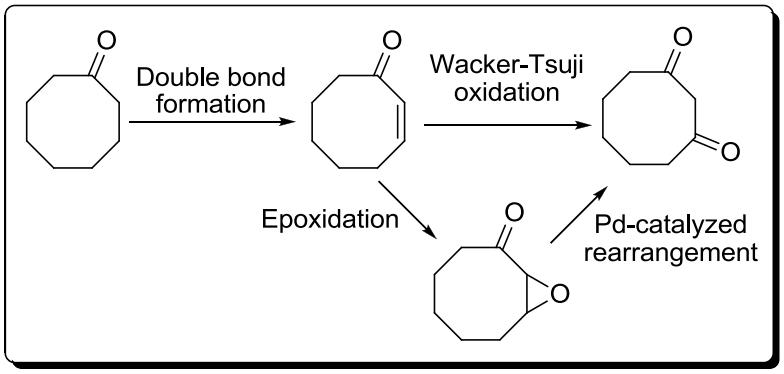

Scheme 9.2 Strategy for synthesis of 1,3-cyclooctanedione.

From the starting cyclooctanone (**1**), enone **5** was synthesized in four steps and 78% yield *via* α-bromination followed by elimination, an established method to introduce an α,β C=C double bond[25]. Bromination of ketone (**1**) was accomplished in excellent yield (90%, Scheme 3) with 1.5 equiv of Br_2 in ethanolic hydrochloric acid and the product was pure enough after standard aqueous workup to obviate chromatographic purification.

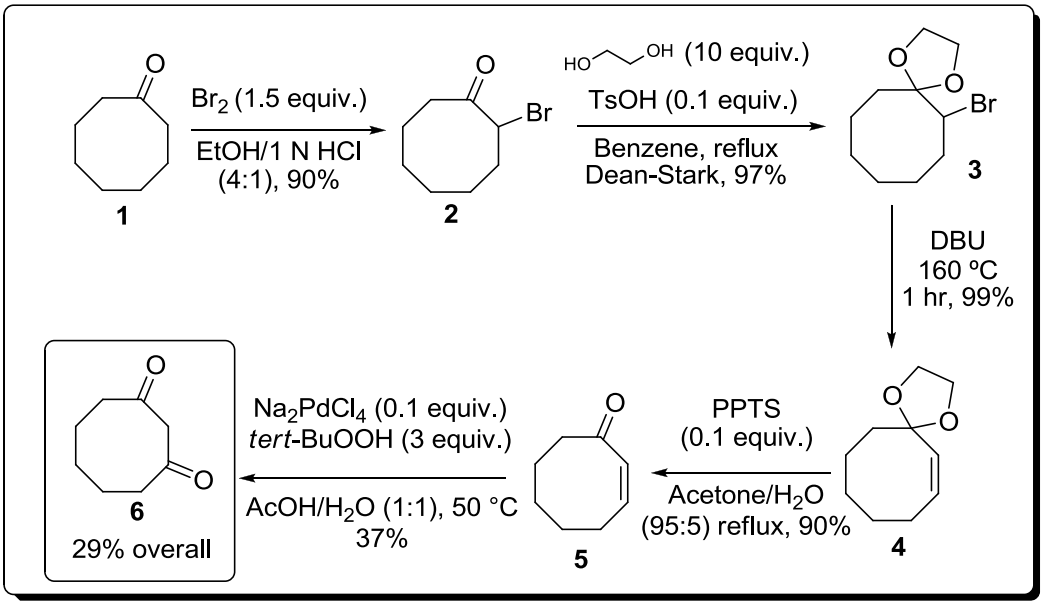

Scheme 9.3 Complete synthesis of 1,3-cyclooctanedione (**6**) from cyclooctanone (**1**) with reaction conditions and obtained yields. Full reaction conditions, as well as ^{1}H, ^{13}C, and COSY NMR and HR-MAS characterization for all compounds can be found in the Supplementary Section 9.5.

Many attempts to effect direct dehydrobromination on **2** with various bases and solvent systems were made (KOH in isopropanol, DBU in toluene or dichloromethane[26], and $LiBr/Li_2CO_3$ in DMF[27]). All such attempts, however, failed to generate significant quantity of enone **5**. Thus, a two-step protection/deprotection of the ketone moiety was adopted[28]. Formation of bromo ketal **3** under Dean-Stark conditions was achieved in near-quantitative yield and reasonable purity. Quantitative dehydrobromination of crude ketal bromide **3** was accomplished after reacting for 1 hr in neat 1,8-diazabicycloundec-7-ene (DBU) at 160 °C. We note that the direct conversion of cyclooctanone **1** to the bromo ketal **3** has been reported elsewhere[29,30]. Crude product **4** was deprotected *via* trans-ketalization in PPTS/acetone/water, and resultant enone **5** was recovered in high yield after purification by flash chromatography. Note that while Plumet[23] reports a method to synthesize enone **5** in two steps from cyclooctanedione, we feel the extra two steps for the present scheme are justified: The overall yield is higher (78% vs 49%), both require just one chromatographic purification (for the final enone), and the palladium reagent used in the Plumet method (73 mol%) would add considerable cost to a large scale preparation.

Two potential methods to convert enone **5** to 1,3-cyclooctanedione (**6**) were identified involving epoxidation then palladium-catalyzed rearrangement[23,31]. However, after an initial attempt to form the epoxide from enone (**5**) under Weitz–Scheffer conditions (aq. H_2O_2 or TBHP and cat. NaOH)[32] failed, we found that Wacker-Tsuji oxidation conditions gave the desired dione in a single step (Scheme 3).[24] After briefly screening reaction conditions (Table 1), conversion of enone **5** to dione **6** was realized in 37% yield by treatment with 0.1 equiv Na_2PdCl_4 and 3 equiv *tert*-BuOOH in $AcOH/H_2O$ (1:1) at 50 °C – undesired formation of unidentified side products resulted in the modest yield of this step. Given the high yields

and simple purifications for the preceding steps, even with a yield <40% for the final step, this represents significant improvement over the standard method for 1,3-cyclooctanedione preparation (Scheme 1)[17]. Furthermore, to the best of our knowledge, no successful application of the Wacker-Tsuji application to a cyclic substrate has ever been reported.

Na_2PdCl_4 (mol equiv)	*tert*-BuOOH (mol equiv)	Temperature (°C)	Yield (%)
0.2	1.5	50	24
0.2	1.5	100	11
0.2	3	50	36
0.2	3	30	36
0.1	1.5	50	30
0.1	3	50	37
0.4	1.5	50	22

Table 9.1 Isolated yields of dione (**6**) *via* the Wacker-Tsuji oxidation of enone (**5**) for a variety of catalyst and reactant amounts, as well as temperature.

In summary, we have described a new method to synthesize 1,3-cyclooctanedione in five steps (Scheme 3) using an inexpensive starting material, robust reactions, and with only two steps requiring chromatographic purification. In addition, the first successful application of the Wacker oxidation in the direct synthesis of a cyclic 1,3-dione is shown. Using this method, we were able to generate 15+ g of dione **6** in 29% overall yield which can be used to further synthesize DIFO3 for SPAAC.

9.4 References

1. Prescher, J.A. & Bertozzi, C.R. Chemistry in living systems. *Nat. Chem. Biol.* **1**, 13-21 (2005).

2. Baskin, J.M. & Bertozzi, C.R. Bioorthogonal click chemistry: Covalent labeling in living systems. *Qsar & Combinatorial Science* **26**, 1211-1219 (2007).

3. Sletten, E.M. & Bertozzi, C.R. Bioorthogonal chemistry: fishing for selectivity in a sea of functionality. *Angew. Chem. Int. Ed. Engl.* **48**, 6974-6998 (2009).

4. Speers, A.E., Adam, G.C. & Cravatt, B.F. Activity-based protein profiling in vivo using a copper(I)-catalyzed azide-alkyne [3+2] cycloaddition. *J. Am. Chem. Soc.* **125**, 4686-4687 (2003).

5. Wolbers, F. et al. Viability study of HL60 cells in contact with commonly used microchip materials. *Electrophoresis* **27**, 5073-5080 (2006).

6. Baskin, J.M. et al. Copper-free click chemistry for dynamic in vivo imaging. *Proc. Natl. Acad. Sci. U. S. A.* **104**, 16793-16797 (2007).

7. Laughlin, S.T., Baskin, J.M., Amacher, S.L. & Bertozzi, C.R. In vivo imaging of membrane-associated glycans in developing zebrafish. *Science* **320**, 664-667 (2008).

8. Chang, P.V. et al. Copper-free click chemistry in living animals. *Proc. Natl. Acad. Sci. U. S. A.* **107**, 1821-1826 (2010).

9. Ning, X.H., Guo, J., Wolfert, M.A. & Boons, G.J. Visualizing metabolically labeled glycoconjugates of living cells by copper-free and fast huisgen cycloadditions. *Angew. Chem. Int. Ed. Engl.* **47**, 2253-2255 (2008).

10. Debets, M.F. et al. Aza-dibenzocyclooctynes for fast and efficient enzyme PEGylation *via* copper-free (3+2) cycloaddition. *Chem. Commun.* **46**, 97-99 (2010).

11. Jewett, J.C., Sletten, E.M. & Bertozzi, C.R. Rapid Cu-free click chemistry with readily Synthesized Biarylazacyclooctynones. *J. Am. Chem. Soc.* **132**, 3688-3690 (2010).

12. Sander, S.v.B. et al. Metal-free triazole formation as a tool for bioconjugation. *Chembiochem* **8**, 1504-1508 (2007).

13. DeForest, C.A., Polizzotti, B.D. & Anseth, K.S. Sequential click reactions for synthesizing and patterning three-dimensional cell microenvironments. *Nat. Mater.* **8**, 659-664 (2009).

14. Johnson, J.A., Baskin, J.M., Bertozzi, C.R., Koberstein, J.T. & Turro, N.J. Copper-free click chemistry for the in situ crosslinking of photodegradable star polymers. *Chem. Commun.*, 3064-3066 (2008).

15. DeForest, C.A., Sims, E.A. & Anseth, K.S. Peptide-functionalized click hydrogels with independently tunable mechanics and chemical functionality for 3D cell culture. *Chem. Mater.* **22**, 4783-4790 (2010).

16. Codelli, J.A., Baskin, J.M., Agard, N.J. & Berozzi, C.R. Second-generation difluorinated cyclooctynes for copper-free click chemistry. *J. Am. Chem. Soc.* **130**, 11486-11493 (2008).

17. Pirrung, M.C. & Webster, N.J.G. Mechanism of intramolecular photocycloadditions of cyclooctenones. *J. Org. Chem.* **52**, 3603-3613 (1987).

18. Bloomfield, J.J. & Nelke, J.M. Acyloin condensation in which chlorotrimethylsilane is used as a trapping Agent - 1,2-Bis(Trimethylsilyloxy)-Cyclobutene and 2-Hydroxycyclobutanone. *Org. Synth.* **50-9**, 167-172 (1988).

19. Kemsley, J. Learning from UCLA. *Chemical & Engineering News* **87**, 29-31 (2009).

20. Ragan, J.A. et al. A practical synthesis of cycloheptane-1,3-dione. *Org. Process Res. Dev.* **2**, 379-381 (1998).

21. Do, N., McDermott, R.E. & Ragan, J.A. Preparation of cycloheptane-1,3-dione *via* reductive ring expansion of 1-trimethylsilyloxy-7,7-dichlorobicyclo[3.2.0]heptan-6-one. *Org. Synth.* **85**, 138-146 (2008).

22. Suzuki, M., Watanabe, A. & Noyori, R. Palladium(0)-catalyzed reaction of alpha,beta-epoxy ketones leading to beta-diketones. *J. Am. Chem. Soc.* **102**, 2095-2096 (1980).

23. Aljarilla, A. et al. Stereochemistry of the tetrabutylammonium cyanide-catalyzed cyanosylilation of cyclic alpha,beta-epoxyketones - Dependence of the diastereoselectivity on the ring size. *Eur. J. Org. Chem.*, 3969-3976 (2006).

24. Tsuji, J., Nagashima, H. & Hori, K. A new preparative method for 1,3-dicarbonyl compounds by the regioselective oxidation of alpha,beta-unsaturated carbonyl-compounds, catalyzed by $PdCl_2$ using hydroperoxides as the reoxidant of Pd^0. *Chem. Lett.*, 257-260 (1980).

25. Larock, R.C. Comprehensive organic transformations: a guide to functional group preparations, Edn. 2nd. (Wiley-VCH, New York ; Chichester [England]; 1999).

26. Paquette, L.A., Ross, R.J. & Springer, J.P. Stereocontrolled Construction of an Ingenol Prototype Having a Complete Array of Oxygenated and Unsaturated Centers. *J. Am. Chem. Soc.* **110**, 6192-6204 (1988).

27. Floyd, M.B. & Weiss, M.J. Prostaglandins and congeners. 21. Synthesis of some cyclohexyl analogs (11a-Homoprostaglandins). *J. Org. Chem.* **44**, 71-75 (1978).

28. Ruedi, G. & Hansen, H.J. Diradical-promoted two-carbon ring-expansion reactions by thermal isomerization: Synthesis of functionalized macrocyclic ketones. *Helv. Chim. Acta* **87**, 1628-1665 (2004).

29. House, H.O., Sieloff, R.F., Lee, T.V. & Detar, M.B. Enones with strained double-bonds. 4. The bicyclo[5.3.1]undecane System. *J. Org. Chem.* **45**, 1800-1806 (1980).

30. Meier, H., Antony-Mayer, C., Schulz-Popitz, C. & Zerban, G. Einführung einer Dreifachbindung in das Bicyclo[6.1.0]nonan-Gerüst. *Liebigs Ann. Chem.* **12**, 1087-1094 (1987).

31. Lehmann, T.E., Kuhn, O. & Kruger, J. Process development and pilot plant scale synthesis of spiro[3.5]nonane-6,8-dione. *Org. Process Res. Dev.* **7**, 913-916 (2003).

32. Weitz, E. & Scheffer, A. The impact of alkali hydrogen superoxyde on unsaturated compounds. *Ber. Dtsch. Chem. Ges.* **54**, 2327-2344 (1921).

9.5 Supplementary Information

Unless otherwise noted, all reactions were performed under an argon atmosphere in flame- or over-dried glassware and were stirred with a Teflon-coated magnetic spinbar. Reaction temperature refers to the bath temperature, not the internal temperature of the reaction vessel. Solvents and liquid reagents were transferred *via* syringe or cannula. All reagents were obtained from commercial suppliers in the highest available purity and used without further purification unless otherwise stated. Solvents were removed by rotary evaporation.

All nuclear magnetic resonance (NMR) spectra were run in deuteriochloroform ($CDCl_3$) obtained from Cambridge Isotope Laboratories. ^1H NMR spectra were recorded on a Varian INOVA 500 MHz instrument. ^{13}C and 2D-COSY experiments were recorded on a Bruker Avance-III 300 MHz instrument. Chemical shifts are reported in parts per million (δ) from TMS and multiplicities are denoted using standard abbreviations. The residual $CHCl_3$ peak was used as an internal reference standard (7.26 ppm for ^1H and 77.16 ppm for ^{13}C). *J* values are reported in Hz.

High-resolution mass spectra (HRMS) were obtained on an electrospray ionization instrument (ESI) at the University of Colorado–Boulder Central Analytical Laboratory.

Flash chromatography was performed on silica gel, standard grade, 60°A, 18-32 μm obtained from Sorbtech following the general procedure by Still. Reaction mixtures and chromatography fractions were analyzed by thin layer chromatography (TLC) on silica gel 60 F_{254} plates from EM Separatory Technologies. TLC plates were developed in the solvent system indicated and compounds were revealed by staining with ceric ammonium molybdate (CAM), or by visualizing with UV light at 254 nm.

9.5.1 Synthesis of 2-Bromocyclooctanone (2)

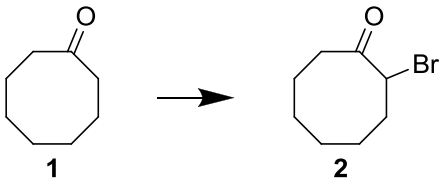

Cyclooctanone (65.75 g, 521 mmol, 1.0 equiv.) and ethanol (700 mL) were added to a 2-L round-bottom flask and stirred until dissolution was complete. 180 mL of 1 N HCl was added and the solution was cooled to 0 °C while purging with argon. Bromine (125 g, 782 mmol, 1.5 equiv.) was then added in a slow, steady stream and the solution was stirred at 0 °C for 72 hr. The reaction was quenched with sat. Na_2SO_3 (150 mL) and most of the ethanol was removed by rotovap. The cloudy, heterogeneous solution was extracted with diethyl ether (4 x 500 mL) and the combined organics were washed with brine, dried over $MgSO_4$, filtered, and concentrated to give a pale yellow liquid (95.95 g, 468 mmol, 90%) that was used without further purification; ^{1}H NMR (500 MHz, $CDCl_3$) δ = 4.27 (dd, *J* = 4.0, 11.4, 1H), 2.87 (td, *J* = 3.7, 12.1, 1H), 2.42 – 2.36 (m, 2H), 2.36 – 2.28 (m, 1H), 1.97 – 1.89 (m, 1H), 1.82 – 1.64 (m, 3H), 1.61 – 1.51 (m, 2H), 1.46 – 1.34 (m, 1H), 1.22 – 1.12 (m, 1H); ^{13}C NMR (75 MHz, $CDCl_3$) δ 208.80, 54.49, 36.30, 32.79, 28.84, 26.66, 25.52, 24.06; HRMS (ESI+): calcd for $[(C_8H_{13}BrO)+H]^+$ 205.0223; found 205.0215.

9.5.2 Synthesis of 6-Bromo-1,4-dioxaspiro[4.7]dodecane (3)

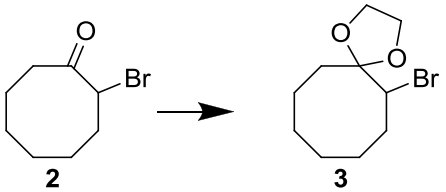

To a 2-L round-bottom flask containing benzene (500 mL) were added 2-bromocyclooctanone (**2**, 86.77 g, 423 mmol, 1.0 equiv.), 1,2-ethanediol (235 mL, 4.230 mol, 10

equiv.), and *p*-toluenesulfonic acid (8.05 g, 42.3 mmol, 10 mol%). The flask was fitted with a Dean-Stark condenser and refluxed (104 °C) until no additional water accumulated in the trap (24 hr), making periodic draw-offs of water as necessary to avoid overflow. The two-phase solution was cooled to rt, washed with water (2 x 400 mL). The water washes were extracted once with benzene (400 mL) and the combined organics were washed with brine (300 mL), dried over $MgSO_4$, filtered, and concentrated to yield a pale yellow liquid (69.96 g, 416 mmol, 97%) that was used without further purification; ^{1}H NMR (500 MHz, $CDCl_3$) δ 4.56 – 4.47 (m, 1H), 4.19 – 4.10 (m, 2H), 4.01 – 3.92 (m, 2H), 2.34 – 2.25 (m, 2H), 2.05 – 1.95 (m, 1H), 1.89 – 1.82 (m, 1H), 1.73 – 1.46 (m, 8H); ^{13}C NMR (75 MHz, $CDCl_3$) δ 111.06, 66.16, 65.24, 59.70, 34.35, 33.89, 27.56, 26.82, 25.07, 22.35; HRMS (ESI+): calcd for $[(C_{10}H_{17}BrO_2)+^7Li]^+$ 255.0566; found 255.0576.

9.5.3 Synthesis of (Z)-1,4-dioxaspiro[4.7]dodec-6-ene (4)

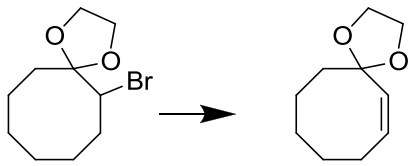

3 **4**

Bromoketal **3** (104.64 g, 420 mmol) and 1,8-Diazabicyclo[5.4.0]undec-7-ene (DBU, 300 mL) were added to a 1-L round-bottom flask and heated at 160 °C for 3 hr. During cooling a rapid precipitation event occurred, causing most of the solution to crystallize. The solidified reaction mixture was dissolved in water (1 L) and extracted with diethyl ether (3 x 600 mL). The combined organics were washed with brine (300 mL), dried over $MgSO_4$, filtered, and concentrated to give a pale yellow liquid (69.95 g, 416 mmol, 99%) that was used without further purification; ^{1}H NMR (500 MHz, $CDCl_3$) δ 5.67 – 5.54 (m, 2H), 3.91 (s, 4H), 2.43 – 2.34 (m, 2H), 1.86 – 1.82 (m, 2H), 1.69 – 1.42 (m, 6H); ^{13}C NMR (75 MHz, $CDCl_3$) δ 133.49, 131.53,

109.91, 64.05, 39.33, 27.91, 24.61, 24.01, 21.78; HRMS (ESI+): calcd for $[(C_{10}H_{16}O_2)+^7Li]^+$ 175.1305; found 175.1303.

9.5.4 Synthesis of (Z)-Cyclooct-2-enone (5)

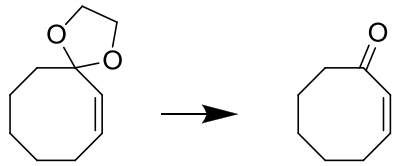

To a solution of acetone/water (95:5, 164.8 mL) in a 500-mL round-bottom flask was added ketal-ene **4** (27.72 g, 164.8 mmol) and pyridinium *p*-toluenesulfonate (4.14 g, 16.5 mmol, 10 mol%). The solution was refluxed (70 °C) overnight then most of the acetone was removed *via* rotovap. Sat. $NaHCO_3$ (250 ml) was added to the reaction mixture, which was then extracted with diethyl ether (3 x 200 mL). The combined organics were washed with brine, dried over $MgSO_4$, filtered, and concentrated. The crude reaction product was purified by flash chromatography (15:1 hexanes/ethyl acetate) to yield a pale yellow liquid (18.46 g, 148.7 mmol, 90%). R_f = 0.28 (10:1 hexanes/ethyl acetate, visualized with CAM stain); ^{1}H NMR (500 MHz, $CDCl_3$) δ 6.34 (dt, *J* = 7.1, 12.5, 1H), 6.00 (d, *J* = 12.5, 1H), 2.68 – 2.61 (m, 2H), 2.55 – 2.46 (m, 2H), 1.85 – 1.78 (m, 2H), 1.67 – 1.52 (m, 4H); ^{13}C NMR (75 MHz, $CDCl_3$) δ 206.08, 141.70, 132.45, 42.78, 28.62, 25.18, 23.15, 22.64; HRMS (ESI+): calcd for $[(C_8H_{12}O)+H]^+$ 125.0961; found 125.0965.

9.5.5 Synthesis of Cyclooctane-1,3-dione (6)

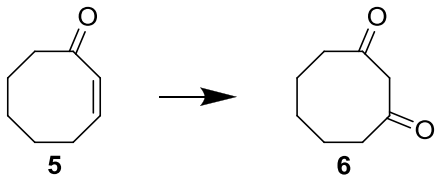

To a solution of 2-propanol and water (50:50, 300 mL) were added enone **5** (37.4 g, 301.4 mmol), *tert*-butylhydroperoxide (129 mL of a 70% aqueous solution, 904 mmol, 3 equiv.), and Na_2PdCl_4 (8.86 g, 30.1 mmol, 10 mol%). The reaction mixture was stirred and heated at 50 °C overnight then diluted with cold water (300 mL) and extracted with dichloromethane (3 x 300 mL). The combined organics were washed with 1 N HCl (500 mL) and brine (300 mL), dried over $MgSO_4$, filtered, and concentrated. The crude product was purified by flash chromatography (10:1 hexanes/ethyl acetate) to yield a pale yellow liquid (15.5 g, 110.6 mmol, 37%). R_f = 0.24 (4:1 hexanes/ethyl acetate, visualized with CAM stain); ^{1}H NMR (500 MHz, $CDCl_3$) δ 3.50 (s, 2H), 2.51 – 2.46 (m, 4H), 1.83 – 1.77 (m, 4H), 1.66 – 1.60 (m, 2H); ^{13}C NMR (75 MHz, $CDCl_3$) δ 206.33, 59.03, 44.08, 27.43, 24.21; HRMS (ESI+): calcd for $[(C_8H_{12}O_2)+H]^+$ 141.0910; found 141.0915.

APPENDIX B

SYNTHESIS OF DIFLUORINATED CYCLOOCTYNE (DIFO3) FOR COPPER-FREE CLICK CHEMISTRY

In collaboration with Senior Thesis student Evan A. Sims

10.1 Synthetic Scheme for the Synthesis of DIFO3

The synthesis of the third generation difluorinated cyclooctyne (DIFO3, **7**) followed the general approach recently reported by Bertozzi *et al.*[1] Our general reaction scheme is shown in Scheme 10.1. Improvements in two key steps were accomplished. First, installation of the vinyl triflate moiety onto ketone **5** was improved by using Comins' reagent instead of *N*-triflimide. Second, the elimination of the vinyl triflate in compound **6** to form cyclooctyne **7** was performed in 69% yield, improving over the reported 59 % yield.

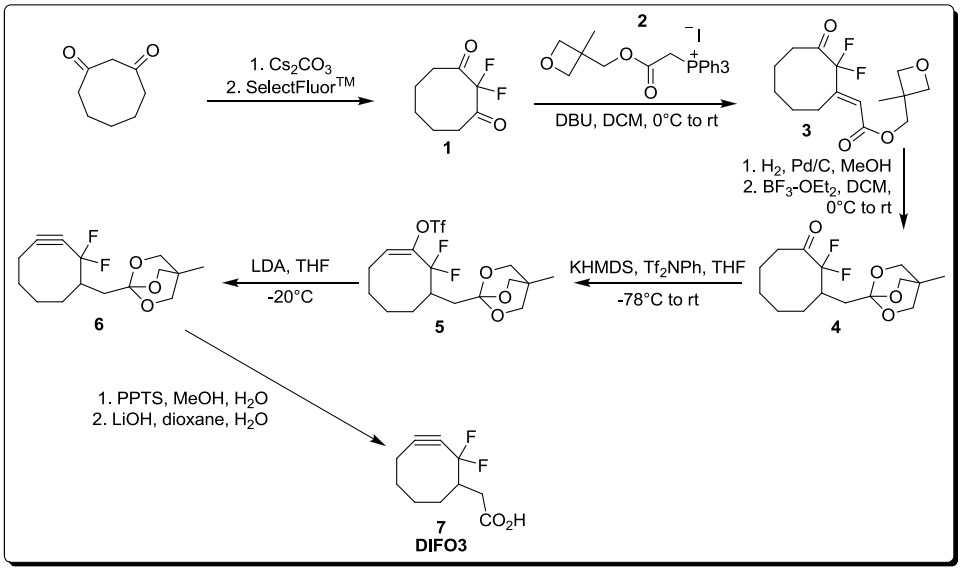

Scheme 10.1 Synthesis route to DIFO3.

10.2 Synthesis of DIFO3

10.2.1 Synthesis of 2,2–difluoro–1,3–cyclooctadione (1)

1,3–cyclooctadione (2.861 g, 20.4 mmol, 1 equiv, as prepared in Appendix A), acetonitrile (146 mL), and Cs_2CO_3 (13.03 g, 40 mmol, 2.0 equiv) were added to a round–bottom flask and stirred for 30 min at rt. The reaction mixture was cooled to 0 °C and SelectFluor (17.00 g, 48 mmol, 2.4 equiv) was added. After stirring at 0 °C for 15 min more, the reaction was removed from the ice–bath, stirred for 30 min then concentrated, diluted with 1 M HCl (120 mL) and extracted with diethyl ether (4 x 120 mL). The combined ether extracts were washed with brine (2 x 60 mL), dried, and concentrated (30 torr at 30 °C) to yield an amber colored oil (2.516 g, 14.28 mmol, 70%) which was carried on without further purification. R_f = 0.31 (4:1 hexanes/EtOAc, stained with CAM). ^{1}H NMR (500 MHz, $CDCl_3$) δ 2.73 – 2.63 (m, 4H), 1.86 – 1.80 (m, 4H), 1.68 – 1.62 (m, 2H). ^{19}F NMR (376 MHz, $CDCl_3$) δ -119.61 (s, 2F). ^{13}C NMR (101 MHz, $CDCl_3$) δ 197.92 (t, J = 25.1), 109.51 (t, J = 261.5), 38.70 (s), 26.17 (s), 24.70 (s). HRMS (ESI+): calculated for $C_8H_{10}F_2LiO_2$ $[M + Li]^+$, 183.0803; found 183.0806 (Δ = + 1.6 ppm).

10.2.2 Synthesis of Phosphonium iodide oxetane ester (2)

Dicyclohexylcarbodiimide (3.66 g, 17.7 mmol, 1.1 equiv), 4–dimethylaminopyridine (98.6 mg, 0.807 mmol, 0.05 equiv), CH_2Cl_2 (20 mL), and 3–methyl–3–oxetanemethanol (1.59 mL, 16.1 mmol, 1 equiv) were added to a round–bottom flask, stirred until dissolution was complete, and brought to 0 °C. Iodoacetic acid (3.00 g, 16.1 mmol, 1 equiv) was added as a solution in CH_2Cl_2 (30 mL) and the reaction was stirred for 1 hr at 0 °C then at rt for 1.5 hr. The reaction was quenched with acetic acid (1.00 mL, 17.5 mmol, 1.1 equiv), stirred for an additional 30 min then diluted with CH_2Cl_2, filtered through Celite, washed with water (200 mL), $NaHCO_3$

(2 x 200 mL), and brine (200 mL). The organic liquid was dried, filtered through Celite, and concentrated. The crude product was diluted with CH_2Cl_2 and again passed through a glass frit to remove addition dicyclohexylurea that had precipitated. This procedure was repeated twice after which the product was taken up in 100 mL of anhydrous THF and transferred to a new round–bottom flask. To this was added triphenylphosphine (4.65 g, 17.7 mmol, 1.1 equiv) and a white precipitate appeared after a few minutes. After stirring for 40 hr, the mixture had become a thick white slurry which was then diluted with CH_2Cl_2 and filtered through a glass frit. The white solid was rinsed with several portions of CH_2Cl_2, collected from the frit and dried in a vacuum oven for 24 hr to yield a white powder (7.24 g, 13.6 mmol, 82% over two steps). ^{1}H NMR (500 MHz, $CDCl_3$) δ 7.91 – 7.85 (m, 6H), 7.82 – 7.76 (m, 3H), 7.70 - 7.64 (m, 6H), 5.55 (d, *J* = 13.5, 2H), 4.25 (dd, *J* = 6.2, 15.6 (variable), 4H), 4.14 (s, 2H), 1.23 (s, 3H). ^{13}C NMR (101 MHz, $CDCl_3$) δ 164.53 (d, *J* = 3.4), 135.53 (d, *J* = 3.0), 134.06 (d, *J* = 10.8), 130.53 (d, *J* = 13.2), 117.57 (d, *J* = 89.1), 79.29 (s), 71.26 (s), 38.95 (s), 33.82 (d, *J* = 56.9), 21.17 (s). ^{31}P NMR (162 MHz, $CDCl_3$) δ 21.61 (s, 1P). HRMS (ESI+): calculated for $C_{50}H_{52}IO_6P_2$ [C+[C+I-]], 937.2278; found 937.2257 (Δ = – 2.2 ppm).

10.2.3 Synthesis of Wittig Product (3)

Phosphonium iodide **2** (7.507 g, 14.1 mmol, 1.05 equiv), DBU (2.045 g, 13.43 mmol, 1 equiv), and CH_2Cl_2 (100 mL) were added to a round-bottom flask and stirred at rt until dissolution was complete then cooled to 0 °C. To this was added compound **1** (2.366 g, 13.43 mmol, 1 equiv) as a solution in CH_2Cl_2 (165 mL) and the reaction was stirred for 72 hr, being allowed to reach rt. The reaction mixture was concentrated and purified by flash chromatography (10:1 hexanes/EtOAc) to yield a clear to pale yellow oil (3.155 g, 10.4 mmol, 78%). R_f = 0.33 revealed by UV light (2:1 hexanes/EtOAc). The doubly-functionalized

compound is also faintly visible at R_f = 0.21 on crude TLC. ^{1}H NMR (500 MHz, $CDCl_3$) δ 6.48 (s, 1H), 4.50 (d, *J* = 6.1, 2H), 4.39 (d, *J* = 6.1, 2H), 4.24 (s, 2H), 2.79 (t, *J* = 6.6, 2H), 2.65 (tt, *J* = 1.6, 6.7, 2H), 1.84 – 1.78 (m, 2H), 1.74 – 1.68 (m, 2H), 1.54 – 1.48 (m, 2H), 1.34 (s, 3H). ^{19}F NMR (376 MHz, $CDCl_3$) δ -113.73 (s, 2F). ^{13}C NMR (101 MHz, $CDCl_3$) δ 200.24 (t, *J* = 28.0), 165.14 (s), 150.48 (t, *J* = 20.1), 121.16 (t, *J* = 9.6), 114.26 (t, *J* = 254.6), 79.71 (s), 69.33 (s), 39.23 (s), 37.52 (s), 26.75 (d, *J* = 6.3), 26.03 (s), 25.56 (s), 21.38 (s). HRMS (ESI+): calculated for $C_{15}H_{21}F_2O_4$ $[M + H]^+$, 303.1402; found 303.1410 (Δ = + 2.6 ppm).

10.2.4 Synthesis of Reduced Wittig Product (3.5)

Wittig product **3** (1.641g, 5.43 mmol, 1 equiv), methanol (75 mL), and 10 wt% palladium on activated carbon (584 mg, 10 mol%) were added to a Parr hydrogenation bottle which was then evacuated and back–filled with hydrogen (ultra-high purity). After shaking for 14 hr under 55 psig of hydrogen, the mixture was diluted with CH_2Cl_2 (100 mL), filtered through Celite to remove the catalyst, and concentrated to obtain the desired product in high purify as a viscous oil which solidified after several days (1.599 g, 5.25 mmol, 97%). R_f = 0.38 stained with DNPH (2:1 hexanes/EtOAc). ^{1}H NMR (500 MHz, $CDCl_3$) δ 4.51 (dd, *J* = 3.1, 6.0, 2H), 4.40 (d, *J* = 6.0, 2H), 4.21 (s, 2H), 2.89 (dd, *J* = 4.0, 16.2, 1H), 2.86 – 2.75 (m, 1H), 2.74 – 2.67 (m, 1H), 2.66 – 2.58 (m, 1H), 2.35 (dd, *J* = 9.0, 16.2, 1H), 2.07 – 1.97 (m, 1H), 1.97 – 1.89 (m, 1H), 1.77 1.62 (m, 2H), 1.61 – 1.45 (m, 4H), 1.34 (s, 3H).

10.2.5 Synthesis of Orthoester Ketone (4)

Two round-bottom flasks containing 4 Å molecular sieves were placed under high-vacuum while heating with a heat-gun then back-filled with argon. After this process was repeated twice more and the flasks were placed under high-vacuum for 2 hr then back-filled a

final time with argon. To one of the flasks was added reduced wittig **3.5** (1.597 g, 5.25 mmol, 1 equiv) as a solution in 10 mL of CH_2Cl_2 which was stirred for 30 min at rt then brought to 0 °C. In the other flask, a 0.2 M solution of $BF_3{\cdot}OEt_2$ was prepared by adding $BF_3{\cdot}OEt_2$ (314 μL) to CH_2Cl_2 (12.186 mL). A portion of the BF3·OEt_2 solution (6.57 mL, 1.3 mmol, 0.25 equiv) was then added to the first flask and the reaction mixture was stirred for 3 hr at 0 °C before quenching with Et_3N (272 μL, 1.95 mmol) and stirring for an additional 20 min. The reaction mixture was transferred to another round–bottom flask *via* syringe, rinsing the first with CH_2Cl_2, concentrated, and purified by flash chromatography over deactivated silica (20:1 hexanes/EtOAc with 1% Et_3N) to yield the desired product as a clear oil (1.311 g, 4.31 mmol, 82%). R_f = 0.37 stained with PMA (2:1 hexanes/EtOAc). ^{1}H NMR (500 MHz, $CDCl_3$) δ 3.89 (s, 6H), 2.71 – 2.63 (m, 1H), 2.62 – 2.46 (m, 2H), 2.22 (dd, *J* = 1.8, 14.6, 1H), 2.10 – 1.95 (m, 2H), 1.90 (s, 1H), 1.66 – 1.57 (m, 2H), 1.55 – 1.42 (m, 2H), 1.42 – 1.30 (m, 2H), 0.80 (s, 3H).

10.2.6 Synthesis of Vinyl Triflate (5)

THF (72 mL) and KHMDS (12.9 mL of a 0.5 M solution in toluene, 6.46 mmol, 1.5 equiv) were added to a round–bottom flask and cooled to -78 °C in a dry–ice/acetone bath. Ketone orthoester **4** (1.311 g, 4.31 mmol, 1 equiv) was added as a solution in 36 mL THF to the above mixture over 30 minutes and the reaction was allowed to stir for an additional 2 hr at -78 °C. N–(5–Chloro–2–pyridyl)bis(trifluoromethanesulfonimide) ('Comins' Reagent,' 2.643 g, 6.46 mmol, 1.5 equiv) was then added as a solution in 36 mL of THF and the reaction was stirred for 10 hr at -78 °C, quenched into deactivated silica, concentrated, and purified by flash chromatography over deactivated silica (20:1 hexanes/EtOAc with 1% Et_3N) to give a white solid (1.667 g, 3.82 mmol, 89%). R_f = 0.61 stained with CAM (2:1 hexanes/EtOAc). ^{1}H NMR (500 MHz, $CDCl_3$) δ 6.04 (t, *J* = 9.6, 1H), 3.89 (s, 6H), 2.72 – 2.58 (m, *J* = 28.4, 1H), 2.51 –

2.34 (m, 2H), 2.21 (dd, J = 1.9, 14.6, 1H), 1.98 – 1.88 (m, 1H), 1.69 – 1.51 (m, 6H), 0.80 (s, 3H). HRMS (ESI+): calculated for $C_{16}H_{21}F_5NaO_6S$ $[M + Na]^+$, 459.0871; found 459.0859 (Δ = – 2.6 ppm).

10.2.7 Synthesis of Cyclooctyne Orthoester (6)

Vinyl triflate **5** (1.529 g, 3.50 mmol, 1 equiv) was dissolved in freshly distilled toluene and concentrated to dryness. This procedure was repeated twice then the compound was dissolved in 10 mL of THF and transferred to a new round bottom flask and cooled to -20 °C in an ice/salt bath. In a separate flask, a 0.22 M solution of lithium diisopropylamide (LDA) was prepared by adding *n*–butyllithium (2.29 mL of a 2.5 M solution in hexanes, 5.72 mmol) dropwise to a stirred solution of diisopropylamine (875 µL, 6.19 mmol) in THF (22.64 mL) at -20 °C. A portion of the LDA solution (19.4 mL, 4.30 mmol, 1.23 equiv) was added to the vinyl triflate solution over 45 min then the reaction was quenched with deactivated silica gel, concentrated, and purified by flash chromatography over deactivated silica gel (20:1 hexanes/EtOAc with 1% Et_3N) to give a white solid (688.5 mg, 2.41 mmol, 69%). R_f = 0.70 stained with CAM (2:1 hexanes/EtOAc). ^{1}H NMR (500 MHz, $CDCl_3$) δ 3.89 (s, 6H), 2.59 – 2.46 (m, 1H), 2.39 – 2.25 (m, 2H), 2.24 – 2.10 (m, 2H), 2.09 – 2.01 (m, 2H), 1.80 – 1.70 (m, 1H), 1.64 (dd, J = 10.3, 14.6, 1H), 1.53 – 1.45 (m, 1H), 1.36 – 1.27 (m, 1H), 0.80 (s, 3H). ^{19}F NMR (376 MHz, $CDCl_3$) δ -96.11 (d, J = 260.5, 1F), -102.95 (ddt, J = 7.0, 23.6, 260.5, 1F). ^{13}C NMR (101 MHz, $CDCl_3$) δ 119.89 (t, J = 238.7), 109.88 (t, J = 11.1), 109.15 (s), 85.36 (dd, J = 41.7, 47.0), 72.81 (s), 51.87 (t, J = 23.8), 35.23 (dd, J = 1.5, 4.4), 32.83 (d, J = 4.8), 32.67 (d, J = 2.0), 30.52 (s), 28.17 (s), 20.53 (s), 14.75 (s). HRMS (ESI+): calculated for $C_{15}H_{21}F_2O_3$ $[M + H]^+$, 287.1453; found 287.1455 (Δ = + 0.7 ppm).

10.2.8 Synthesis of Cyclooctyne Free Acid (DIFO3) (7)

To a scintillation vial containing compound **6** (76.8 mg, 0.268 mmol, 1.0 equiv) were added MeOH (4 mL), H_2O (400 μL) and pyridinium p-toluenesulfonate (PPTS, 134.9 mg, 0.527 mmol, 2.0 equiv). The solution was stirred at rt under an air atmosphere for 24 hr then quenched with $NaHCO_3$ (2 mL) and concentrated under reduced pressure (35 °C at 60 torr) to remove most of the MeOH. Brine (7 mL) was added and the solution was extracted with EtOAc (3 x 10 mL). The combined organics were washed with brine (10 mL) and brine/HCl (1:1 1 M HCl/brine, 2 x 13 mL) then dried, and concentrated to yield a white solid (74.5 mg, 0.245 mmol, 91%). This material was redissolved in 1,4-dioxane (3 mL). To this were added H_2O (200 μL) and LiOH (69 mg, 2.9 mmol, 11.8 equiv) and the heterogeneous mixture (the LiOH did not dissolve completely) was stirred under an air atmosphere for 18 hr. The reaction was quenched with 1 M HCl, diluted with brine (4 mL), and extracted with EtOAc (3 x 11 mL). The combined organic extracts were washed with brine/HCl (1:1 1 M HCl/brine, 12 mL), dried, concentrated, and purified by flash chromatography (20:1 hexanes/EtOAc with 2% AcOH) to provide a white solid (37 mg, 0.183 mmol, 75% over one step or 68% over two steps). R_f = 0.70 (20:1 hexanes/EtOAc with 2% AcOH). ^{1}H NMR (500 MHz, $CDCl_3$) δ 11.72 (br s, 1H), 2.82 – 2.69 (m, 2H), 2.43 – 2.28 (m, 3H), 2.19 – 2.05 (m, 2H), 1.87 – 1.74 (m, 2H), 1.70 – 1.61 (m, 1H), 1.45 – 1.35 (m, 1H). ^{13}C NMR (101 MHz, $CDCl_3$) δ 178.53 (s), 119.10 (dd, *J* = 237.7, 239.4), 110.71 (t, *J* = 11.1), 84.62 (dd, J = 41.6, 46.9), 52.60 (t, *J* = 24.3), 33.80 (d, *J* = 3.1), 32.84 (d, *J* = 4.5), 32.65 (d, *J* = 1.9), 27.87 (s), 20.45 (s). ^{19}F NMR (376 MHz, $CDCl_3$) δ -95.84 (d, *J* = 259.9, 1F), -102.05 (ddt, *J* = 7.0, 21.1, 260.2, 1F). HRMS (ESI+): calculated for $C_{10}H_{12}F_2LiO_2^+$ $[M + {}^7Li]^+$, 209.0960; found 209.0965 (Δ = + 2.4 ppm).

10.3 References

1. Codelli, J.A., Baskin, J.M., Agard, N.J. & Berozzi, C.R. Second-generation difluorinated cyclooctynes for copper-free click chemistry. *J. Am. Chem. Soc.* **130**, 11486-11493 (2008).